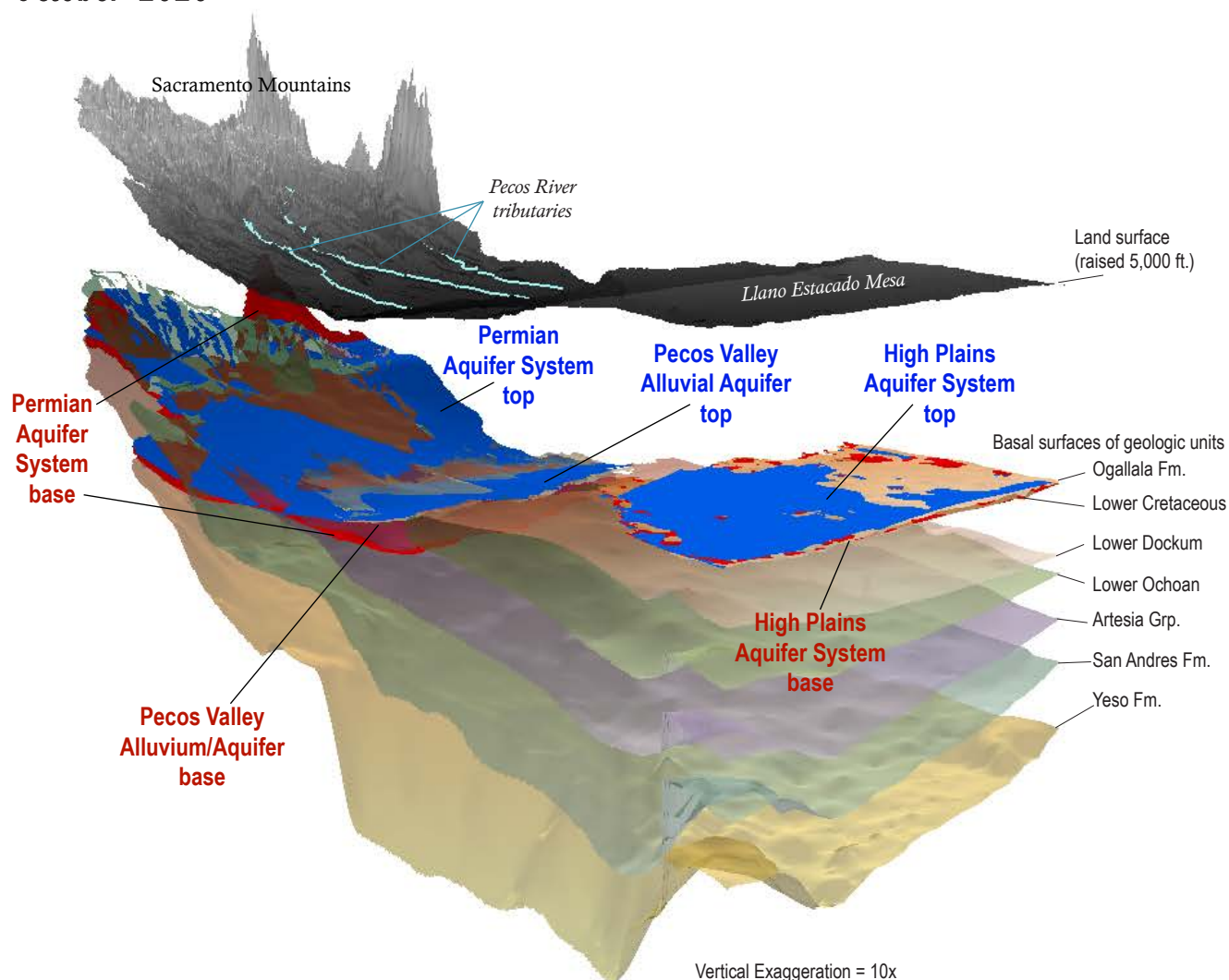
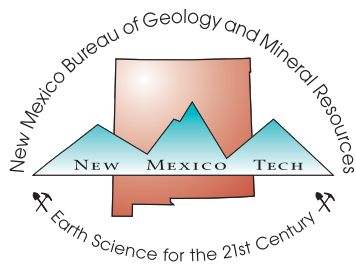


# A Three-Dimensional Hydrogeologic Model from the Pecos Slope to the Southern High Plains, Southeastern New Mexico

Colin Cikoski, Marissa Fichera, Ethan Mamer, and Laila Sturgis

Open-File Report 614  
October 2020





New Mexico Bureau of Geology and Mineral Resources

A Research Division of New Mexico Institute of Mining and Technology

Socorro, NM 87801

(575) 835-5490

[www.geoinfo.nmt.edu](http://www.geoinfo.nmt.edu)

# A Three-Dimensional Hydrogeologic Model from the Pecos Slope to the Southern High Plains, Southeastern New Mexico

<sup>1</sup>Colin Cikoski, <sup>2</sup>Marissa Fichera, <sup>2</sup>Ethan Mamer, and <sup>2</sup>Laila Sturgis

<sup>1</sup>Wyoming Department of Environmental Quality–Land Quality Division, [Colin.Cikoski@wyo.gov](mailto:Colin.Cikoski@wyo.gov)

<sup>2</sup>New Mexico Bureau of Geology and Mineral Resources

Open-File Report 614  
October 2020

New Mexico Bureau of Geology and Mineral Resources

# PROJECT FUNDING

Funding for this project was provided by the Healy Foundation and the New Mexico Bureau of Geology and Mineral Resources Aquifer Mapping Program.

Stacy Timmons, *Associate Director for Hydrogeology Programs*  
Laila Sturgis, *Aquifer Mapping Program Manager*

## Disclaimer

The reports and data provided here are intended to aid in the understanding of the geologic and hydrologic resources of New Mexico. However, there are limitations for all data, particularly when subsurface interpretation is performed, or when data are aggregated that may have been collected at different times, by different agencies or people, and for different purposes. The information and results provided are also dynamic and may change over time. Users of these data and interpretations should exercise caution, and site-specific conditions should always be verified. These materials are not to be used for legally binding decisions. Any opinions expressed do not necessarily reflect the official position of the New Mexico Bureau of Geology and Mineral Resources, New Mexico Tech, or the State of New Mexico.

Although every effort is made to present current and accurate information, data is provided without guarantee of any kind. The data are provided “as is,” and the NM Bureau of Geology assumes no responsibility for errors or omissions. No warranty, expressed or implied, is made regarding the accuracy or utility of the data for general or scientific purposes. The user assumes the entire risk associated with its use of these data. The NM Bureau of Geology shall not be held liable for any use or misuse of the data described and/or contained herein. The user bears all responsibility in determining whether these data are fit for the user’s intended use.

## Suggested citation:

Cikoski, C., Fichera, M., Mamer, E., Sturgis, L., 2020, A Three-Dimensional Hydrogeologic Model from the Pecos Slope the Southern High Plains, Southeastern New Mexico. New Mexico Bureau of Geology and Mineral Resources Open-File Report 614.

Cover: Three-dimensional visualization of the subsurface geology from the Sacramento Mountains to the Southern High Plains of southeastern New Mexico. *Figure by Marissa Fichera*



# CONTENTS

Executive Summary .....	vi
<i>by Laila Sturgis</i>	

Pecos Slope Digital Framework Geologic Model—Overview of Methods .....	1
---	---

*by Colin Cikoski*

Summary .....	3
I. Introduction .....	5
II. Background .....	9
III. Input data .....	19
IV. Methods .....	25
V. Results .....	79
Acknowledgments .....	80
References .....	81
Appendix 1 - Model assessment .....	7 pages

[Map package](#)

3D Aquifer Mapping of the Pecos Slope and Southern High Plains Regions, Southeast New Mexico .....	85
--	----

*by Marissa Fichera and Ethan Mamer*

Summary .....	87
I. Previous work .....	88
II. Introduction .....	89
III. Methods .....	97
IV. Regional aquifer systems .....	101
V. Summary .....	119

Acknowledgments .....	121
-----------------------	-----

References .....	121
------------------	-----

Appendix 2 - Aquifer volume calculation methods .....	3 pages
--	---------

## EXECUTIVE SUMMARY

Understanding and managing groundwater resources has become more important than ever, especially in New Mexico, which relies on groundwater more than any other state in the southwest. Accurate information on the depth to groundwater, water quality, and thickness of the state's aquifers is needed for a variety of reasons, including: improving well drilling success, informing regional water planning, and reducing oil and gas well interference with fresh water zones. Currently, this type of data is found in regional maps, or buried in databases, and extrapolating the data to determine site-specific conditions can be tedious and, oftentimes, inaccurate. The New Mexico Bureau of Geology and Mineral Resources is investigating the feasibility of using the robust suite of spatial analysis tools available in ArcGIS to create publicly available, three-dimensional maps of the major aquifers in the state to fill this data gap.

The southeastern portion of New Mexico, specifically the Pecos Slope region of the Sacramento Mountains and the lower Pecos River valley, was selected for this initial study of 3-D mapping due to its wealth of geologic data, including thousands of well logs from oil and gas exploration. The major aquifers in this region are divided up as the Pecos Valley Alluvium, the Southern High Plains Aquifer System, and the Permian Aquifer System. The water resources in this area are in high demand and under intense active management: groundwater is relied upon to support large agricultural and dairy/cattle industries, as well as a booming oil and gas industry; surface water use is strictly limited by the terms of the Pecos River Compact, further highlighting the need for this project.

This collection includes three parts. The first part, work by Colin Cikoski, provides an in-depth look at the feasibility of using ArcGIS to build a digital, three-dimensional hydrogeologic model. There are several 3D geologic modeling software packages, ultimately, however, ArcGIS was selected for this study due to its widespread use in several fields, the ability to utilize the final data with free or open source software, and the ease of importing the final data files into other modeling software. In addition to focusing on a model system that was widely available, the project was designed to create a model that would minimize modeler bias and maximize objective utilization of a wide variety of input data. The geologic surfaces were created through an iterative process of developing regional surfaces, comparing that surface to raw control points to calculate local deviance models, then incorporating the deviance model into the next iteration of the surface. Uncertainty was quantified through each of the stages of the model building and combined to create uncertainty maps. The results of Cikoski's analysis show that the modeling method is unbiased and faithfully captures complex large and medium scale geologic structures. The model is reflective of the current understanding of the geology of the area and had reduced accuracy with increased distance from control points.

The second part of the collection, by Marissa Fichera and Ethan Mamer, is the application of the completed geologic model to calculate aquifer extents and volumes. Defining freshwater aquifer boundaries is more complicated than looking at the geologic contacts alone, as hydraulic properties and water quality often vary spatially within the same formation. To constrain these variables, water-quality and water-level information from the USGS, the New Mexico Office of State Engineer, and the Texas Water Development Board were compiled into a relational database and plotted in 3-dimensions. Water quality was broken into two zones, fresh to low-salinity brackish (below 3,000 mg/L TDS) and brackish (above 3,000 mg/L TDS). Water-level surfaces were contoured from control points measured in wells between 2010 and 2019. After creating these water quality and water-level zones within the geologic model, relevant hydraulic properties were applied to estimate current extractable volumes. The result of this analysis estimate the Pecos Valley Alluvial Aquifer volume of 4–6 million acre-feet (maf), Southern High Plains Aquifer System volume of 20–50 maf, and Permian Aquifer System volume of 90–260 maf.

The third part of this collection is an ArcGIS map package containing digital hydrogeologic model data, including raster surfaces, and contours of the subsurface elevations of geologic units and relevant hydrologic surfaces. Basal surfaces of the following geologic units are included in the map package: the Pecos Valley Alluvium, the Ogallala Formation, Lower Cretaceous strata, upper and lower Dockum Groups, upper and lower Ochoan strata, the Artesia Group, the San Andres Formation, and the Yeso Formation. Aquifer extents, water-table elevation and saturated thickness contour maps, and estimated basal aquifer extents are also included.

While great care was taken to create an accurate and user friendly set of maps and model layers, this data should still be used with caution. The Pecos Slope model has a horizontal resolution of no more than 1 km and is intended primarily for visualization and communication, and for regional or preliminary studies. Users of this model should be aware of the levels of uncertainty in each surface and conduct site-specific studies, especially in structurally complex areas, as needed.

—By *Laila Sturgis*



Lea Lake is located in Bottomless State Park about 15 miles southeast of Roswell in the Roswell Artesian Basin.  
*Photograph by Peter A. Scholle.*

# PECOS SLOPE DIGITAL FRAMEWORK GEOLOGIC MODEL: OVERVIEW OF METHODS

*Colin Cikoski*

<b>Summary</b> .....	3	<b>Figures</b>	
<b>I. Introduction</b> .....	5	1. General location of the study area in southeastern New Mexico .....	6
Terminology .....	6	2. Select structural features of the study area .....	9
<b>II. Background</b> .....	9	3. Distribution of data collected, geologic map and geologic unit description .....	11–13
Study area.....	9	4. Stratigraphy of the study area .....	14
Geology.....	10	5. Conceptual stratigraphic diagram of the model units .....	15
<b>III. Input Data</b> .....	19	6. Diagram depicting the core relationships of the Pecos Slope model database .....	24
Sources of data.....	19	7. Example of linear data to point data conversion .....	27
Database structure.....	23	8. Example of the conversion of cross-section data to synthetic well data .....	30
<b>IV. Methods</b> .....	25	9. Example correlation of units diagram .....	32
Modeling methods background research.....	25	10. Illustration of the leave-one-out cross-validation method used for data quality assessment .....	34
General.....	26	11. Example of leave-one-out cross-validation identification of an influential control point .....	34
Data synchronization.....	27	12. Example of the unequal distribution of control data for adjacent model units .....	37
Quality control and compatibility assessment.....	31	13. Example uses of offset control estimates .....	38
Offset control estimates.....	36	14. Example of the initial contact surface generation method .....	40
Contact surface generation.....	39	15. Example of the build-down method of creating the final model .....	43
Combining the contact surfaces–3D.....	42	16. Validation point residuals versus the standard deviations between contact surface realizations .....	47
Model creation.....	42		
Uncertainty assessment.....	45	<b>Tables</b>	
<b>V. Results</b> .....	79	1. Definitions of terms .....	7
Discussion of methods.....	79	2. General description of model units .....	20–21
Summary.....	80	3. Summary of processing steps .....	28–29
Intended uses and limitations .....	80		
<b>Acknowledgments</b> .....	80		
<b>References</b> .....	81		

## Plates

1. Unit thickness model for the Abo Formation .....	49	16. Basal contact regional trend for Upper Cretaceous .....	64
2. Unit thickness model for the Yeso Formation .....	50	17. Basal contact regional trend for Sierra Blanca .....	65
3. Unit thickness model for the San Andres Formation .....	51	18. Geologic framework for Yeso Formation base .....	66
4. Unit thickness model for the Artesia Formation .....	52	19. Geologic framework for San Andres Formation base .....	67
5. Unit thickness model for the Lower Ochoan Formation .....	53	20. Geologic framework for Artesia Formation base .....	68
6. Unit thickness model for the Upper Ochoan Formation .....	54	21. Geologic framework for Lower Ochoan Formation base .....	69
7. Unit thickness model for the Lower Dockum Formation .....	55	22. Geologic framework for Upper Ochoan Formation base .....	70
8. Unit thickness model for the Upper Cretaceous .....	56	23. Geologic framework for Lower Dockum Formation base .....	71
9. Basal contact regional trend for Yeso Formation .....	57	24. Geologic framework for Upper Dockum base .....	72
10. Basal contact regional trend for San Andres Formation .....	58	25. Geologic framework for Lower Cretaceous .....	73
11. Basal contact regional trend for Artesia Formation .....	59	26. Geologic framework for Upper Cretaceous .....	74
12. Basal contact regional trend for Lower Ochoan Formation .....	60	27. Geologic framework for Sierra Blanca .....	75
13. Basal contact regional trend for Upper Ochoan Formation .....	61	28. Geologic framework for Ogallala-PVAunit .....	76
14. Basal contact regional trend for Lower Dockum Formation .....	62	29. Geologic framework for Alluvium unit base formation base .....	77
15. Basal contact regional trend for Upper Dockum Formation .....	63		
		<b>Appendix I</b>	
		Model assessment.....	7 pages

## SUMMARY

Three-dimensional, digital, geographic information system (GIS)-ready, subsurface geologic models are becoming increasingly common tools for visualizing, evaluating, and managing the subsurface and subsurface resources. This project developed such a model for a portion of southeastern New Mexico using methods designed to combine a variety of input data sources and formats, maximize objective utilization of data, minimize modeler subjective choice, and explicitly evaluate and quantify the uncertainty in the modeling process and results.

The study area extended from the crest of the Sacramento Mountains eastward across the lower Pecos River valley to the New Mexico-Texas stateline, including portions of the Southern High Plains and covering the cities of Roswell, Artesia, Hobbs, Lovington, and Ruidoso. Geologically, this area includes portions of the shallow-dipping, east-facing, homoclinal Pecos Slope; the Laramide Sierra Blanca Basin and mid-Cenozoic Sierra Blanca volcanic field; the southwesternmost Ogallala aquifer; the northernmost margin of the Delaware Basin (a structural feature of the greater Permian Basin oil and gas region); and numerous smaller-scale uplifts, basins, folds, and faults. The modeled strata are dominantly Permian in age (Wolfcampian through Ochoan), with lesser extents of Triassic, Cretaceous, Tertiary, and Quaternary rocks and deposits occurring beneath the Pecos River valley and Southern High Plains as well as within the Sierra Blanca Basin.

Input data was collected from surface geologic mapping; well data compilations and individual well logs and records; cross-section and structure contour interpretations; and existing published georeferenced rasters of geologic contact elevations. To the extent possible, these input data were collected “as found” into a relational geodatabase that facilitated preserving original geologic unit designations (despite the wide variety of unit designations in use in the area), data formats (e.g., points versus lines versus cross-section data), data sources, and data quality evaluations. Input data was subsequently simplified to datasets of control points that followed a synchronized model stratigraphy. The control point data quality and the compatibility between different

data sources was subsequently evaluated using leave-one-out cross-validation of geostatistical models (krige models) to identify influential or outlier control points, which were subsequently scrutinized for accuracy and corrected or removed as needed. Control point datasets for individual contact surfaces were supplemented with offset control estimates, which are estimated control point locations calculated by adding or subtracting a (apparent) thickness of strata to/from the elevation of a control point for an adjacent contact. Apparent thickness models were developed using ordinary kriging, and these models were also used in part to estimate the preserved extents of units in the subsurface. Offset control estimates were allowed to lie above the land surface, to lie along the bases of laterally equivalent units (due to facies changes), or to lie along the bases of truncating unconformities, in order to provide point locations to project a contact surface to where the contact has been eroded or transitions to another unit’s contact (in the case of a facies change). Offset control estimate quality and compatibility was assessed using the same leave-one-out cross-validation of geostatistical models as was applied to the original control point dataset.

The final geologic model consists of a suite of model unit basal contact surfaces in GIS-ready raster formats. Each contact surface was interpolated from a dataset of control points and offset control estimates, using known mapped faults as barriers in the interpolation process to accommodate discrete offsets across these faults. The interpolation process involved three stages: 1) development of a regional trend surface that is offset by a selection of applicable faults; 2) kriging of the residuals of the control points and offset control estimates from the regional trend surface to develop a geostatistical ‘local deviance’ model; and 3) combination of the regional trend and local deviance models to derive an initial contact surface. As offset control estimates were allowed to lie above the land surface or continue into truncating unconformities and across facies changes, these initial contact surfaces similarly project above the land surface and into unconformities. The final contact surfaces were generated by iteratively comparing initial contact surfaces to one another to enforce truncating relationships.



Uncertainty was quantified at several stages in the model generation process as the ‘standard predication error’ associated with the various geostatistical models used. In addition, a dataset uncertainty model was developed using n-fold cross-validation. The dataset uncertainty, regional trend surface uncertainty, and local deviance model uncertainty were combined to calculate a map of total estimated contact uncertainty, and each contact surface is presented alongside its uncertainty map. In general, the uncertainty maps conform to the expectation that uncertainty increases with distance from control points and with increasing structural complexity of an area.

Results were compared to previous studies that published structure contours for some of the units modeled herein. In summary, the comparisons suggest:

- 1) This geologic model is generally comparable to works produced by previous authors and reflective of the current understanding of the geology of the area at a large scale;
- 2) The methods used herein do not bias the final results, as separate interpolation strategies used by prior studies on similar datasets determined similar contact surfaces; and
- 3) The geologic model successfully captures complex large- and medium-scale structures (structures with widths greater than ~5 km) given adequate data coverage, but that small-scale structures, and in particular dense collections of small-scale structures, are difficult to capture.

These conclusions suggest that the model is an adequate regional model for the area studied, and may be useful as a framework for regional studies or a starting point for site-specific, more detailed studies. The model should not be used on its own for such site-specific studies, and users should, in particular, recognize the limitations of the model in terms of its spatial resolution and capacity to capture complex, small-scale structures.



# I. INTRODUCTION

Three-dimensional (3D), digital, geographic information system (GIS)-ready, subsurface geologic models are becoming increasingly common tools for visualizing, evaluating, and managing the subsurface and subsurface resources (e.g., Berg et al., 2011; GeoMol Team, 2015). Berg et al. (2011) compiled the current uses, challenges, and strategies of 3D geologic modeling being used by geological survey organizations (GSOs) worldwide. Their compilation demonstrates an increasing interest in, use of, and development of 3D modeling techniques at GSOs in response to an increasing need for detailed, quantitative subsurface information. Overlapping interests in subsurface resources, particularly in areas of dense development, increasingly require accurate subsurface information to properly manage contrasting interests (GeoMol Team, 2015). Past implementation of 3D modeling at GSOs has largely been on-demand and project-driven, with specific focused goals dictated by clients. However, many GSOs are working toward, or maintain a goal to work toward, regional framework models that can serve multiple needs.

Given the interest in and utility of 3D models for geologic research and resources management, the NMBGMR Aquifer Mapping Program (AMP) is engaged in a long-term project to develop 3D subsurface framework geologic models of the major aquifers in the state of New Mexico.

Framework models provide a regional picture of the subsurface by mapping geologic contacts as digital surfaces across a study area. Large-scale trends and structural features are captured in the surfaces, which can then be visualized using 3D visualization software or as “2.5D” maps (e.g., structure contour maps or hillshade maps; maps that themselves are two-dimensional but display the variation in elevation across the map area), or used in regional spatial data processing. While these regional framework models should not be used in lieu of detailed, location-specific subsurface studies for planning, infrastructure development, environmental decision making, etc., they do provide a framework that can serve as a starting point for more detailed studies. Several GSOs worldwide have generated and utilize framework models, by one name or another, in their geologic research and management

duties (e.g., Mathers et al., 2014; Branscombe et al., 2018; van der Meulen et al., 2013).

Despite a growing body of methods and previous studies in the field of 3D geologic modeling, subsurface geologic model development continues to be a challenging endeavor. The state of New Mexico, in particular, presents a difficult area to model, as the variety of physiographic and geologic terrains present in the state, as well as the varying qualities and densities of available subsurface data, nearly ensures that no single methodology can be applied to all parts of the state. In addition, structural complexity varies across the state, and methods may need adjustment or revision to fit the complexity of an area. Finally, many geologic units are of only limited extent through the state, such that model stratigraphy itself will need to be modified for different regions of the state. Given these challenges, model development is progressing region-by-region, and modeling methods are expected to similarly evolve region-by-region.

The goal of this project was to generate a 3D, digital, GIS-ready, subsurface geologic model using methods designed to incorporate a variety of input data, maximize objective utilization of data, minimize modeler subjective choice, and explicitly evaluate and quantify the confidence in the modeling process and results. Ideally, the methods used would facilitate incorporating new data as it becomes available as well as repeatability in model generation. Maximizing objective data utilization and minimizing subjective choice simultaneously facilitates scripting and automation and should ensure that different modelers would generate similar results. The disadvantage to this approach is the loss of small-scale, expert-knowledge-driven or experience-derived adjustments to model contact surfaces. However, as the methods are designed to facilitate incorporating new data as it becomes available, expert knowledge can be added to the model in subsequent revisions by generating interpretive products such as cross-sections or structure contours that are later incorporated into the modeling process.

This report presents the methods and results of subsurface geologic modeling efforts in the Pecos Slope to Southern High Plains region of southeastern

New Mexico (Figure 1). This region provides an excellent “pilot study” location because 1) a variety of prior studies provide input datasets covering the entirety of the region as well as prior subsurface interpretations against which to test the results; 2) oil and gas interests in the area provide a relative abundance of “hard” geologic data for model development; 3) structural and stratigraphic complexity is generally low to moderate through the area, providing a good initial study area for developing and testing methods; and 4) water resource concerns in the region provide a strong impetus and need for a subsurface model. One goal of this “pilot study” was to develop generic methods that could be applied to the variety of geologic settings found in New Mexico, and hence the input data, quality control methods, interpolation schemes, and results are presented with additional discussion of their strengths and weaknesses for later reference in developing models of other regions of New Mexico. Additional

discussion of prior studies’ methods by other agencies are also presented for comparison.

## Terminology

This project utilizes a variety of terms that are either not in common usage or are used in a particular way herein. These terms are summarized in Table 1. A few particularly significant terms are expanded upon here.

In this report, “geologic units” are separate from “model units,” in that geologic units are the original stratigraphic units for which data was collected, while model units are aggregates of geologic units for which enough data was found to construct a basal contact surface across the study area. This distinction was

kept in order to facilitate preserving as much of the acquired data in its original “as found” state in the Pecos Slope model database. Geologic unit data was subsequently aggregated to model unit data during data processing.

“Rasters” are grids of pixels or cells that each contain a single numeric value (here, most commonly an elevation) or a “null value” indicating no

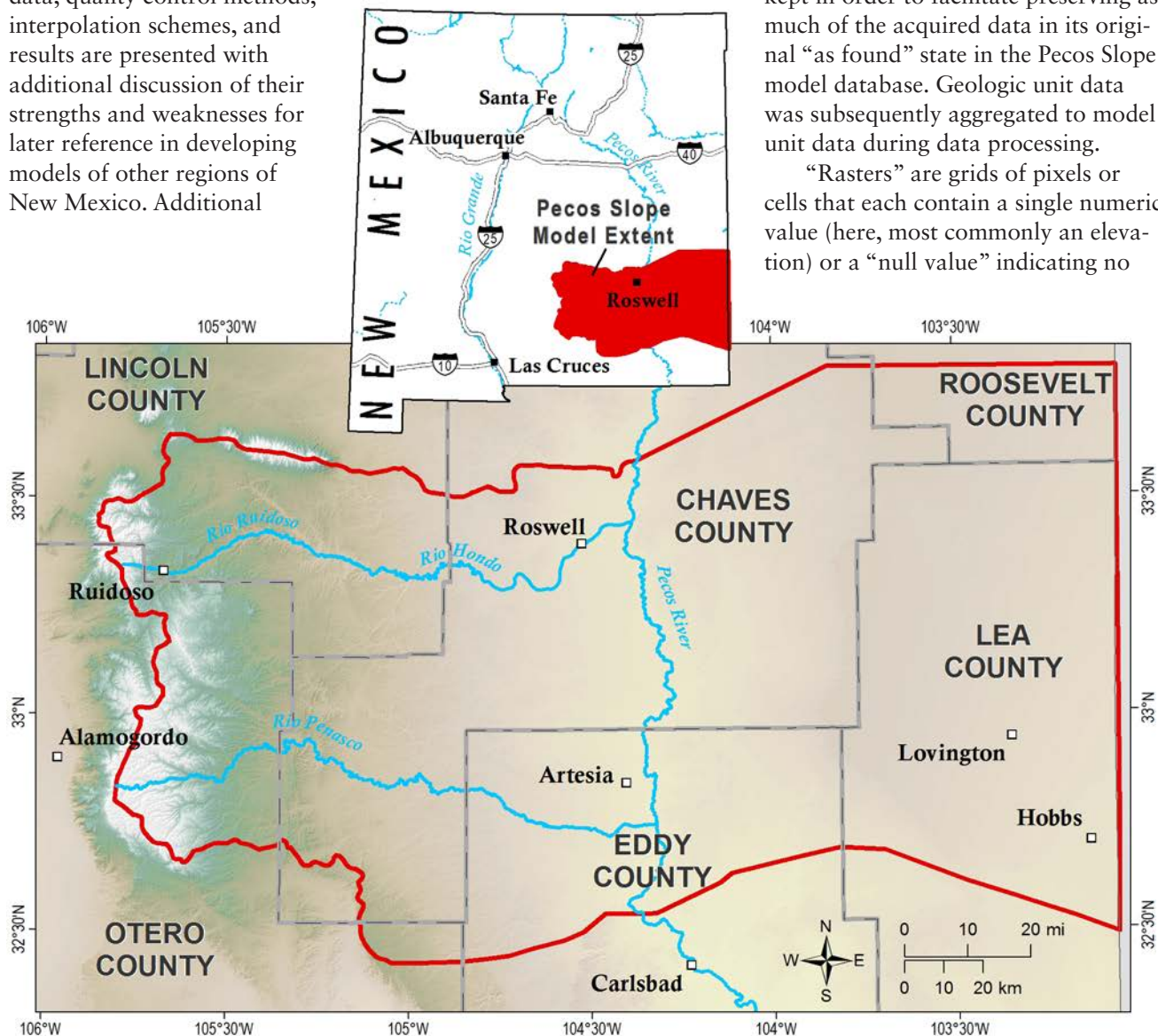


Figure 1. General location of the study area in southeastern New Mexico.

**Table 1.** Definitions of terms.

Term	Definition as used in this report
Geologic unit	A defined body of rock or sediment material, most commonly associated with a formal definition (e.g., Yesso Formation), although in places it is an informal unit (e.g., Alluvium).
Model unit	An aggregate of geologic units, combined so as to provide a unit with sufficient data across the study area for a 3D body to be modeled.
Geologic or model unit contact	A 2.5D surface that estimates the elevation of the contact between two distinct model units at every point in the model domain where the two units are present. Contacts are interpolated between control points.
Sealed geologic model	A geologic model with no topological errors such as crossing contacts or contacts that terminate within a model unit (Caumon et al., 2004).
Discrete (contact) surface	A contact surface that is only defined where the contact is present in the subsurface, and only defined where the model units to either side of the contact are present and preserved. These surfaces therefore have gaps where the model units are eroded, and may not extend across the entire model domain.
Continuous (contact) surface	A contact surface that is defined at every location in the model domain even where the units to either side of the contact are not present. Where the units are present, the continuous contact surface lies along the contact between the two; where the units have been eroded, however, the continuous contact surface continues along the surface of erosion.
Control data	Any dataset that provides information on the elevation of a geologic contact at a point in space.
Hard data	Control data where the elevation of a contact can or has been observed, such as a formation pick in a well record or a surface exposure of a geologic contact.
Soft data	Interpreted or projected data, such as geologist-drawn cross-sections or structure contour lines.
Control point	A point in 3D space where the elevation of a contact is known or estimated. It may come from hard or soft data.
Influential control point	A control point is influential if it has a particularly strong impact on the interpolation methods used, typically as determined through cross-validation of a geostatistical model. A point may be 'influential' because, as examples, it is erroneous and distorting the interpolated surface; because it lies near a structural deformation; or because it lies along the margin of the study area where little other data is found to control the surface. Influential points are not necessarily in error.
Offset control estimate	A point in 3D space where the elevation of a contact is estimated based on the elevation of an adjacent contact control point. The control point is offset by the (apparent) thickness of the intervening model unit, which is interpolated between control points where the (apparent) thickness is constrained. These are "soft" data as they are interpretations of the dataset.
Trend surface	A regional 2.5D surface that estimates large-scale trends in the geometry of a contact surface. A trend surface may be a constant average value (i.e., a horizontal plane), a curvilinear surface, or include steps along faults. Trend surfaces do not necessarily pass directly through control points.
Snap raster	A raster used to define the locations and sizes of raster cells/pixels during data processing. Used to ensure that all rasters generated during processing have the same resolution and have colocated cells.

applicable numeric value exists at that location (e.g., for a contact surface, a null value may be assigned to cells where the contact has been eroded and is not physically present). A "snap raster" is a template raster that locates pixel/cell centers and is used to ensure that all rasters generated during data processing have colocated pixels of the same dimensions. "Surfaces" are rasters displaying the topography of a contact or the land surface. Two types of model unit contact surfaces were generated for this model. With "continuous contact surfaces," every pixel location across the study area has a defined, numeric value (no null values), even where the contact is not present due to erosion. Where the contact is not present, the values of the raster cells in the continuous contact surface are identical to those of the surface that truncates the contact (e.g., the land surface or an

unconformity). Because the values of the continuous contact surface are equal to those of the overlying, truncating continuous contact surface, the thickness of the unit is readily calculated as zero, and the preserved extent of the unit is readily determined as the extent over which the calculated thickness is greater than zero. The "discrete contact surface" of the same model unit contact is the same as the continuous contact surface, but clipped to the preserved extent of the model unit. Where the thickness of the model unit is zero, the discrete contact surface pixels are assigned null values. Discrete contact surfaces are only defined where the model unit is preserved. In contrast to the contact surfaces, which are exact interpolations that pass directly through control points, a "trend surface" is an inexact interpolation that averages the variability between control points. These trend

surfaces may be a flat constant value, a flat dipping plane, or a curvilinear surface. Both contact and trend surfaces may accommodate sharp jumps (breaks) such as would be present along a fault.

“Control data” is any form of data that provides information on the elevation of a model unit contact surface. “Hard data” is control data derived from direct observations, while “soft data” is derived from interpretations and projections. Examples of hard data include surface-mapped geologic contacts, contacts located in well cuttings or core, or a contact located on a geophysical log. Examples of soft data include structure contours and cross-sections derived from projecting surface features into the subsurface. “Control points” are control data distilled down to single points that define the location of a contact in 3D space as Easting-Northing-Elevation locations. Contact surfaces are interpolated between control points, and an “influential control point” is one that has a particularly strong effect on the interpolation. This is determined through leave-one-out cross-validation, as described in the Methods section. Influential control points may have a strong effect due to an error (e.g., a mislocated well), imprecise data, low data density, or because the point accurately defines a rapid change in elevation of

the contact, possibly due to a structure. Because these points have a strong effect on the interpolated contact surface, they were given extra scrutiny to ensure their accuracy, and were removed from the control point dataset if they could not be verified. “Offset control estimates” are estimated control points generated by offsetting a control point from an adjacent model unit contact surface by adding or subtracting the expected (apparent) thickness between the surfaces. The expected thickness was determined using geostatistical models that predict thickness trends across the study area between control points. Offset control estimates are a form of soft data in that they are interpretations of the available data. Offset control estimates were also assessed for their degree of influence on the interpolation process, and scrutinized if they were found to have a strong effect on the interpolation.

As used here, a “geologic model” is a suite of model unit contact surfaces that partition the model space into model units. Finally, a “sealed geologic model” is one where the geologic model has no topological errors, such as intersecting contact surfaces or a contact surface that ends abruptly within a model unit (Caumon et al., 2004).



## II. BACKGROUND

### Study Area

The study area extends from the crest of the Sacramento Mountains eastward along the Pecos Slope and across the lower Pecos River valley to the Southern High Plains and the New Mexico-Texas state border (Figures 1 and 2). This area includes the cities of Roswell, Artesia, Lovington, and Hobbs, as well as smaller communities such as Ruidoso and Hope. The lower Pecos River nearly bisects the study area into eastern and western halves. Portions of the counties of Lincoln, Otero, Chaves, Eddy, Lea, and Roosevelt lie within the study area boundaries.

Elevations are as great as about 11,981 ft amsl at the top of Sierra Blanca Peak in the Sacramento Mountains, and generally decrease eastward along the Pecos Slope to lows around the Pecos River. The Southern High Plains lie along the eastern margin of the study area. The area is generally sparsely populated, with oil and gas and agricultural interests dominating the local economy.

The nature, density, and quality of control data varies substantially through this study area (Figure 3). A significant subsurface dataset is available for the eastern half of the study area, where nearly a century of oil and gas exploration provides substantial well

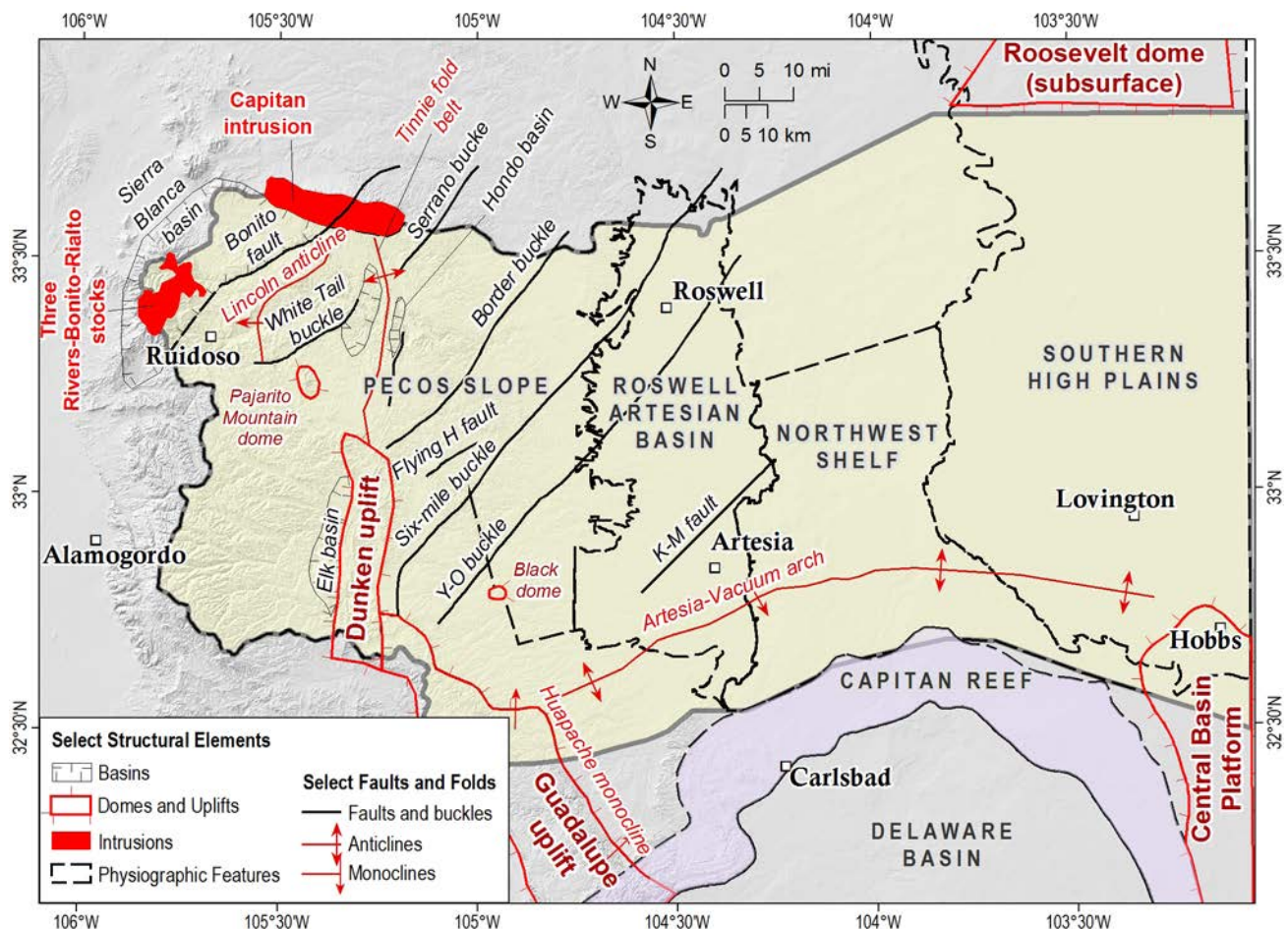


**Figure 2.** Select structural features of the study area. Adapted from Kelley (1971), NMBGMR (2003), Standen et al. (2009), and Broadhead et al. (2009). Physiographic features are all approximately located.

control. In contrast, the west half of the study area, which lacks significant deep subsurface economic resources, is nearly devoid of well control. Instead, here most subsurface research has been associated with hydrogeologic research (e.g., Newton et al., 2012), and subsurface data is largely from surface mapping and interpretative products such as cross-sections and structure contours. Sediment aquifers, such as along the lower Pecos River in the Roswell Artesian Basin and the Ogallala aquifer, have been studied by the U.S. Geological Survey (USGS) for decades (cf., Cronin, 1969; Lyford, 1973), and aquifer units extending into Texas have been studied by the Texas Water Development Board (TWDB) as a part of their groundwater availability modeling program (e.g., Meyer et al., 2012; Deeds et al., 2015). Overall, the study area is relatively well covered by existing subsurface datasets.

## Geology

The geology of the area is treated only briefly here. More detail is available from Kelley (1971), who provides a detailed review of the stratigraphy and structure of the Pecos Slope region from the Sacramento Mountains to the Pecos River valley; from Deeds et al. (2015) and references therein for discussion of the geology of the High Plains region; and in papers collected by Ruppel (2009) for review of the subsurface geology pertinent to oil and gas interests in the greater Permian Basin region.

### Stratigraphy and generalized geologic history

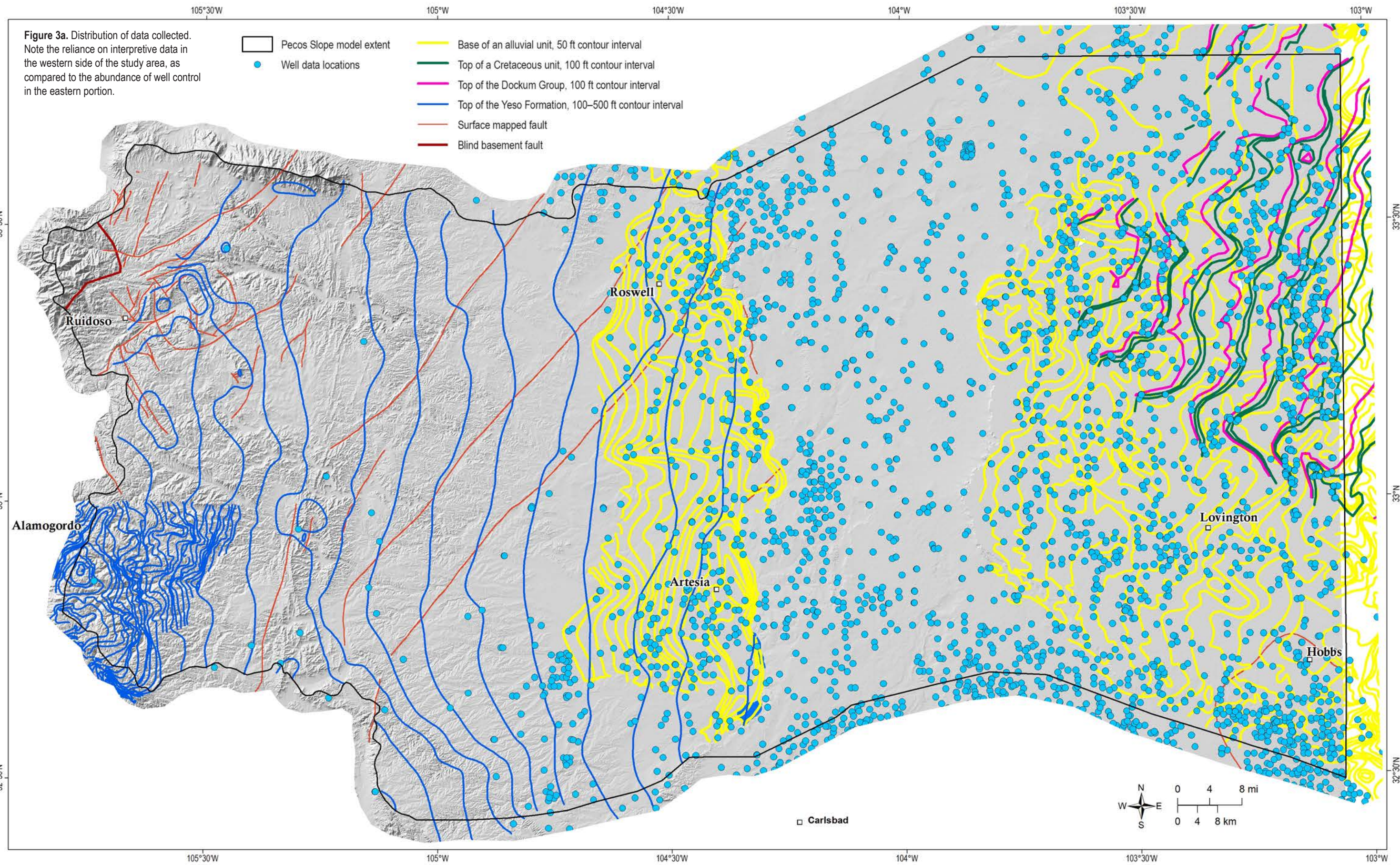
A variety of stratigraphic nomenclature is in use through this study area (Figure 4). This diversity has several origins. For one, throughout most of Permian time the environment consisted of a broad, shallow-gradient continental shelf/tidal flat/floodplain environment (Northwest Shelf) that graded southeastward to a continental shelf break along the margin of the Delaware Basin (circa the Capitan Reef trend on Figure 2), then descended rapidly into the often-marine Delaware Basin. Each of these environments (shelf, basin-margin, and basin) accumulated a distinctly different package of sedimentary rocks that earned distinctly different names (e.g., the Leonardian and Guadalupian intervals in Figure 4). In addition, workers from different backgrounds extended their understanding of the stratigraphy into the subsurface in this area, resulting in contrasting names such as Clear Fork

and Yeso or Dewey Lake and Quartermaster for strata that are commonly interpreted to be largely, if not entirely, equivalent. Additional complexity stems from regional and local stratigraphers providing contrasting nomenclatures, as is seen for the Triassic section (summarized by Lehman, 1994, and depicted in Figure 4). Finally, geologic complexity masks the precise relationship between the youngest sediments, particularly the Gatuña and Ogallala Formations (cf., Hawley, 1993). The correlations between these units are generally understood, however, such that units can be readily combined during processing to simplify the stratigraphy (e.g., Table 2, Figure 5). Note, however, that during data collection every attempt was made to preserve the original name assigned to a geologic unit, regardless of the final nomenclature used for the model. Although this approach complicated data compilation, an advantage to this approach was the preservation of the original details of the data collected, which proved useful in later data assessment. Certain input geologic units were later recognized as being associated with more uncertain control points, and these units were subsequently given greater scrutiny during the data quality and compatibility assessment.

Rocks from the Precambrian, Permian, Triassic, Cretaceous, Tertiary, and Quaternary time periods are found at or near the surface within the study area (Figure 3). In the subsurface, strata of Cambrian through Pennsylvanian age are found as well (cf., Meyer, 1966, and papers collected by Ruppel, 2009). However, this report concerns only strata of Wolfcampian (Lower Permian) through Quaternary age (Figures 4 and 5). This interval consists nearly entirely of sedimentary rocks, with some intrusive and extrusive igneous rocks present in the Sierra Blanca volcanic field in the northwest corner of the study area. Broadly, the depositional settings and strata can be grouped as Permian Delaware Basin margin strata; Permo-Triassic continental strata; Cretaceous marine and marginal marine strata; and Cenozoic continental strata.

**Permian Delaware Basin margin strata**—During the Lower to Middle Permian, the Ouachita–Marathon orogeny, driven by collision along a subduction zone located present-day-south of the study area, and the Ancestral Rocky Mountains orogeny caused Delaware Basin subsidence and uplift of the ancient Pedernal mountains, the axis of which roughly co-locates with the present-day crest of the Sacramento Mountains (Kelley, 1971). The resultant paleotopography was a highland along the western margin of the study area that descended gently eastward







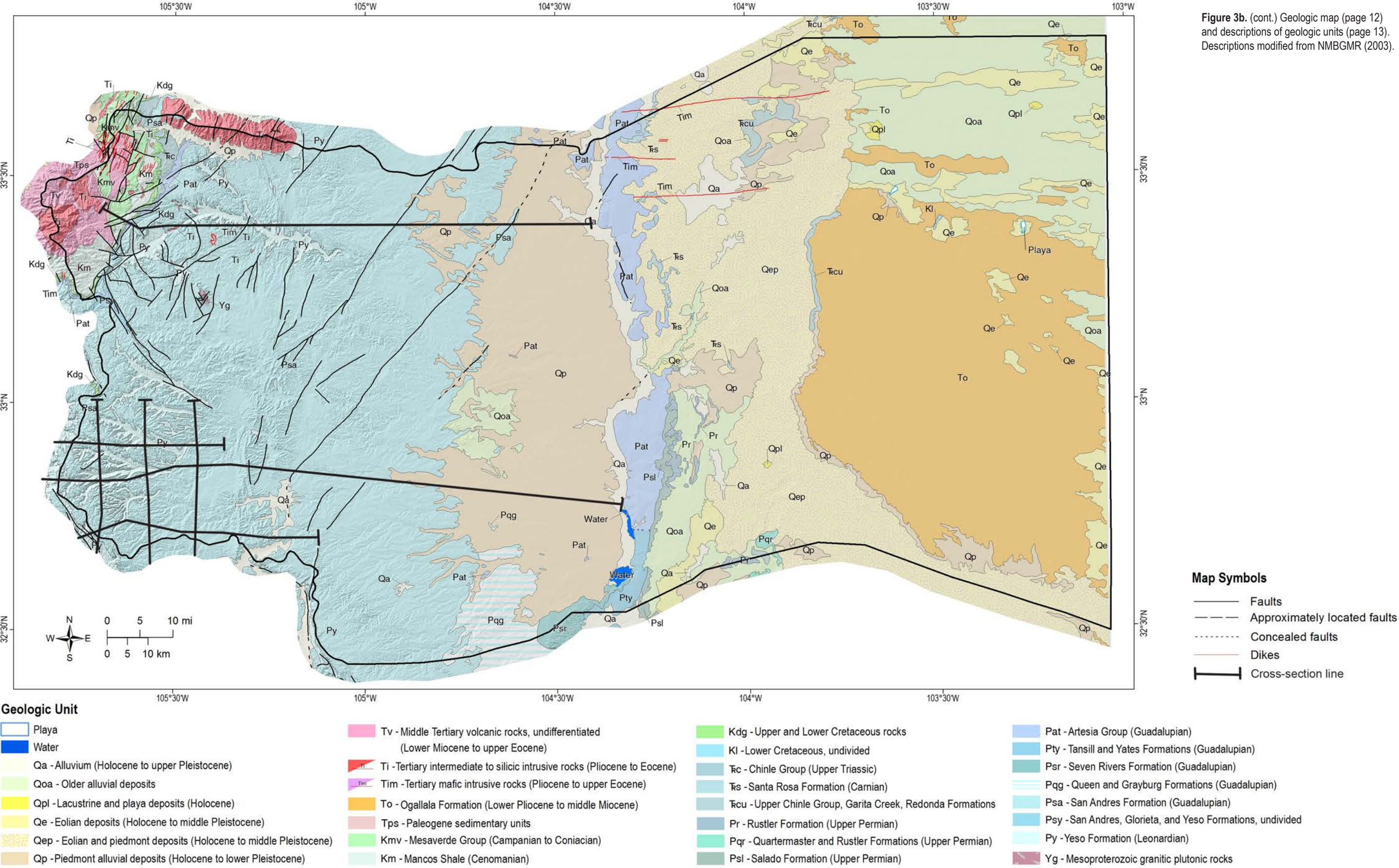


Figure 3b. (cont.) Geologic map (page 12) and descriptions of geologic units (page 13). Descriptions modified from NMBGMR (2003).



## Cenozoic

Water-Perennial standing

Playa- Alluvium and evaporite deposits (Holocene)

Qa- Alluvium (Holocene to upper

Qep- Eolian and piedmont deposits (Holocene to middle Pleistocene) - Interlayered eolian sands and piedmont-slope deposits

Qp- Piedmont alluvial deposits (Holocene to lower Pleistocene)

Qe- Eolian deposits (Holocene to middle Pleistocene)

Qeg- Gypsiferous eolian deposits (Holocene to middle Pleistocene)

Qpl- Lacustrine and playa deposits (Holocene) - Includes associated alluvial and eolian deposits of major lake basins

Qoa- Older alluvial deposits of upland plains and piedmont areas, and calcic soils and eolian cover sediments of High Plains region (middle to lower Pleistocene)

Qb- Basaltic to andesitic lava flows (Holocene to middle Pleistocene)

QTS- Upper Santa Fe Group (middle Pleistocene to uppermost Miocene)

To- Ogallala Formation (lower Pliocene to middle Miocene) - Alluvial and eolian deposits, and petrocalcic soils of the southern High Plains. Locally includes Qoa

Tps- Paleogene sedimentary units - Includes Baca, Galisteo, El Rito, Blanco Basin, Hart Mine, Love Ranch, Lobo, Sanders Canyon, Skunk Ranch, Timberlake, and Cub Mountain Formations

Ti- Tertiary intrusive rocks of intermediate to silicic composition (Pliocene to Eocene)

Tv- Sierra Blanca volcanics- Middle Tertiary volcanic rocks, undifferentiated (lower Miocene to upper Eocene)

## Cretaceous

K- Cretaceous rocks,

Kmv- Mesaverde Group (Campanian to Turonian) - Includes Cliff House Sandstone, Menefee Formation and Point Lookout Sandstone.

Kmd- Intertongued Mancos Shale and Dakota Sandstone of west-central New Mexico (Cenomanian)

Km- Mancos Shale (Cenomanian to Campanian) - Divided into upper and lower parts by Gallup Sandstone

Kdg- Dakota Group - Upper and Lower Cretaceous rocks of east-central and northeast New Mexico

Kl- Lower Cretaceous rocks,

## Triassic

Tc- Chinle Group (Upper Triassic) - Map unit includes Moenkopi Formation (Middle Triassic) at base in many areas

Tcu- Upper Chinle Group, Garita Creek through Redonda Formations, undivided (Upper Triassic)

Ts- Santa Rosa Formation (Carnian) - Includes Moenkopi Formation (Middle Triassic) at base in most areas

Tm- Moenkopi Formation (Middle

## Permian

PP- Permian and Pennsylvanian rocks, undivided - Includes Concha, Scherrer, Colina, Epitaph, and Earp Formations (Permian) and Horquilla Limestone (Permian to Pennsylvanian)

Pqr- Upper Ochoan- Quartermaster and Rustler Formations (Upper Permian)

Pqm- Dewey Lake and Quartermaster Formations (Upper Permian) - Red sandstone and siltstone

Pr- Rustler Formation (Upper Permian) - Siltstone, gypsum, sandstone, and dolomite

PsL- Salado Formation (Upper Permian) - Evaporite sequence, dominantly halite

Pc- Castile Formation (Upper Permian) - Dominantly anhydrite sequence

Pat- Artesia Group (Guadalupean) - Shelf facies forming broad south-southeast trending outcrop from Glorieta to Artesia area; includes Tansill, Yates, Seven Rivers, Queen and Grayburg Formations (Guadalupean)

Pty- Tansill and Yates Formations- Sandstone, siltstone, limestone, dolomite, and anhydrite

Psr- Seven Rivers Formation (Guadalupean) - Gypsum, anhydrite, salt, dolomite, and siltstone

Pgg- Queen and Grayburg Formations (Guadalupean) - Sandstone, gypsum, anhydrite, dolomite, and red mudstone

Pcp- Capitan Formation (Guadalupean) - Limestone (reef facies)

Psy- Lower Permian- San Andres, Glorieta, and Yeso Formations, undivided

Psg- San Andres Limestone and Glorieta Sandstone (Guadalupean and Leonardian)

Psa- San Andres Formation (Guadalupean in south, in part Leonardian to north) - Limestone and dolomite with minor shale

Pg- Glorieta Sandstone (Leonardian) - Texturally and mineralogically mature, high-silica quartz sandstone

Pbc- Bell Canyon Formation (Guadalupean) - Basin facies - sandstone, limestone, and shale

Pcc- Cherry Canyon Formation (Guadalupean) - Basin facies - sandstone, limestone, and shale

Pco- Cutoff Shale (Leonardian) - In Brokeoff Mountains only

Py- Yeso Formation (Leonardian) - Sandstones, siltstones, anhydrite, gypsum, halite, and dolomite

Pvp- Victorio Peak Limestone (Leonardian) - In Brokeoff Mountains only

Pa- Abo Formation (Wolfcampian) - Red beds, arkosic at base, finer and more mature above

Pau- Upper part of Abo Formation (Wolfcampian)

Pal- Lower part of Abo Formation (locally Virgilian to Upper Pennsylvanian)

Ph- Hueco Formation or Group (Wolfcampian) - Limestone

Pb- Bursum Formation (lowermost Permian to uppermost Pennsylvanian) - Shale, arkose, and limestone

## PrePermian

IP- Pennsylvanian rocks undivided

IPs- Panther Seep Formation (Virgilian) - In Organ, Franklin, and San Andres Mountains

MD- Mississippian and Devonian rocks, undivided

OC- Ordovician and Cambrian rocks, undivided - Includes Montoya Formation (or Group), El Paso Formation, and Bliss Sandstone

SO- Silurian through Cambrian rocks, undivided

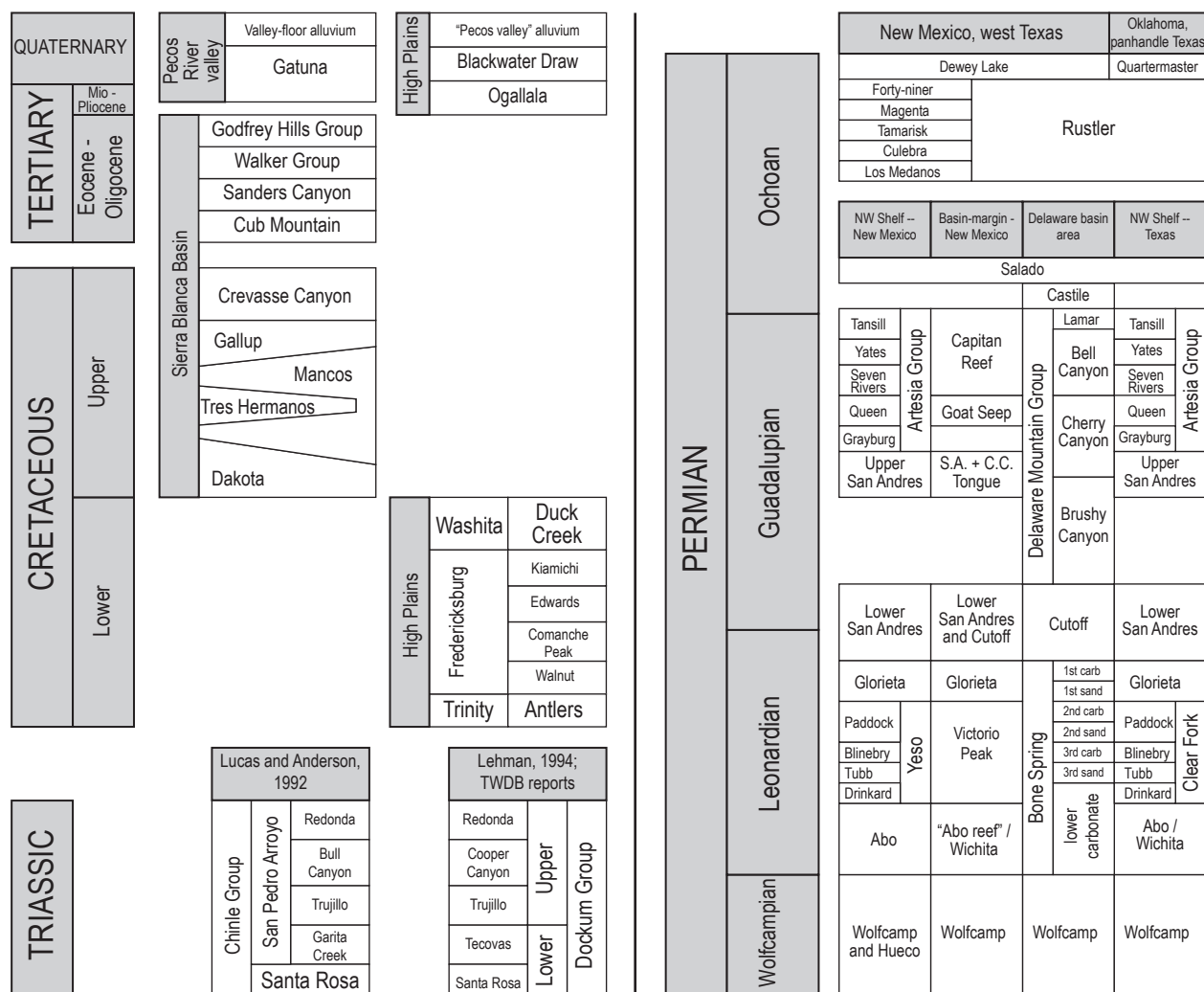
Yg- Precambrian- Mesoproterozoic granitic plutonic rocks - Mainly 1.45-1.35 Ga megacrystic granites, generally weakly foliated except locally at their margins

Ys- Precambrian- Mesoproterozoic sedimentary rocks - Exposed in Sacramento Mountains, present in subsurface in southeastern New Mexico as De Baca Group

and southward to a horseshoe-shaped marine basin margin at the southeast corner of the study area (cf., paleogeographic maps in Kues and Giles, 2004; Figure 2). The broad gentle slope is often referred to as the Northwest Shelf. The geometry and location of the margin as well as the sharpness of the transition from continental margin to marine basin changed through time. In Guadalupian time, the transition was sharp and marked by the Capitan Reef complex, while in earlier time periods the transition was broader and more gradational. Depositional settings varied with sea levels; during lowstands, continental fluvial to tidal flat settings were found along the Northwest Shelf (e.g., Abo and Yeso Formations), while during highstands shallow marine or marginal marine conditions prevailed (e.g., San Andres Formation, Artesia Group). Paleoclimates were hot and arid, and as a consequence variable abundances

of evaporites, as trace constituents up to thick beds, are present in many Lower to Middle Permian units. In Upper Permian time, as basin subsidence slowed and sea levels retreated, evaporite deposition came to dominate, and salts subsequently filled the Delaware Basin and then blanketed the Northwest Shelf (Castile and Salado formations).

Stepping through the Permian section sequentially, during Wolfcampian time, shallow marine conditions dominated the Northwest Shelf, in which the Hueco Limestone accumulated. Closer to, and within, the Pedernal Uplift, subaerial exposure resulted in non-deposition or net erosion, and no Wolfcampian strata are preserved. Closer to, and within, the Delaware Basin, deeper marine conditions accumulated shaly limestones and shales (often referred to as simply “Wolfcamp,” e.g., Figures 4 and 5). In later Wolfcampian and early Leonardian



time, marine regression resulted in largely continental settings through the Northwest Shelf, with early fluvial settings in which the Abo Formation deposited and later a variety of depositional environments, including some shallow marine conditions, in which the Yeso Formation accumulated. Each of these graded into marginal marine and marine carbonates and shaly carbonates along the margin of and within the Delaware Basin (“Abo reef” and Wichita formations associated with the Abo Formation; Victorio Peak and Bone Spring Limestone associated with the Yeso Formation). In later Leonardian and early Guadalupian time, eolian (Mack and Bauer, 2014) and possibly littoral sands of the Glorieta Sandstone interfingered with shallow marine carbonates of the San Andres Formation along the Northwest Shelf and basin-margin area. Rising and falling sea levels through this time resulted in periods of non-deposition or erosion, as well as incursions of the basinal Delaware Mountain Group fine sandstones and siltstones into the basin margin area (Cherry Canyon Sandstone Tongue, Figure 4). In later Guadalupian time, tidal flat to lagoonal conditions dominated the Northwest Shelf, in which Artesia Group (Grayburg, Queen, Seven Rivers, Yates, and Tansill formations) carbonates, mudstones, sandstones, and evaporites

accumulated. These graded into the Goat Seep Dolomite and Capitan Limestone along the margin of the Delaware Basin, while within the basin the fine sandstones and siltstones of the Delaware Mountain Group continued to accumulate.

Sea levels regressed substantially following Guadalupian time. Periodic marine incursions brought salts into the area and accumulated first the gypsum-dominated Castile Formation that filled the Delaware Basin and subsequently the halite-dominated Salado Formation, which accumulated within the basin as well as across the Northwest Shelf. At this time, the Delaware Basin largely ceased to exist as a distinct entity, although some magnitude of faulting appears to offset strata through to the close of the Permian at least along the eastern margin of the basin (cf., Schiel, 1988). In upper Ochoan time, marine incursions become increasingly rare and tidal flat/salt flat and more continental conditions progressively came to dominate. Interbedded fine-grained clastic rocks, carbonates, and evaporites of the Rustler Formation (Powers and Holt, 2000) reflect this transition, while fluvial and lesser eolian sedimentary rocks of the Dewey Lake Formation reflect purely continental settings by the close of the Permian (Schiel, 1988).

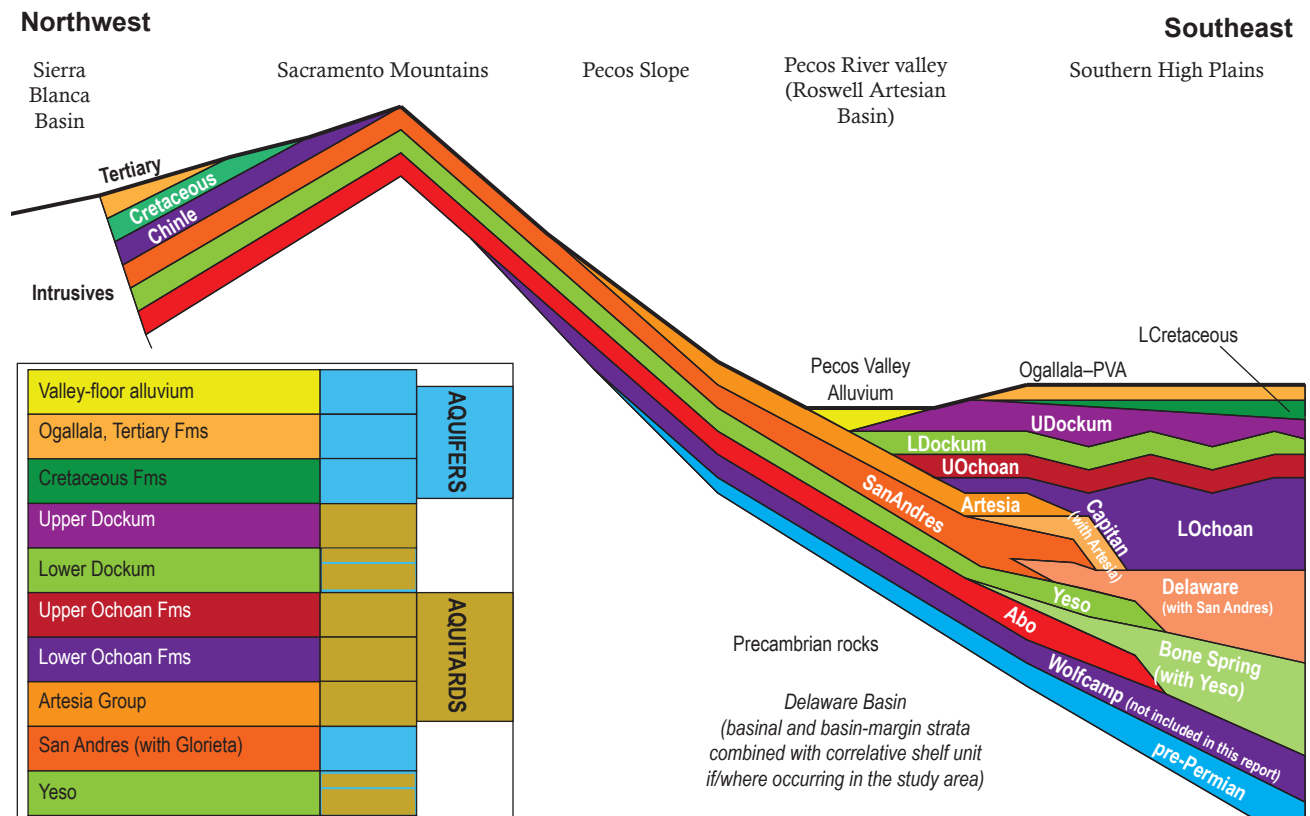


Figure 5. Conceptual stratigraphic diagram of the model units.



**Permo-Triassic continental strata**—Continental, largely fluvial, environmental settings dominated the end of the Permian through the Triassic and likely the Jurassic time period as well. Dewey Lake deposition may have continued into the lower Triassic, with uppermost Dewey Lake strata potentially correlative to the more widespread Moenkopi Formation (Schiel, 1988), although this is in dispute (Lucas and Anderson, 1993). Regardless of correlations, a substantial unconformity separates the Dewey Lake from the overlying Upper Triassic Dockum / Chinle group. The lowermost formation of these groups, the Santa Rosa Formation, can be traced using detrital zircons from Texas through New Mexico to Nevada (Riggs et al., 1996), demonstrating the scale of the fluvial system as well as the equivalence of at least the lower Dockum and lower Chinle groups. The Santa Rosa Formation is a sandstone-dominated unit that fines upsection into a more mudstone-dominated unit, which is typically referred to as the Tecovas Formation. A second fining upwards sequence, the Trujillo-to-Cooper Canyon interval, overlies the lower sequence with local unconformity. Both consist dominantly of fluvial strata with local lacustrine deposits that are potentially associated with paleodepressions that may have formed over areas of preferential subsurface salt dissolution (Lehman and Chatterjee, 2005). The two fining-upwards sequences define the informal Lower and Upper Dockum Group subunits (cf., McGowen et al., 1977; Ewing et al., 2008) in common usage by the TWDB and used here. Continental settings presumably continued through the Jurassic as well, but no strata is preserved in this area from this time period.

**Cretaceous marine and marginal marine strata**—Shallow marine conditions returned to the area during a transgression originating from the southeast (Fallin, 1988, 1989). This transgression deposited a sequence characterized by a basal sandstone interval (Antlers Formation) overlain by clay and limestone and a cap of shale and clay (Walnut through Duck Creek formations, Figure 4). These strata are areally restricted to a broadly synclinal zone in the northeastern corner of the study area; elsewhere, pre-Ogallala erosion removed these rocks from the area. Equivalent are found locally in northeastern New Mexico (e.g., Tucumcari Shale: Brand and Mattox, 1972), but in general Lower Cretaceous rocks are rare along the eastern flank of New Mexico. These rocks accumulated in shallow marine and near-marine settings, including littoral, open marine, lagoonal, and carbonate platform settings (Fallin, 1989).

Upper Cretaceous marine and near-marine strata are found in the northwest corner of the study area preserved in the Sierra Blanca Basin, although the accumulation of these strata are not necessarily affiliated with development of this basin. Upper Cretaceous strata include the Dakota and Mancos Groups, the Gallup Sandstone, the Tres Hermanos Formation, and the Crevasse Canyon Formation (Lucas and Anderson, 1994; Koning et al., 2014a; Rawling, 2014). The sequence reflects several transgressive-regressive cycles of the Cretaceous interior seaway, and culminate in largely continental (fluvial) strata (Crevasse Canyon Formation). Overall, these strata consist of inter-bedded sandstones, shales, siltstones, mudstones, and some coal, reflecting various littoral, marine, and finally fluvial depositional settings.

**Cenozoic continental strata**—Since the Cretaceous, subaerial conditions have persisted across the study area, and deposition has been dominated by alluvial and eolian processes. The Laramide orogeny drove subsidence of the Sierra Blanca Basin, in which fluvial sediments derived from basement-cored uplifts accumulated to form the Cub Mountain Formation (Cather, 2004; Koning and Roberts, 2014). Volcanism accompanied the tail end of the Laramide, and volcanic and volcanoclastic sedimentary rocks of the Walker and Godfrey Groups subsequently accumulated in the same general Basin (Cather, 2004; Koning et al., 2014b; Kelley et al., 2014).

Laramide compressional forces gave way to Rio Grande Rift extensional tectonics, in this area perhaps as early as latest Eocene (~38 Ma: Koning et al., 2014b), and reorganized the landscape. The Sacramento Mountains uplifted and tilted eastward, and streams derived from this highland traversed the study area eastward into Texas, beveling earlier strata and carving now-buried paleovalleys. These streams subsequently aggraded in a generally dry, windswept setting in which a mix of alluvial and eolian sediment accumulated to form the Ogallala and Blackwater Draw Formations. Presumably, these streams extended across the modern lower Pecos River valley. Subsequent development of a north-south flowing Pecos River separated the High Plains Ogallala deposits from source highlands in the Sacramento Mountains, and incision of the Pecos River carved the modern lower Pecos River valley. Alluvial sedimentation along the Pecos River and its tributaries emplaced Quaternary valley-floor deposits, which constitute the youngest deposits considered in this report.

## Structure

The regional structure is dominantly a shallow-dipping, east-facing homocline (Pecos Slope) extending from the Sacramento Mountains crest eastward to the New Mexico-Texas state line (Figure 2 and stylized in Figure 5). A variety of buckles and faults, folds, uplifts, and domes break this regional pattern, and the Laramide-age Sierra Blanca Basin in the northwest corner of the study area represents a significant departure from the regional trend (Figures 2 and 5). Kelley (1971) discusses structures through the western half of the study area individually, and provides an excellent reference for more detail. Through the eastern half of the study area, structural development consists of Permian tectonic structures largely now-buried by later sediments and sedimentary rocks, and smaller-scale salt dissolution-related structures. Large-scale structures in this area include the Delaware Basin, which consists of a deep, north-south-elongate structural trough in the far southeastern corner of the study area (Figure 2). The southern flank of the Roosevelt Dome or uplift occurs in the far northeastern corner of the study area, but contour mapping by Broadhead and Jones (2002) suggests the effect of this structural feature on Abo Formation and younger strata is limited or nonexistent. Although not explicitly discussed as such, structure contours for the top of the Abo Formation released by Broadhead et al. (2005) suggest the presence of buried horst structures in the subsurface in the eastern half of the study area, e.g., in the vicinity of T10 and 11S R32E, and T11 and 12S R33E (cf., Plate 5–18). Salt dissolution-related structures vary in scale from small sinkholes to elongate troughs to regional deflation (cf., Bachman, 1980, 1987). Bachman (1987) suggests that closed depressions apparent in the contours of the elevation of the base of the Pecos Valley alluvium around Roswell may be the product of buried collapse sinks. Lakes and wetlands of Bottomless Lakes State Park and Bitter Lake National Wildlife Refuge fill sinkholes formed by localized subsidence of the Seven Rivers Formation (Land and Huff, 2010). Although Gustavson (1986) documents evidence of large scale land subsidence associated with salt dissolution north of the Roosevelt Dome, no similar large scale salt dissolution-related features appear to have been documented for this study area.

For the interval modeled in this study (Wolfcampian strata and younger), the primary periods of structural development are the Ouachita–Marathon orogeny and associated Ancestral

Rocky Mountains orogeny (here, OM-ARM), the Laramide orogeny, Sierra Blanca volcanism, and Rio Grande Rift extension. Episodic subaerial exposure throughout this time period superimposes periods of salt dissolution and localized collapse on top of these regional structural periods. The OM-ARM produced the overall paleotopographic setting for the pre-Ochoan Permian strata by down-dropping the Delaware Basin and uplifting the Central Basin Platform and Pedernal Uplift. The OM-ARM may also have affected the Huapache monocline and Roosevelt Dome, as Pennsylvanian strata are missing from uplifted portions of both features (cf., Meyer, 1966). Structural segregation of the area into basins and uplifts extended from Pennsylvanian time into early Permian time (through at least Wolfcampian time; Ewing, 1993; Kues and Giles, 2004), and this development may have significantly deformed strata as young as the Abo Formation. Subsidence would continue beyond Wolfcampian time, and indeed Delaware Basin-margin faults appear to offset strata as young as Ochoan in age (cf., Schiel, 1988), but the magnitude of differential movement along faults within the greater Permian Basin was much reduced relative to earlier times.

The Upper Cretaceous to Eocene Laramide orogeny impacted most pre-Cenozoic strata at least along the western half of the study area; the extent of Laramide deformation, if there is any, of strata in the eastern half of the study area is not well known. Laramide compression uplifted numerous fault blocks west of the study area (cf., Cather, 2004; Seager, 2004) that were in many places denuded down to Precambrian basement. Concomitant basins, such as the Sierra Blanca Basin, accumulated fluvial sediment derived from these uplifts. Although timing is poorly constrained, lateral shear along the northeast-trending Pecos Buckles (e.g., Y-O Buckle, Six-mile Buckle, Border Buckle, etc., on Figure 2); deformation of Guadalupian-age strata along the Huapache monocline; and small-scale deformations in the Guadalupe Mountains and Delaware Basin have also been interpreted as effects of the Laramide (cf., Kelley, 1971; Erdlac, 1993; Koša and Hunt, 2006; Hill, 2006).

Regionally, the onset of Rio Grande Rift extensional deformation was diachronous, beginning in some places of southern New Mexico as early as late Eocene (e.g., Mack, 2004; Koning et al., 2014b). Evidence supports significant Rio Grande Rift-related uplift of the Sacramento and Guadalupe Mountains since at least the Mio-Pliocene (Mack, 2004; Polyak et al., 2006; DuChene and Cunningham, 2006). To the

east, the Ogallala and Gatuña Formations, sourced at least in part from the Sacramento Mountains, are at least as old as late Miocene in age (Hawley, 1993). On a large scale, the effect of Rio Grande Rift deformation on the area is quite prominent as it largely generated the current topographic setting by driving uplift of the Sacramento Mountains, eastward tilting of the Pecos Slope, and accumulation of Ogallala sediments that underlie the Southern High Plains. On a smaller scale, individual extensional features throughout the Sacramento Mountains may be the product of extensional deformation, although timing of deformation is rarely well established.

Regionally, within the Delaware Basin area, salt dissolution as old as Ochoan (syndepositional with the Salado Formation) has been documented

(Johnson, 1993). For the area of this study, no documentation of specific periods of salt dissolution was found. Hawley (1993) suggests that thickness trends of the late Miocene–Pliocene Gatuña Formation are in part influenced by local salt dissolution, while closed depressions in contours of the elevation of the base of the valley-floor alluvium along the Pecos River valley have been interpreted as reflecting local buried sinkholes (Bachman, 1987). Otherwise, the influence of salt dissolution on the structure of the area is poorly documented and not well understood. As only local examples of salt dissolution-related structures are documented in the literature for this area, it is possible that no large-scale structures (i.e., structures at the scale of the 3D model constructed here) are found in this area.

### III. INPUT DATA

**G**eologic contact control data was acquired from the 1:500,000, statewide geologic map of New Mexico (NMBGMR, 2003); a variety of compiled well data (Broadhead and Gillard, 2005b; Broadhead and Gillard, 2005a; Broadhead et al., 2005; Broadhead et al., 2009; Broadhead and Ulmer-Scholle, 2012; NM OCD, 2018; the TWDB BRACS database: cf., Meyer, 2017); cross-sections drawn at a variety of scales as a part of geologic mapping in the area as well as for hydrogeologic studies of the area (Newton et al., 2012; NMBGMR, 2018); structure contours drawn as a part of hydrogeologic studies in the area (Blandford et al., 2003; Blandford et al., 2008; Ewing et al., 2008; Ewing et al., 2012; Newton et al., 2012); and several TWDB geologic and hydrogeologic reports (Blandford et al., 2003; Blandford et al., 2008; Ewing et al., 2008; Standen et al., 2009; Ewing et al., 2012; Meyer et al., 2012; Deeds et al., 2015; Figure 3, Table 2). Utilizing this variety of input data required the development of 1) an adaptable database, 2) strategies to synchronize the data formats and stratigraphies, and 3) data quality and compatibility assessment methods. Data was acquired from within the study area boundary as well as within a 5 km buffer around the study area, with the goal of mitigating edge effects.

#### Sources of Data

##### Topography

Land surface topographic data was derived from Intermap Technologies (2008) 4.5-meter resolution digital terrain models (DTMs). DTMs covering the area were merged, down-sampled to 30 m resolution by way of a median function, and clipped to an area encompassing the full study area plus the 5 km buffer. This 30 m DTM was used for extracting elevation data where needed as a part of the data processing, such as identifying the elevation of a well head where not specified in the input data, or for identifying the elevation of a surface geologic contact. The 30 m DTM was further downsampled to 500 m, also by way of a median function, to generate a land surface

DTM with pixel size and location coincident with the snap raster for the final 3D model. The coarser-resolution DTM was also used in the generation of contact surfaces (see Methods section).

##### Surface geology and faults

Surface geologic contacts, faults, and geologic units were acquired from the 1:500,000-scale statewide surface geologic map of New Mexico (NMBGMR, 2003). This map is available from the NMBGMR as a GIS-ready geodatabase complete with digital contact and fault lines and geologic unit polygons. For this project, contact lines were ‘draped’ over the 30 m DTM to convert these lines to 3D, and scripts were utilized to extract the nature of the geologic units juxtaposed across each contact line. Fault lines were extracted for later use as ‘breaks’ in the interpolated contact surfaces (see Methods section).

An additional source of fault lines was the Precambrian subsurface mapping by Broadhead et al. (2009), which included a set of digitized basement faults. Although these basement faults do not necessarily continue to the surface or offset the geologic units modeled here, the influence of at least some of these faults on the surface structure is apparent, and therefore using the basement faults as faults in the geologic model could potentially improve the model results. Therefore, the effect of each basement fault on the model was evaluated to decide whether or not to include the fault in the model. For example, the Huapache monocline, which trends northwest-southeast through the southwest quarter of the study area (Figure 2), is a fault at depth in the basement but a fold closer to the surface (Hayes, 1964; Kelley, 1971). The monocline is fairly sharp, however, such that modeling the fold as a fault could potentially result in a more accurate model. Both approaches were tried, and it was determined that enough data was found through this area to model the fold accurately as a fold, rather than as a discrete structure, and the fault was not used as a fault in the final model. On the other hand, the sharp descent from the Dunken Uplift to the Elk Basin (of Kelley, 1971; Figure 2), which is a fold at the surface but overlying a fault in the

**Table 2.** General description of model units

Model unit	Model unit abbreviation	General description	Included geologic units	Primary input data (for the base of the model unit)
Valley-floor alluvium	Alluvium	Alluvial deposits along current valleys, including along the lower Pecos River and the Rios Hondo, Peñasco, and Ruidoso. Only modeled where extensive enough to show at a 500 m pixel resolution.	unnamed alluvium that is mappable at a 1:500,000 scale (e.g., NMBGMR, 2003)	Contours and well points locating the base of the alluvium from Lyford (1971); geologic map from NMBGMR (2003).
Ogallala-Pecos Valley alluvium	Ogallala–PVA	The Southern High Plains Ogallala Formation and overlying or adjacent Pecos Valley alluvial and eolian deposits (PVA). PVA term is as used by Meyer et al. (2012) and Deeds et al. (2015).	Ogallala Formation and overlying eolian and alluvial deposits. Thin alluvial deposits along slopes descending from the Ogallala Formation.	Raster surface from Deeds et al. (2015) [resampled to fit snap raster, with no additional data processing]
Sierra Blanca	SierraBlanca (combined SierraBlancaCap, SierraBlancaSB)	Volcanic and volcanoclastic strata and intrusive rocks of the Sierra Blanca volcanic field.	Capitan pluton (SierraBlancaCap); Walker Group and post-Walker Group strata in the Sierra Blanca volcanic field core (SierraBlancaSB).	Cross sections by NMBGMR geologists and affiliates; geologic map from NMBGMR (2003).
Upper Cretaceous	UCretaceous	Upper Cretaceous strata and Eocene sedimentary rocks. Preserved only in the Sierra Blanca basin.	Dakota Sandstone, Mancos Shale, Gallup Sandstone, Mesaverde Formation, Cub Mountain Formation, Sanders Canyon Formation.	Cross sections by NMBGMR geologists and affiliates; geologic map from NMBGMR (2003).
Lower Cretaceous	LCretaceous	Lower Cretaceous strata beneath the Ogallala Formation in the northeast corner of the model area. Preserved only in an isolated synclinal zone beneath the sub-Ogallala unconformity.	May include: Antlers Fm (Trinity Group); Walnut, Comanche Peak, Edwards, Kiamichi Fms (Fredericksburg Group); Duck Creek Fm (Washita Group). Cf., Fallin (1989) and Deeds et al. (2015).	Raster surface from Deeds et al. (2015) [resampled to fit snap raster, with no additional data processing]
Upper Dockum	UDockum	Upper Dockum Group strata, as defined by McGowen et al. (1977) and in common usage by TWDB contractors. Dominantly sandstones and mudstones, generally fining upwards.	Cooper Canyon and Trujillo formations of the upper portion of the Dockum Group. Cf., McGowen et al. (1977), Ewing et al. (2008), and Deeds et al. (2015).	Well data from the BRACS database and Broadhead and Ulmer-Scholle (2012); structure contours from Blandford et al. (2008).
Lower Dockum	LDockum	Lower Dockum Group strata, as defined by McGowen et al. (1977) and in common usage by TWDB contractors. Dominantly sandstones and mudstones, generally fining upwards.	Tecovas and Santa Rosa formations of the lower portion of the Dockum Group. Cf., McGowen et al. (1977), Ewing et al. (2008), and Deeds et al. (2015).	Well data from the BRACS database, Broadhead and Ulmer-Scholle (2012), and NM OCD (2018); structure contours from Ewing et al. (2012); geologic map from NMBGMR (2003).
	LDockumNW	Lower Dockum Group strata occurring around the Sierra Blanca basin. Separated from the remaining Dockum by a preservation gap, and modeled separately. Combined with the remaining LDockum in the final model.	Principally Santa Rosa Formation.	Cross sections by NMBGMR geologists and affiliates; geologic map from NMBGMR (2003).
Upper Ochoan	UOchoan	Upper Ochoan series (uppermost Permian) strata. Clastic sedimentary rocks, evaporites, and local carbonates.	Dewey Lake and Rustler formations.	Well data from the BRACS database, Broadhead and Ulmer-Scholle (2012), and NM OCD (2018); structure contours from Ewing et al. (2012); geologic map from NMBGMR (2003).
Lower Ochoan	LOchoan	Lower Ochoan series (uppermost Permian) strata. Principally evaporites.	Principally the Salado Formation; may include some Castile Formation along the margin of the Delaware Basin.	Well data from the BRACS database, Broadhead and Ulmer-Scholle (2012), NM OCD (2018), and Standen et al. (2009) [for the Capitan Limestone, shelf margin-equivalent to the Artesia Group]; cross sections from Newton et al. (2012) and G.C. Rawling (unpublished); geologic map from NMBGMR (2003).
Artesia	Artesia	Artesia Group shelf, lagoonal, mudflat, and/or backreef strata.	Tansill, Yates, Seven Rivers, Queen, and Grayburg formations of the Artesia Group.	Well data from Broadhead and Ulmer-Scholle (2012) and NM OCD (2019); cross sections from Newton et al. (2012) and G.C. Rawling (unpublished); geologic map from NMBGMR (2003).
	ArtesiaNW	Artesia Group strata found around the Sierra Blanca basin. Separated from the remaining Artesia by a preservation gap, and modeled separately. Combined with the remaining Artesia in the final model.	Grayburg Formation.	Cross sections by NMBGMR geologists and affiliates; geologic map from NMBGMR (2003).



**Table 2.** (cont.) General description of model units

Model unit	Model unit abbreviation	General description	Included geologic units	Primary input data (for the base of the model unit)
San Andres	SanAndres	San Andres limestones and Glorieta sandstones. Model unit includes some correlative or interfingering Delaware Mountain Group strata along the margin of the Delaware Basin.	San Andres and Glorieta formations. Includes some Delaware Mountain Group sandstones (principally the Cherry Canyon Sandstone tongue) around the margin of the Delaware Basin.	Well data from Broadhead and Ulmer-Scholle (2012), NM OCD (2018), and Broadhead and Gillard (2005) [for the Bone Spring Limestone, Delaware Basin-equivalent to the Yeso Formation]; cross sections from Newton et al. (2012) and G.C. Rawling (unpublished); structure contours from Newton et al. (2012); geologic map from NMBGMR (2003).
Yeso	Yeso	Yeso Formation/Group carbonates, mudstones, and evaporites. Model unit includes some correlative Bone Spring Limestone along the margin of the Delaware Basin.	Yeso Formation or Group. Includes some Bone Spring Limestone ( $\pm$ Victorio Peak Dolomite) along the margin of the Delaware basin. The term Clear Fork/Clearfork is commonly used along the Texas border; Yeso and Clear Fork do not appear to be perfect synonyms, but the Yeso model unit would include the Clear Fork strata.	Well data from Broadhead and Ulmer-Scholle (2012), NM OCD (2018), and Broadhead et al. (2005, 2009); cross sections from Newton et al. (2012) and G.C. Rawling (unpublished); structure contours from Newton et al. (2012); geologic map from NMBGMR (2003).
Abo	Abo	Implicitly modelled as it underlies the Yeso through nearly all of the study area (locally missing at structurally-highest portions of the Pedernal uplift, e.g. at Pajarito Mountain). Mostly mudstones and local sandstones; grades into shelfal clastic dolomites ("Abo reef") along the margin of the Delaware Basin.	Abo Formation, "Abo reef," Wichita Formation (Group). Includes some Hueco Group/Formation limestones along the margin of the Delaware Basin.	The base of the Abo was not modeled in this report.

basement, is better modeled when the basement fault is incorporated as a barrier in the interpolation; this basement fault was therefore included in the modeling effort. The fault bounding the Central Basin Platform, which lies in the subsurface in the far southeastern corner of the study area, was similarly used as a barrier in the interpolation process.

As discussed later in the Methods section, the set of faults used as barriers during the interpolation of geologic contacts varies depending on the geologic unit being modeled and the age of the faults as described in previous studies. For example, faults cut through rocks as young as Tertiary in age in the Sierra Blanca Basin, while structures along the Central Basin Platform appear to only affect units older than Triassic in age (Schiell, 1988). Faults through the Sierra Blanca Basin are therefore used as barriers for contacts between nearly all model units, while faults through the Delaware Basin are only applied to contacts between Permian-age model units.

## Well control

Two main sources of well control were leveraged: from reports and compilations by Ron Broadhead (Senior Petroleum Geologist, NMBGMR) and his associates and from projects sponsored by the TWDB. Published reports by R. Broadhead include NMBGMR Open-File Reports 487, 488,

489, and 512, which compile formation tops for the Abo Formation, Bone Spring Limestone, Tubb Sandstone (a member of the Yeso Formation), and the Precambrian basement (Broadhead and Gillard, 2005b; Broadhead and Gillard, 2005a; Broadhead et al., 2005; Broadhead et al., 2009). Additionally, Broadhead and Ulmer-Scholle (2012) compiled a collection of formation tops for select wells throughout the state for many of the major geologic units, and this unpublished compilation was used with permission. All of R. Broadhead's reports are careful to document the source of the formation tops (e.g., scout card, original log interpretation, another report, etc.), and this information was captured in the geodatabase for later reference, particularly during the data quality assessment step. These reports also document where a major geologic unit is missing from a drill hole, providing additional control on the subsurface extents of units.

The TWDB sponsored several reports on west Texas aquifers and brackish water resources that extended into New Mexico. Much of the data collected as a part of these reports was compiled into their Brackish Resources Aquifer Characterization System (BRACS) database (cf., Meyer, 2017), a Microsoft Access-based database that is made publicly available through the TWDB website. However, this database was designed and began concurrent with some parallel aquifer studies in the region, and

it was noted that some data was missing from the BRACS database that was available in the databases released with these parallel studies. These databases were provided upon request by the TWDB, and data from these databases found to be missing from the BRACS database were incorporated into the Pecos Slope database. Most studies sponsored by the TWDB specifically study a single aquifer unit, with variable amounts of data collected on adjacent units. As such, these well controls are not uncommonly incomplete and restricted to only the shallowest geologic units. Regardless, the data collected and reported in the BRACS and supplementary TWDB databases provide substantial numbers of well controls for the Cenozoic, Triassic, and Ochoan (uppermost Permian) units along the Texas-New Mexico border.

The New Mexico Oil Conservation Division (NM OCD) maintains a database of oil and gas wells throughout the state, and for a fraction of these wells the formation tops reported by the driller or operator have been entered into their digital database. The full NM OCD database was not available at the time of data collection, and manual extraction of data from their website at this scale was impractical. Therefore, after compiling data from the R. Broadhead and TWDB reports, select regions were identified with either low well control density or high structural complexity and wells from the NM OCD database in these areas were specifically searched for digitized formation tops data. Any records found were added to the Pecos Slope database.

Well data is typically reported as the depth to the top of a unit from a known datum elevation. To convert the depth-based well data to elevation-based control data, one simply subtracts the depth to the top of the unit from the datum to calculate the elevation of the top of the unit. The datum may be the surface elevation, but more commonly, particularly for formation tops picked from geophysical logs, the datum is the elevation of the kelly bushing, which is often about 10 to 25 ft above the ground level. The derrick or driller's floor, which is again several feet above the ground level, is another less common datum. Data compiled by R. Broadhead and TWDB projects commonly identify and record the datum point (ground level, kelly bushing, etc.), datum height above ground level, and datum elevation in feet above mean sea level. Other data sources are less reliable as to determining and specifying the nature of the reference datum, even where a datum elevation is provided in the database. Local examination of some well records suggests these unspecified reference elevations are most often ground level elevations and

not kelly bushing elevations. Given the size of the database and available resources, it was not feasible to check or correct all unspecified datum elevations, and therefore a ~25 ft uncertainty exists for many formation tops elevations. In the rare case that no reference datum elevation was provided in the well database, a ground level elevation was extracted from the 30 m resolution DTM to use as the datum, and again this would impart a ~25 ft uncertainty to the control data. All formation tops were converted from depths to elevations for processing and interpolation.

An early quality assessment step was to compare the datum elevation specified in the input dataset to the elevation of the 30 m DTM at that location. Well locations and records were scrutinized if the given datum elevation was >100 ft above the 30 m DTM, or >50 ft below the 30 m DTM. Particularly large discrepancies were not uncommonly associated with misspecified datum elevations or mislocated wells, and these were corrected. Wells with more moderate discrepancies were compared to surrounding wells and the surrounding topography. If the well were located in an area of moderate to high topographic relief and the formation tops elevations calculated for the well were comparable to those in nearby wells, the discrepancy was interpreted to be the result of topographic relief, and no change was made to the datum. However, if the calculated formation tops elevations were significantly different from those of nearby wells, and if recalculating the formation tops elevations using the DTM elevation as the datum would improve the compatibility, then the given datum was interpreted to be in error. In addition, in areas of low topographic relief, the given well datum was compared to those of nearby wells, and if the given datum were >100 ft above or below those of nearby wells then the datum was interpreted to be in error. If the given datum was interpreted to be in error, and the well appeared to be correctly located, then the datum was reset to the ground level elevation from the 30 m DTM and the elevations of formation tops in that well were recalculated.

### Well reports

Additional data was manually read from reports and logs available from the OCD website and the NMBGMR Subsurface Library. After compiling already-digitized well control data, areas with low well data density or high structural complexity were identified, and records were sought for wells in these areas on the OCD website and in the Subsurface Library. Reports assessed included drillers and well

completion reports; lithologic logs; sample logs (strip-logs); scout cards; and geophysical logs. In general, original interpretations of lithologies or geophysical logs were not performed, unless clear contacts were apparent. Most often, previous geologist interpretations of lithologic and geophysical data were recorded and utilized. Data acquired from these sources was saved locally for reference and manually entered into the Pecos Slope database.

### Cross sections

Digitized cross sections were available for the Pecos Slope region of the Sacramento Mountains. Cross-section scales varied from 1:24,000 to 1:250,000, and were typically derived from surface geologic mapping efforts at the 1:24,000 quadrangle scale. Along most of these sections, well control was sparse; sections are principally the product of surface geologic data extrapolated to depth by geologist expert knowledge. Digitized cross-section data was compiled or converted to GIS feature classes in “MZ space,” wherein the X coordinate of the GIS file is the distance along the cross-section and the Y coordinate is the elevation. Digitized cross-section line locations were also compiled to the GIS database in traditional Easting-Northing space, and Esri ArcTools (“Linear Referencing” tools; Esri Inc., 2017) can be used to locate MZ data from the cross-section data GIS files to Easting-Northing-Elevation locations by referencing the cross-section data to the cross-section line location. Regional cross-sections were compiled by Newton et al. (2012) for the southern Sacramento Mountains, and G.C. Rawling (pers. comm., 2017) provided additional large-scale cross-sections for the northern Sacramento Mountains. Additional cross-section data was acquired for individual quadrangles mapped by a variety of authors (Rawling, 2004a, 2004b, 2006; Zeigler, 2008a, 2008b; Skotnicki, 2009b, 2009a, 2010b, 2010a; Timmons and Zeigler, 2010; Goff et al., 2011).

### Structure contours

Several of the studies listed above produced structure contours for various geologic contacts, which are contour lines showing the elevation of a contact in the subsurface or projected above the land surface. Kelley (1971) contoured the top of the Rio Bonito Member of the San Andres Formation over a large portion of the study area. The Rio Bonito Member is, however, entirely within the San Andres Formation and therefore the contours cannot be used directly for the units

modeled here. Newton et al. (2012) generated contours for the top of the Yeso Formation throughout much of the Pecos Slope. Ewing et al. (2012) released hand-drawn contours for the contacts between the Salado, Rustler, Dewey Lake, and Santa Rosa Formations; however, their study area was largely to the south of this present study and only a few segments of their contours occur within the southeastern corner of this study. Lyford (1973) contoured the base of the alluvium along the Pecos River in the Roswell Artesian Basin. Fallin (1989) contoured portions of the Lower Cretaceous section occurring beneath the Southern High Plains, and these contour lines were digitized and released as GIS files by Blandford et al. (2008). The base of the Ogallala Formation was contoured by Cronin (1969) and Weeks and Gutentag (1981), and these contours were digitized and released as digitized GIS files by Blandford et al. (2003).

### Existing raster surfaces

Most of the TWDB-sponsored aquifer studies conclude with a set of raster surfaces that represent the contacts bounding hydrogeologically-important units. This includes surfaces for the bases of the Ogallala and “Pecos Valley alluvium” (Ogallala-PVA); various units in the Lower Cretaceous section beneath the Southern High Plains; various units in the Dockum Group; and the Dewey Lake and Rustler Formations (Blandford et al., 2003; Blandford et al., 2008; Ewing et al., 2008; Ewing et al., 2012; Meyer et al., 2012; Deeds et al., 2015). While most of these surfaces are of limited extent in New Mexico, a few covered the entirety of the extent of the unit within this study area, and it was considered unlikely that this work would improve upon these rasters. The raster surfaces that were not modified as a part of this study but instead used as released by Deeds et al. (2015) were the base of the Ogallala-PVA and the base of the Lower Cretaceous section.

## Database Structure

Considerable time was spent designing an adaptable, expandable, spatial/GIS-ready, relational database for storing the variety of datasets acquired for this project. Challenges in database design centered on the diversity of data types, of underlying stratigraphies and levels of stratigraphic detail, and of data sources and qualities. In addition, it was considered desirable to store as much of the original data as possible in the database, while using scripts and workflows to

later synchronize the stratigraphies and data types for actual modeling. The core of the geodatabase scheme is illustrated in Figure 6. The structure was inspired by the GeMS model developed by the USGS for surface geologic maps (<https://ngmdb.usgs.gov/Info/standards/GeMS/>), with the intention to facilitate transferring data between NMBGMR geologic maps and 3D modeling efforts. All tables and feature classes were stored in a single ArcGIS-format geodatabase. The relational nature of the database facilitated

querying records through relationship classes, while simultaneously allowing for additional geologic units and datasets from new data sources to be added to the database. As an inherently spatially-aware database, the geodatabase also facilitates spatial querying of datasets. However, the original input data types and stratigraphies are not conducive to data processing; pre-processing steps were required to synthesize the data types to control points for a simplified, consistent stratigraphy of model units.



**Figure 6.** Diagram depicting the core relationships of the Pecos Slope model database. Arrows depict fields used to define inter-table relationships. "M:1": many-to-one relationship; "1:M": one-to-many relationship.



## IV. METHODS

### Modeling Methods Background Research

Berg et al. (2011) summarized the variety of 3D subsurface geologic modeling methods in use by a variety of GSOs worldwide. This summary addressed many of the challenges associated with such models, and provided a starting point for developing techniques for this project. One interpretation of this summary is that no clearly preferred or superior modeling methodology has yet been accepted. Most 3D modeling is performed on an as-needed, project-by-project basis, with methods adapted to fit the needs of and available data for the model. However, some programmatic methods have been developed, and these were particularly scrutinized for their potential to achieve the modeling goals as described in the introduction. Cross-section-based methods are in relatively widespread use (e.g., Mathers et al., 2011; Keefer, 2011); however, these methods require either abundant well control or extensive interpretation to utilize. As mentioned above, well control is only abundant in this area through the eastern side in an area of extensive oil and gas interests, while along the Pecos Slope most data is derived from surface geologic mapping, structure contours, and a few widely-spaced cross-sections. In addition, the stated goals for the modeling approach include minimizing direct modeler involvement and maximizing the capacity to incorporate new data for later model revisions; drawing cross-sections would require direct interpretive involvement, while the generally time-consuming nature of generating cross-sections would discourage incorporating new data and model updates. Similarly, hand-drawn structure contours are commonly used for developing surfaces for structurally-complex contacts (e.g., Ewing et al., 2012), as this provides precise control over the shape of the contact, but such an approach requires direct involvement of the modeler and is time-consuming to update or incorporate new data.

Interpolating contact surfaces between control points is another popular option that can be executed using a variety of interpolation schemes. An added benefit to interpolating between points is the multiple geostatistical techniques that utilize points as

inputs and can generate maps depicting the spatial variability in uncertainty (common referred to as ‘error’ or ‘prediction standard error’). Geostatistical methods can also be leveraged to identify potentially erroneous points and influential control points by quantifying their effect on the interpolation through cross-validation. Branscombe et al. (2018) describe a systematic methodology for evaluating extensive datasets of well control points for potentially erroneous or influential control points that identifies those points that require additional scrutiny due to their influence on the interpolation. Although Branscombe et al. (2018) specifically evaluated a dataset of principally well control data, the same method can be applied to any dataset consisting of data points, and input data consisting of lines (e.g., structure contours, surface geologic contacts) can similarly be assessed if first decomposed to points. The Branscombe et al. (2018) method is systematic in its approach to identifying outliers and influential control points, and provides an effective method of quality assessment of a point dataset. As such, it facilitates combining disparate datasets and adding new data, as the method implicitly evaluates the compatibility between datasets and identifies potentially erroneous new data objectively.

As the Branscombe et al. (2018) method of data evaluation effectively addresses several of the methodologic goals (maximize objective utilization of data, minimize modeler subjective influence, facilitate incorporating new data, quantify confidence in the data), it was adapted as a crucial step in creating the Pecos Slope model. This required a pre-processing step of synchronizing data formats and stratigraphies for direct comparison between datasets. As an addition to the evaluated data compatibility and quality using formation top elevations, model unit apparent thickness data compatibility was also assessed. This was done for several reasons: 1) model unit thicknesses tended to vary less rapidly across the area; 2) evaluating thickness trends was useful in delineating the expected extents of units in the subsurface, and to estimate subsurface model unit pinchout locations; and 3) apparent thickness trends were used to constrain model unit contacts in areas with low data

density by locating offset control estimates. It was therefore desirable to directly assess the quality of the thickness data.

For the final contact surface interpolations, many algorithms are in use depending on the input data and available software resources. Kessler et al. (2011) describe a suite of common 3D software packages in use by GSOs worldwide, many of which were specifically designed to facilitate 3D modeling and incorporate geologic rules in their modeling algorithms. For this project, only interpolation schemes available through Esri ArcGIS tools (Esri Inc., 2017) were considered and experimented with. Strengths and weaknesses considered here included 1) geologic reasonability; 2) capacity to directly estimate uncertainty across the study area; and 3) capacity to incorporate known discrete structures (faults). The final approach used relied on two separate interpolations: 1) an inexact interpolation algorithm to generate a regional trend that could accommodate discrete breaks (faults) in a trend surface, and 2) a geostatistical (kriging) interpolation of the deviations from the regional trend that was better suited to capturing local structures and estimating local uncertainty.

## General

The 3D model consists of a suite of “2.5D” contact surfaces, which are raster (pixel-based, regularly-gridded) datasets which show the predicted elevation of the geologic contact in the subsurface (as feet above mean sea level [ft amsl]) as the pixel value at each pixel or cell location of the raster. Most of the geologic contact surfaces used in this 3D model were generated new as a part of this project. However, some contact surfaces were available from the Texas Water Development Board (TWDB) for a few of the geologic units present in the area along the Texas-New Mexico border. These surfaces were assessed, and it was determined that little improvement would likely result from recreating these surfaces. Therefore, surfaces for the bases of the Lower Cretaceous section and the Ogallala Formation released by Deeds et al. (2015) were used directly without any modification besides resampling to the Pecos Slope framework model target pixel resolution and snap raster pixel locations. Although the TWDB also released contact surfaces for various Triassic and Ochoan (Upper Permian) geologic units as well, none of these covered the extent of the Pecos Slope study area, and hence new surfaces were created that combined the TWDB control datasets with additional input data to provide

contact surfaces spanning the study area. The base of the alluvium along the Pecos River in the Roswell Artesian Basin was also treated separately from the remaining geologic unit contacts, as a fully contoured surface was available from the work of Lyford (1973), and a raster surface was generated from his contours directly with only modest modification to extend this contact surface westward along the valley floors of the Rios Hondo, Peñasco, and Ruidoso (shown on Figure 1).

Initially, the model was to be extended down to the top of the Precambrian basement. However, the input data quality assessment steps proved too time consuming to develop the model to this depth with confidence in a time-efficient manner, particularly as the degree of structural complexity increases significantly below the Permian section. It was therefore determined that the model would only extend through the interval of most importance to water resource concerns, that is, the interval above the Abo Formation (Wolfcampian, Lower Permian).

Table 3 summarizes the data processing steps used to generate the Pecos Slope model. The target horizontal resolution was 1000 m, and the initial target vertical resolution was 100 ft; as processing progressed, it was realized that this vertical target resolution was too idealistic for the deeper geologic units given the available time, and hence the resolution was relaxed to 200 ft for the deeper units. The uncertainty in contact surface elevations was later assessed at several stages in the model building process, as discussed below. All raster processing was conducted with the snap raster used to enforce colocation of pixels and a processing pixel size of 500 m by 500 m; a higher horizontal resolution was used during processing so as to preserve details during processing, with the intention of downsampling to the final target resolution as a final processing step.

The processing steps described below were applied to all model unit contact data except the Lower Cretaceous, Ogallala–Pecos Valley Alluvium (Ogallala–PVA), and the alluvium model unit data. The bases of the Lower Cretaceous and Ogallala–PVA were acquired directly from TWDB reports, and the only processing applied to these was to resample the published rasters to fit the snap raster pixel location and size. The base of the alluvium unit was compiled principally from contours determined by Lyford (1973).

Some model units were processed in areal subsets then combined. In particular, the Artesia and Lower Dockum model units are found in two distinctly different and non-continuous portions of the study area (cf., Plates 20 and 23). These natural subsets of

the Artesia and Lower Dockum control data were therefore processed separately, and the results subsequently combined. In addition, although the Sierra Blanca model unit is well-constrained to a small area in the northwest of the study area, the two areas of its occurrence are geologically distinct. Around Capitan Mountain (“SierraBlancaCap”), the unit is principally an intrusive body interpreted to be a laccolith, while around Sierra Blanca and the northern Sacramento Mountains (“SierraBlancaSB”) the base of the model unit is often a depositional contact. The two areas were therefore processed separately as natural subsets.

## Data Synchronization

### Format synchronization

In order to leverage point-based geostatistical methods, the linear control data (e.g., surface geologic contacts and structure contours) were converted to point data for processing. Two distinctly different forms of line data were acquired and processed in separate ways: planar line data (lines in XY or Northing-Easting space, such as surface contacts

and structure contours) and cross-section data (with contact lines in MZ space along cross-section lines in a vertical plane). The general governing philosophy underlying the line-to-point conversion was to identify those vertex points along each line that dictate the shape of the line at the target spatial resolution and preserve only those points as control data. The Esri ArcToolbox provides a “Simplify Line” tool with a “Point Remove” option that removes all line vertices based on a maximum allowable perpendicular distance between each vertex along the line and the simplified line. If removing a vertex results in a simplified line that deviates from the original line by a magnitude less than the specified allowable distance, the vertex is removed; if the simplified line would deviate by more than this allowable distance, the vertex is kept.

For surface geologic contacts and structure contours (that is, lines in Northing-Easting coordinates), the “Point Remove” tolerance was set to the final target horizontal resolution of 1000 m. This successfully removed many points along all lines while retaining those that were important to defining the curvilinear shape of the line at the target resolution (e.g., Figure 7). For structure contours,

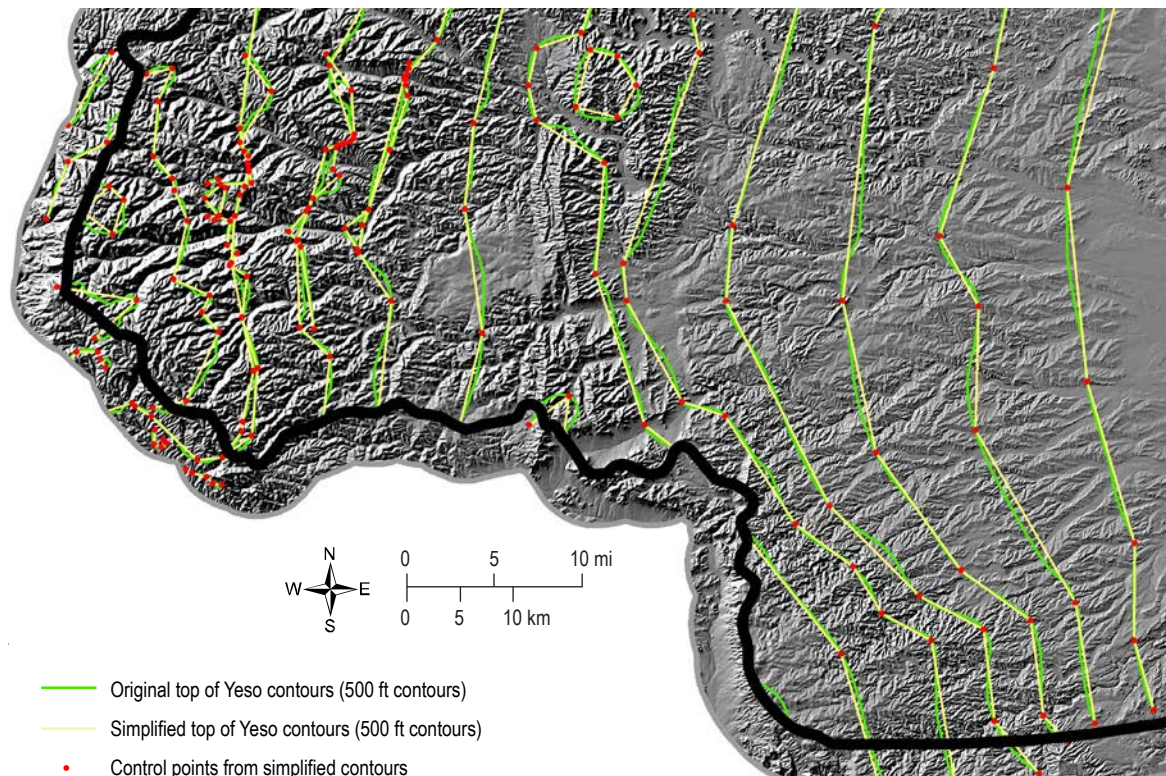


**Figure 7.** Example of linear data to point data conversion. Vertices from the top of the Yeso Formation structure contours are removed unless removal of the vertex would cause the line to move more than 1 km from its original location. After line simplification, the remaining vertices are converted to control points.



**Table 3.** Summary of processing steps

Stage	Step	Summary
(parameters)	Processing extent	Data was collected for and processing was conducted on the study area plus a 5 km buffer around the study area. Results were subsequently clipped to the actual extent of the study area.
	Snap raster	A 500 m cell size snap raster was used to ensure that rasters generated during processing had co-located and equal-sized raster cells.
	Existing rasters	Rasters for the bases of the Ogallala–PVA and Lower Cretaceous units were available from Deeds et al. (2015) that covered the extent of the study area. Contours for the base of the valley-floor alluvium from Lyford (1971) were used to construct the base of the Alluvium model unit.
	New rasters	Rasters for the bases of the Upper and Lower Dockum, Upper and Lower Ochoan, Artesia, San Andres, and Yeso model units were generated as a part of this project from data collected and quality assessed for this project.
Data collection	Data management	An expandable relational geodatabase scheme was developed specifically for this project to store data in a compact, readily queryable format. The adaptable design to the geodatabase was developed with the intention of further utilizing the database schema in later projects.
	Data sources	Data was harvested from published and unpublished compilations of formation tops in well data; published structure contours; published and unpublished cross-sections; surface geologic mapping; and data collected from the NMBGMR Subsurface Library and NM OCD website.
Data synchronization	Format synchronization - line data	Line data (surface-mapped geologic contacts; structure contours) were converted to points by 1) running the cartographic "Simplify Line" ArcGIS tool to reduce the vertices of lines to those that define the shape of the line at the target resolution, then 2) converting the vertices to points that record the elevation of the geologic contact or structure contour at that location.
	Format synchronization - cross-sections	Cross-sections were converted to point data by sampling the cross-sections with 'synthetic wells', which are lines drawn vertically across the cross-sections and intersected with the cross-sections to locate geologic contacts at depth in each cross-section at each 'synthetic well' location. Synthetic wells were drawn to so as to 1) avoid faults, 2) sample the cross-section at no finer than the target resolution of the final model, and 3) locate synthetic wells at or close to important features such as anticline crests or syncline troughs, fold axis, and unit pinchouts.
	Input geologic units to model units	Data was collected on geologic units, then aggregated to model units. Aggregation was done using spatially-aware graphics (feature classes); each model unit was drawn as a polygon and each geologic unit drawn as a line within its respective model unit polygon. The relative geometries of lines and polygons defined whether or not a geologic unit can be the top of the model unit, bottom of the model unit, both, or neither. These relationships were then used to map geologic unit data to model unit data. At any location where both the top and bottom of the model unit is defined, an apparent thickness was calculated.
Data assessment	Iterative leave-one-out cross-validation	Model unit control data was evaluated for outliers ('influential control points') using a leave-one-out cross-validation (LOO CV) of ordinary kriging models. Kriging models were developed for both apparent thickness and model unit top elevation data. A constant trend was removed from the apparent thickness data, while a local 1st order local polynomial trend was removed from the model unit top elevation data. Data with LOO CV magnitudes of 'error' of >200 ft (Abo, Yeso, San Andres, and Artesia model units) or >100 ft (Upper and Lower Dockum and Upper and Lower Ochoan units) or normalized magnitudes of 'error' (z-scores) of >2 were considered 'influential' data points in need of evaluation.
	Influential point evaluation	Influential data were evaluated by checking available well records, lithologic logs, and geophysical logs for errors. Erroneous data was corrected, verified data was kept unchanged, and control points for which supporting data could not be found or was equivocal were removed. If any changes were made, the cross-validation was repeated, until all influential points had been identified and evaluated.
Data densification	Apparent thickness modeling	An ordinary kriging model was developed for the apparent thickness data across the study area. Locations where model units were known to be absent were included as 0 thickness values. Thinned preserved thicknesses resulting from surface erosion were not included. Each kriging model used a constant trend and a spherical variogram model. Apparent thickness prediction models were extrapolated throughout the study area.
	Unit preserved extent estimation	For units that pinchout or transition to other units laterally (particularly around the Delaware Basin), the kriging models were used to estimate the probability that model unit thickness is less than 50 ft (Upper and Lower Ochoan units) or less than 100 ft (Abo and Yeso units) throughout the study area. Probability values were contoured, and these contours, plus locations where each unit was known to be absent, were used to estimate the extents across which each unit is present in the subsurface. The extent across which each unit was exposed at the land surface and subject to surface erosion were also delineated, using the 1:500,000-scale geologic map (NMBGMR, 2003).
	Offset control estimates	Offset control estimates were generated by using the apparent thickness models to estimate the bottom and top elevations of adjacent model units at locations with control data for only some model units. Offset control estimates were used to 1) densify data-poor datasets, 2) project contacts above the land surface where a unit has been eroded, and 3) provide controls to project a contact toward where a unit pinches out or transitions to another unit in the subsurface.
	Exceptions	Offset control estimates were not imported from the base of the Yeso (top of the Abo) to the base of the San Andres (top of the Yeso) except along the margins of the study area, as the Abo was inferred to have potentially undergone a greater degree of structural deformation than the Yeso and San Andres, and the offset control estimate approach risked importing these deformations where they were not present.
	Unit pinchout control estimation	Where a unit is inferred to pinchout in the subsurface, offset control estimates are imported (with 0 offset) from the base of the next overlying unit. Using these estimates ensures that the basal contact of the unit that pinches out will project to basal contact of the next overlying unit.
	Facies transition control estimation	Where a unit is inferred to transition to another unit, offset control estimates are imported (with 0 offset) from the base of the unit to which the unit transitions. Using these estimates ensures that the basal contact of the unit that undergoes the transition soles into the base of the unit to which this unit transitions.



**Table 3. (cont.) Summary of processing steps**

Stage	Step	Summary
Data den-sification (cont.)	Quality assessment	Offset control estimates were assessed using the same ordinary kriging-based LOO CV method outlined above. Influential offset control estimates were judiciously removed, as they were assumed to likely be erroneous estimates of a contact's location.
	General	Contact surfaces were generated by first interpolating regional trend prediction surface, then interpolating a raster predicting the local deviance from the regional trend based on control point residuals from the regional trend. This was done primarily to over-come a common limitation in geostatistical models, which is the lack of capacity to incorporate discrete steps in an interpolation surface such as caused by faults. The regional trend prediction method can accommodate 'barriers' across which the prediction surface is allowed to 'jump' stepwise, as should occur across a fault. The local deviance raster is added to the regional trend raster to generate the contact surface raster.
Initial surface generation	Regional trend development	Regional trend surfaces were generated using the "Kernel Interpolation with Barriers" ArcGIS tool that was specifically parameter-ized to average large swaths of data points and generate a smooth, regional trend surface. Faults mapped on the 1:500,000-scale geologic map (NMBGMR, 2003) and two basement faults mapped by Broadhead et al. (2009) were used as barriers, across which the interpolated surface was allowed to 'jump' stepwise. The two basement faults were 1) that bounding the Central Basin Platform in the far southeast of the study area, and 2) a fault juxtaposing the Elk Basin from the Dunken Uplift (terms after Kelley, 1971) in the southwest of the study area. Inclusion of these faults was found to improve the agreement between structural trends mapped by Kelley (1971) and those that occurred in the model.
	Local deviance/resid-uals interpolation	At each control point, the residual between the control point elevation and the regional trend prediction surface was calculated, and an ordinary kriging model of the residuals developed. The residuals kriging model was interpolated across the study area to develop a model of 'local deviance' from the regional trend surface. The local deviance model was added to the regional trend model to calculate the contact surface raster.
	"Build-down" of the geologic model	A 'sealed' geologic model was developed by progressively comparing each contact surface raster to the overlying contact surface raster, keeping the lower value of the two at each raster cell location. This method constructs a series of 'continuous' contact sur-faces that are defined at every raster cell location in the study area. Where a unit is absent, either due to erosion or a subsurface pinchout, the continuous contact surface will lie at the same elevation as the continuous contact surface of the overlying unit, and thus the model unit thickness will be 0. Discrete contact surfaces are generated by clipping each continuous contact surface to the extent across which the model unit thickness is greater than 0.
	Comparison to Kelley (1971)	Discrete contact surfaces were contoured, and the contours compared to the structure contours of Kelley (1971) to assess for agreement in structural trends. Disagreements were noted.
Model assessment and refinement	Refinements	Where feasible, data was added or adjusted to provide better correlation between the Kelley (1971) documented structural trends and those occurring in the geologic model. For example, disagreement between a structure contour dataset and the traces of the Pecos Buckles resulted in an incorrect sense of offset across some buckles. Control points were relocated accordingly to provide a correct sense of offset.
	Refinements (cont.)	For model units with distinct gaps in their extent, better results were attained by subsetting the control data to create distinct control data sets for each area that the model unit occurred. Separate basal contact surfaces were generated for each subset, and the separate surfaces were then merged to form a single basal contact surface spanning the model domain. The units that were subset were: LDockum, Artesia, and SierraBlanca.
Model assessment and refinement (cont.)	Final surfaces	After control data was refined, contact surfaces were regenerated following the same methodology as before. In the Sierra Blanca basin, where little data is available for the deeper Permian strata, a minimum thickness of 800 ft was applied to the San Andres and Yeso model units to prevent anomalous thinning at depth away from control points.
	Data density uncertainty	Uncertainty associated with data gaps was not quantified. However, the distribution of control data is shown on all maps for assessment.
Uncertainty assessment	Prediction standard error maps	Geostatistical models provide an estimate of the expected uncertainty across an interpolation extent. The apparent thickness, regional trend, and local deviance models' prediction standard error maps were generated and are shown on appropriate maps. The regional trend and local deviance uncertainty maps are combined with the dataset uncertainty map to estimate each contact surface's total uncertainty.
	Dataset uncertainty maps	Following Branscombe et al. (2018), uncertainties in the dataset were assessed using an n-fold cross-validation method. Prediction surfaces were generated for each fold, and the standard deviation between surfaces calculated. Actual prediction errors, as determined from the residuals of validation points for each fold, were then used to scale the standard deviation map to a predicted uncertainty map.
	Contact surface estimated uncertainty maps	The total uncertainty in each contact surface was estimated by summing the regional trend predicted standard error map, the local deviance predicted standard error map, and the dataset uncertainty map.

the elevation of the contour line was taken to be the elevation of the contact at that point. For surface contacts, the elevation of the contact at that point was extracted from the 30 m DTM. At each surface contact point, both the younger, overlying geologic unit and the older, underlying geologic unit were recorded (although overturned contacts do occur very locally along the Pecos Slope [cf., Kelley, 1971], they are local features and were not considered relevant at this scale).

For cross-section geologic contacts (those in MZ space along cross-section lines), an additional consideration for the line-to-point conversion was the utility of recording apparent thicknesses of strata at control points in addition to recording the elevations of formation tops. Thus, rather than simply breaking down contact lines to control points, vertical lines were drawn at select locations along the cross-sections and intersected with the cross-section data to derive 'synthetic well' data. Synthetic wells were located, by script, according to the following steps (cf., Figure 8):

- 1) The cross-section was divided horizontally into 1000 m-wide intervals; this interval width corresponds to the target horizontal resolution of the final model.
- 2) Intervals containing faults were removed from consideration for drawing synthetic wells by clipping cross-section contacts to the extents of intervals that do not contain faults. This was done to avoid drawing well through the faults, and to avoid local deformations that are often inferred to be present near to faults by geologists drawing cross sections but that do not have regional significance.
- 3) Following clipping, cross-section contacts were converted to points using the "Simplify Line" tool with the "Point Remove" option and a tolerance of 30 m, which is approximately the initial target vertical resolution of 100 ft. As the clipping step above trims each line to the edge of any interval containing a fault, and the end point of a line is always preserved by the Simplify Line tool, contact line vertex points are always preserved just outside the intervals containing faults.
- 4) Within each interval, the horizontal locations of all remaining line vertices for all geologic contacts within that interval were averaged, and at this average horizontal location a synthetic well was drawn. No synthetic wells were drawn in any interval that did not contain any preserved vertex

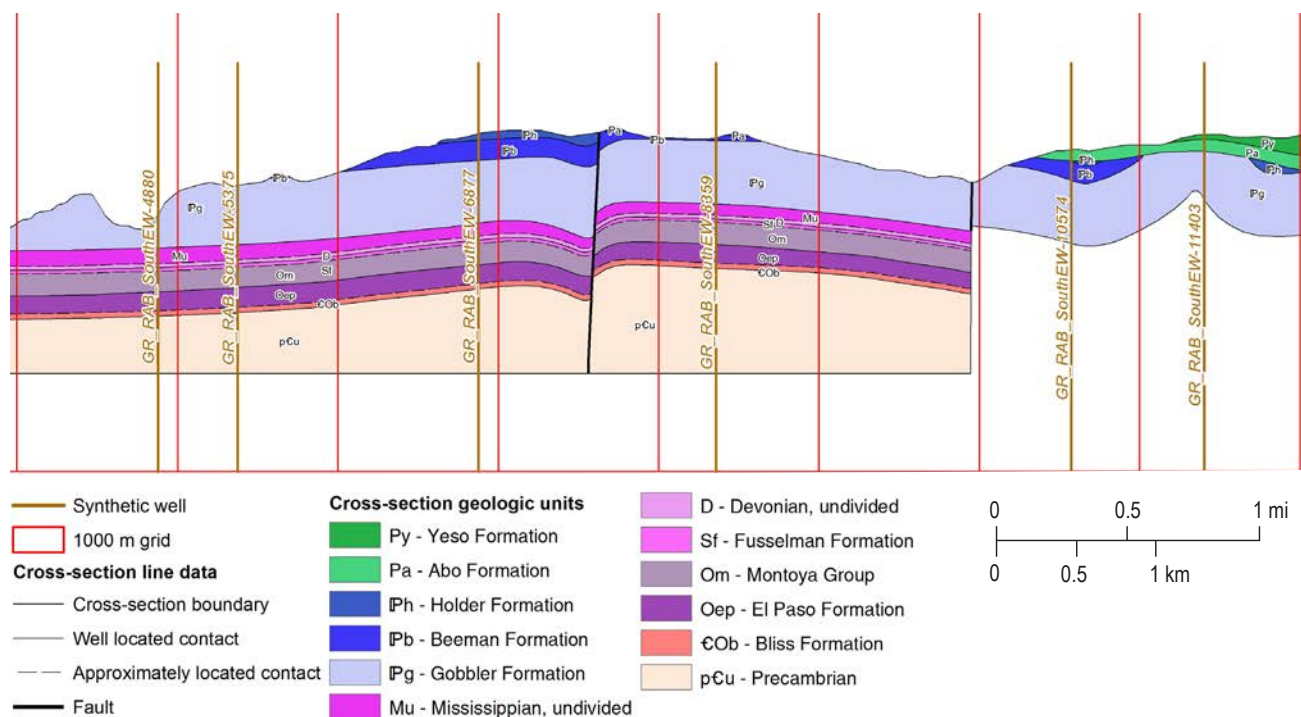


**Figure 8.** An example of the conversion of cross-section data to synthetic well data. The cross section is divided into 1 km-width intervals, and synthetic wells are located within these cells so as to avoid faults and target bends in contact lines. Synthetic well names are arbitrary but designed to be unique, and reflect the name of the cross section and the location of the well as a distance along the cross-section line origin.

points. The goal of this step was to 1) draw no more than one synthetic well within a single pixel of the final model; 2) have that single synthetic well be representative of the geologic unit top elevations and thicknesses within that pixel; and 3) to limit the number of synthetic wells drawn to only those intervals of the cross-section in which influential contact line vertices lie.

Subsequently, the cross-sections and initial synthetic well locations were visually assessed and some were adjusted. Most frequently, synthetic well locations were adjusted to capture specific features such as the crests of anticlines or troughs of synclines, or to avoid local features such as tight folds. The final suite of synthetic well lines were then intersected with the geologic unit polygons in the cross-section to locate the tops and bottoms of each geologic unit in the synthetic wells. Synthetic wells were then located in Northing-Easting space by using the Linear Referencing tools from the Esri ArcToolbox, which can relocate points in MZ space to Northing-Easting space given information about the distance along a Northing-Easting line at which the point is located (i.e., given an “M” coordinate). The result is a set of synthetic well location points in Northing-Easting space and a table of geologic unit tops, bottoms, and apparent thicknesses at each of these points, in a format that is comparable to how the collected well data was stored. This synthetic well data was then processed alongside the well data.

Intrusive bodies around the Sierra Blanca volcanic field in the northwest corner of the study area provided an additional challenge in using cross-section and geologic map data. Small intrusive plugs and stocks as well as dikes and sills are frequently captured in 1:24,000 and even 1:500,000 scale maps and sections that cannot be preserved at the target model scale. Therefore, intrusive polygons in either the geologic map or in cross-section data that were less than 1,000 m wide or 30 m thick were manually removed prior to processing the contacts and cross-section data. In addition, around Sierra Blanca itself the subsurface is interpreted to be rich in intrusive bodies that may completely entrain older sedimentary rocks at depth (cf., Goff et al., 2011). Modeling these entrained bodies would be superfluous, as they are not continuous sequences of sedimentary rocks, and in many instances are not of sufficient width to appear in the model. Therefore, a “Sierra Blanca core” area was designated and manually drawn based on cross-section data and the surface geologic map. Within this area, the subsurface is interpreted to be

dominated by intrusive bodies, and no depositional contacts were extended into this region.

### Stratigraphy synchronization

As much as was feasible, the stratigraphy and nomenclature of each collected dataset was preserved in the database, using relational tables to associate comparable and related units to one another and to model units. After all data was converted to sets of point data, the stratigraphy was simplified to the set of model units using Esri feature classes as a visual method of associating the geologic units to the model units (Figure 9, Table 2). Geologic units were drawn as lines that roughly illustrated their relative time extents, lateral correlations, overlaps, and sequences. Model units were then drawn around these geologic unit lines as polygons that encompassed the geologic units associated with each model unit as well as dictated which geologic units defined the top and/or bottom of the model unit. As these are feature classes, they can be intersected and compared using Esri ArcTools to generate a key that relates the geologic units to the model units, and, using scripts, the sets of data points are filtered through this key to develop sets of control points for each model unit. Control points were generated anywhere an input data point constrains the elevation of the top and/or bottom of the model unit, constrains the thickness of the model unit, or specifies that the model unit is absent in the subsurface at that location.

All remaining quality assessment and processing steps were conducted on the model unit control data. However, where feasible, quality assessments and changes to geologic unit top or bottom interpretations were applied to the original geologic unit data in the Pecos Slope database.

### Quality Control and Compatibility Assessment

After converting input data to model unit control points, the control points were assessed for their quality and for the compatibility between datasets from different sources by comparing data points to each other and identifying outliers and influential control points. These points are not necessarily in error, but given their apparent influence on the interpolation process they do require additional scrutiny to ensure their accuracy. Influential control points were identified and scrutinized iteratively. With each iteration, a set of influential points to investigate was determined, available records for these data were pulled and

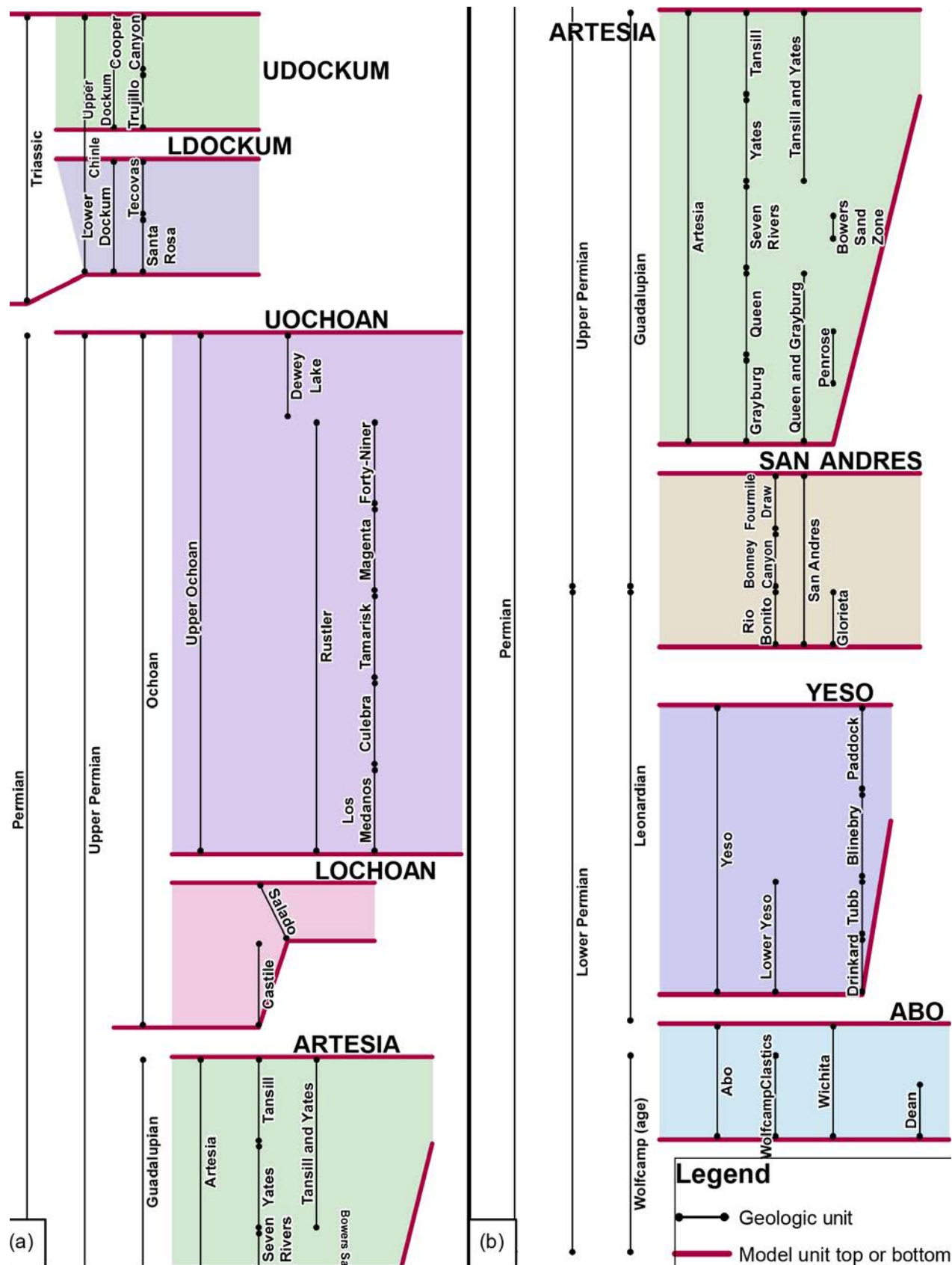


**Figure 9.** Example correlation of units diagram. Model units and geologic units are in spatially-aware feature classes, and scripts aggregate the geologic unit control data to model unit control data. The right panel (b) is a downward continuation of the left panel (a).



assessed, the control data was updated as needed, and the outlier identification method repeated. This was iterated until all influential control points had been scrutinized and determined to be in agreement with the available records. For all model units, both model unit elevation top and apparent thickness values were assessed for outliers and influential control points.

### Examination of influential control points

Influential control points and outliers were scrutinized by checking the original data source; acquiring well completion reports and geophysical logs from the OCD website (NM OCD, 2018); and accessing sample logs, lithologic logs, well records, and scout cards from the NMBGMR Subsurface Library to look for inconsistencies and alternative formation tops interpretations. If no well records, sample logs, or geophysical logs could be acquired to validate the control point, the point was removed. If an alternative formation top elevation was found that would be more consistent with nearby control points, then the formation top was adjusted. If the control point value was consistent with all the available records accessed, then the value was left unchanged, and flagged as a value that had been checked. When assessing apparent thickness values, the data for the underlying unit was also checked against available records. In general, raw lithologic or geophysical data was not interpreted for this project, but instead compared against the control point data for consistency. Original interpretations were not conducted due to limitations in time available for the project. A tracking table was used to record changes that were performed as they occurred and to record what points had been assessed previously. For geostatistical quality assessment steps, the trend surface, variogram model, and prediction surface parameters from each iteration were recorded for later reference.

Interpretive data (cross-sections, structure contours) was more difficult to assess rigorously. Each interpretive data point had to be considered in its geologic context and compared to neighboring controls. Quadrangle-scale (1:24,000-scale) geologic maps were often acquired, mainly from the NMBGMR website (NMBGMR, 2018), to compare to the interpretive data and assess their validity. Interpretive data points that contrasted with nearby hard data points were often simply removed, unless the available maps justified the contrast, such as if mapped folds or faults justified rapid changes in model unit top elevations or apparent thicknesses.

### Cursory quality control

Cursory evaluations included graphing control data values as box-and-whisker plots and histograms that identified outlier values in the full dataset; using Esri Geostatistical Analyst exploratory data maps and graphs to scan for outliers; and visually scanning maps of control data locations and values to identify obvious outliers. These cursory examinations principally identified incorrectly transcribed data, incorrectly located data, and some compatibility issues between interpretive data (cross-sections, structure contours) and hard data (well control, surface contacts).

### Geostatistical quality control

Branscombe et al. (2018) utilized a leave-one-out cross validation (hereafter, LOO CV) technique to identify influential data points for assessment, and their method was adapted here to provide a rigorous, quantitative, iterable method of identifying influential control points. In general, the method involves developing an ordinary kriging-based geostatistical model of the control data, then removing one control point at a time from the dataset and using the remaining data to predict the value at the location of the removed control point (e.g., Figure 10). The predicted value is compared against the actual control point, and the magnitude of the difference, referred to as the ‘error,’ is recorded. The distribution of errors is then used to determine which errors are statistically significant (“normalized score”). Both magnitudes of ‘error’ and normalized scores were considered in identifying influential control points (e.g., Figure 11). All processing was conducted in Esri’s ArcMap, using the Geostatistical Analyst Wizard that steps through developing a trend, fitting a variogram model to the semivariogram of the data, then generating a prediction surface based on the resulting geostatistical model. Cross-validation was similarly performed using tools in the Esri ArcToolbox. Both apparent thickness data and model unit tops elevations were evaluated in this manner; thicknesses were evaluated first, followed by tops. This order was used because the apparent thickness data 1) consisted mainly of control points from sources considered to be of higher reliability (e.g., from Broadhead and Ulmer-Scholle, 2012, and geologist cross-sections), and 2) is essentially a subset of the tops elevations data, as the thickness control points consist of only those locations where the elevations of both the model unit top and bottom are known. Therefore, assessing the apparent

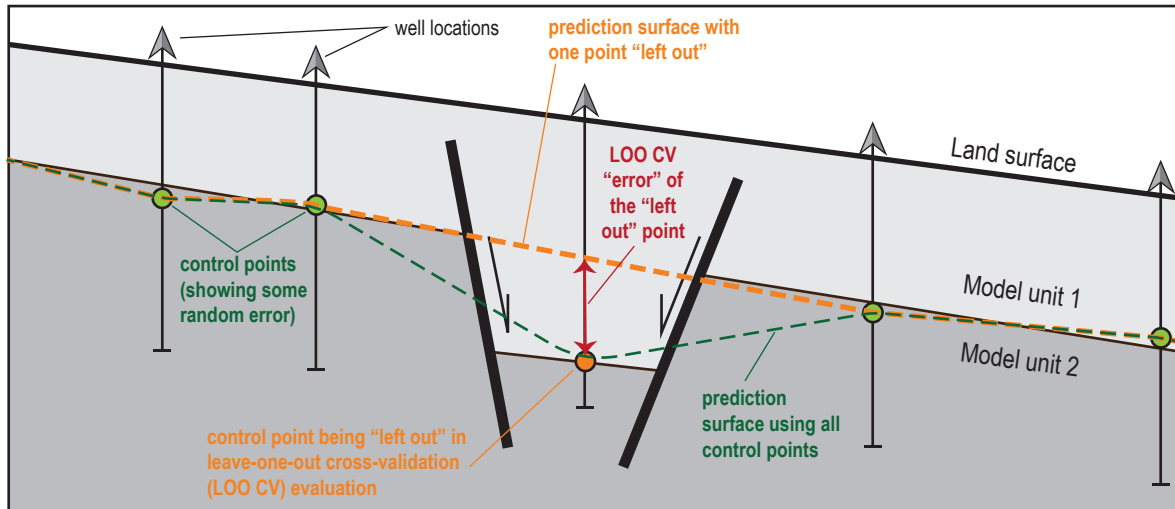


**Figure 10.** Illustration of the leave-one-out cross-validation method used for data quality assessment. The prediction surface is generated with and without the control point being evaluated, and the difference between the two surfaces calculated. The difference is not necessarily a result of error in the evaluated point, however. For example, a small structural feature could result in a large magnitude of 'error' between the two surfaces that is associated with accurate data, as illustrated above. LOO CV = Leave-one-out Cross-validation.

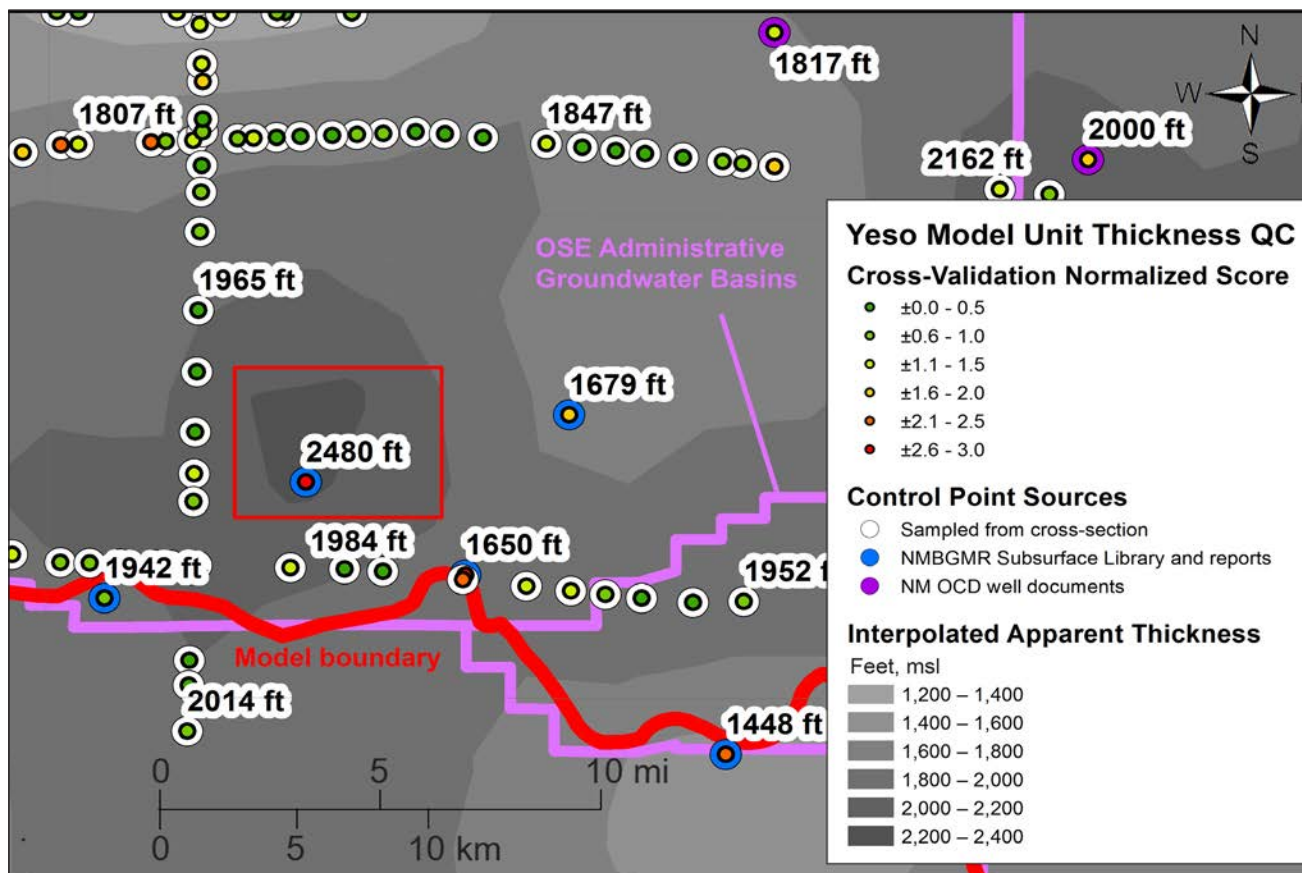


**Figure 11.** Example of leave-one-out cross-validation identification of an influential control point (red rectangle). Possible reasons for the disagreement between nearby points: 1) the influential point was erroneously entered into the database; 2) the influential point was inaccurately interpreted; 3) the influential point is accurate, but the nearby cross-section interpretations are inaccurate; or 4) all points are accurate, and the influential point reflects a local structure that results in an unusual apparent thickness of Yeso strata.



thickness data first developed a core subset of quality-assessed data that the full set of model unit top elevations were subsequently evaluated against in later steps. Note that for thickness data, although units recorded as absent in the subsurface were given a 0 thickness in the database, only non-zero apparent thicknesses were evaluated at this stage.

For both attributes, exploratory graphs were used to determine the type of trend surface to apply prior to fitting a variogram. For apparent thicknesses, an average constant trend surface was applicable in all cases. For the model unit tops, a first-order local polynomial trend surface was fit to each dataset, using an exponential kernel and Esri Geostatistical Wizard-optimized parameters. For both, a new trend surface was generated with each quality assessment iteration. The difference in the type of trend surface used for the thickness data versus the elevation data reflects the geologic setting of the area. Most of the geologic units modeled accumulated in broad, low-relief depositional settings such as floodplain, mudflat, or sabkha environments, which are conducive to forming broad geologic units with only relatively moderate changes in thickness. Subsequent to deposition, however, the area was regionally tilted down-to-the-east, inducing a large scale trend to the model unit top elevations. Smaller-scale structures throughout the study area are superimposed on this regional tilt, however, and as a consequence a local polynomial function was fit to the data to account for this superposition. Although this risks overfitting the trend surface to the data, for the purpose of identifying influential control points and outliers this was not a significant concern.

For both attributes, both spherical and Gaussian variogram models were fit to the semivariogram of the detrended data. Spherical models were preferred, but the better-fitting model, as determined visually, was used. The prediction surface was generated using a neighborhood defined by a minimum of 2 and maximum of 5 nearby points within each of 4 sectors, with the remaining parameters copied from the variogram model. No anisotropy was applied.

Branscombe et al. (2018) applied their iterative method while tracking the reduction of the root mean square error (RMSE) calculated by the LOO CV, and they continued their iterations until the RMSE stabilized. Due to time constraints, this project utilized a different approach to determine when the quality control iterations were complete. For the apparent thickness data evaluation, data with LOO CV errors with magnitudes >200 ft or magnitudes of normalized scores >2 were scrutinized as described

above. This was done iteratively, beginning with magnitudes of error >500 ft, then >400 ft, >300 ft, and finally >200 ft. Overall, six iterations were performed. After the first two iterations, it was determined that apparent thicknesses from the synthetic wells drawn along the cross-sections were commonly in disagreement with those from hard well data for the Abo and Yeso model units. Assessment of the cross-sections suggested that the top and bottom of the Abo unit was largely projected in these cross-sections or located by assuming a constant thickness for the Yeso and Abo from sparse well controls. The Abo tops and bottoms from the cross-sections were therefore inferred to be more suspect and lower quality than the hard well data, and the tops and bottoms as determined from synthetic wells along the cross-sections were removed from the database where within 10 km of a hard well data-derived control point. Few wells contained both the top and bottom of the Upper Ochoan model unit (top of the Dewey Lake Formation / bottom of the Lower Dockum Group and bottom of the Rustler Formation / top of the Salado Formation). This may in part be due to the challenge of locating the top of the Dewey Lake Formation with confidence, as its geophysical signature can be subtle and ambiguous. In contrast, the tops of the Rustler (within the Upper Ochoan model unit) and Salado (at the top of the Lower Ochoan unit) Formations are generally clear in geophysical logs. Hence, in many wells it was noted that the Upper Ochoan model unit is present, and the location of the base of the model unit documented, but the top of the model unit was unknown. In order to provide some quality control during the apparent thickness evaluation, top elevations for the Upper Ochoan model unit were extracted from a raster for the base of the Dockum Group compiled by Deeds et al. (2015). Apparent thicknesses for the Upper Ochoan model unit were then calculated with respect to this raster, and these thicknesses used in the quality assessment process.

For the model unit top elevations evaluation, data with LOO CV errors with magnitudes >200 ft or magnitudes of normalized scores >2 were scrutinized for all model units, and for the shallower Upper and Lower Ochoan, Lower Dockum, and Upper Cretaceous model units errors with magnitudes >100 ft were scrutinized. Overall, eight iterations were performed. Structure contour and surface geologic contact control points, which were not evaluated in the previous stage as these do not provide thickness data, were the most common outlier points through this step, particularly for the

top of the Yeso model unit, which is exposed and contoured throughout the Pecos Slope. In early iterations, due to the density and abundance of such outlier points many were simply deleted. Where control point density was high, contact and structure contour points were manually thinned so as to preferentially keep values closer to the median value of the cluster of points. Influential control points from structure contour lines that were located close to (within about 10 km) of a hard control point (well data) that were in sharp contrast to the hard control point were frequently removed, unless they appeared to define a model-scale structure that was not captured by the hard data.

**Discussion and uncertainties**—The goal of this quality assessment was to identify data points that differ significantly from neighboring points and would have a strong influence on the contact surface interpolation. This can rapidly identify inaccurate outliers. However, as the method is comparing points to one another, the method can be sensitive to systematic errors in the dataset. For example, an area with multiple poor data points and a single accurate point may flag the accurate point as the outlier, and fail to recognize the poor data. This could happen particularly with interpretive data points, as the interpreting geologist may impart a systematic bias to their results (cf., Figure 11). The method is incapable of identifying the cause of an outlier point, and provides little information on whether an outlier is an accurate influential point or in error. Local structural deformations may result in outlier control points that are accurate representations of the subsurface geology, and in many situations it relies on data analyst judgement to determine whether the influential point is accurate or in error.

As used here, the method also does not account for directionality or for known or unknown discrete deformations such as faults. Accounting for anisotropy by preferentially comparing points along structures rather than across structures would be an improvement on the method. However, this anisotropic direction changes across the study area and cannot be incorporated with a single azimuth. Varying anisotropy is not easily accommodated by Esri Geostatistical Tools, and may require original programming to accomplish.

As used here, the method only flags points with magnitudes of ‘error’ >200 ft, or >100 ft for top elevations of the Upper and Lower Ochoan, Lower Dockum, and Upper Cretaceous model units. Any erroneous data point with a magnitude of error below

these thresholds would not be expected to be identified using this method.

As used here, the method is reliant on previous geologists’ interpretations to identify or correct erroneous data. Few original interpretations were conducted for this study. A potential improvement would be to identify particularly well-constrained control points and use geophysical correlation techniques to improve the dataset.

## Offset Control Estimates

Control data abundance varied significantly between model units (e.g., Figure 12). For example, due in part to the depth of erosion, the top of the Yeso model unit is particularly well exposed throughout the west half of the study area, and its top was contoured by Newton et al. (2012). Distinct marker units such as the Abo Formation are commonly identified in well records, and the database compiled by Broadhead and Gillard (2005a) provides an abundance of control for the top of this model unit particularly throughout the eastern half of the study area. Although there are significant exceptions, much of the geologic sequence is conformable or nearly so, such that control data for the top of one model unit can be ‘offset’ to provide offset control estimates for the top of an adjacent model unit by using model unit thickness trends (Figure 13). Additionally, where a model unit is exposed at the surface and subjected to erosion, the pre-erosion top elevation of the unit can be estimated in the same way, by adding the predicted thickness of the model unit at that location to the elevation of the top of the underlying unit. The advantage of doing this projection is that it provides a set of offset control estimates to which the interpolated contact surface can be projected to reduce edge effects (e.g., left side of Figure 13a). Similarly, where a model unit is in the subsurface and truncated by an unconformity, offset control estimates can be added to a model unit dataset in order to ensure that the top of the unit projects into the contact between the overlying unit and the next underlying unit (left side of Figure 13b). As the thickness of the model unit is zero in this instance, the control point for the top of the underlying unit is not truly ‘offset,’ but is incorporated into the model unit dataset as a point to which the top of the model unit should project as it pinches out in the subsurface. A final use of offset control estimates is to ensure that a shelf unit transitions into the equivalent basinal unit by importing basin model unit top elevations as control estimates for the

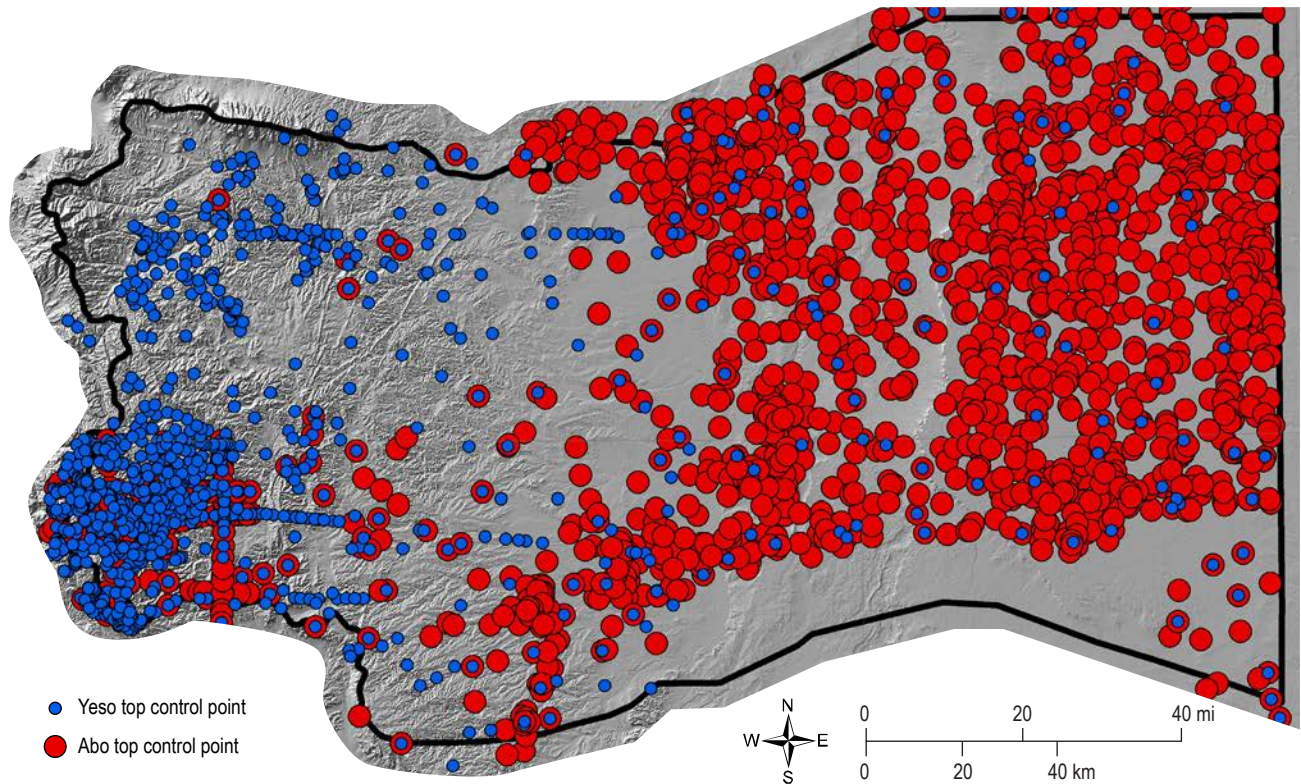


**Figure 12.** Example of the unequal distribution of control data for adjacent model units.

shelf model unit (right side of Figure 13b). The use of offset control estimates helps to preserve subparallel contacts between conformable units and helps to accurately project contacts away from control points where the unit is preserved to where the unit pinches out, transitions to another unit, or is eroded.

Generating offset control estimates requires developing a thickness model for each model unit and, for units that pinch out or transition into other units in the subsurface, developing maps that predict the extents of model units in the subsurface. To do this, for each model unit a geostatistical model of apparent thickness was developed using ordinary kriging, a constant average trend surface, and a best-fit spherical variogram model. All models were constructed using the Esri Geostatistical Wizard in ArcMap. Prediction neighborhoods used the 'smooth' neighborhood type with a smoothing factor of 0.5. Both apparent thickness prediction maps and prediction standard error maps were generated (Plates 1 through 8). In addition, for units that were known to pinch out or transition into other units in the subsurface, the probability of the thickness of the unit in the subsurface dropping below a threshold value (50 ft for the shallower Upper and Lower Ochoan units, 100 ft for the deeper Yeso and Abo units) was contoured in 0.1 probability increments (Plates 1, 2,

4, 5, 6, and 7). Polygons defining the extents of where units were absent in the subsurface were hand drawn around control points where the unit is known to be absent in the subsurface using the contour trends as guides. Typically, these extent polygons were drawn along the 0.3, 0.4, and/or 0.5 probability contours, as these contours frequently appeared to best separate locations where a unit was known to be present from locations where it was known to be absent. In addition, for all model units the 1:500,000 scale surface geologic map was used to identify regions where a model unit was exposed at the surface. In these locations, offset control estimates were derived from the underlying geologic unit in order to project the contact of the exposed unit above the land surface.

For each model unit, offset control estimates of the top of the model unit were generated from the top control points of both the next overlying and next underlying model unit. For control points from the overlying unit, the thickness model of the overlying unit was used to generate offset control estimates by subtracting the predicted thickness of the overlying unit. For control points from the underlying unit, the thickness model of the model unit itself was used to generate offset control estimates by adding the predicted model unit thickness. Where the model unit is inferred to be absent, the predicted thickness



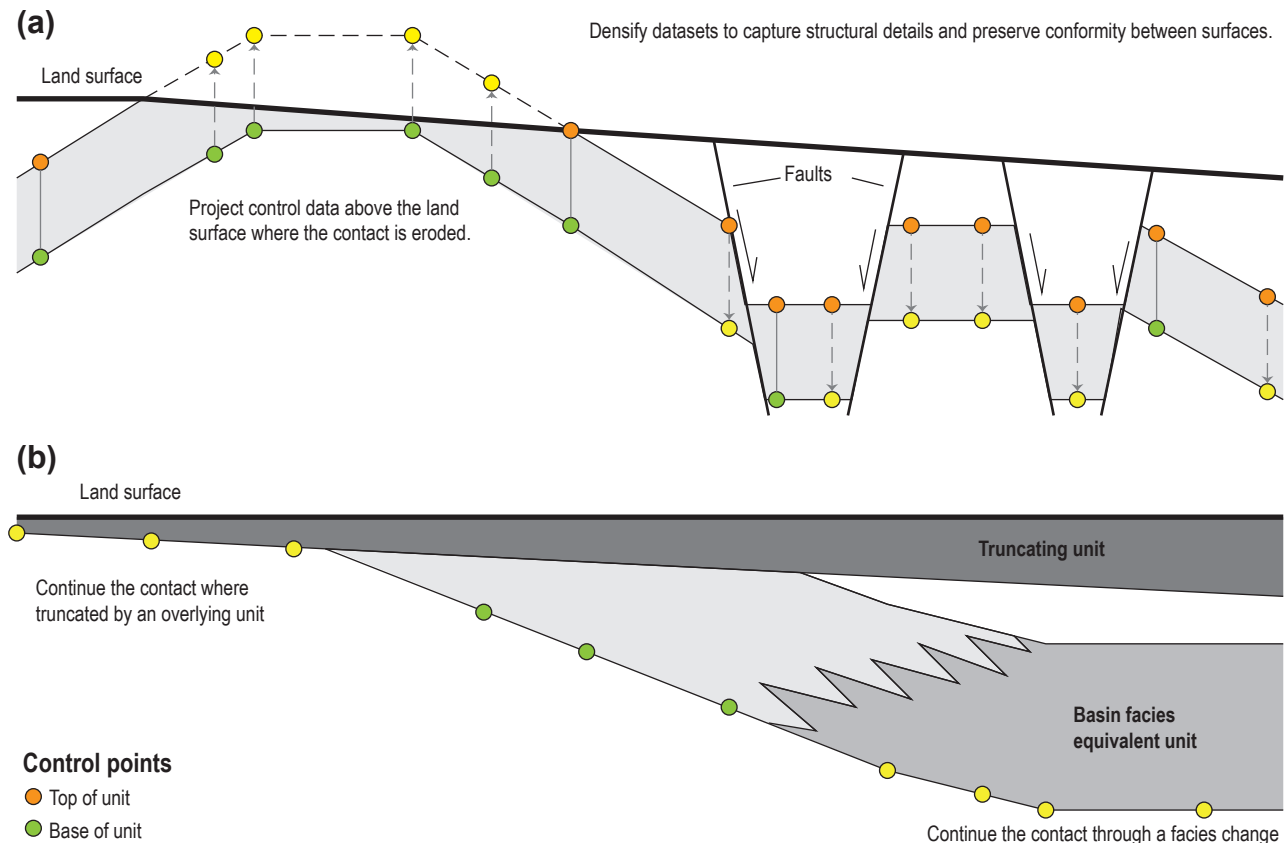


**Figure 13.** Example uses of offset control estimates. (a) To provide control data to project a contact to where the contact has been eroded (left), or to densify control-poor datasets to preserve conformity and capture structural details (right). (b) To provide controls that will cause the interpolated contact to sole into the base of an overlying, truncating unit (left) or into the equivalent contact of a laterally-equivalent unit across a facies change (right).

is taken to be zero, but otherwise the method is the same (e.g., left side of Figure 13b). Where a shelf unit transitions to a basin unit, basin units are treated as underlying units, and the offset is again zero; offset control estimates from basin units are only used where the shelf unit is inferred to be absent (right side of Figure 13b).

Control points for the top of the Abo model unit were only locally offset to provide control estimates for the top of the Yeso model unit. Regionally, the Ancestral Rocky Mountains orogeny caused substantial fault-bounded uplift and basin development throughout Abo deposition that largely ceased in Yeso time (Kues and Giles, 2004). Subsidence rate maps by Ewing (1993) similarly suggest that uplift and subsidence in the Permian Basin is more localized in Abo and Yeso time. Syndepositional horst and graben development, or horst and graben development between the depositions of these geologic units, could violate the implicit assumption that the two model unit top surfaces are subparallel and offset by similar amounts across structures (such as illustrated on the

right side of Figure 13a). Therefore, control points from the top of the Abo were only selectively offset for estimates of the top of the Yeso, particularly along the edges of the model area where control points were generally scarce (Plate 18).

The prediction standard uncertainty in the thickness models is shown alongside contours of the thickness models in Plates 1 through 8; these uncertainty estimates are produced by the Esri Geostatistical Wizard with no additional modification. Faults mapped from surface exposures or from basement studies (i.e., from Broadhead et al., 2009) are shown as well. Although these structures were not explicitly included in the thickness models, relatively rapid thickness changes perpendicular to fault trends are apparent in the Abo and Yeso model units and suggest some structural control in thickness trends. Thickness trends appear to be more gradual across mapped structures in younger units.

After generating offset control estimates, an additional stage of iterative data compatibility assessments were performed. As before, geostatistical models of

the model unit top elevations data were constructed using ordinary kriging of the residuals from a first order local polynomial trend surface. Unlike before, local influence on the polynomial surface was minimized so as to compare individual points to larger scale trends. This was thought to be a better approach at this stage so as to ensure the offset control estimates are compared to actual control points and not just to other offset control estimates. Some local influence was necessary to produce an adequate semivariogram, however. To balance minimizing local influence and the need for an adequate semivariogram, the “Exploratory Trend Surface Factor” in the Esri Geostatistical Wizard trend surface step was iteratively increased from 0 by increments of 5 until a satisfactory semivariogram in the detrended data occurred. This factor adjusts both the kernel bandwidth and prediction surface search neighborhood simultaneously so as to increase local influence as the factor increases. Semivariograms were fit with spherical variogram models with parameters optimized by the Geostatistical Wizard. Prediction surfaces were generated using a smooth search neighborhood with the smoothing factor set to 0.5 and other parameters copied from the variogram model. LOO CV was performed as before, and magnitudes of error >200 ft (>100 ft for the shallower Upper and Lower Ochoan, Lower Dockum, and Upper Cretaceous units) or with magnitudes of normalized scores >2 were scrutinized. As the offset control estimates are only estimates of the elevation of the top of the model unit at a point, they were frequently assumed to be in error where displaying a large magnitude of LOO CV error and hence removed from the dataset. Six iterations of this final data quality assessment were performed.

**Discussion and uncertainties**—The offset control estimate points are intended to constrain the interpolation of contact surfaces in areas away from established control points, and to provide subparallel contact trends between conformable units. For conformable model units with gradually changing apparent thicknesses, these estimates provide a method of importing dense data collected for some units as controls to adjacent units. An example of where this would be particularly useful is where structure contour lines drawn on a single unit help to define structural trends across an area but only for this single unit; estimating the tops of adjacent units as offset from these structure contours can assist in imposing these structural trends on the adjacent units. In addition, the offset control estimates can provide interpolation targets along the edges of datasets,

including providing control estimates above the land surface in areas where a unit has been eroded but previously would have extended to higher elevations. However, the validity of importing control estimates from adjacent units in this way is sensitive to the geologic setting and may even vary across a study area. Structures in this area span a variety of ages, and some may offset older model units but not younger units, resulting in deformations in the surfaces of the older units that should not be imported to the younger units. Local structures likely play a role in the quite variable thicknesses observed for the Abo and Yeso model units (Plates 1 and 2), and hence importing offset control estimates across these model units was done with caution. Control data and offset control estimate compatibility should be assessed prior to interpolating contact surfaces.

Plates 1 through 8 show the prediction standard uncertainties for the apparent thickness models as they vary in space. Uncertainty primarily varies with distance from a control point, as shown in the maps, and as a consequence the largest uncertainties are seen in model units with sizeable gaps in data coverage, particularly the Artesia model unit. Uncertainty is secondarily a function of the variability in thickness across the area. Low-variability units such as the San Andres, Upper Ochoan, and Lower Dockum units have uncertainties dominantly between about 50 and 100 ft, while those with more variability such as the Lower Ochoan, Artesia, and Abo units have uncertainties between 100 and 200 ft. The Yeso model unit appears to suffer from both high variability and areas of low data density. Variability in thickness, and hence uncertainty in the thickness model, may relate to how certain structures influenced deposition of a unit. For example, several units either thicken (Lower Ochoan) or pinchout/transition to another unit (Yeso, Abo) into the Delaware Basin, while the older Abo and Yeso unit thicknesses appear to be influenced by faults throughout the Pecos Slope area. Model unit apparent thickness uncertainties were not propagated in later uncertainty estimates.

## Contact Surface Generation

The method used to generate the final contact surfaces involved three steps (Figure 14): 1) fitting a faulted regional trend surface to the control points and offset control estimates, 2) fitting a geostatistical model to the residuals between the trend surface and the control points and estimates (local deviance model), and 3) combining the regional trend surface and local



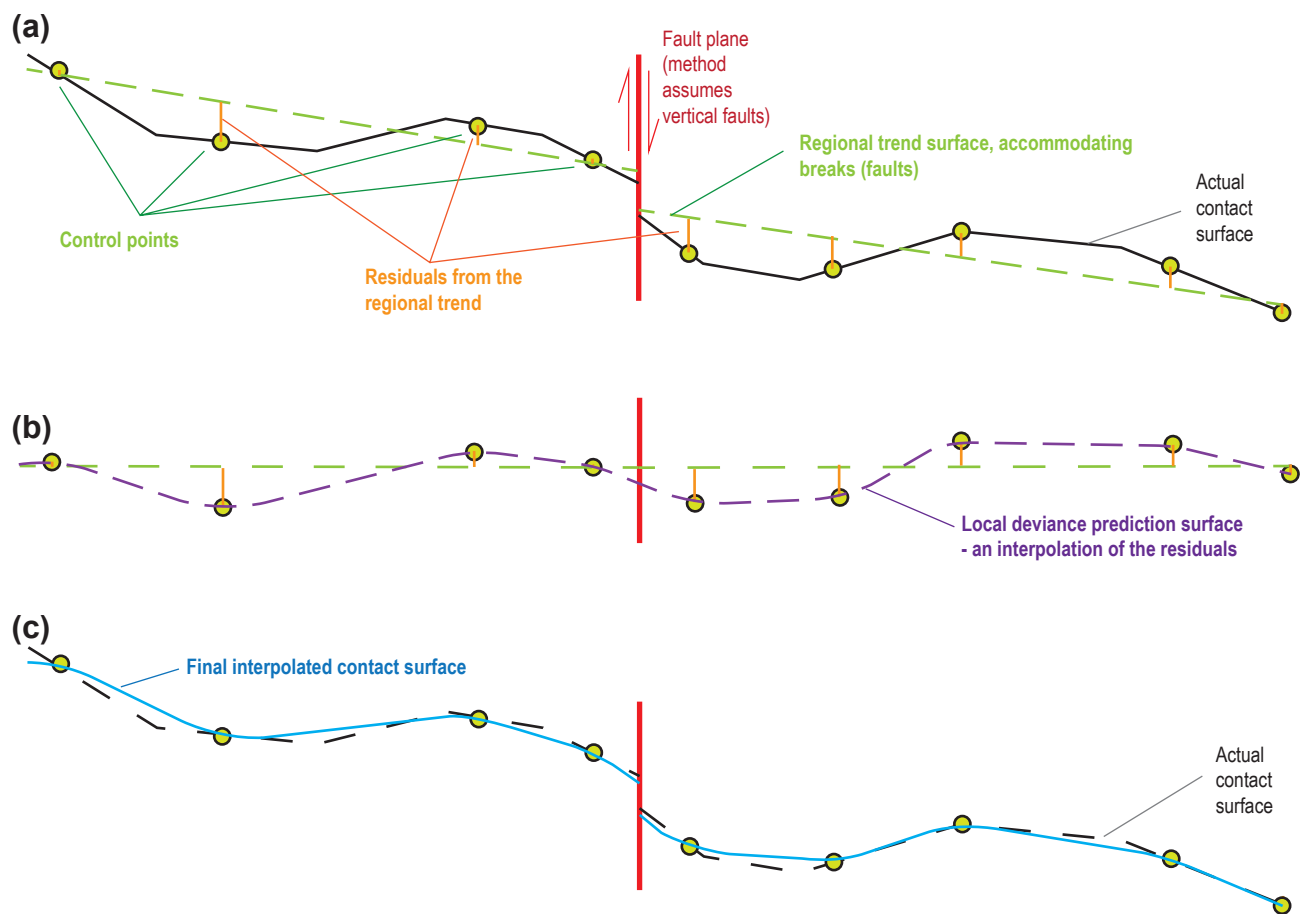


**Figure 14.** Example of the initial contact surface generation method. (a) A regional trend surface is developed that accommodates vertical steps at fault lines. (b) The residuals from each data point to the regional trend surface is then fit with an ordinary kriging model. Removing the faulted regional trend has the effect of re-aligning control points across faults so a single smooth surface can be fit to the data. (c) Adding the local deviance surface to the regional trend creates a faulted contact surface.

deviance model to create a set of faulted contact surfaces. This stepwise approach was taken in order to overcome a common limitation of many interpolation methods, which is that they lack the capacity to handle discrete offsets in the interpolated surface such as should occur across faults. Deliberately creating a regional trend surface using an inexact interpolation scheme that can accommodate breaks in the interpolated surface, followed by developing a separate prediction model for the residuals from this faulted trend surface, can circumvent this limitation.

Up to this point in the processing, much of the focus of data assessment focused on the top elevations of the model units. This was for consistency with the existing datasets, which frequently, if not ubiquitously, provided control on the top elevations of geologic units rather than the bases. However, as processing continued it became apparent that rephrasing the datasets in terms of the bases of units facilitated the 3D model construction. For most of the model units,

this shift was simple: the top contact surface of the underlying model unit was the base contact surface of the overlying model unit. The major notable exception was the base of the Lower Dockum model unit, which, geologically, is a profound unconformity that truncates the Upper and Lower Ochoan and in places lies atop the Upper Ochoan, the Lower Ochoan, or the Artesia Group (in the Sierra Blanca Basin). The model unit extent polygons determined from the apparent thickness models were used to determine where the Lower Dockum overlay each of these model units.

#### Faulted regional trend development

The regional trend surfaces were generated and residuals calculated with scripts that used the Esri Kernel Smoothing Interpolation with Barriers tool. This interpolation method is similar to the first order local polynomial interpolation used previously, with

the exception that this tool can accept a feature class of lines to use as barriers in the interpolation process, across which the interpolated surface can ‘jump’ vertically. Tool parameters were chosen to emphasize the regional trend in the data and generate a highly smoothed surface; the trend surfaces were generated using a first order polynomial interpolation with an exponential kernel function using a neighborhood search radius and bandwidth of 65 km (one quarter the largest lateral dimension of the study area) and a ridge parameter of 100 (the maximum amount). The large search radius and bandwidth ensured that at every location in the prediction surface the interpolation incorporates control points from about one quarter to one half of the study area. The high ridge parameter helped to provide a numerical solution to the interpolation at all locations in the study area; while the use of a ridge parameter can introduce bias in the solution, this was not considered a detriment here as this interpolation was intended to provide a regional trend surface and not an exact interpolation. The set of barrier lines initially consisted of all surface-mapped faults and faults inferred to offset the basement from Broadhead et al. (2009). The basement faults, with the exception of that lying along the west flank of the Dunken Uplift of Kelley (1971) and that encircling the Central Basin Platform (cf., Figure 2), were subsequently removed, as were many small surface-mapped faults that bounded areas with too little input data to solve the interpolation algorithm, or that did not show evidence of displacing geologic contacts greater than 1,000 m laterally in either the 1:500,000 scale geologic map or the available structure contour data (see “Revisions” section below); the final suite of faults used as barriers is shown on Figure 3 and all plates. Faults were not applied as barriers to all contact surfaces. Structure contouring by Schiel (1988) suggests that faults around the Central Basin Platform do not offset units younger than Upper Ochoan in age, and hence this fault was not used as a barrier for the regional trend surfaces fit to the Lower Dockum or Upper Ochoan model unit top elevations data. In contrast, faults through the Sierra Blanca Basin offset units as young as Tertiary in age, and these faults were applied as barriers during the interpolation process for units older than the valley-floor alluvium. Both prediction maps and prediction standard error maps were generated, and are shown in Plates 9 through 17.

**Discussion and uncertainties**—Prediction standard uncertainties are shown alongside contours depicting the elevation of the regional trend surfaces of the

bases of the model units in Plates 9 through 17. In general, uncertainties in these surfaces are relatively low. Uncertainties are higher where significant deviations from a regional trend are observed. For example, somewhat higher uncertainties occur in the Sierra Blanca Basin in the far northwest of the study area, where reversal of the regional dip (from dominantly eastward outside the Basin to northwestward within the Basin) causes significant deviation from the regional trend in the San Andres and Yeso surfaces. Smaller elevated uncertainties are observed along several of the buckles, as well as along the south-central margin of the study area in the area of the Huapache monocline. Elevated uncertainties are also seen along the margin of the Central Basin Platform in the southeast of the study area, and finally along the edges of the study area in general, likely due to low data density and edge effects. The generally low uncertainties likely result from the geologic setting. Many of the strata accumulated in relatively low-relief settings and were subsequently tilted down-to-the-east by Rio Grande Rift extension, and now the dominant, regional structural trend is relatively simple: an east-dipping homocline descending from a structural high along the Sacramento Mountains crest to a structural low along the margin of the Delaware Basin. Most of the control data, as well as the offset control estimates, generally lie along this regional trend, resulting in relatively low uncertainties.

### Local deviance model development

Following generation of the regional trend surfaces, the residuals between the trend surfaces and each control point and control estimate were calculated (Figure 14a). Geostatistical models of the distributions of residuals were then generated (Figure 14b) using ordinary kriging in ArcMap using the Geostatistical Wizard. Each kriging model used a constant trend surface and a spherical variogram model. Although the residuals are, in a sense, already detrended by the regional trend surface, the average of the residuals was typically slightly off from zero, and hence a constant-value trend (i.e., the average of the residuals) was removed from the residuals. Variogram parameters were typically those optimized by the Geostatistical Wizard, although in some instances the fit of the variogram model was visually poor, and hence the model was manually adjusted to better fit the semivariogram of the data. The prediction surface used a smooth neighborhood type with a smoothing factor of 0.5 and, in general, all other parameters were copied from the variogram model. In

some instances, however, a short range in the variogram model resulted in gaps in the prediction surface, and the neighborhood search range was therefore increased to provide full coverage of the study area (without adjusting the range of the variogram model). Both prediction maps and prediction standard error maps were generated, and the predicted residuals added to the regional trend surfaces to create the initial contact surfaces (Figure 14c).

#### Base of valley-floor alluvium surface

The base of the valley floor alluvium model unit was constructed using a separate method. For the Roswell Artesian Basin valley floor alluvium along the Pecos River, Lyford (1973) published a set of well control points, contours for the elevation of the base of the alluvium, and an (incomplete) alluvium extent polygon. This dataset well-constrains the base of valley floor alluvium surface along the Pecos River within this study area, and it was considered unlikely that any of the geostatistical processing described above would improve upon his mapping. However, comparison of Lyford's map to the 1:500,000 scale geologic map (NMBGMR, 2003) suggested that significant amounts of tributary stream valley floor alluvium would not be captured by using Lyford's data alone. At the 1:500,000 scale, and considering the locations of pixels in the designated snap raster, alluvium could be mapped along the tributary Rios Ruidoso, Peñasco, and Hondo. Therefore, two methods were combined to produce the base of valley floor alluvium surface. Within the extent of Lyford's work, his base of alluvium contours, well points, and extent polygon were combined to a raster surface using the Esri ArcToolbox "Topo to Raster" interpolation tool without drainage enforcement. Elevations along the edge of the extent of the alluvium were extracted from the 30 m DTM. Along the tributary streams, water-well records were searched but few wells with adequate data to constrain the base of the alluvium were found in these areas, and an arbitrary constant thickness of 20 ft was subsequently assumed. To derive the base of alluvium surface along the tributary streams, the valley floor alluvium map unit polygons from the 1:500,000 scale geologic map were used to select valley floor pixels from the 500 m DTM, then the arbitrary 20 ft thickness subtracted from the surface elevation of these pixels. Only pixels with centers and >50% of their area within a valley floor alluvium polygon were selected. Although this method results in a discontinuous raster surface, as gaps exist between pixels that satisfy the selection criteria, given

the narrow width of the tributary streams and the resolution of the model this was considered an acceptable depiction of the base of the tributary alluvium at this scale. The Roswell Artesian Basin and tributary stream rasters were then combined to a single base of valley floor alluvium raster surface.

## Combining the Contact Surfaces—3D Model Creation

#### Initial contact surfaces

The suite of initial contact surfaces included (Table 2):

- 1) The topographic DTM downsampled to the 500 m pixel size and snap raster cell locations.
- 2) The base of the valley floor alluvium. This included the alluvium along the lower Pecos River in the Roswell Artesian Basin and locally along the Rios Peñasco, Ruidoso, and Hondo.
- 3) The base of the Ogallala and "Pecos Valley alluvium" (term as used by Meyer et al., 2012). This included the Ogallala Formation and post-Ogallala unconsolidated sediments blanketing the broad slopes grading to the Pecos River away from the Ogallala aquifer that are or are potentially hydraulically connected to the Ogallala. This raster was resampled from a similar surface produced by Deeds et al. (2015).
- 4) The base of the Sierra Blanca volcanic pile and laccolithic intrusions. This surface was constructed from Sierra Blanca model unit base elevation control points and offset control estimates, as described above. Two subsets of the Sierra Blanca control data were modeled separately, one for the Capitan pluton and one for the Sierra Blanca volcanic field, with the results of each subset model subsequently combined.
- 5) The Upper Cretaceous-Lower Dockum contact where it is preserved in the Sierra Blanca Basin. This surface was constructed from Upper Cretaceous model unit base elevation control points and offset control estimates, as described above.
- 6) The base of the Lower Cretaceous section locally preserved beneath the Ogallala in the north-eastern corner of the study area. This raster was resampled from a similar surface produced by Deeds et al. (2015).
- 7) The Upper Dockum-Lower Dockum contact. This surface was constructed from Upper Dockum

model unit base elevation control points and offset control estimates, as described above.

- 8) The basal Lower Dockum contact, which in places overlies the Upper Ochoan, Lower Ochoan, or the Artesia model units. This surface was constructed from Lower Dockum model unit base elevation control points and offset control estimates, as described above. Two subsets of the control data were modeled separately, one for within the Sierra Blanca Basin and one for outside the Sierra Blanca Basin, with the results of each subset model subsequently combined.
- 9) The Upper Ochoan-Lower Ochoan contact. This surface was constructed from Upper Ochoan model unit base elevation control points and offset control estimates, as described above.
- 10) The Lower Ochoan-Artesia contact. This surface was constructed from Lower Ochoan model unit base elevation control points and offset control estimates, as described above.
- 11) The Artesia-San Andres contact. This surface was constructed from Artesia model unit base elevation control points and offset control estimates, as described above. Two subsets of the control data were modeled separately, one for within the Sierra Blanca Basin and one for outside the Sierra Blanca Basin, with the results of each subset model subsequently combined.
- 12) The San Andres-Yeso contact. This surface was constructed from San Andres model unit

base elevation control points and offset control estimates, as described above.

- 13) The Yeso-Abo contact. This surface was constructed from Yeso model unit base elevation control points and offset control estimates, as described above.

Each of these initial contact surfaces was unconstrained by adjacent surfaces; that is, initial contact surfaces were allowed to intersect, and, in particular, initial contact surfaces were allowed to project above the land surface. Initial contact surfaces were also not constrained by or clipped to the inferred or known preserved extents of the geologic units.

#### “Build-down” method for combining surfaces into a model

Once model unit contacts were rephrased as basal surfaces, rather than top surfaces, the method of combining the individual initial contact surfaces to a complete 3D model was a simple iterative procedure (Figure 15). The procedure begins with the land surface raster as the initial continuous contact surface, then at each raster cell location the elevation of the land surface raster is compared to the elevation of the corresponding base of valley floor alluvium raster, and the lower of the two is preserved. Wherever the base of the valley floor alluvium is not defined (i.e., wherever there is no valley floor alluvium), the topographic surface elevation is recorded. In this way, a continuous contact raster is developed for the base

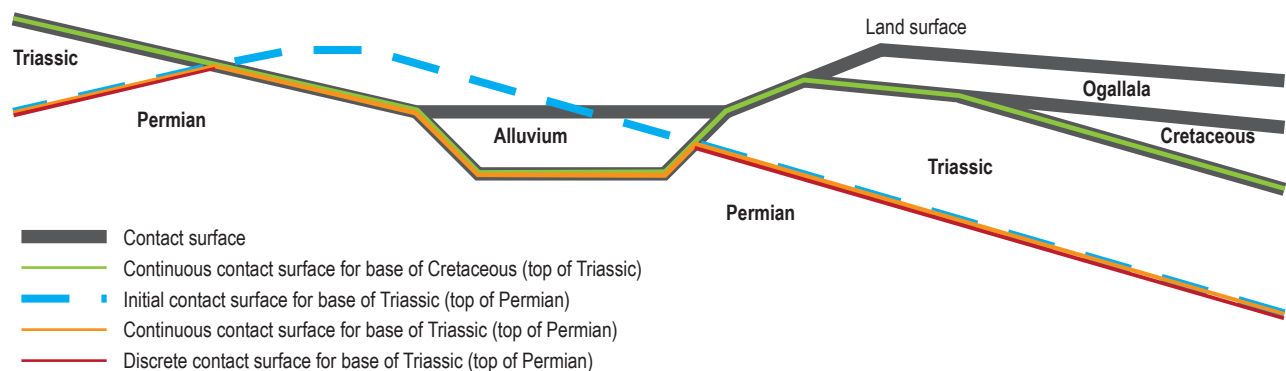


**Figure 15.** An example of the build-down method of creating the final model. To create the final contact surface between the Triassic and Permian, the initial contact surface, which projects above younger units and the land surface, is compared to the contact surface between the Cretaceous and the Triassic, and the lower of the two surfaces is kept at each raster cell location in the model area. This creates a continuous contact surface for the Triassic–Permian contact, the elevation of which is defined at every raster cell location in the model area. Where the Triassic is missing, the continuous contact surface between the Triassic and Permian co-locates with that between the Triassic and Cretaceous, such that the thickness of the Triassic calculated by subtracting the two surfaces is zero. The discrete contact surface between the Triassic and Permian is only defined where the Triassic is present, and is determined by clipping the continuous contact surface to the extent over which the thickness of the Triassic is greater than zero.

of the valley floor alluvium model unit which has elevation values defined at every raster cell location across the study area. The continuous contact raster lies along the base of the valley floor alluvium where there is alluvium, and merges with the topographic surface where there is no alluvium. Each subsequent model unit is added to the 3D model in a comparable fashion (Figure 15). The elevations of the continuous contact surface for the base of the valley floor alluvium is compared to the elevations of the initial base of Ogallala-PVA surface to construct a continuous contact surface for the base of the Ogallala-PVA model unit, and this continuous contact surface is then compared to the initial base of the Sierra Blanca model unit, etc. These calculations are performed using a simple iterative script. Note that at this stage anywhere a model unit contact projects above the contact of an overlying unit it will be truncated by the base of the overlying model unit; in this way, erosional truncations of contacts are accounted for.

The end result is a 3D subsurface geologic model, where for every model unit there is a basal raster contact surface that has a defined elevation at every pixel location in the model extent, and the basal contact surface merges with the basal contact surface of the next overlying model unit where the model unit is not present. The thickness of the model unit at every pixel location can then be calculated by simple subtraction, and the extent of the model unit in the subsurface is simply every location where the thickness is greater than 0. To convert the suite of continuous contact surfaces to discrete contact surfaces, a script calculates the thickness at each raster cell location of each model unit, then clips each continuous raster surface to the extent over which the model unit thickness is greater than 0 (Figure 15).

### Initial model assessment and revisions

The initial 3D model was assessed for reasonability by comparing the model to known geologic structures and comparing contours of discrete contact surfaces to the hand-drawn structure contours of Kelley (1971). To illustrate the structure of the Pecos Slope area, including portions of the Northwest Shelf and Delaware Basin, Kelley divided the region into three areas and for each area contoured a representative unit with distinct characteristics. Through most of the area, he contoured the top of the Rio Bonito Member of the San Andres Limestone, while along the shelf margin of the Delaware Basin he contoured the top of the Yates Sandstone (Formation) of the Artesia Group. Each of these units is internal to one

of the model units used here, and hence neither set of structure contours can be directly compared to any model unit top or base contours. However, as many of the Permian strata are conformable or nearly so with subparallel contacts, the trends in Kelley's structure contours should be mirrored in the contours for the bases of the Yeso, San Andres, Artesia, and Lower and Upper Ochoan model units. Contours for these surfaces were overlain on georeferenced digital versions of Kelley's structure contour maps in a GIS in order to directly compare trends. In addition, each of the model unit surfaces were scrutinized for their capacity to reflect the structural features described by Kelley in the text of his report. Although many of the structures described by Kelley are of too small a scale to be captured in this model, it was expected that the uplifts, basins, and buckles described by Kelley should be apparent in the model. In general, there was decent agreement between the large scale structures mapped and described by Kelley and the contours of the model unit contacts. Some notable disagreements were:

- 1) Incorrect sense of offset along some buckles, which appeared to be caused by mislocation of some control points derived from structure contours as compared to the fault lines used as barriers in the regional trend interpolation. This was corrected by adjusting control point locations.
- 2) Some basement faults from Broadhead et al. (2009) detracted from the interpolation results, such as along the east flank of the Dunken Uplift and underlying the Huapache monocline. These faults were subsequently removed from the set of barrier faults.
- 3) The Pajarito Mountain Dome was poorly captured by the initial control point datasets, particularly along the east flank. Some control points were added along structure contour lines to better capture the sharp eastern rise of the uplift.
- 4) The transition to the Delaware Basin was poorly captured for the Yeso model unit. Additional control data was located in a set of Bone Spring well data (Broadhead and Gillard, 2005a) and incorporated into the database.

After applying the corrective measures described above, the contact surfaces were regenerated as above.

In addition to the structure contour comparison, several artifacts of the processing method were identified and corrected. These artifacts originated from the extrapolation of a unit's contact surface away



from control point locations and in places outside the extent of the model unit. These artifacts were corrected by trimming the extent of each contact surface to the inferred preserved extent of the model unit. The one complication to this was that each unit's extent was re-assessed at this stage by examining the original inferred extent of the unit (as derived in the Offset Control Estimates step above), the distribution of control data for the unit, the 1:500,000 scale surface geologic map, and the extent of the unit determined by the initial 3D model to determine if the inferred preserved extent of the unit should be revised. Although most unit extents were unaffected by the reevaluation, the extent of the Lower Ochoan was adjusted locally in response to the results of the initial 3D model. Each contact surface was clipped to the inferred preserved extent of the model unit, then the 3D model was recreated using the iterative approach described above.

A second projection-related artifact was noted in the far northwest corner of the study area, where poor control on the bases of the San Andres and Yeso model units resulted in anomalous thinning and, locally, pinching out these units. Although it is possible that such pinch outs do occur in the subsurface, as the available data is scarce, these units have not been documented nor interpreted to pinch out here in the reviewed literature. The thinning of these model units was therefore interpreted to be an artifact of projecting surfaces away from control data. To prevent this thinning, the well data in the area was scrutinized for the range of thicknesses of these units observed in nearby wells, and for each there appeared to be a minimum thickness of about 800 ft. This minimum thicknesses was applied to each model unit by shifting their basal contact surfaces downward in elevation to preserve this minimum. The final base of model unit surfaces are shown as contours in Plates 18 through 29.

## Uncertainty Assessment

A crucial stage of any modeling effort is to adequately describe the uncertainty in the model (Bardossy and Fodor, 2001; Keefer et al., 2011). In fact, a leading factor in choosing to utilize geostatistical methods for data interpolation and quality assessment was the capacity for these methods to calculate and map expected uncertainty ('prediction standard error') across the study area. Uncertainty can enter the model through multiple channels, some of which can be quantitatively addressed while others can only be

qualitatively described. Generally speaking, contributions to uncertainty include data quality, density, and ambiguity; compatibility between the data processing methods used and the nature of the geology; the complexity of the geology; and uncertainty associated with the interpolation algorithms used. The evaluated forms of uncertainty are described below: data quality, data density, offset control estimate uncertainty (a form of methodologic uncertainty), regional trend interpolation uncertainty, local deviance interpolation uncertainty, and uncertainty associated with the data distribution (dataset uncertainty). The last three of these uncertainties are combined to calculate the total estimated uncertainty.

### Data quality and dataset intercompatibility

This project sought to address uncertainty in data quality and dataset intercompatibility by adapting the geostatistical methods of Branscombe et al. (2018), as described above. Due to time constraints, this process only addressed influential data points as determined by magnitudes of LOO CV 'error' of >200 ft (>100 ft for the Ochoan and younger units). Control data with errors of lower magnitude would likely not be identified using this method. This places an expected limit of confidence for the control data itself at  $\pm 200$  ft for the Abo, Yeso, San Andres, and Artesia model units and  $\pm 100$  ft for the Ochoan and younger model units.

### Data density uncertainty

Although a dense dataset is not necessarily required to adequately model an area, a low density dataset is less capable of identifying areas of structural complexity or identifying data errors using cross-validation. In addition, model confidence always decreases away from control data locations. The uncertainty associated with distance from control point locations is generally reflected in the prediction standard error maps for the local deviance models, described below.

### Offset control estimate uncertainty

Offset control estimates were generated to provide additional contact location estimates away from model unit control points. The quality of these estimates relies on the accuracy of the model unit thickness models and the applicability of the method given the geologic setting. These uncertainties are discussed above, and are shown overlain by control data point locations and contours of the thickness models in

Plates 1 through 8. These uncertainties are not directly propagated into the total estimated uncertainty.

### Contact surface uncertainties

Each contact surface was generated by a set of interpolation steps that each carry a measure of uncertainty. Uncertainty in the regional trend and local deviance models each carry a separate predicted standard error determined by the Esri Geostatistical Analyst tools. An additional uncertainty lay in the datasets themselves, and this was quantified by adapting the n-fold cross-validation method of Babakhani (2016).

**Regional trend uncertainty**—Regional trend uncertainty was quantified as the predicted standard error derived from the Esri Kernel Interpolation with Barriers tool used to generate the regional trend surface, and these uncertainty maps are shown in Plates 9 through 17. Regional trend uncertainty is discussed in more detail above, and is combined with the local deviance and dataset uncertainties to derive the total estimated contact surface uncertainty.

**Local deviance uncertainty**—Local deviance model uncertainty was quantified as the predicted standard error derived from the Esri ordinary kriging method used to generate the local deviance model surface. Local deviance uncertainty is discussed in more detail above, and is combined with the regional trend and dataset uncertainties to derive the total estimated contact surface uncertainty.

**Dataset uncertainty**—Uncertainty in the dataset and its effect on the interpolation process can be quantified using n-fold cross-validation. This general method divides the dataset into training and validation sets, recreates the contact surface with the training set alone, and compares the validation set to the resulting surface. This method can also assess the range in contact elevations that may occur at any given location that could result from different datasets (i.e., from different training sets). Branscombe et al. (2018) applied the method of Babakhani (2016) to address this form of uncertainty by generating ten contact surface variations, each based on a randomly-selected training set consisting of 80% of the total input data points. At each cell location, the standard deviation between the ten individual contact surface realizations was calculated, and this was used as an estimate of the contact surface uncertainty. In this project, we expand upon their method. For each of ten realizations, a

randomly-selected 80% of the total input dataset was used as a training dataset to generate the contact surface. Realizations were generated using the same regional trend model and ordinary kriging model as was used to generate the original contact surface; each realization therefore uses the same underlying geostatistical model but with a different set of input points to interpolate between. At each cell location, the standard deviation between these realizations was calculated, as per the Babakhani approach. In addition, for each contact surface realization, the residuals from the surface to the remaining 20% of the data that were not used to create the contact surface (i.e., the residuals between the validation set points and the surface) were calculated. These residuals reflect the actual error of the contact surface determined from the training data alone. At each validation point location (from all ten subsets), the standard deviation between the ten contact surface realizations was recorded and compared to the validation point residual; not surprisingly, the larger residuals correlated to areas with larger standard deviations nearly linearly (Figure 16). For each model unit or model unit subset (in the case of the Sierra Blanca, Artesia, and Lower Dockum model units), a line was fit to the standard deviation-versus-actual error data, and these linear equations suggest that the actual error is often roughly twice the standard deviation between the ten realizations (see equations on Figure 16). As the actual errors (i.e., the validation point residuals) are often noticeably higher than what the standard deviation maps would suggest, the standard deviation maps were scaled by the linear equations on Figure 16 to derive ‘calibrated’ uncertainty maps. The one exception was for the Lower Dockum model unit Sierra Blanca-area subset (LDockumNW on Figure 16). These data do not display a linear relationship, and the equation shown was not used in ‘calibrating’ the uncertainty map. Instead, the steepest slope (2.92 from the Upper Ochoan model unit) and the highest y-axis intercept (32.525 from the Sierra Blanca SB model unit) were used as the coefficients to ‘calibrate’ the uncertainty map for this model unit subset in a conservative fashion. These uncertainty maps are combined with the regional trend and local deviance uncertainty maps to derive the total estimated uncertainty.

**Total estimated uncertainty**—As used here, the total estimated uncertainty for the surfaces that comprise the 3D model is the sum of the regional trend, local deviance, and dataset uncertainties. These uncertainty maps are shown alongside contours depicting the

## Cross-validation-observed error vs. standard deviation between N-fold surfaces

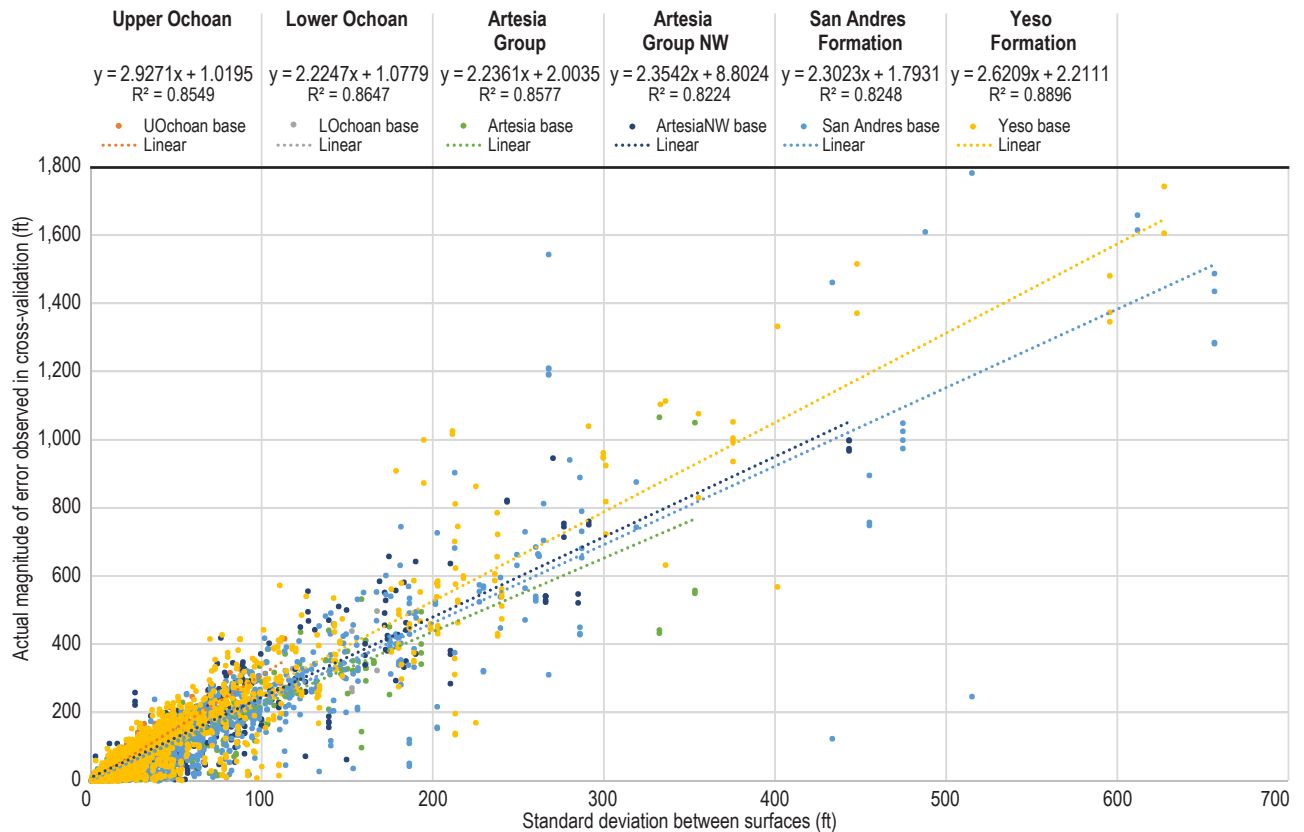
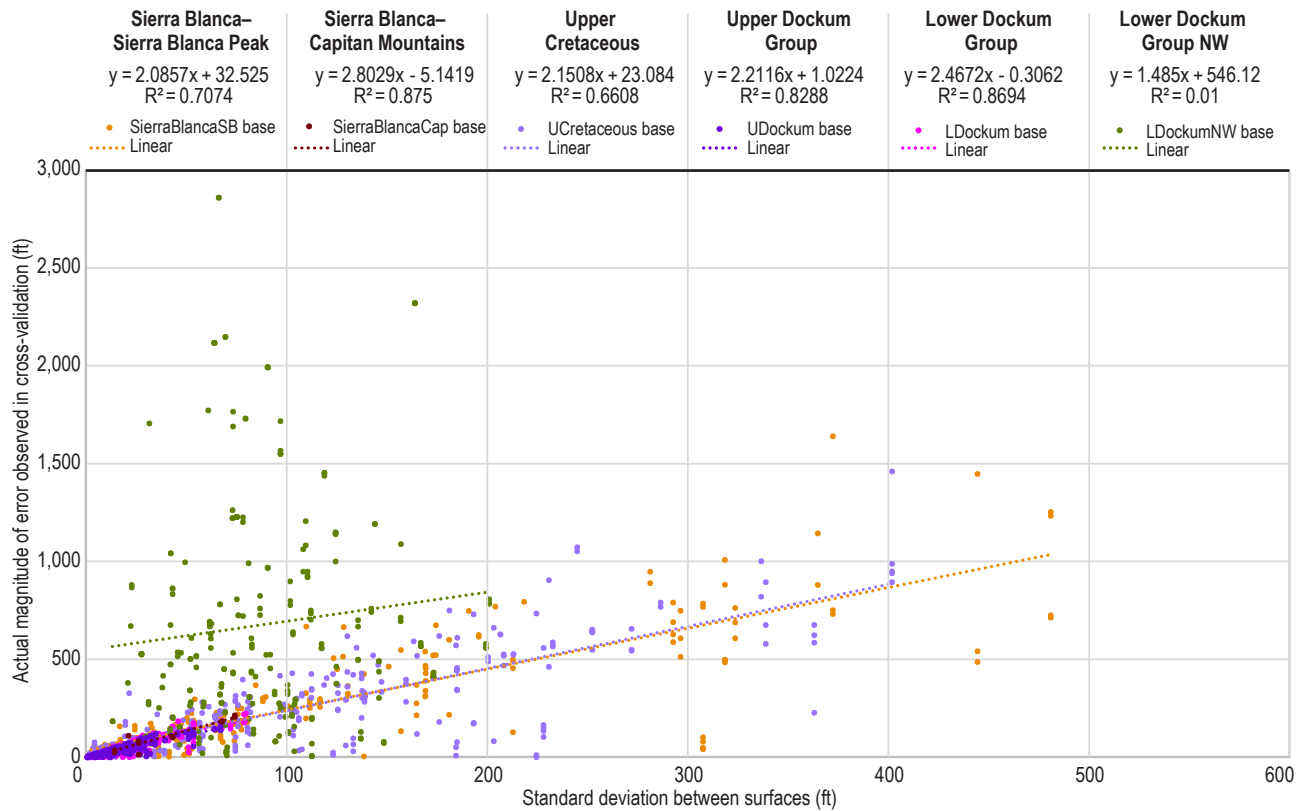


Figure 16. Validation point residuals versus the standard deviations between contact surface realizations.

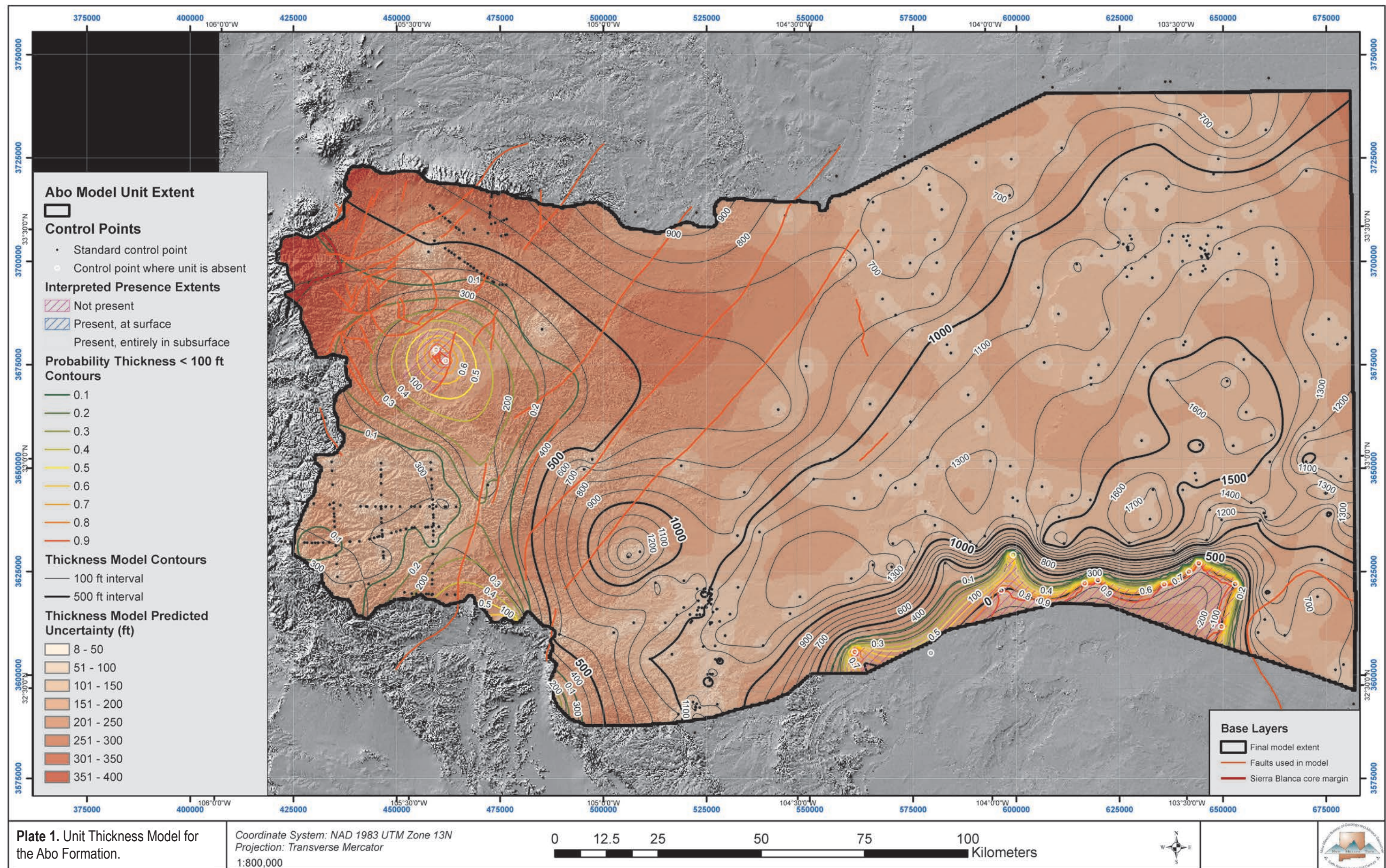
elevations of the contact surfaces in Plates 18 through 24 and 26 through 27. Note that the surfaces for the bases of the valley floor alluvium, Ogallala–PVA, and Lower Cretaceous model units do not have this uncertainty determined as these surfaces were imported directly from previous studies, and their uncertainty was not evaluated here.

Comparing the maps of the individual contributions to uncertainty to the maps of the total estimated uncertainty suggest that the dataset uncertainty is the main contributor of uncertainty, followed by the uncertainty from the local deviance kriging model. Uncertainties are highest around particularly influential control points. This reflects the significance of certain points in dictating the shape of the contact surface, particularly in areas with significant

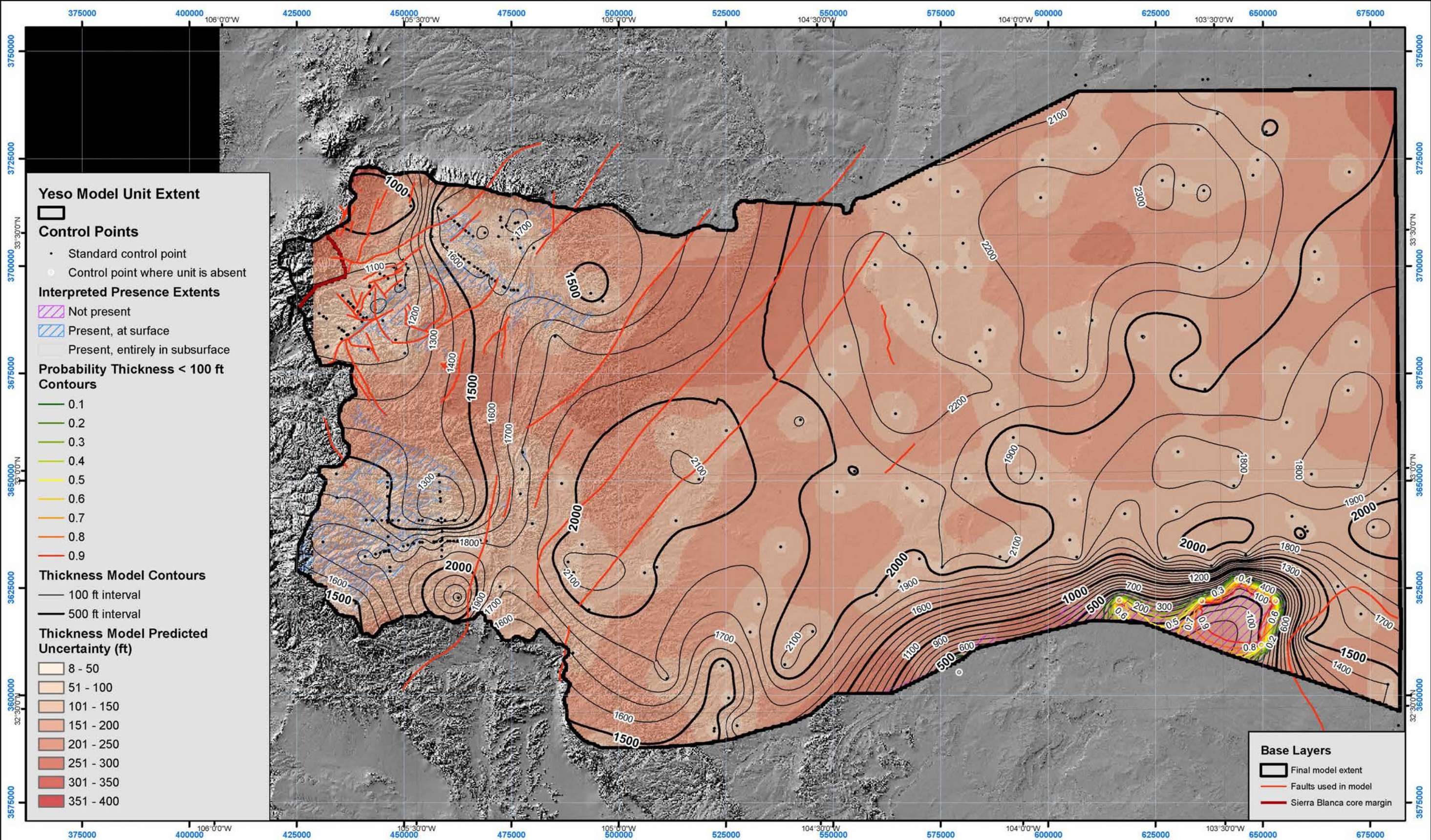
structural deformation and few control points that illustrate the structure. High uncertainties are particularly apparent along the flanks of the Pajarito Mountain structural high and the Delaware and Sierra Blanca Basins. Away from influential control points, uncertainty generally scales with distance from control points; here, uncertainty is mostly influenced by the local deviance uncertainty.

Overall, the total estimated uncertainty trends appear to demonstrate the anticipated patterns. The highest uncertainties occur in deformed areas with few control points to constrain the structure, and lowest uncertainties occur directly around control points in areas with low structural relief.



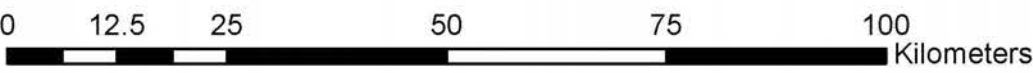




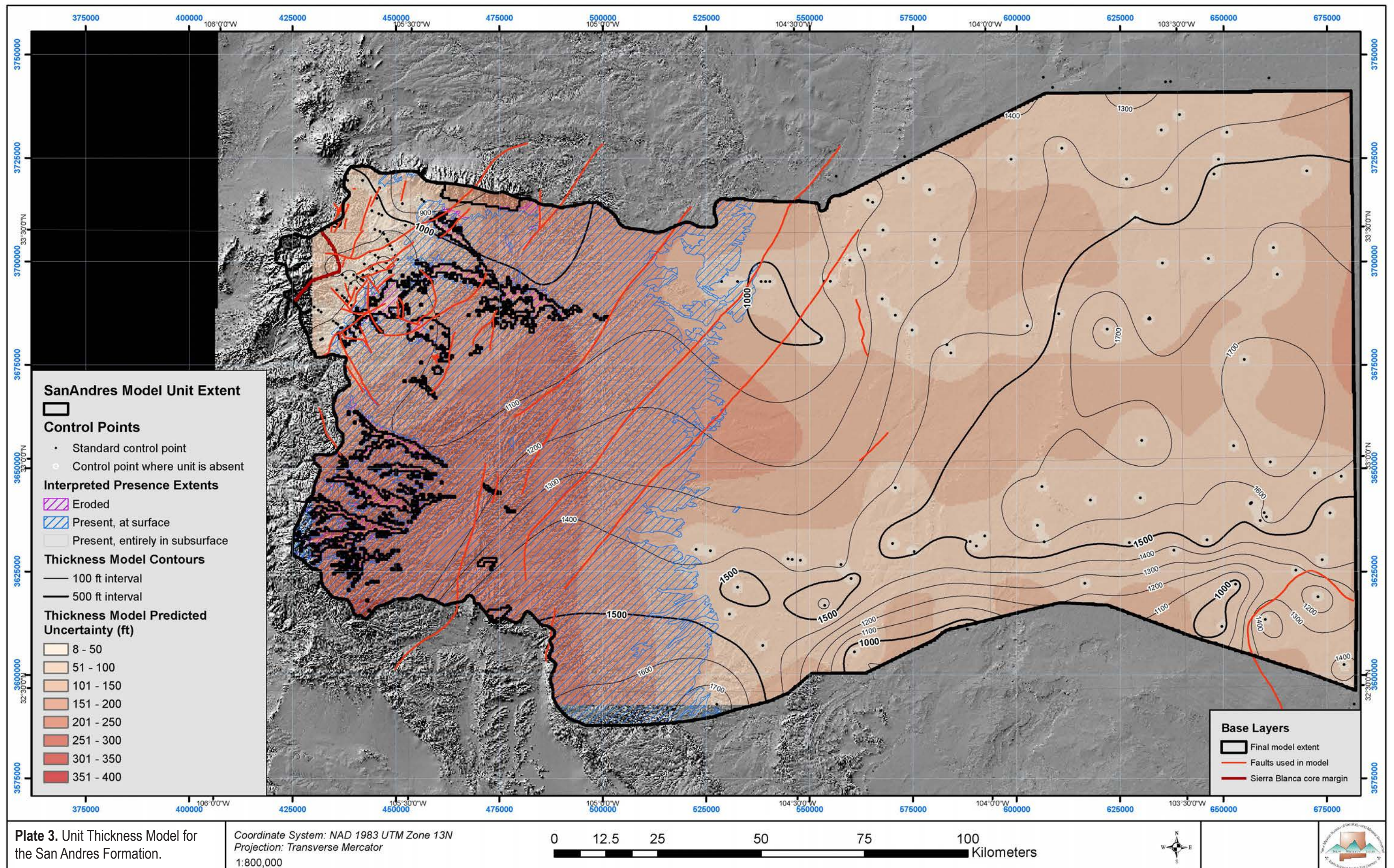


**Plate 2.** Unit Thickness Model for the Yeso Formation.

Coordinate System: NAD 1983 UTM Zone 13N  
 Projection: Transverse Mercator  
 1:800,000









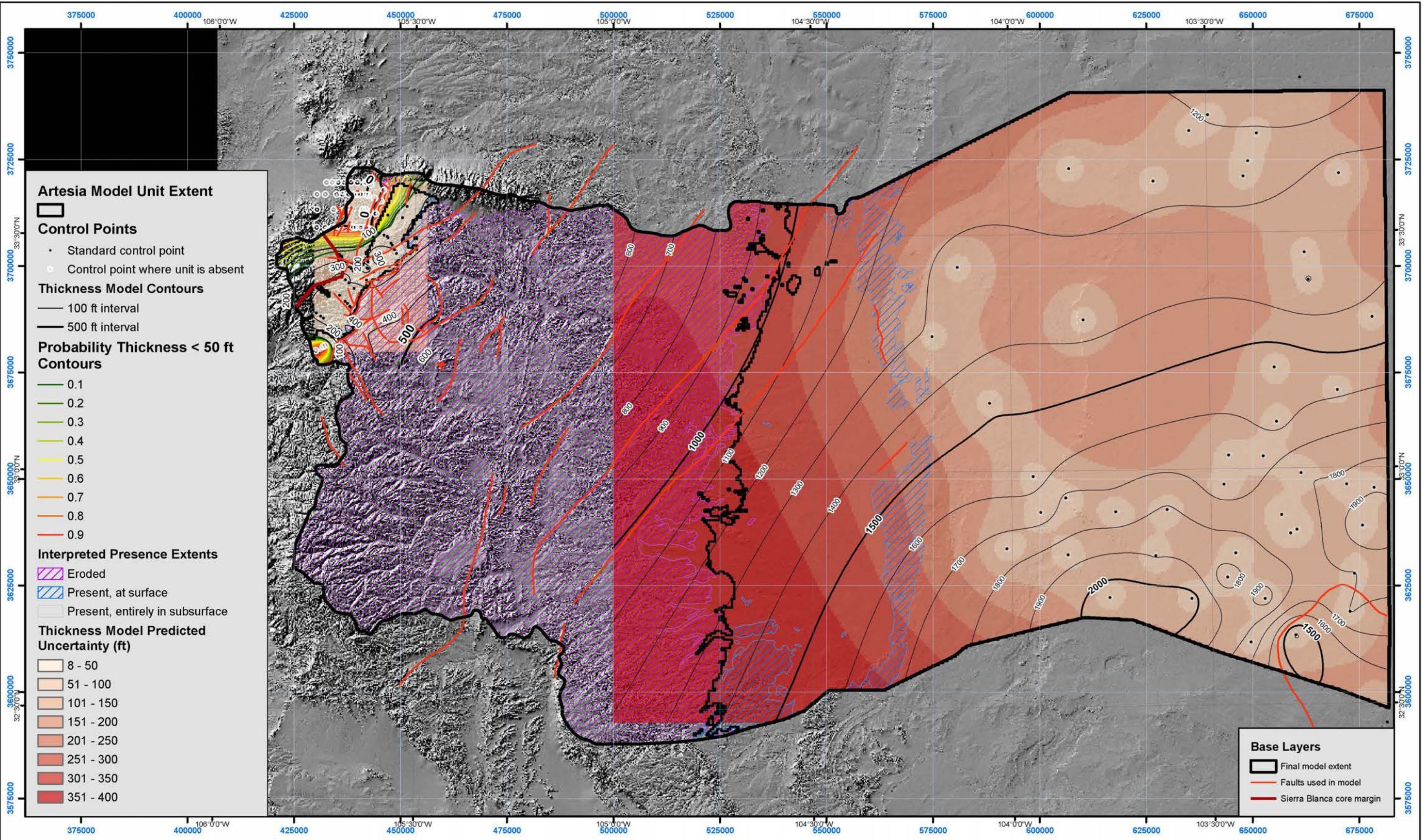
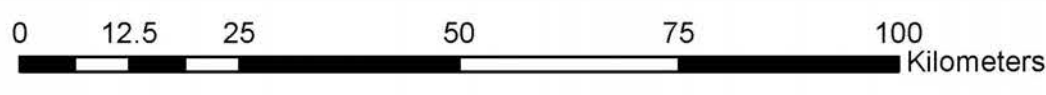
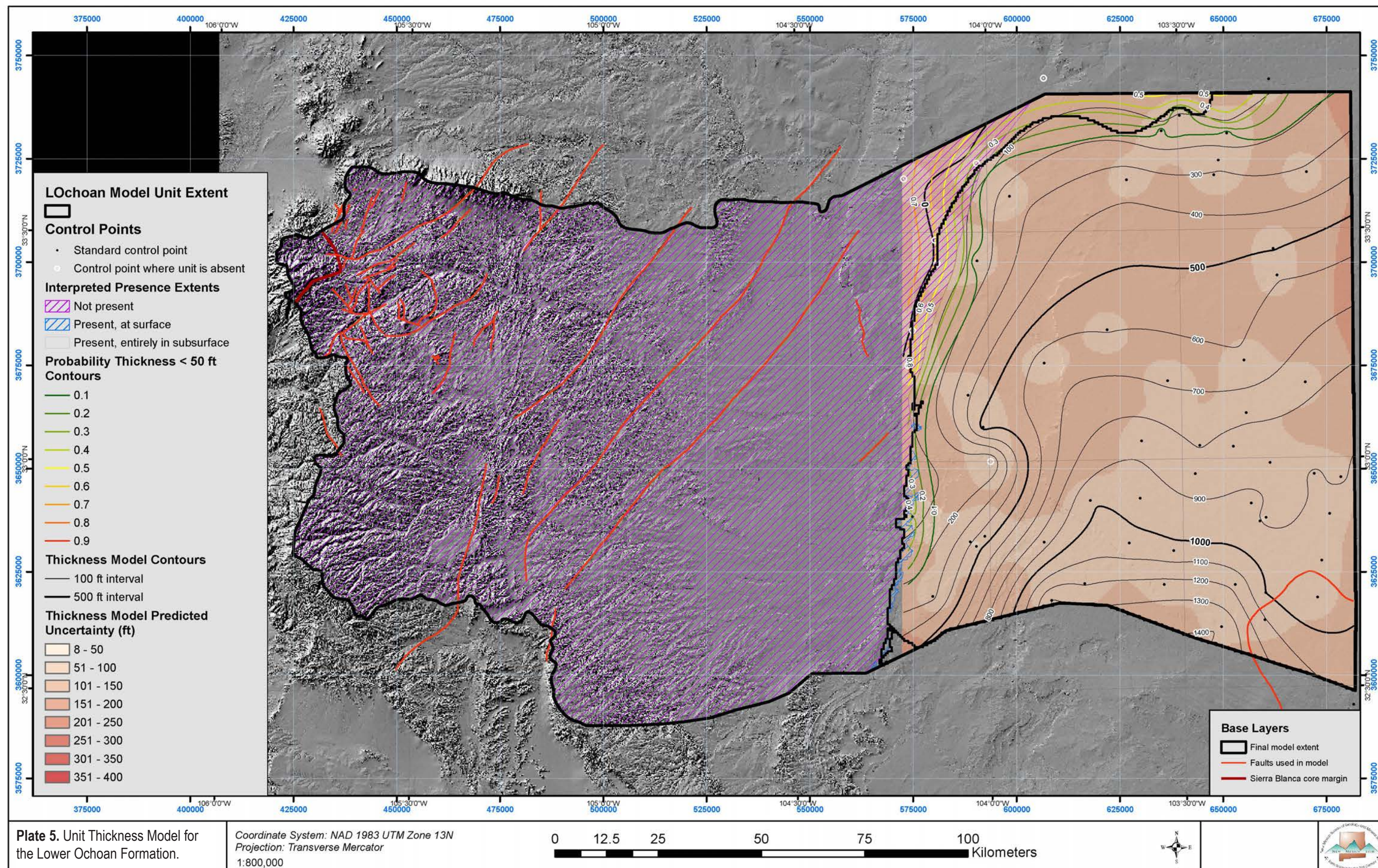


Plate 4. Unit Thickness Model for the Artesia Formation.

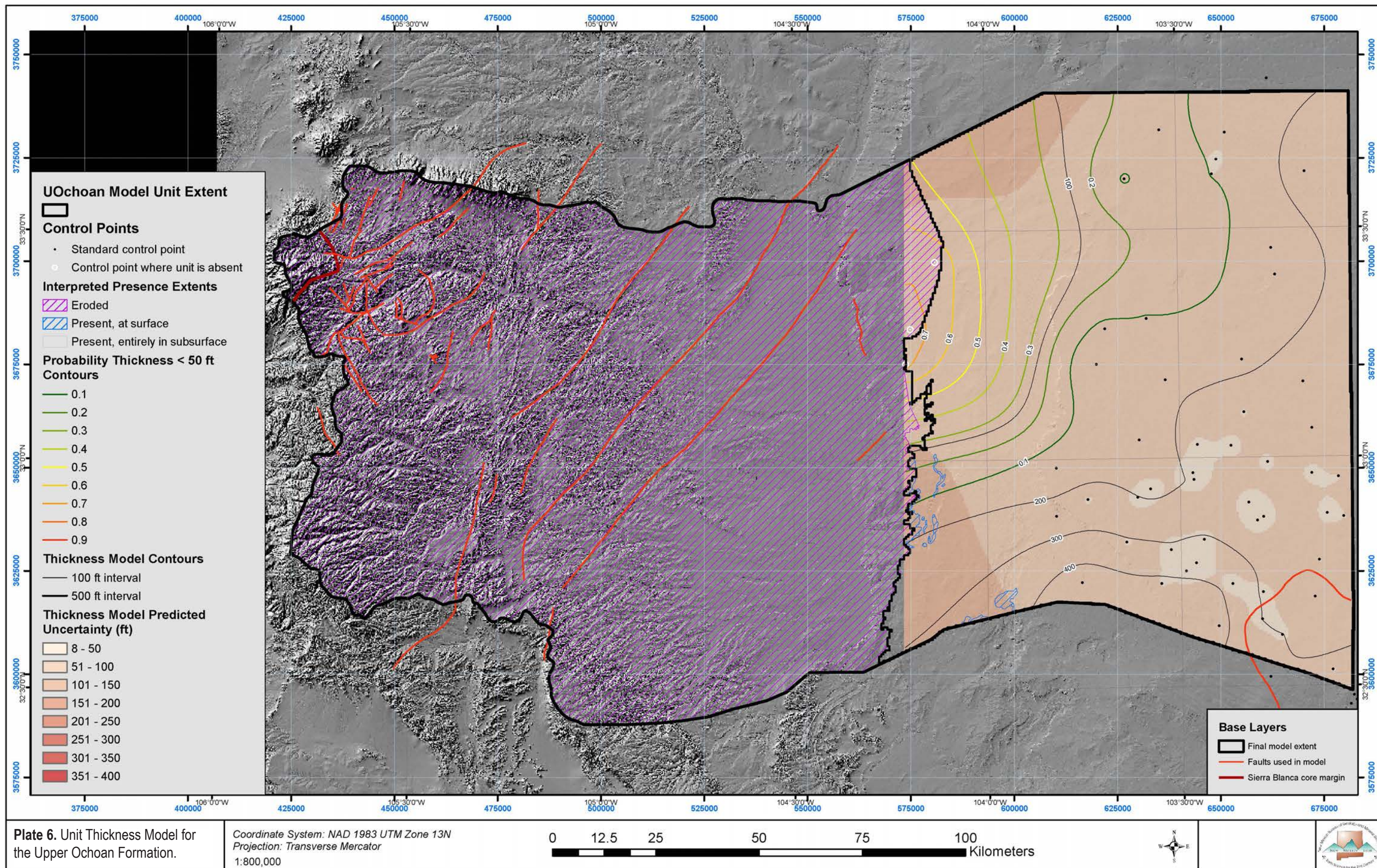
Coordinate System: NAD 1983 UTM Zone 13N  
Projection: Transverse Mercator  
1:800,000



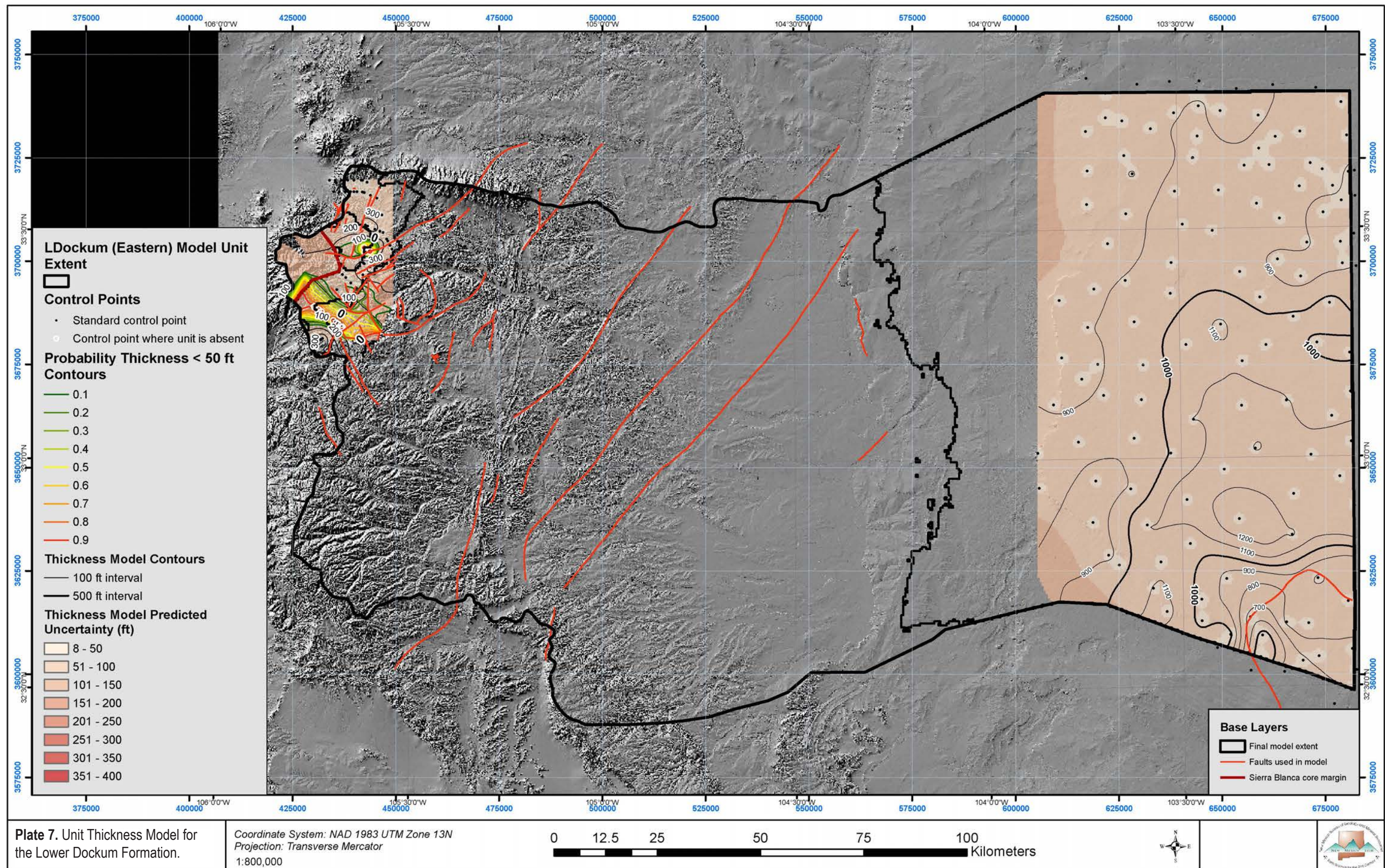




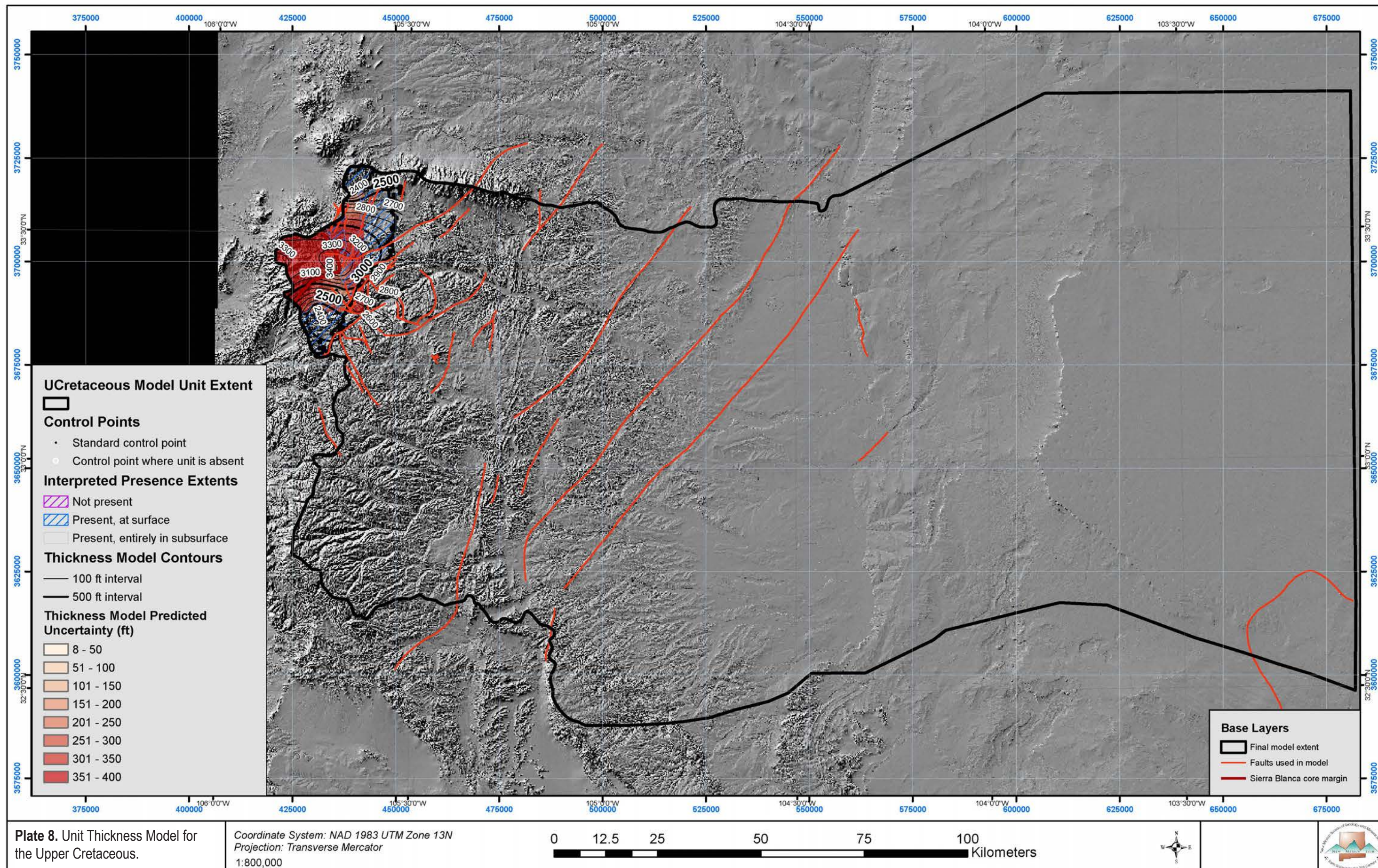




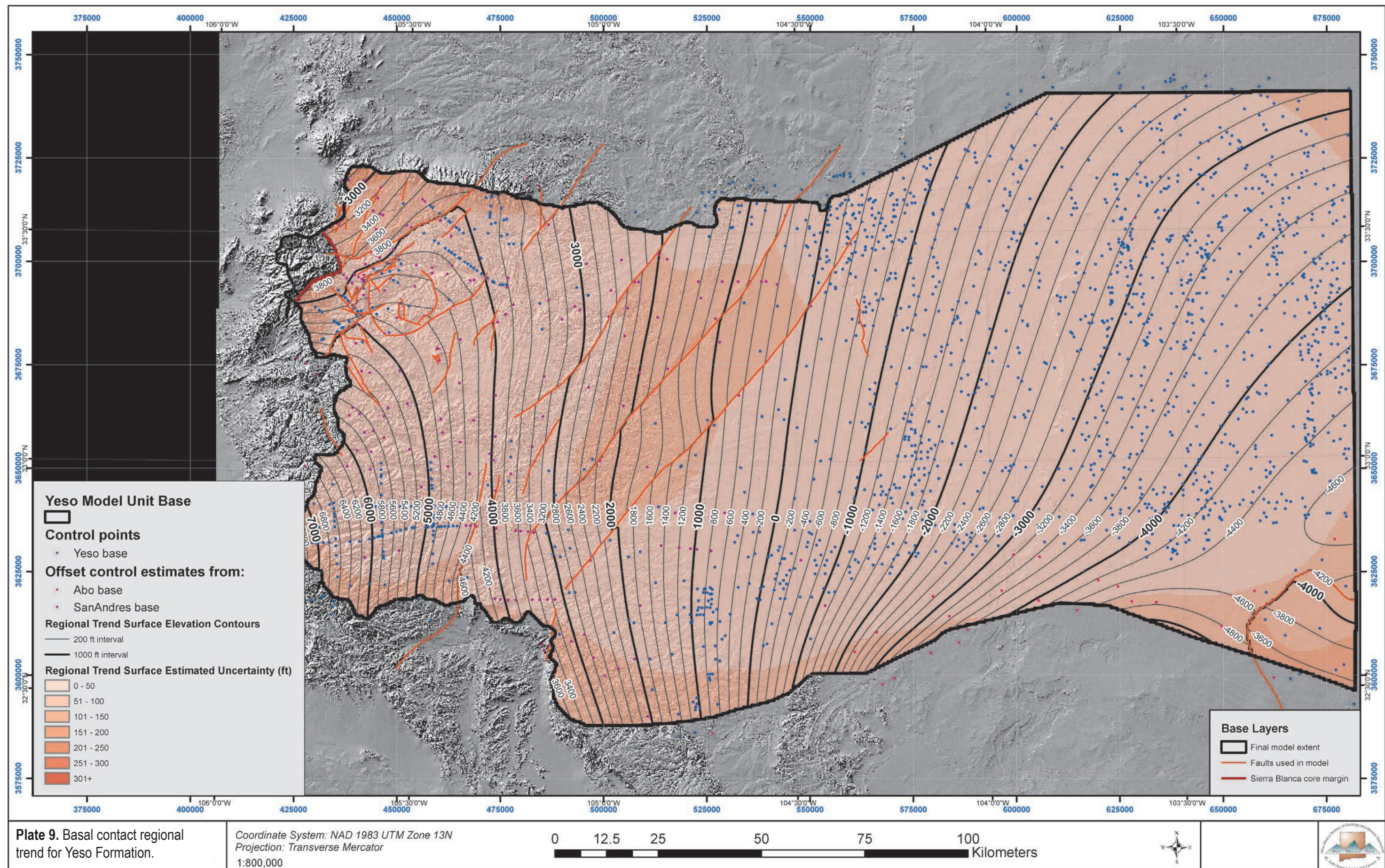




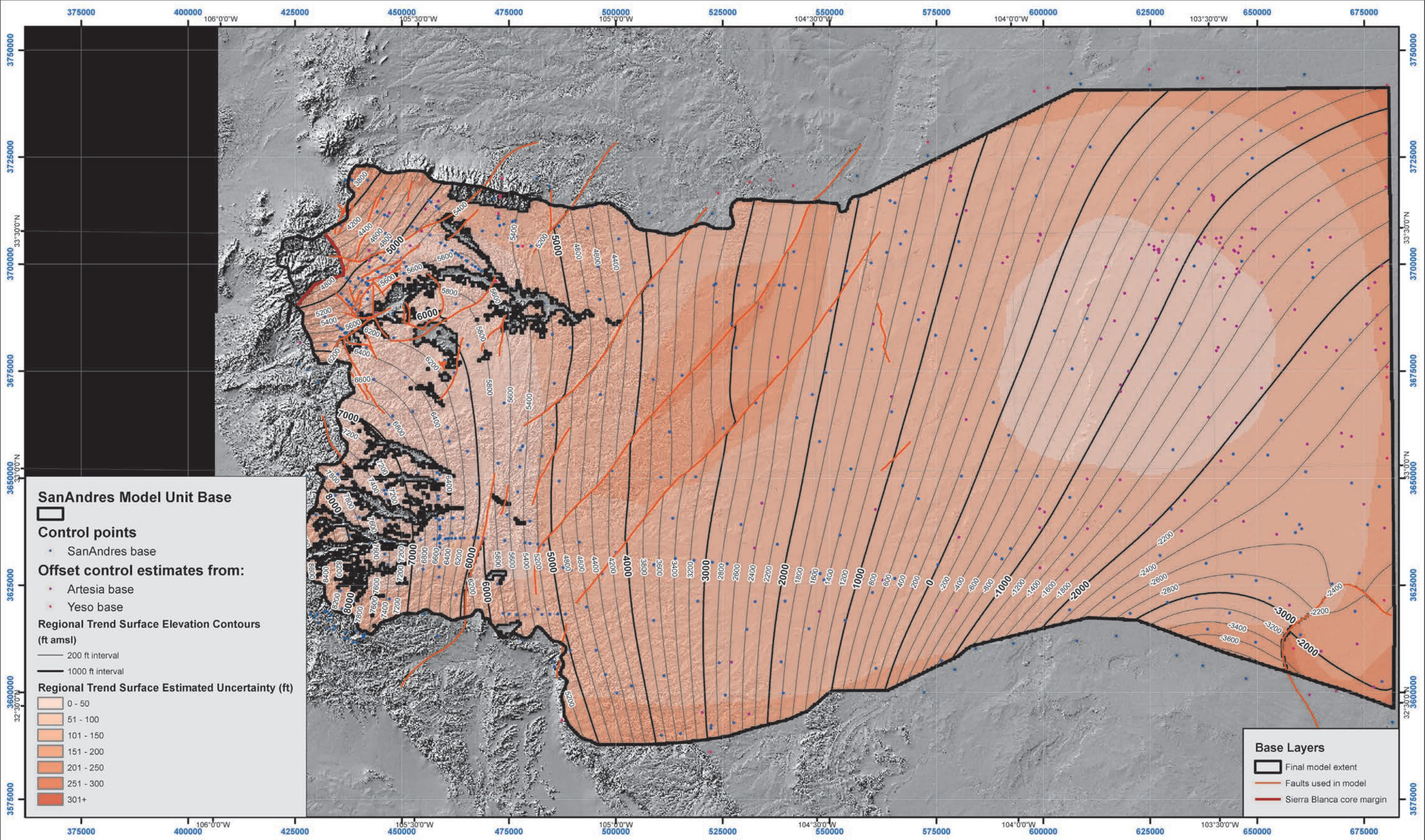






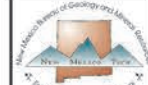




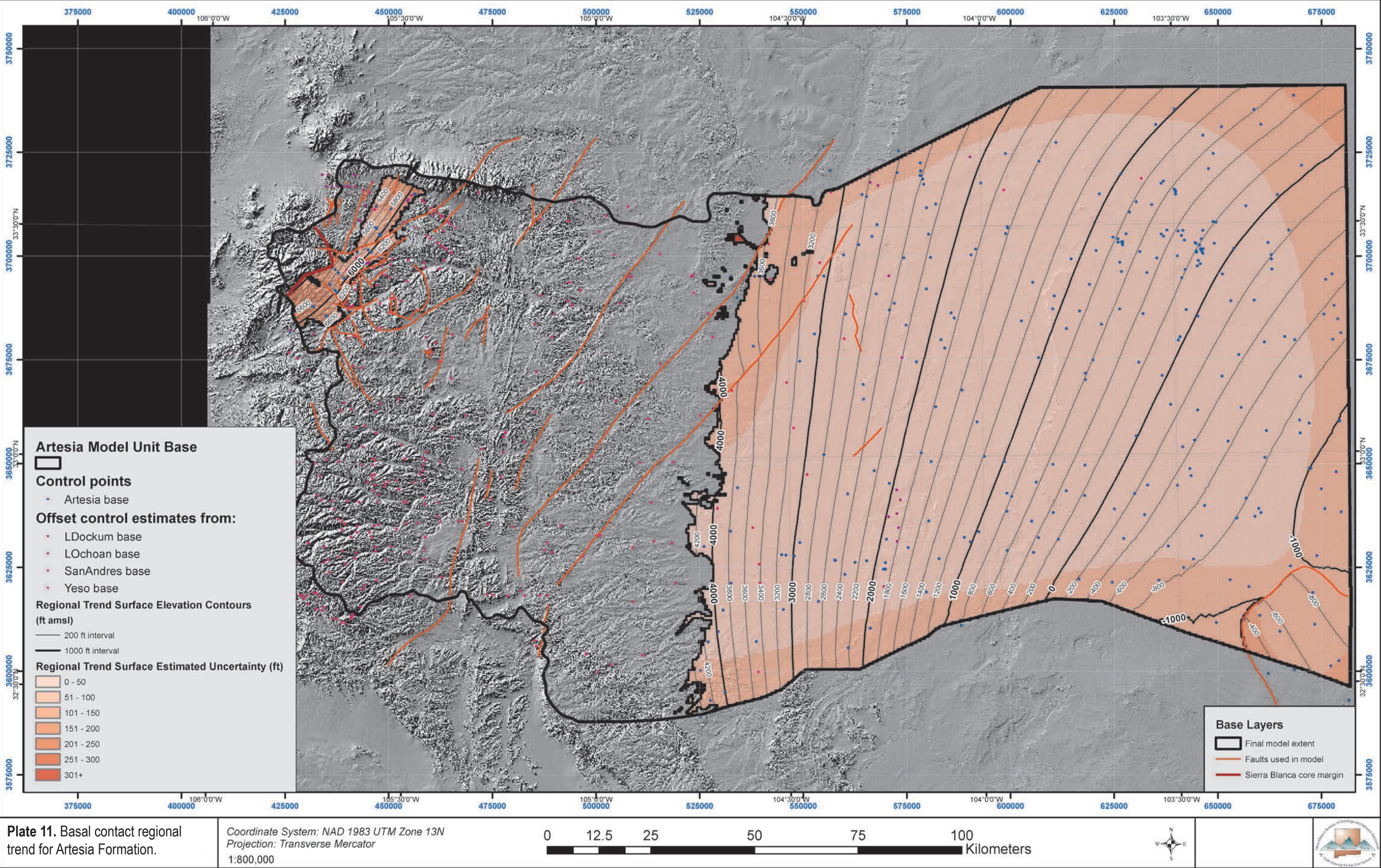


**Plate 10.** Basal contact regional trend for San Andres Formation.

Coordinate System: NAD 1983 UTM Zone 13N  
Projection: Transverse Mercator  
1:800,000









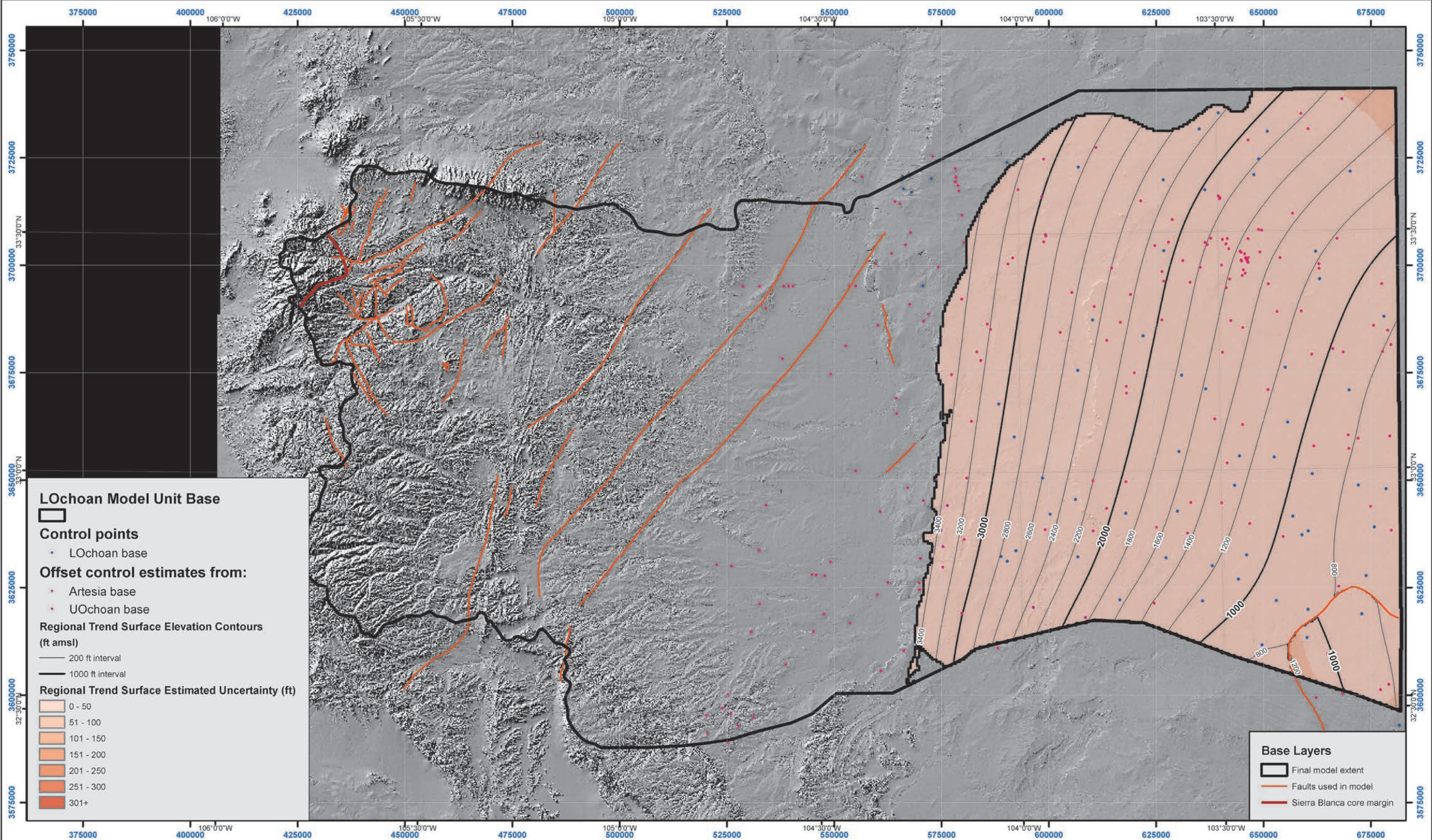
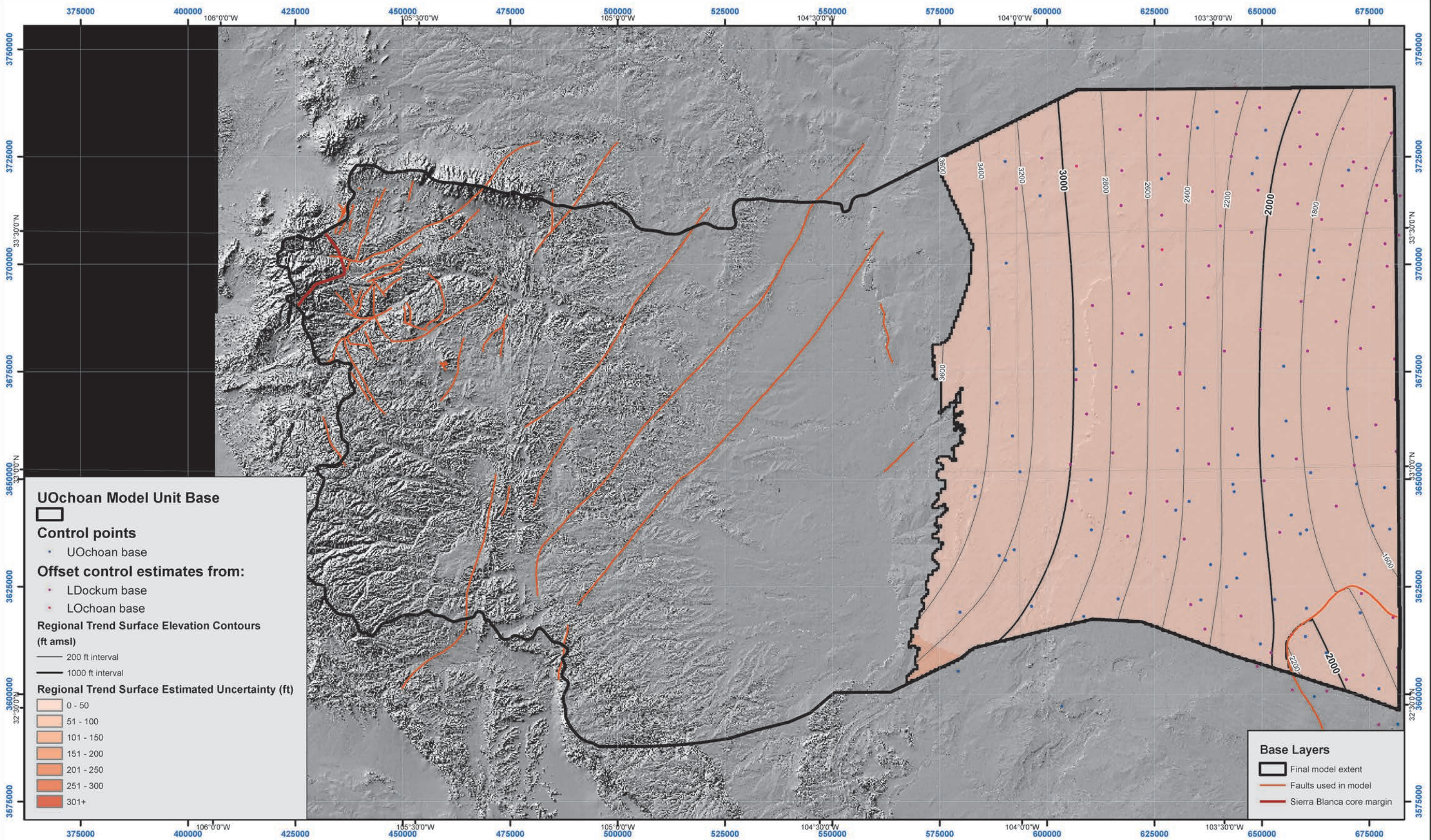


**Plate 12.** Basal contact regional trend for Lower Ochoan Formation.

Coordinate System: NAD 1983 UTM Zone 13N  
Projection: Transverse Mercator  
1:800,000

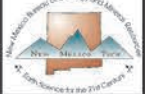




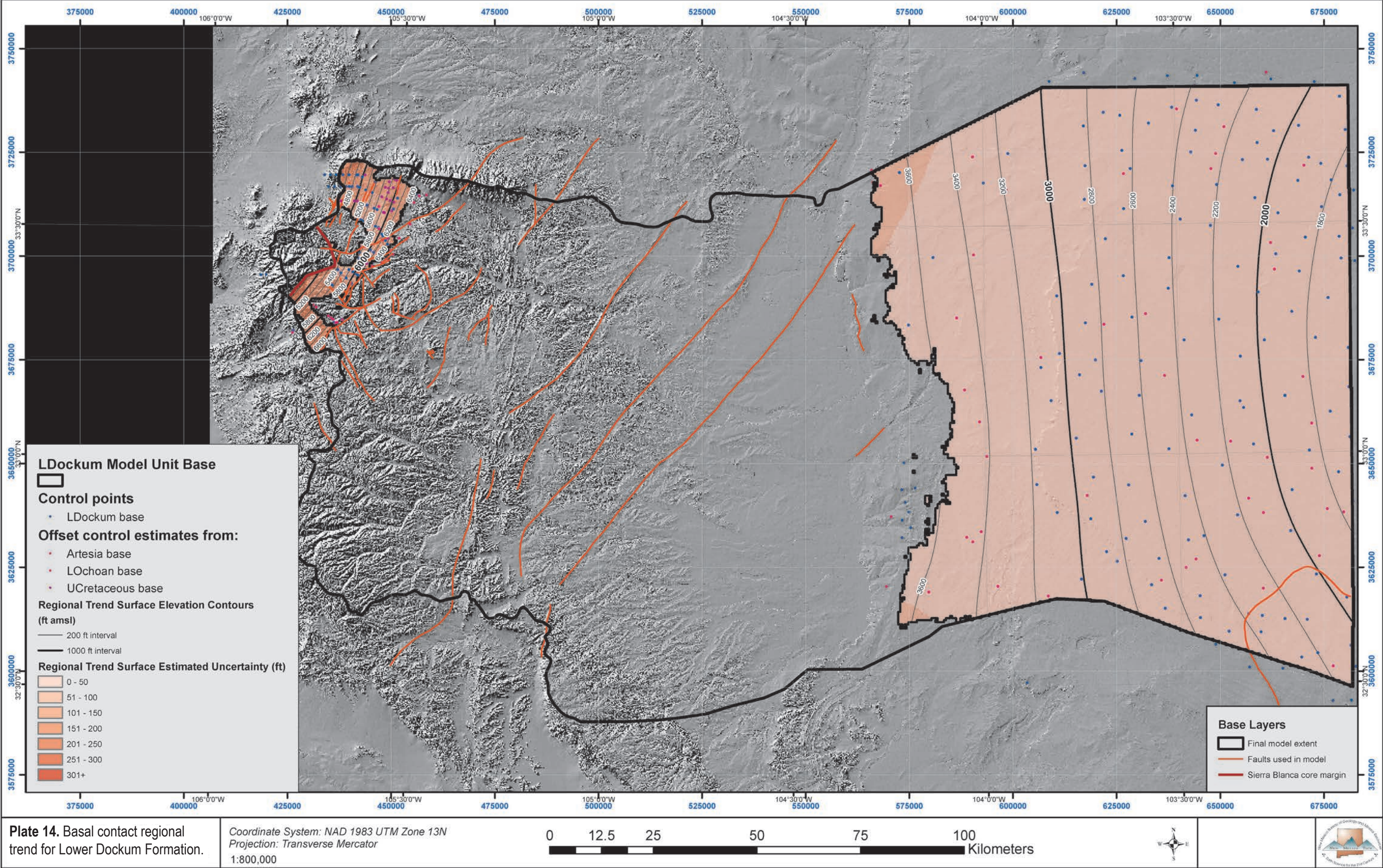


**Plate 13.** Basal contact regional trend for Upper Ochoan Formation.

Coordinate System: NAD 1983 UTM Zone 13N  
Projection: Transverse Mercator  
1:800,000









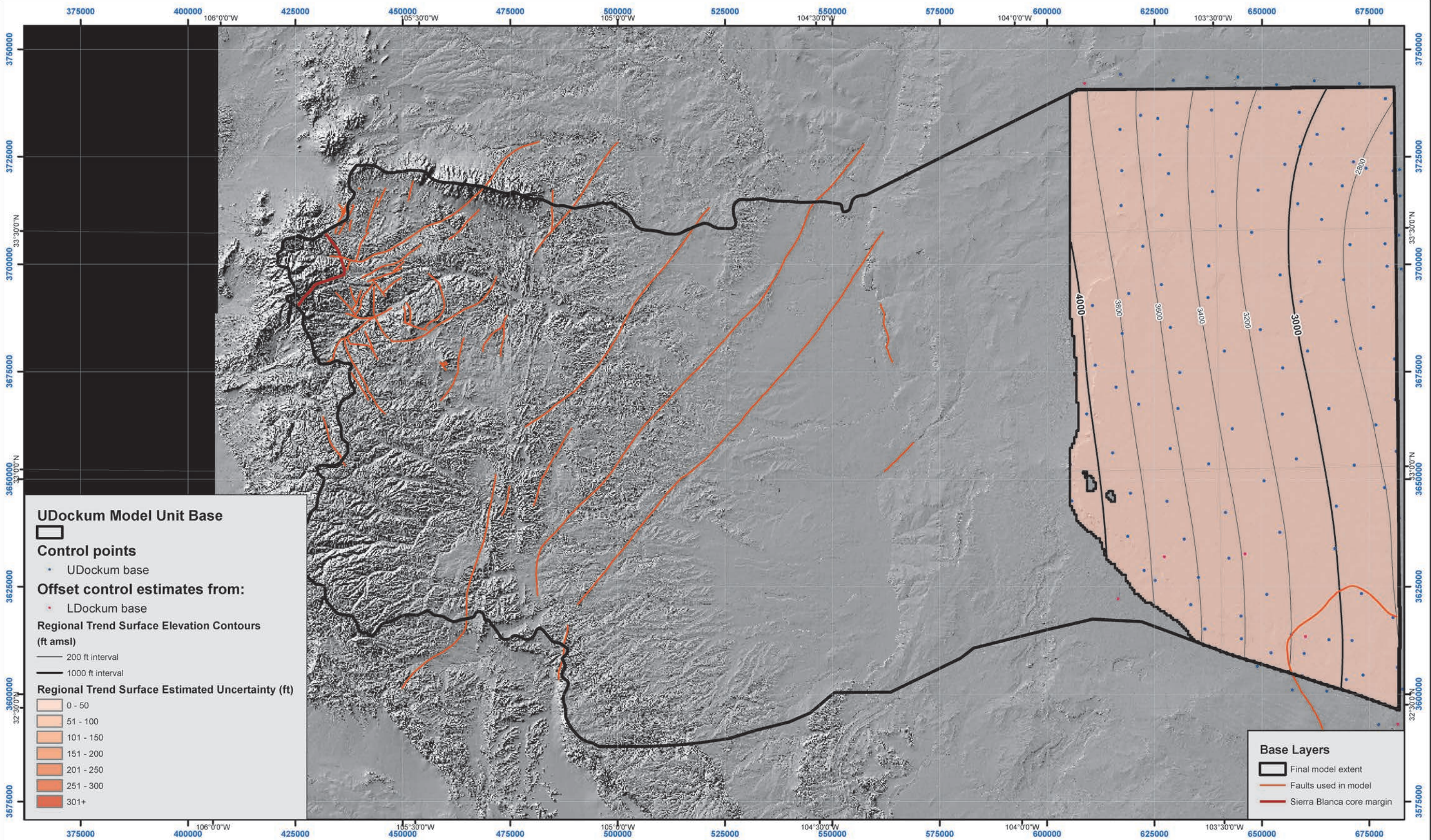
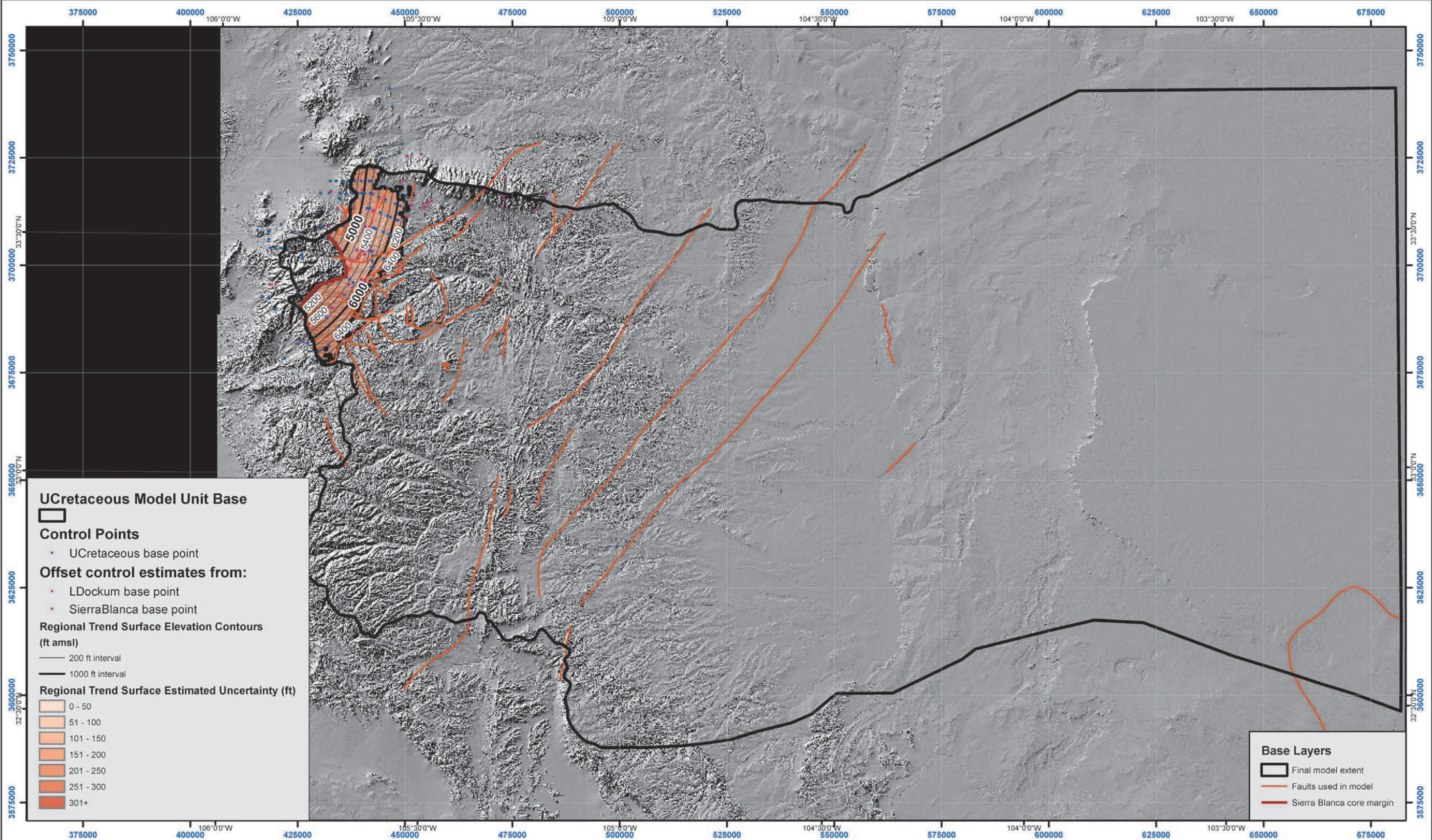


Plate 15. Basal contact regional trend for Upper Dockum Formation.

Coordinate System: NAD 1983 UTM Zone 13N  
Projection: Transverse Mercator  
1:800,000



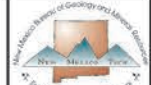




**Plate 16.** Basal contact regional trend for Upper Cretaceous.

Coordinate System: NAD 1983 UTM Zone 13N  
Projection: Transverse Mercator  
1:800,000

0 12.5 25 50 75 100 Kilometers





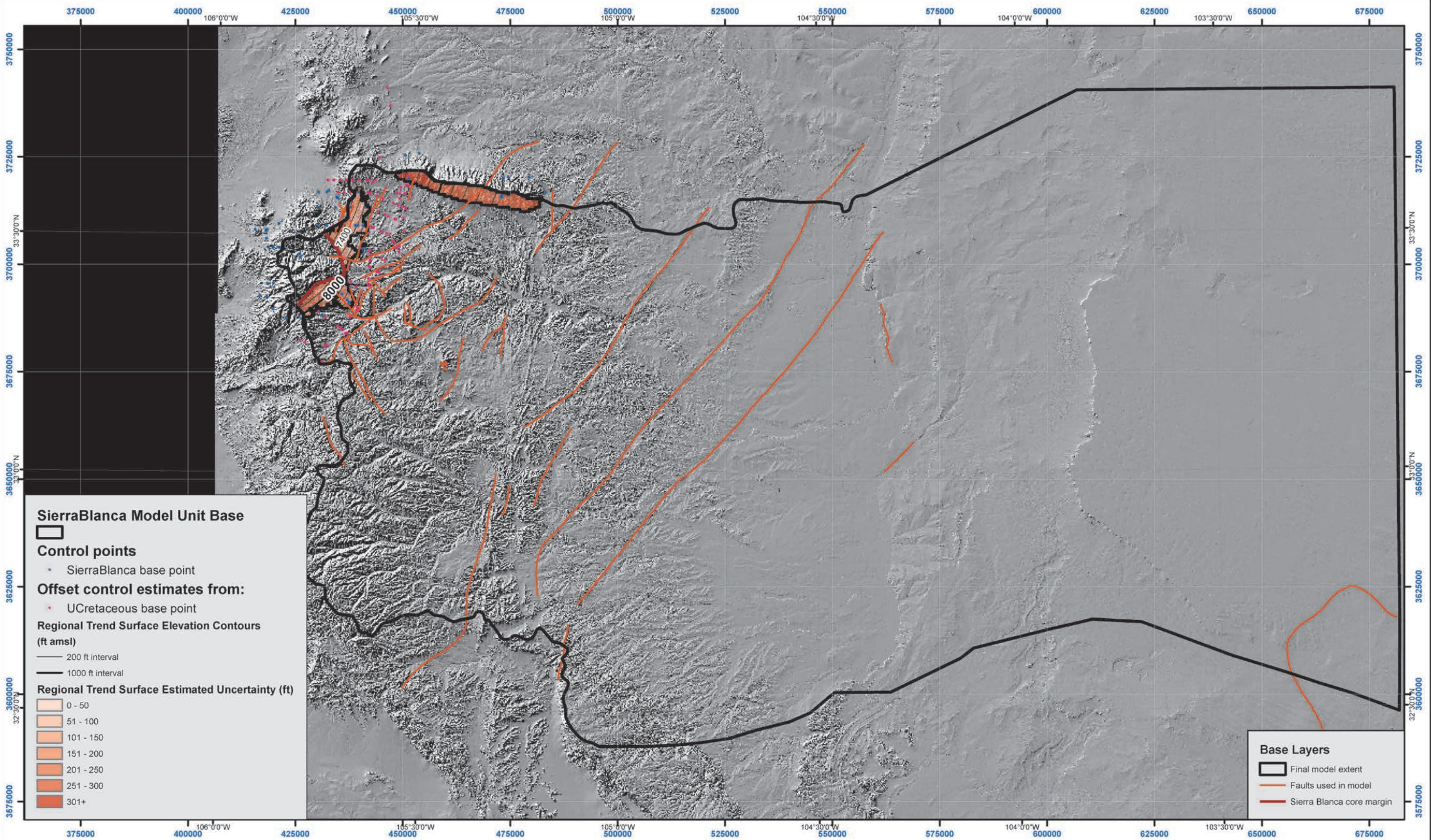
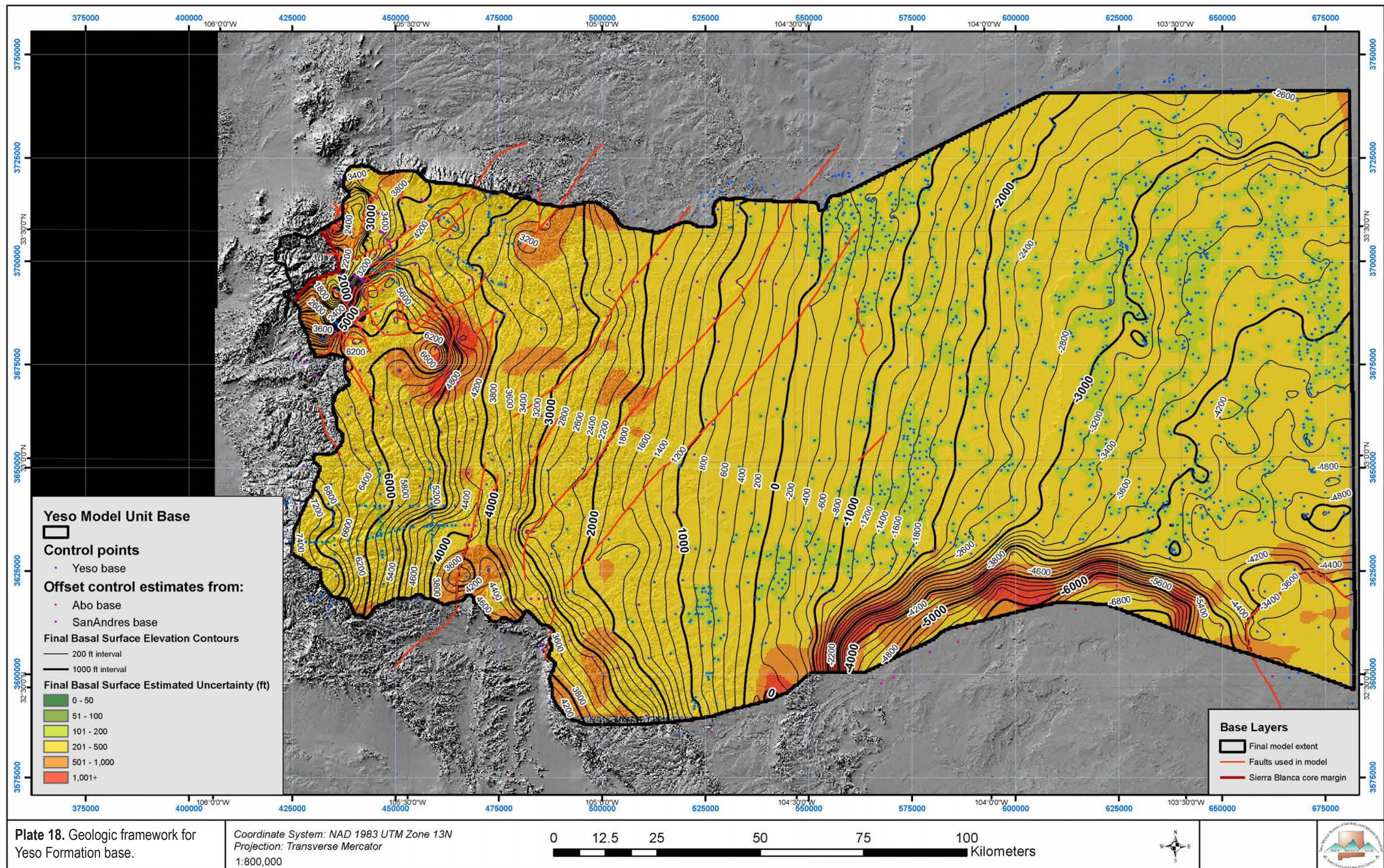


Plate 17. Basal contact regional trend for Sierra Blanca.

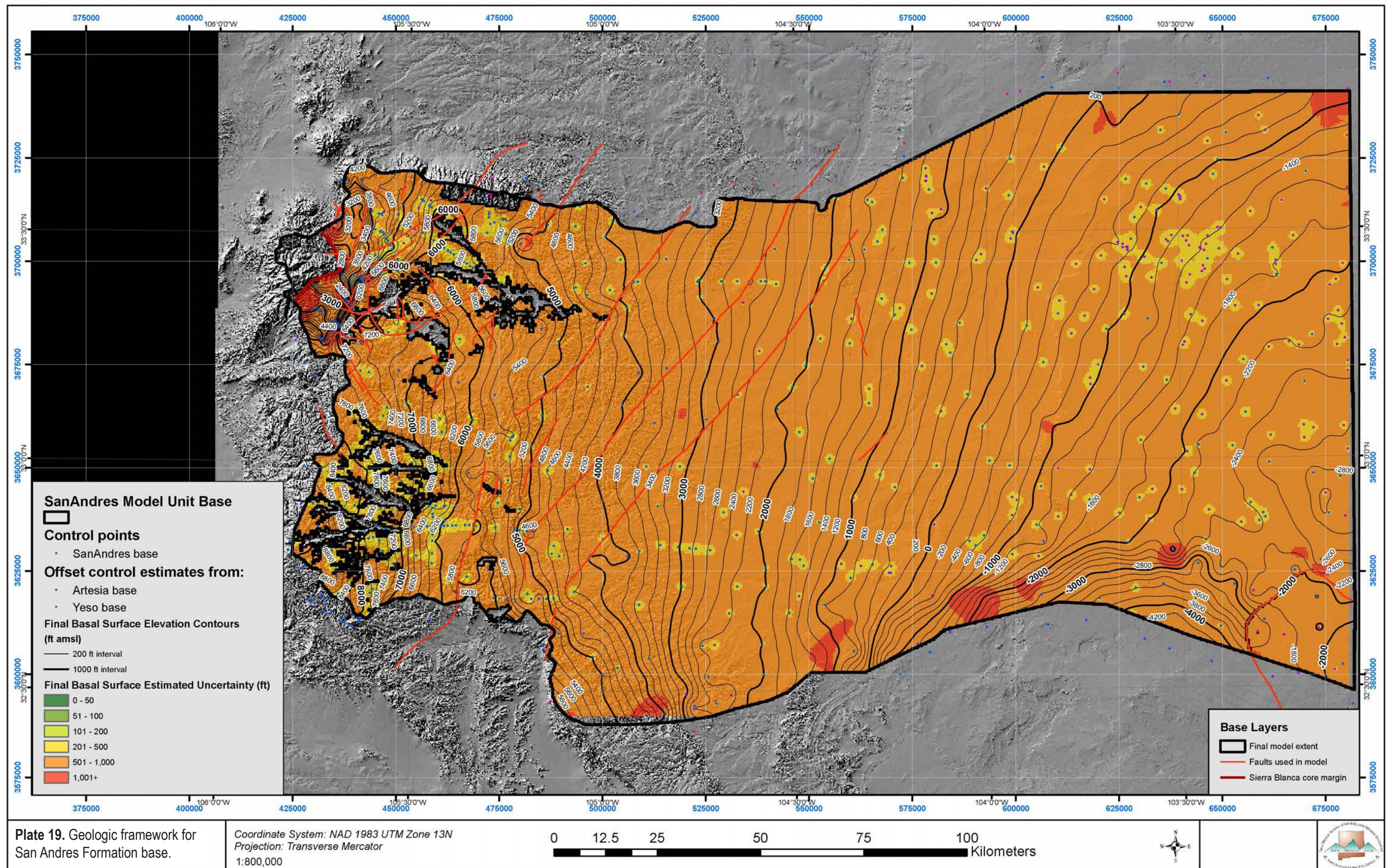
Coordinate System: NAD 1983 UTM Zone 13N  
Projection: Transverse Mercator  
1:800,000



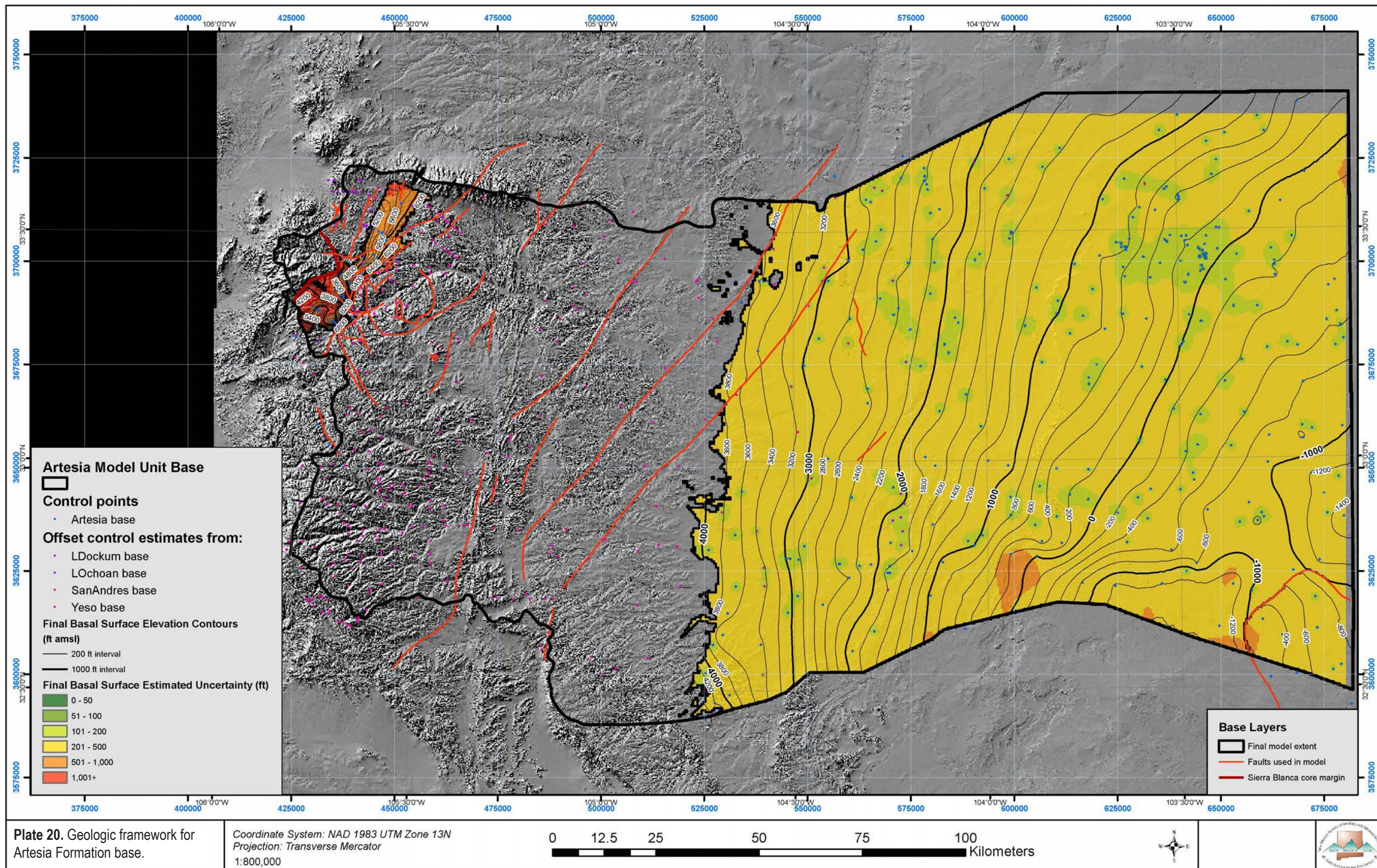




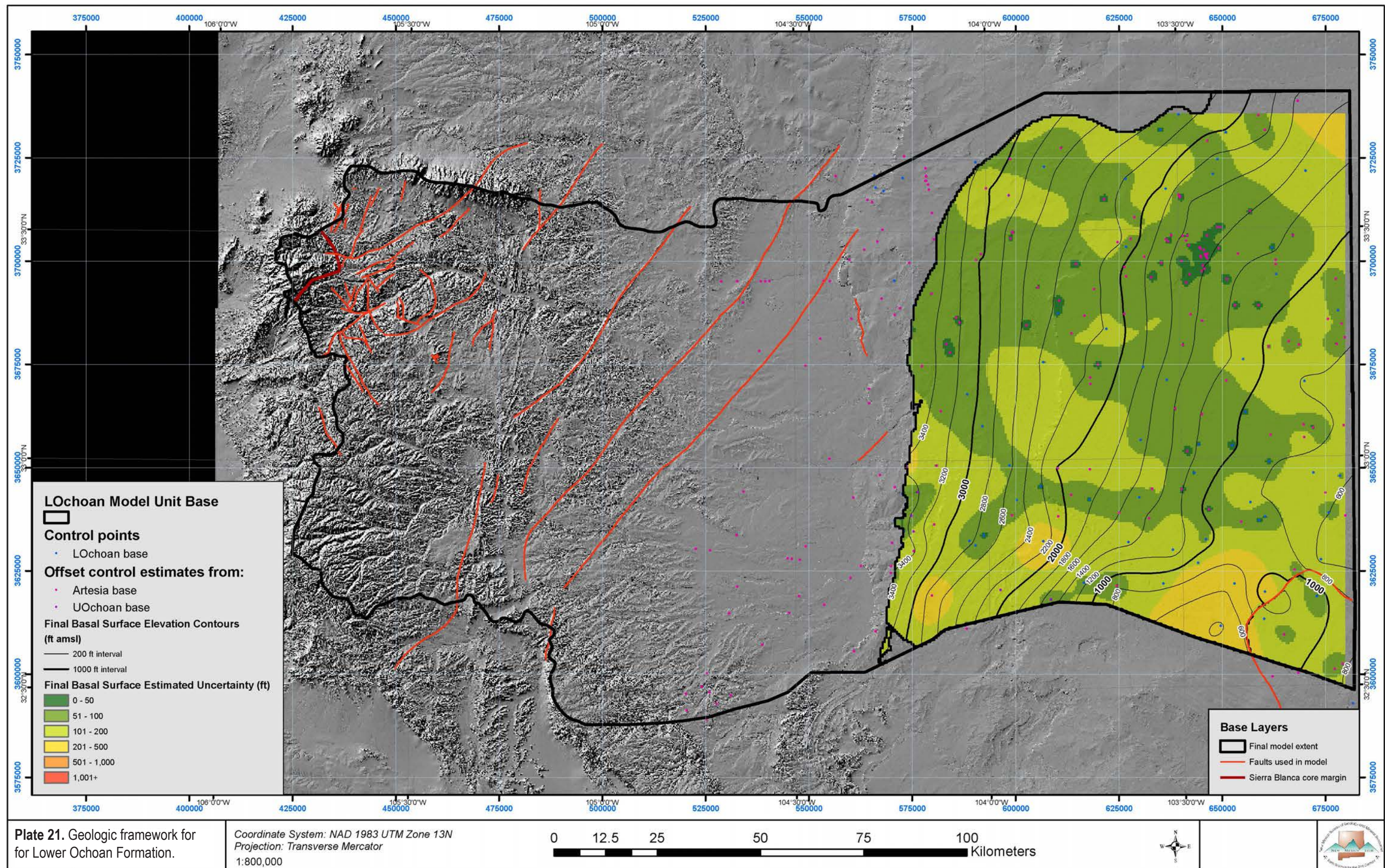




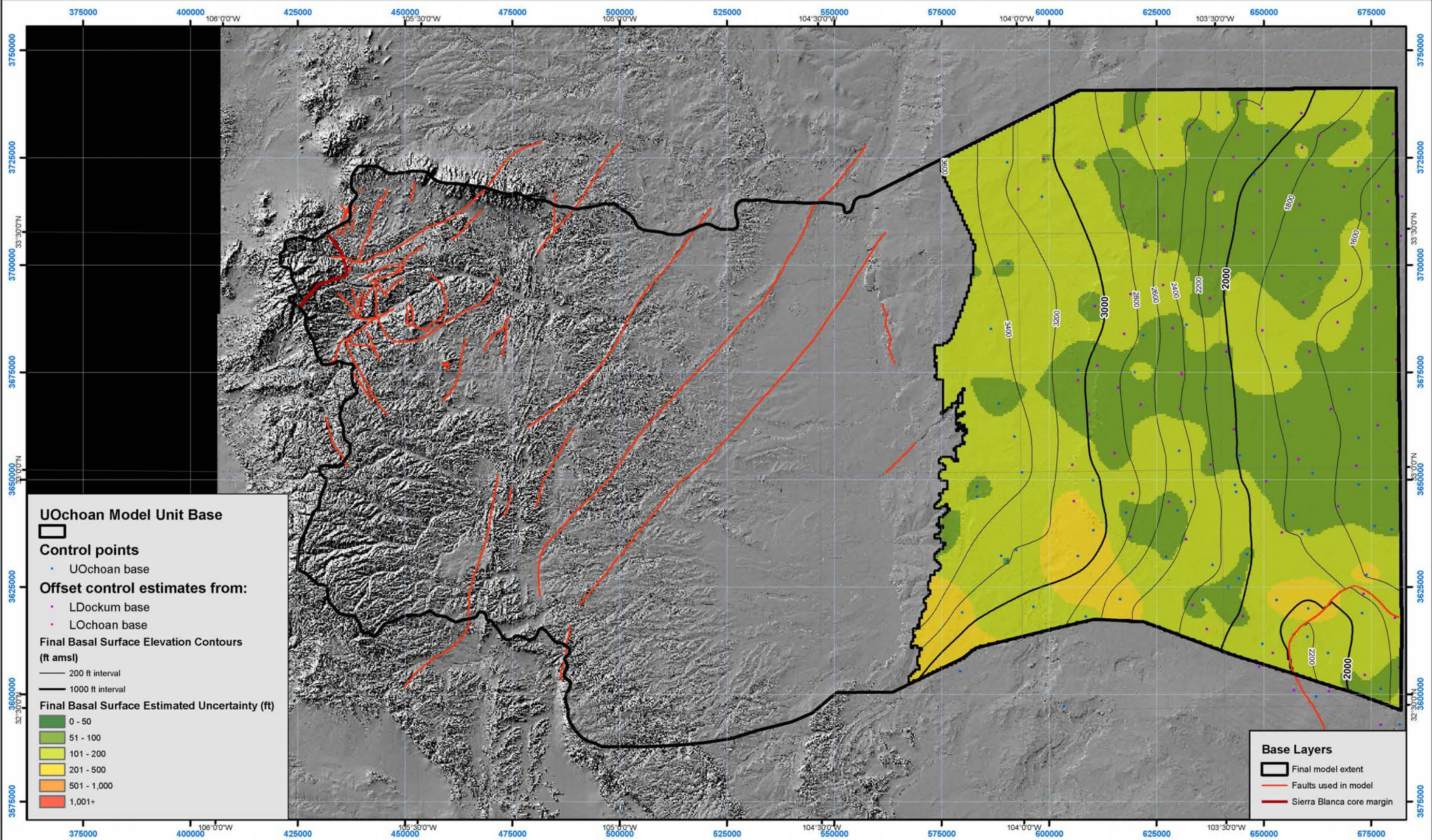






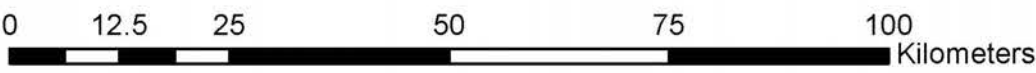




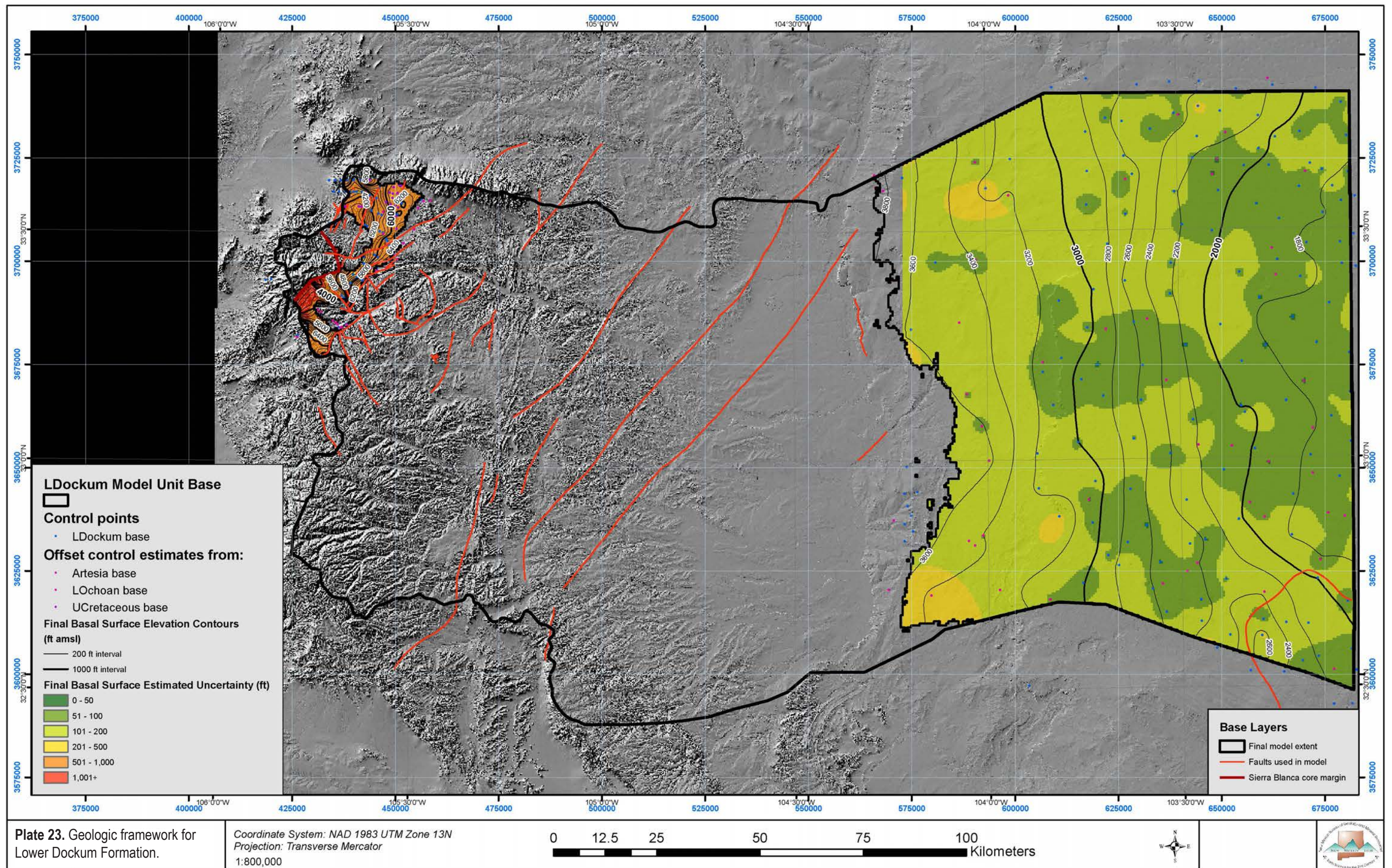


**Plate 22.** Geologic framework for for Upper Ochoan Formation.

Coordinate System: NAD 1983 UTM Zone 13N  
Projection: Transverse Mercator  
1:800,000









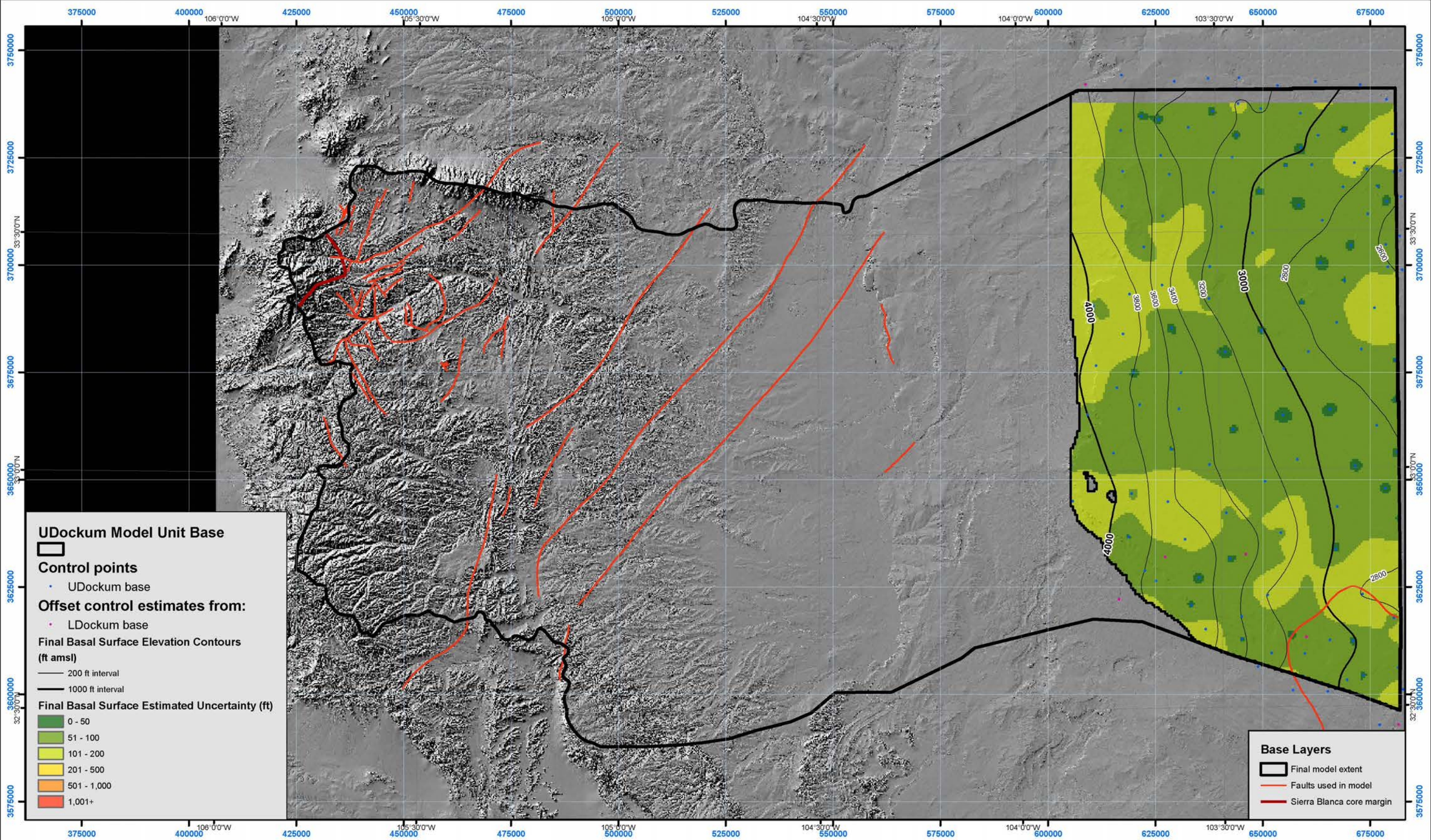
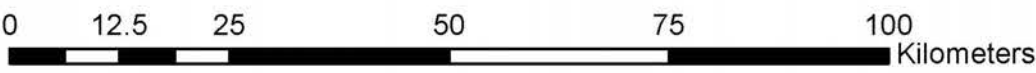
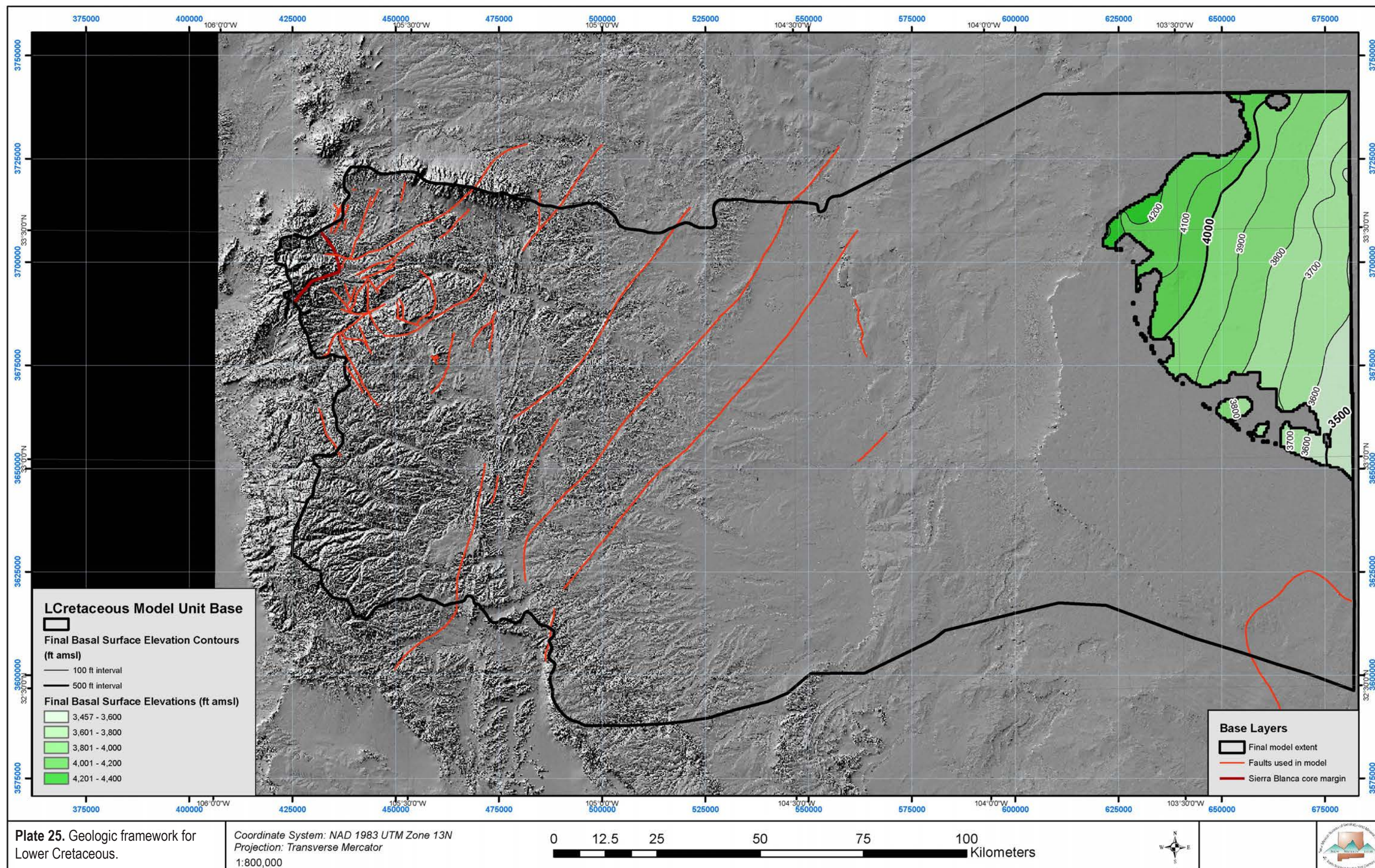


Plate 24. Geologic framework for Upper Dockum Formation.

Coordinate System: NAD 1983 UTM Zone 13N  
Projection: Transverse Mercator  
1:800,000









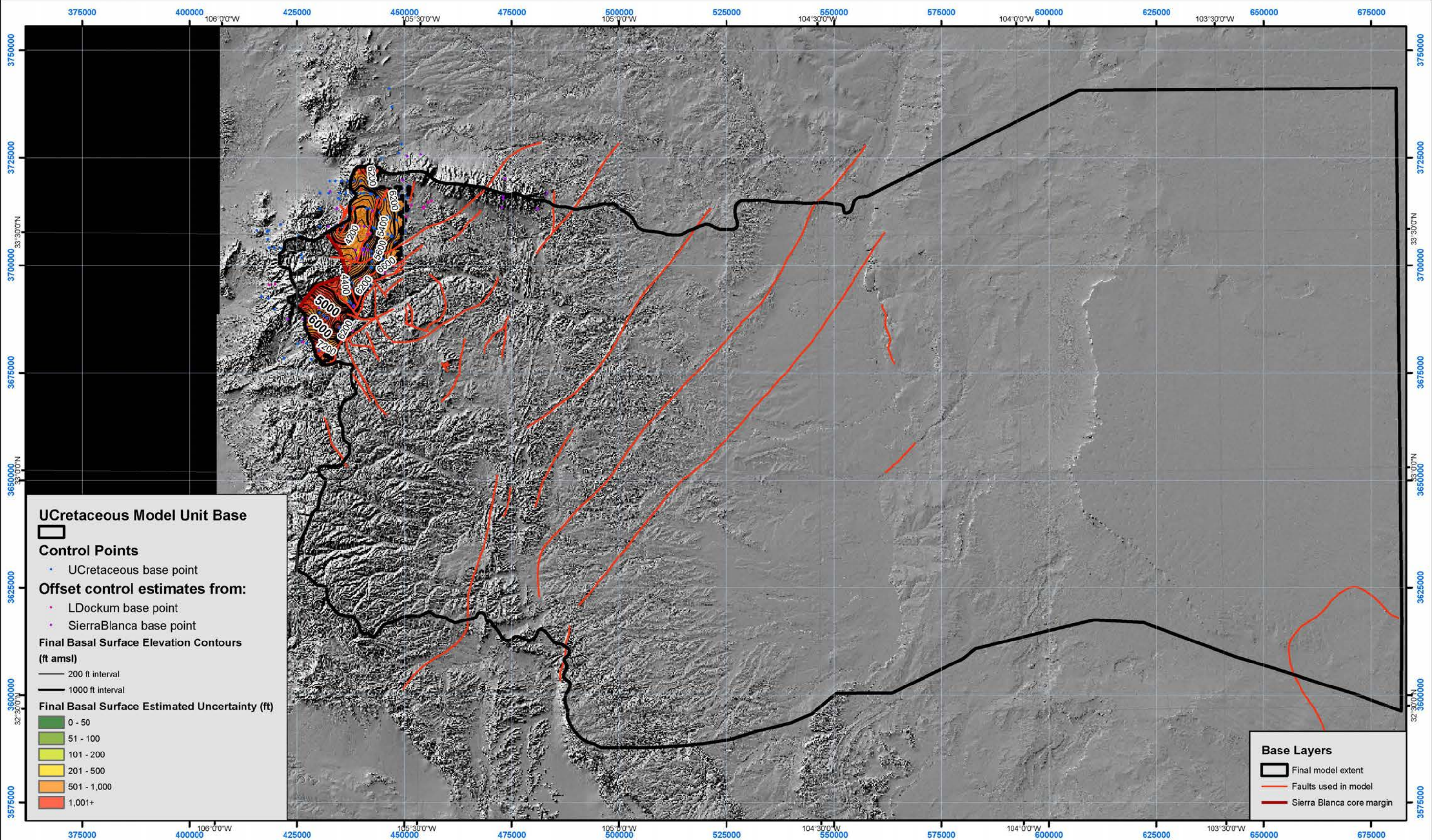


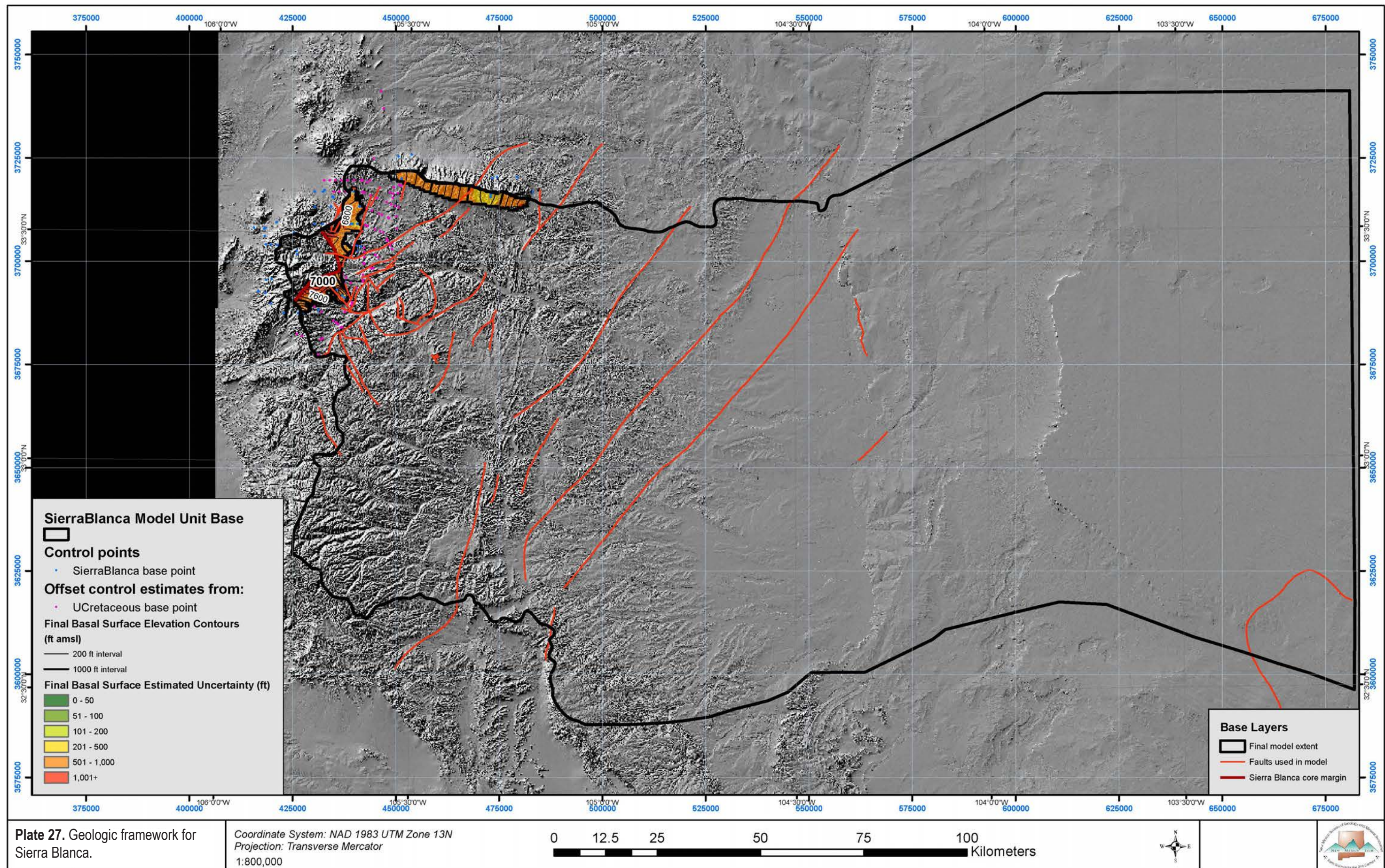
Plate 26. Geologic framework for Upper Cretaceous.

Coordinate System: NAD 1983 UTM Zone 13N  
Projection: Transverse Mercator  
1:800,000

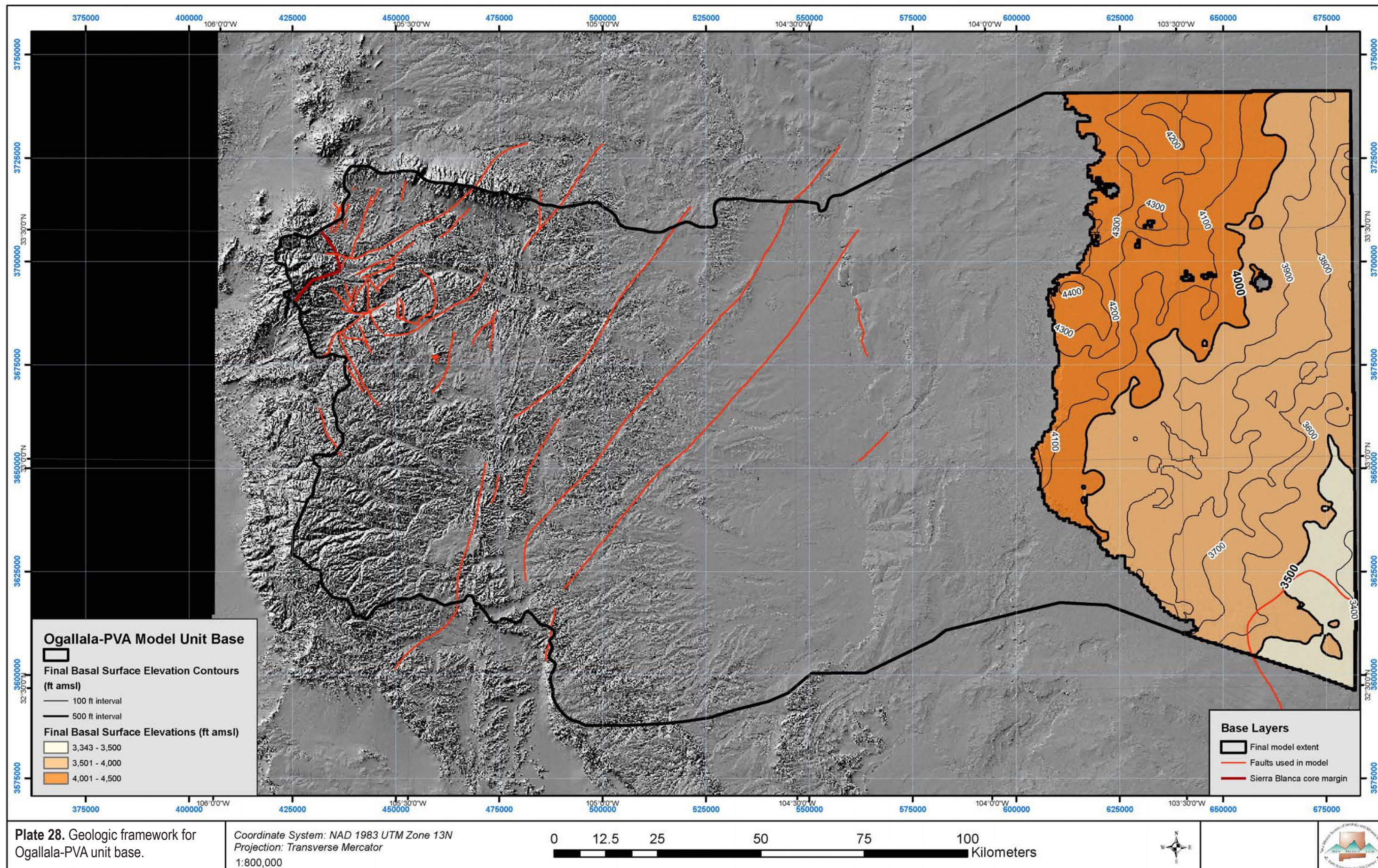
0 12.5 25 50 75 100 Kilometers



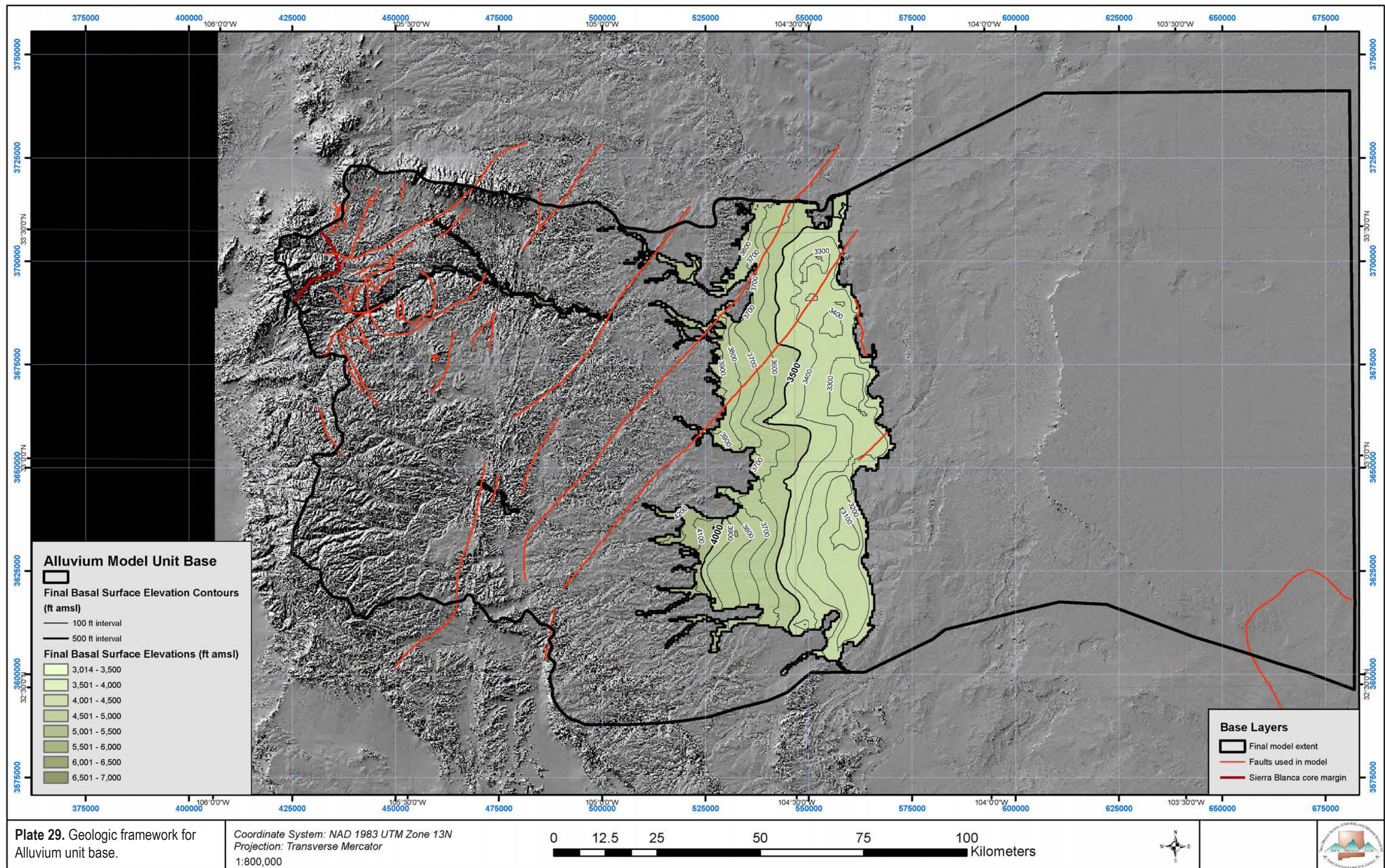
















Bitter Lake is sourced from the Lost River (also known as Bitter Creek). The lake is seasonally dessicated, as in this July 2016 photo.  
*Photograph by David J. McCraw*



## V. RESULTS

The goals of this project were to develop a 3D, digital, GIS-ready, subsurface geologic model using methods designed to incorporate a variety of input data, maximize objective utilization of data, minimize modeler subjective choice, and explicitly evaluate and quantify the confidence in the modeling process and results. The capacity of the developed methods and model to achieve these goals is described below. Particular challenges are also discussed.

### Discussion of Methods

In general, the methods developed address the goals outlined above. In terms of combining a variety of datasets, the LOO CV technique used appeared to adequately identify incompatible data points. A major challenge was in combining soft projected data (structure contours, cross-sections) with hard well data in structurally deformed regions of the Pecos Slope. One admitted subjective choice was to emphasize the hard data by preferentially removing soft data control points in the vicinity of hard data points. A perhaps superior method would include both but apply weights to the different datasets that would reflect the confidence in each data source. Unfortunately, the final interpolation strategy used here had limited opportunities for applying weights to individual data points.

Objective use of data was sufficiently emphasized and subjective modeler choice minimized. Some arbitrary choices were made, such as in evaluating data points during quality and compatibility assessment and particularly during thinning of points from data sources that resulted in many control points, such as structure contours and surface-mapped contacts. One weakness of the method used that was noted was the challenge of mixing datasets of strongly contrasting data point densities. Variable point density across the study area had a noticeable effect on semivariogram plots and the optimized variogram models. Thinning the dense datasets was necessary, but, on the other hand, one reason for the high data point densities in portions of the Pecos Slope was the relatively high degree of structural deformation, and

thinning the data here risked losing the capacity to model this deformation. Methods of managing varying data densities while minimizing data loss should be researched. Alternatively, subdivision of the study area into domains and processing these domains separately may improve results (cf., MacCormack et al., 2018), albeit at the expense of adding additional modeling time.

One success of the methods used was in quantifying uncertainty in the final model across the study area. Conceptually, confidence should decrease with decreasing data density and increasing structural complexity, and the uncertainty maps well reflect this and appear to well quantify the degree of uncertainty. Two potential improvements would be to quantify and incorporate the varying confidence in individual data points (e.g., offset control estimates versus control points, or hard versus soft data) and the uncertainty associated with the interpolation approach itself. Accounting for the former would map higher uncertainties around offset control estimates or data points from less robust sources. To account for the latter, one could interpolate the contact surfaces using different software or interpolation schemes and compare the results to each other and the final contact surfaces to quantify the effect of the exact interpolation method and algorithm on the end results (cf., MacCormack et al., 2013; Jessell et al., 2014).

The final interpolation methods successfully combine smooth (folds, homoclines) and discrete (faults) changes in contact surface elevations. The methods are limited in their capacity to handle non-vertical structures, however. A potential improvement would be to use a few iterations during regional trend development to project fault locations along reasonable dip angles to better locate their intersections with each contact surface. Another weakness in the methods used is a lack of anisotropy, as along-strike and across-strike data points are compared equally and interpolations weight each direction equally. However, the anisotropic direction would need to vary across the study area, as structural grain varies from northeast-trending (such as around the Pecos Buckles) to northwest-trending (such as around the Huapache monocline). This again suggests that subdivision of the



domain may improve results (cf., MacCormack et al., 2018). At the scale of a regional framework model, however, the contact surfaces, in general, appear to adequately capture the subsurface structure.

A final comparison of the contact surfaces generated in this model to contours drawn or generated by separate authors is discussed in Appendix 1.

1. This analysis shows that in general the model and the other data sets show similar trends and contour spacing, but that small scale features were harder to capture with a model of this scale and resolution.

## Summary

These comparisons show that the surfaces generated using the methods above are:

- 1) Not biased by the method used. In portions of the study area where a surface was generated using a similar dataset to a previous study, the surface generated here is nearly identical to the surface generated by the previous study.
- 2) Capable of capturing complex large- and medium-scale structures (structures with widths greater than perhaps ~5 km) given adequate data coverage. Small scale structures are not reliably

captured, and dense collections of small scale structures, such as around the Tinnie fold belt, may impact results.

- 3) Generally comparable to works produced by previous authors and reflective of the current understanding of the geology of the area at a large scale.

These conclusions suggest that the model is an adequate framework model for the region modeled.

## Intended Uses and Limitations

The Pecos Slope framework model is intended for use at a horizontal resolution of no more than 1 km. It is intended for such uses as visualization and communication, and regional or preliminary studies. The model should not be used in lieu of site-specific studies, such as for well planning or design and environmental or hazard studies. Users of this dataset should be aware of the varying levels of uncertainty in each surface and incorporate this uncertainty in their considerations. In particular, structurally complex areas are difficult to model, and studies in areas with such complexity should be aware of this challenge and include more detailed, site-specific data as needed in their work.

# ACKNOWLEDGMENTS

I thank Ron Broadhead (NMBGMR) for sharing his geologic knowledge of the subsurface of the area and providing a useful critical review of a previous draft of this model, and Donald Sweetkind (USGS) for a critical review of the methodology. I also thank Phil Miller (NMBGMR), Coordinator of the Map Production Group, for digitizing many of the cross-sections used as input data for this model. J. Michael Timmons, Associate Director for Mapping Programs, provided additional support for attending digital geologic mapping conferences. Gabriel Parrish, formerly of the New Mexico Tech Earth and Environmental Science Department, assisted in the data quality control process. Finally, this report could never have been completed without the tenacious efforts of Marissa Fichera and Laila Sturgis (NMBGMR), who carried this work through to the end after the author's departure from the NMBGMR.



# REFERENCES

- Babakhani, M., 2016, Uncertainty analysis in geological surface modelling (Duvernay and Leduc Formation case studies): Closing the Gap III: Advances in applied geomodeling for hydrocarbon reservoirs (conference), Lake Louise, Alberta, Canada, Canadian Society of Petroleum Geologists, October 8–11.
- Bachman, G.O., 1980, Regional geology and Cenozoic history of Pecos region, southeastern New Mexico: U.S. Geological Survey, Open-File Report 80-1099, 116 p.
- Bachman, G.O., 1987, Karst in evaporites in southeastern New Mexico: Sandia National Laboratories, SAND86-7078, 82 p.
- Bardossy, G., and Fodor, J., 2001, Traditional and new ways to handle uncertainty in geology: Natural Resources Research, v. 10, no. 3, p. 179–187.
- Berg, R.C., Mathers, S.J., Kessler, H., and Keefer, D.A., 2011, Synopsis of current three-dimensional geological mapping and modeling in geological survey organizations: Illinois State Geological Survey, Circular 578, 92 p.
- Blandford, T.N., Blazer, D.J., Calhoun, K.C., Dutton, A.R., Naing, T., Reedy, R.C., and Scanlon, B.R., 2003, Groundwater availability of the southern Ogallala aquifer in Texas and New Mexico: Numerical simulations through 2050: Texas Water Development Board, Groundwater Availability Model (GAM) Report, 160 p.
- Blandford, T.N., Kuchanur, M., Standen, A., Ruggiero, R., Calhoun, K.C., Kirby, P., and Shah, G., 2008, Groundwater availability model of the Edwards–Trinity (High Plains) aquifer in Texas and New Mexico: Texas Water Development Board, Groundwater Availability Model (GAM) Report, 176 p.
- Brand, J.P., and Mattox, R.B., 1972, Pre-Dakota Cretaceous formations of northwestern Texas and northeastern New Mexico, *in* Kelley, V. C., and Trauger, F. D., eds., “East-Central New Mexico”: New Mexico Geological Society, Fall Field Conference Guidebook 23, p. 98–104.
- Branscombe, P., MacCormack, K.E., and Babakhani, M., 2018, 3D provincial geological framework model of Alberta, version 1 - Methodology: Alberta Energy Regulator / Alberta Geological Survey, Open-File Report 2017-09, 141 p.
- Broadhead, R.F., and Gillard, L., 2005a, Structure contours on Bone Spring Formation (Lower Permian), Delaware basin: New Mexico Bureau of Geology and Mineral Resources, Open-File Report 488, 10 p.
- Broadhead, R.F., and Gillard, L., 2005b, Structure contours on Tubb sandstone member of Yeso Formation (Lower Permian), Central Basin Platform, southeastern New Mexico: New Mexico Bureau of Geology and Mineral Resources, Open-File Report 489, 10 p.
- Broadhead, R.F., Gillard, L., and Engin, N., 2005, Structure contours on Abo Formation (Lower Permian), Delaware basin: New Mexico Bureau of Geology and Mineral Resources, Open-File Report 487 [CD-ROM], 10 p.
- Broadhead, R.F., and Jones, G.E., 2002, Petroleum potential of the Sin Nombre area, De Baca, Roosevelt, Curry, Lincoln, Guadalupe, and Chaves Counties, New Mexico: New Mexico Bureau of Geology and Mineral Resources, Open-File Report 467, 42 p.
- Broadhead, R.F., Mansell, M.M., and Jones, G., 2009, Carbon dioxide in New Mexico: Geologic distribution of natural occurrences: New Mexico Bureau of Geology and Mineral Resources, Open-File Report 514, 131 p.
- Broadhead, R.F., and Ulmer-Scholle, D., 2012, New Mexico Saline Aquifer Database [unpublished]: compiled for the U.S. Geological Survey, New Mexico Bureau of Geology and Mineral Resources, Socorro, NM.
- Cather, S.M., 2004, Laramide orogeny in central and northern New Mexico and southern Colorado, *in* Mack, G. H., and Giles, K. A., eds., “The Geology of New Mexico: A Geologic History”: New Mexico Geological Society, Special Publication 11, p. 203–248.
- Caumon, G., Lepage, F., Sword, C.H., and Mallet, J.-L., 2004, Building and editing a sealed geological model: Mathematical Geosciences, v. 36, no. 4, p. 405–424.
- Cronin, J.G., 1969, Ground water in the Ogallala Formation in the southern high plains of Texas and New Mexico: U.S. Geological Survey, Hydrologic Investigations Atlas HA-330.
- Deeds, N.E., Harding, J.J., Jones, T.L., Singh, A., Hamlin, S., Reedy, R.C., Yan, T., Jigmond, M., Lupton, D., Scanlon, B.R., Seni, S., and Dutton, A., 2015, Final conceptual model report for the High Plains aquifer system groundwater availability model: report to the Texas Water Development Board, 546 p.
- DuChene, H.R., and Cunningham, K.I., 2006, Tectonic influences on speleogenesis in the Guadalupe Mountains, New Mexico and Texas, *in* Land, L., Lueth, V. W., Raatz, W., Boston, P., and Love, D. W., eds., “Caves and Karst of Southeastern New Mexico”: New Mexico Geological Society, Fall Field Conference 57, p. 211–217.
- Erdlac, R.J., 1993, Small-scale structures in the Guadalupe Mountains region: Implication for Laramide stress trends in the Permian basin, *in* Love, D. W., Hawley, J. W., Kues, B. S., Austin, G. S., and Lucas, S. G., eds., “Carlsbad Region (New Mexico and West Texas)”: New Mexico Geological Society, Fall Field Conference Guidebook 44, p. 167–174.
- Esri Inc., 2017, ArcGIS Desktop (v. 10.5.1.7333) [Software].
- Ewing, J.E., Jones, T.L., Yan, T., Vreugdenhil, A.M., Fryar, D.G., Pickens, J.F., Gordon, K., Nicot, J-P., Scanlon, B.R., Ashworth, J.B., and Beach, J., 2008, Groundwater availability model for the Dockum aquifer - Final Report, report to the Texas Water Development Board, 420 p.
- Ewing, J.E., Kelley, V.A., Jones, T.L., Yan, T., Singh, A., Powers, D. W., Holt, R. M., and Sharp, J.M., 2012, Final groundwater availability model report for the Rustler aquifer: report to the Texas Water Development Board, 394 p.



- Ewing, T. E., 1993, Erosional margins and patterns of subsidence in the late Paleozoic west Texas basin and adjoining basins of west Texas and New Mexico, *in* Love, D. W., Hawley, J. W., Kues, B. S., Austin, G. S., and Lucas, S. G., eds., "Carlsbad Region (New Mexico and West Texas)": New Mexico Geological Society, Fall Field Conference Guidebook 44, p. 155–166.
- Fallin, J.A.T., 1988, Hydrogeology of Lower Cretaceous strata under the southern High Plains of Texas and New Mexico: New Mexico Geology, v. 10, no. 1, p. 6–9.
- Fallin, J.A.T., 1989, Hydrogeology of Lower Cretaceous strata under the southern High Plains of Texas and New Mexico: Texas Water Development Board, Report 314, 39 p.
- GeoMol Team, 2015, GeoMol - Assessing subsurface potentials of the Alpine Foreland Basins for sustainable planning and use of natural resources: Project report, Augsburg, Germany, Bavarian Environment Agency, 188 p.
- Goff, F., Kelley, S.A., Lawrence, J.R., Cikowski, C.T., Krier, D., Goff, C.J., and McLemore, V.T., 2011, Geologic map of the Nogal Peak 7.5-minute quadrangle, Lincoln and Otero Counties, New Mexico: New Mexico Bureau of Geology and Mineral Resources, Open-File Geologic Map OF-GM-134, scale 1:24,000.
- Gustavson, T.C., 1986, Geomorphic development of the Canadian River Valley, Texas Panhandle: An example of regional salt dissolution and subsidence: Geological Society of America Bulletin, v. 97, p. 459–472.
- Hawley, J. W., 1993, The Ogallala and Gatuna Formations in the southeastern New Mexico region: A progress report, *in* Love, D. W., Hawley, J. W., Kues, B. S., Austin, G. S., and Lucas, S. G., eds., "Carlsbad Region (New Mexico and west Texas)": New Mexico Geological Society, Fall Field Conference Guidebook 44, p. 261–269.
- Hayes, P.T., 1964, Geology of the Guadalupe Mountains, New Mexico: U.S. Geological Survey, Professional Paper 446, 69 p.
- Hill, C.A., 2006, Geology of the Guadalupe Mountains: An overview of recent ideas, *in* Land, L., Lueth, V. W., Raatz, W., Boston, P., and Love, D. W., eds., "Caves and Karst of Southeastern New Mexico": New Mexico Geological Society, Fall Field Conference 57, p. 145–150.
- Intermap Technologies, Inc., 2008, Digital Terrain Models, Core Product Version 4.2, Edit Rule Version 2.2: Englewood, CO.
- Jessell, M.W., Ailleres, L., De Kemp, E., Lindsay, M., Wellmann, F., Hillier, M., Laurent, G., Carmichael, T., and Martin, R., 2014, Next generation three-dimensional geologic modeling and inversion, *in* Kelley, K. D., and Golden, H. C., eds., "Building Exploration Capability for the 21st Century": Society of Economic Geologists, Special Publication 18, p. 261–272.
- Johnson, K.S., 1993, Dissolution of Permian Salado salt during Salado time in the Wink area, Winkler County, Texas, *in* Love, D. W., Hawley, J. W., Kues, B. S., Austin, G. S., and Lucas, S. G., eds., "Carlsbad Region (New Mexico and west Texas)": New Mexico Geological Society, Fall Field Conference Guidebook 44, p. 211–218.
- Keefer, D.A., 2011, Chapter 10: Illinois State Geological Survey: A modular approach for 3-D mapping that addresses economic development issues, *in* Berg, R. C., Mathers, S. J., Kessler, H., and Keefer, D. A., eds., "Synopsis of current three-dimensional geological mapping and modeling in geological survey organizations": Illinois State Geological Survey, Circular 578, p. 53–59.
- Keefer, D.A., Kessler, H., Cave, M., and Mathers, S.J., 2011, Chapter 2: Major mapping and modeling issues, *in* Berg, R. C., Mathers, S. J., Kessler, H., and Keefer, D. A., eds., "Synopsis of current three-dimensional geological mapping and modeling in geological survey organizations": Illinois State Geological Survey, Circular 578, p. 6–10.
- Kelley, S., Koning, D.J., Goff, F., Cikowski, C.T., Peters, L., and McIntosh, W., 2014, Stratigraphy of the northwestern Sierra Blanca volcanic field, *in* Rawling, G., McLemore, V. T., Timmons, S., and Dunbar, N., eds., "Geology of the Sacramento Mountains Region": New Mexico Geological Society, Fall Field Conference Guidebook 65, p. 197–208.
- Kelley, V. C., 1971, Geology of the Pecos country, southeastern New Mexico: New Mexico Bureau of Mines and Mineral Resources, Memoir 24, 78 p.
- Kessler, H., Mathers, S.J., Keefer, D.A., and Berg, R.C., 2011, Chapter 4: Common 3-D mapping and modeling software packages, *in* Berg, R. C., Mathers, S. J., Kessler, H., and Keefer, D. A., eds., "Synopsis of current three-dimensional geological mapping and modeling in geological survey organizations": Illinois State Geological Survey, Circular 578, p. 13–16.
- Koning, D.J., Kelley, S., and Goff, F., 2014a, Preliminary geologic map of the northeastern Tularosa basin and western Sierra Blanca basin, Lincoln and Otero Counties, New Mexico: New Mexico Bureau of Geology and Mineral Resources, Open-File Report 563, scale 1:50,000.
- Koning, D.J., Rawling, G.C., Kelley, S., Goff, F., McIntosh, W., and Peters, L., 2014b, Structure and tectonic evolution of the Sierra Blanca basin, *in* Rawling, G., McLemore, V. T., Timmons, S., and Dunbar, N., eds., "Geology of the Sacramento Mountains Region": New Mexico Geological Society, Fall Field Conference Guidebook 65, p. 209–226.
- Koning, D.J., and Roberts, L., 2014, Redefinition of the base of the Cub Mountain Formation and preliminary depositional and tectonic interpretations of the Early-Middle Eocene strata in the Sierra Blanca basin, New Mexico, *in* Rawling, G., McLemore, V. T., Timmons, S., and Dunbar, N., eds., "Geology of the Sacramento Mountains Region": New Mexico Geological Society, Fall Field Conference Guidebook 65, p. 273–286.
- Koša, E., and Hunt, D.W., 2006, The effect of syndepositional deformation within the Upper Permian Capitan platform on the speleogenesis and geomorphology of the Guadalupe Mountains, New Mexico, USA: Geomorphology, v. 78, p. 279–308.
- Kues, B.S., and Giles, K. A., 2004, The Late Paleozoic ancestral Rocky Mountains system in New Mexico, *in* Mack, G. H., and Giles, K. A., eds., "The Geology of New Mexico: A geologic history": New Mexico Geological Society, Special Publication 11, p. 95–136.
- Land, L., and Huff, G.F., 2010, Multi-tracer investigation of groundwater residence time in a karstic aquifer: Bitter Lakes National Wildlife Refuge, New Mexico, USA: Hydrogeology Journal, v. 18, p. 455–472.
- Lehman, T.M., 1994, The saga of the Dockum Group and the case of the Texas/New Mexico boundary fault, *in* Ahlen, J., Peterson, J., Bowsher, A. L., and Zidek, J., eds., "Geologic activities in the 90s -- Southwest Section of AAPG 1994, Ruidoso, New Mexico": New Mexico Bureau of Mines and Mineral Resources, Bulletin 150, p. 37–51.
- Lehman, T.M., and Chatterjee, S., 2005, Depositional setting and vertebrate biostratigraphy of the Triassic Dockum Group of Texas: Journal of Earth System Science, v. 114, no. 3, p. 325–351.



- Lucas, S.G., and Anderson, O.J., 1993, Stratigraphy of the Permian-Triassic boundary in southeastern New Mexico and west Texas, *in* Love, D. W., Hawley, J. W., Kues, B. S., Austin, G. S., and Lucas, S. G., eds., "Carlsbad Region (New Mexico and west Texas)": New Mexico Geological Society, Fall Field Conference Guidebook 44, p. 219–230.
- Lucas, S.G., and Anderson, O.J., 1994, Ochoan (Late Permian) stratigraphy and chronology, southeastern New Mexico and west Texas, *in* Ahlen, J., Peterson, J., and Bowsher, A. L., eds., "Geologic activities in the 90s, Southwest Section of AAPG 1994, Ruidoso, New Mexico": New Mexico Bureau of Geology and Mineral Resources, Bulletin 150, p. 29–36.
- Lyford, F.P., 1973, Valley fill in the Roswell-Artesia area, New Mexico: United States Geological Survey, Open-File Report 73-163, 26 p.
- MacCormack, K.E., Arnaud, E., and Parker, B.L., 2018, Using a multiple variogram approach to improve the accuracy of subsurface geological models: Canadian Journal of Earth Science, v. 55, no. 7, p. 786–801.
- MacCormack, K.E., Brodeur, J.J., and Eyles, C.H., 2013, Evaluating the impact of data quantity, distribution and algorithm selection on the accuracy of 3D subsurface models using synthetic grid models of varying complexity: Journal of Geographical Systems, v. 15, p. 71–88.
- Mack, G.H., 2004, Middle and late Cenozoic crustal extension, sedimentation, and volcanism in the southern Rio Grande rift, Basin and Range, and southern transition zone of southwestern New Mexico, *in* Mack, G. H., and Giles, K. A., eds., "The Geology of New Mexico: A geologic history": New Mexico Geological Society, Special Publication 11, p. 389–406.
- Mack, G.H., and Bauer, E.M., 2014, Depositional environments, sediment dispersal, and provenance of the early Permian (Leonardian) Glorieta Sandstone, central New Mexico, *in* Rawling, G., McLemore, V. T., Timmons, S., and Dunbar, N., eds., "Geology of the Sacramento Mountains Region": New Mexico Geological Society, Fall Field Conference Guidebook 65, p. 261–271.
- Mathers, S.J., Kessler, H., and Napier, B., 2011, Chapter 6: British Geological Survey: A nationwide commitment to 3-D geological modeling, *in* Berg, R. C., Mathers, S. J., Kessler, H., and Keefer, D. A., eds., "Synopsis of current three-dimensional geological mapping and modeling in geological survey organizations": Illinois State Geological Survey, Circular 578, p. 25–30.
- Mathers, S.J., Terrington, R.L., Waters, C.N., and Leslie, A.G., 2014, GB3D - a framework for the bedrock geology of Great Britain: Geoscience Data Journal, v. 1, p. 30–42.
- McGowen, J.H., Granata, G.E., and Seni, S.J., 1977, Depositional systems, uranium occurrence and postulated groundwater history of the Triassic Dockum Group, Texas Panhandle-eastern New Mexico: The University of Texas at Austin, Bureau of Economic Geology, contract report prepared for the United States Geological Survey, 104 p.
- Meyer, J.E., 2017, Brackish Resources Aquifer Characterization System Database Data Dictionary: Texas Water Development Board, Open-File Report 12-02, 3rd ed., 195 p.
- Meyer, J.E., Wise, M.R., and Kalaswad, S., 2012, Pecos Valley aquifer, west Texas: Structure and brackish groundwater: Texas Water Development Board, Report 382, 86 p.
- Meyer, R.F., 1966, Geology of Pennsylvanian and Wolfcampian rocks in southeast New Mexico: New Mexico Bureau of Mines and Mineral Resources, Memoir 17, 123 p.
- Newton, B.T., Rawling, G.C., Timmons, S.S., Land, L., Johnson, P.S., Kludt, T.J., and Timmons, J.M., 2012, Sacramento Mountains hydrogeology study: Final technical report, prepared for Otero Soil and Water Conservation District: New Mexico Bureau of Geology and Mineral Resources, Open-File Report 543, 77 p.
- NM OCD, 2018, OCD well files imaging server [on-line], from: <http://ocdimage.emnrd.state.nm.us/imaging/>, New Mexico Oil Conservation Division.
- NMBGMR, 2003, Geologic map of New Mexico: New Mexico Bureau of Geology and Mineral Resources, scale 1:500,000.
- NMBGMR, 2018, New Mexico geologic map search [on-line], from: <https://geoinfo.nmt.edu/publications/maps/geologic/home.cfm>, New Mexico Bureau of Geology and Mineral Resources.
- Polyak, V.J., McIntosh, W.C., Provencio, P.P., and Guven, N., 2006, Alunite and natroalunite tell a story-the age of and origin of Carlsbad Cavern, Lechuguilla Cave, and other sulfuric-acid type caves of the Guadalupe Mountains, *in* Land, L., Lueth, V. W., Raatz, W., Boston, P., and Love, D. W., eds., "Caves and Karst of Southeastern New Mexico": New Mexico Geological Society, Fall Field Conference 57, p. 203–209.
- Powers, D. W., and Holt, R. M., 2000, The salt that wasn't there: Mudflat facies equivalents to halite of the Permian Rustler Formation, southeastern New Mexico: Journal of Sedimentary Research, v. 70, no. 1, p. 29–36.
- Rawling, G.C., 2004a, Geologic map of the Angus quadrangle, Lincoln County, New Mexico: New Mexico Bureau of Geology and Mineral Resources, Open-File Geologic Map OF-GM-95, scale 1:24,000.
- Rawling, G.C., 2004b, Geologic map of the Ruidoso 7.5-minute quadrangle, Lincoln and Otero Counties, New Mexico: New Mexico Bureau of Geology and Mineral Resources, Open-File Geologic Map OF-GM-93, scale 1:24,000.
- Rawling, G.C., 2006, Geologic map of the Fort Stanton quadrangle, Lincoln County, New Mexico: New Mexico Bureau of Geology and Mineral Resources, Open-File Geologic Map OF-GM-119, scale 1:24,000.
- Rawling, G.C., 2014, Geology of the Capitan and Nogal quadrangles, Lincoln County, New Mexico: New Mexico Bureau of Geology and Mineral Resources, Open-File Report 538, scale 1:24,000.
- Riggs, N.R., Lehman, T.M., Gehrels, G.E., and Dickinson, W.R., 1996, Detrital zircon link between headwaters and terminus of the Upper Triassic Chinle-Dockum paleoriver system: Science, v. 273, p. 97–100.
- Ruppel, S.C., ed., 2009, Integrated synthesis of the Permian Basin: Data and models for recovering existing and undiscovered oil resources from the largest oil-bearing basin in the U.S., Bureau of Economic Geology and the University of Texas at Austin, Austin, TX, prepared for the U.S. Department of Energy contract DE-FC26-04NT15509, 959 p.
- Schiel, K.A., 1988, The Dewey Lake Formation: End stage deposit of a peripheral foreland basin [M.S. Thesis]: The University of Texas at El Paso, El Paso, Texas, 180 p.



- Seager, W.R., 2004, Laramide (Late Cretaceous-Eocene) tectonics of southwestern New Mexico, *in* Mack, G. H., and Giles, K. A., eds., "The Geology of New Mexico: A Geologic History": New Mexico Geological Society, Special Publication 11, p. 183–202.
- Skotnicki, S.J., 2009a, Geologic map of the Lincoln 7.5-minute quadrangle, Lincoln County, New Mexico: New Mexico Bureau of Geology and Mineral Resources, Open-File Geologic Map OF-GM-188, scale 1:24,000.
- Skotnicki, S.J., 2009b, Geologic map of the San Patricio 7.5-minute quadrangle, Lincoln County, New Mexico: New Mexico Bureau of Geology and Mineral Resources, Open-File Geologic Map OF-GM-189, scale 1:24,000.
- Skotnicki, S.J., 2010a, Geologic map of the Capitan Pass quadrangle, Lincoln County, New Mexico: New Mexico Bureau of Geology and Mineral Resources, Open-File Geologic Map OF-GM-208, scale 1:24,000.
- Skotnicki, S.J., 2010b, Geologic map of the Capitan Peak quadrangle, Lincoln County, New Mexico: New Mexico Bureau of Geology and Mineral Resources, Open-File Geologic Map OF-GM-209, scale 1:24,000.
- Standen, A., Finch, S., Williams, R., Lee-Brand, B., and Kirby, P., 2009, Capitan reef complex: Structure and stratigraphy: report to the Texas Water Development Board, 53 p.
- Timmons, J.M., and Zeigler, K.E., 2010, Preliminary geologic map of the Nelson Canyon West quadrangle, Lincoln County, New Mexico: New Mexico Bureau of Geology and Mineral Resources, Open-File Geologic Map OF-GM-197, scale 1:24,000.
- van der Meulen, M.J., Doornenbal, J.C., Gunnink, J.L., Stafleu, J., Schokker, J., Vernes, R.W., van Geer, F.C., van Gessel, S.F., van Heteren, S., van Leeuwen, R.J.W., Bakker, M.A.J., Bogaard, P.J.F., Busschers, F.S., Griffioen, J., Gruijters, S.H.L.L., Kiden, P., Schroot, B.M., Simmelink, H.J., van Berkel, W.O., van der Krogt, R.A.A., Westerhoff, W.E., and van Daalen, T.M., 2013, 3D geology in a 2D country: perspectives for geological surveying in the Netherlands: *Netherlands Journal of Geosciences*, v. 92, no. 4, p. 217–241.
- Weeks, J.B., and Gutentag, E.D., 1981, Bedrock geology, altitude of base, and 1980 saturated thickness of the High Plains aquifer in parts of Colorado, Kansas, Nebraska, New Mexico, Oklahoma, South Dakota, Texas, and Wyoming: U.S. Geological Survey, Hydrologic Investigations Atlas HA-648.
- Zeigler, K.E., 2008a, Geologic map of the Elk 7.5-minute quadrangle map, Otero and Chaves Counties, New Mexico: New Mexico Bureau of Geology and Mineral Resources, Open-File Geologic Map OF-GM-175, scale 1:24,000.
- Zeigler, K.E., 2008b, Geologic map of the Thimble Canyon 7.5-minute quadrangle map, Chaves County, New Mexico: New Mexico Bureau of Geology and Mineral Resources, Open-File Geologic Map OF-GM-176, scale 1:24,000.



# 3D AQUIFER MAPPING OF THE PECOS SLOPE AND SOUTHERN HIGH PLAINS REGIONS, SOUTHEAST NEW MEXICO

*Marissa Fichera and Ethan Mamer*

<b>Summary</b> .....	87	5. B-B' west-east cross-section of northern half of study area displaying complex geologic structure and stratigraphy .....	92
<b>I. Previous Work</b> .....	88	6. Areal extent of relevant aquifer systems/aquifer units .....	93
<b>II. Introduction</b> .....	89	7. 3-dimensional representation of total dissolved solids concentration within study area .....	94–95
Regional physiography .....	89	8. Locations of water-level measurements used in model development for each aquifer system .....	98
Geologic setting .....	90	9. Network of wells not used in aquifer characterization of this region .....	99
Hydrogeologic overview .....	93	10. Conceptual model of Yeso aquifer in the Sacramento Mountains .....	102
<b>III. Methods</b> .....	97	11. Location of wells drilled into San Andres and Yeso Formations.....	103
Overview .....	97	12. Locations of water wells with relevant water level data in the Permian Aquifer System .....	103
Water-data summary .....	97	13. Locations of water wells with relevant water level data in the Permian Aquifer System .....	104
<b>IV. Regional Aquifer Systems</b> .....	101	14. Potentiometric surface map of the Permian Aquifer System. ....	106
Permian aquifer system.....	101	15. 3D geometry of the Permian Aquifer System, visualized in ArcScene with geologic surfaces .....	108
Pecos Valley alluvial aquifer .....	107	16. Potentiometric surface map of the Pecos Valley Alluvial Aquifer.....	109
Southern High Plains aquifer system .....	111	17. Total well network of formations associated with the Pecos Valley Alluvial Aquifer—location of wells drilled into the Pecos Valley Alluvium or the Artesia group .....	110
<b>V. Summary</b> .....	119	18. Locations of wells with water levels reported after 2009 for the Pecos Valley Alluvial Aquifer .....	110
<b>Acknowledgments</b> .....	121	19. 3D geometry of the Pecos Valley Alluvial Aquifer, visualized in ArcScene with geologic surfaces. Panels a, b, and c visualize aquifer geometry in 2D .....	112
<b>References</b> .....	121		
<b>Figures</b>			
1. Area of hydrogeologic study and 3D model within New Mexico.....	89		
2. Generalized surficial geologic map of study area .....	90		
3. Block diagram showing simplified regional subsurface geology and surficial landscape .....	91		
4. A-A' west-east cross-section of southern half of study area displaying subsurface geology and water-table elevation .....	92		



20. Upper caliche caprock of Ogallala Formation forming the Mescalero Escarpment in southeast New Mexico .....	113
21. Location of wells drilled into Southern High Plains Aquifer System units .....	114
22. Locations of wells with water levels reported after 2009 for the Southern High Plains Aquifer System .....	114
23. Hydrostratigraphic cross-section of Southern High Plains Aquifer System, displaying water quality projected from data points .....	115
24. Potentiometric surface map of the Southern High Plains Aquifer System .....	116
25. 3D geometry of the Southern High Plains Aquifer System .....	117
26. 3D hydrogeologic model of Lower Pecos Slope and Southern High Plains region .....	120

## Tables

1. Aquifer assignment based on well depth .....	98
2. A summary of water-well coverage in the Permian Aquifer System extent .....	104
3. A summary of water-well coverage in the Pecos Valley Alluvial Aquifer extent .....	109
4. A summary of water-well coverage in the Southern High Plains Aquifer System extent.....	113
5. Summary of estimated aquifer volumes .....	119

## Appendix 2

Aquifer volume calculation methods.....	3 pages
---	---------



## SUMMARY

The New Mexico Bureau of Geology and Mineral Resources is investigating the feasibility of creating three dimensional hydrogeologic maps using existing water data and tools available in ArcGIS. This study focuses on the Lower Pecos Slope and Southern High Plains region in southeast New Mexico. Three-dimensional hydrogeologic maps are beneficial for a variety of reasons, including: 1) better visualization and comprehension of the subsurface as it relates to groundwater resource management; 2) the ability to calculate volumetric data and cross-sectional data as it relates to groundwater supply and water quality; 3) create a publicly available hydrogeologic framework capable of being used in development of groundwater flow models; and 4) analyzing water quality data at depth, and potentially identify zones of brackish groundwater resources. This study has accomplished creating 3D digital subsurface data, in the form of raster surfaces and contour maps, compiled into an ArcGIS map package which accompanies this report. During development of the 3D hydrogeologic model, vast amounts of data were compiled and organized into geodatabases. The compilation of this data into geodatabases proved useful in identification of data gaps and, in the future, will allow for seamless updates to the hydrogeologic models as new data is collected.

The Lower Pecos Slope and Southern High Plains region of New Mexico was chosen as one of the first areas to develop a 3D hydrogeologic framework because of the high density of subsurface geologic data and water data. The region encompasses portions of Lincoln, Otero, Chaves, Roosevelt, and Lea Counties. Lea County is the top producer of oil and gas in the state, lending to tens of thousands of wells with subsurface geologic data. West of Lea

County resides the Roswell Artesian Basin and the Sacramento Mountains. This region is used extensively for agriculture, lending to a dense water-well network with well measurements going back to the early 1900s (Rinehart and Mamer, 2017).

Mapping aquifers in three dimensions required aquifer boundaries to be delineated in areal extent and at depth. Approximating aquifer boundaries is challenging due to complexities in how aquifers are defined. For example, aquifers are often defined by administrative water management zones, watershed boundaries, and geologic structural and stratigraphic boundaries in the subsurface. Oftentimes, there is no one simple boundary, but rather “zones” of good quality water, contained within certain extents of geologic units. For this study, defining these zones and the extents of geologic units was done, in general, by mapping geologic surfaces and TDS content in 3D. Conceptual boundaries were estimated based on water-level, water-quality, and well-depth data, combined with literature review. Aquifer tops and aquifer bases were then created and contoured using tools in ArcGIS. As a result, three major aquifer systems were defined and mapped in 3D within the Lower Pecos Slope/Southern High Plains region: 1) the Permian Aquifer System; 2) the Pecos Valley Alluvial Aquifer, and; 3) the Southern High Plains Aquifer System. The resulting 3D aquifer maps facilitate enhanced visualization of groundwater supply as it pertains to groundwater resource management, estimation of groundwater volumes, and identification of water-level and water quality data gaps. This study is part of an on-going, multiyear effort to improve and update aquifer maps using modern, three-dimensional mapping techniques based in ArcGIS, which are a joint product of this report.



## I. PREVIOUS WORK

Numerous studies have been completed on aquifer systems in southeast New Mexico. A hydrogeology study of the southern Sacramento Mountains and the Lower Pecos Slope was completed in 2012 by the New Mexico Bureau of Geology and Mineral Resources (NMBGMR), resulting in a regional-scale hydrogeologic conceptual model. In the multi-scale study, geologic mapping, water-level data, and streamflow measurements were used to analyze groundwater/surface water interactions, while geochemical methods (including major ions and trace metals, stable isotopes, tritium, tritium-helium, noble gases, carbon isotopes, and chlorofluorocarbons) were used in assessing groundwater ages, groundwater movement, and recharge mechanisms. Rawling and Newton (2016) published an additional study outlining groundwater recharge and the hydraulic connection between the High Mountain Aquifer System and Roswell Artesian Basin (hereto referred conjunctively as the Permian Aquifer System). Newman et al. (2016) identified and analyzed hydrochemical facies within the Roswell Artesian Basin in order to examine stratigraphic and structural controls on geochemical variability within the aquifer. Land and Timmons (2016) published a report sum-

marizing water chemistry parameters within major groundwater basins in New Mexico in order to assess brackish water resource potential. Water use, demand, and supply were evaluated in the Lower Pecos Valley Regional Water Plan (2016) and the Lea County Regional Water Plan (2016). Additionally, both water plans outlined future demand projections and water conservation strategies.

Deeds et al. and the Texas Water Development Board (TWDB) completed an extensive report in 2015 on the High Plains Aquifer System across New Mexico and Texas, using data from multiple agencies to create a conceptual model and a groundwater availability numerical model. This study documented the physiography, geology, hydrostratigraphy, hydrostratigraphic framework, water levels, recharge, surface water interaction, hydraulic properties, discharge, and water quality for the Ogallala, Edwards–Trinity, and Dockum aquifers. As used here, a “geologic model” is a suite of model unit contact surfaces that partition the model space into model units. Finally, a “sealed geologic model” is one where the geologic model has no topological errors, such as intersecting contact surfaces or contact surface that end abruptly within a model unit (Caumon et al., 2004).



## II. INTRODUCTION

### Regional Physiography

The study area is bounded to the west by the ridge of the Sacramento Mountains, to the east by the New Mexico-Texas border, to the south by Guadalupe Mountains and the northern boundary of the Delaware Basin, and to the north by the Capitan Mountains and a break in the regional High Plains Aquifer System (represented by an area of low groundwater saturation caused by thinning of the Ogallala Formation) (Fig. 1). The Sacramento Mountains are one of the largest and most conspicuous mountain ranges in southern New Mexico. The north-south trending profile of the Sacramento Mountains is strongly asymmetric, with a steep, west-facing escarpment that rises abruptly for more than a mile above the desert

floor of the Tularosa Basin. East of the crest, the land surface merges almost imperceptibly with the Pecos Slope, a sparsely populated, nearly treeless plain that slopes gently downward toward the Pecos River 80 miles away and about 6,000 ft lower in elevation (Land, 2003). The eastern boundary of the Pecos River Valley is defined by the Mescalero Escarpment and the Llano Estacado Mesa. The Mescalero Escarpment forms a steep west-facing cliff approximately 300 ft tall and bounds the Llano Estacado Mesa which dips gently to the southeast at an approximate gradient of 10 ft/mile. The northern and northwestern boundaries of the study region are defined by the volcanic and granitic highlands of Sierra Blanca and the Capitan Mountains batholith (Land and Timmons, 2016).

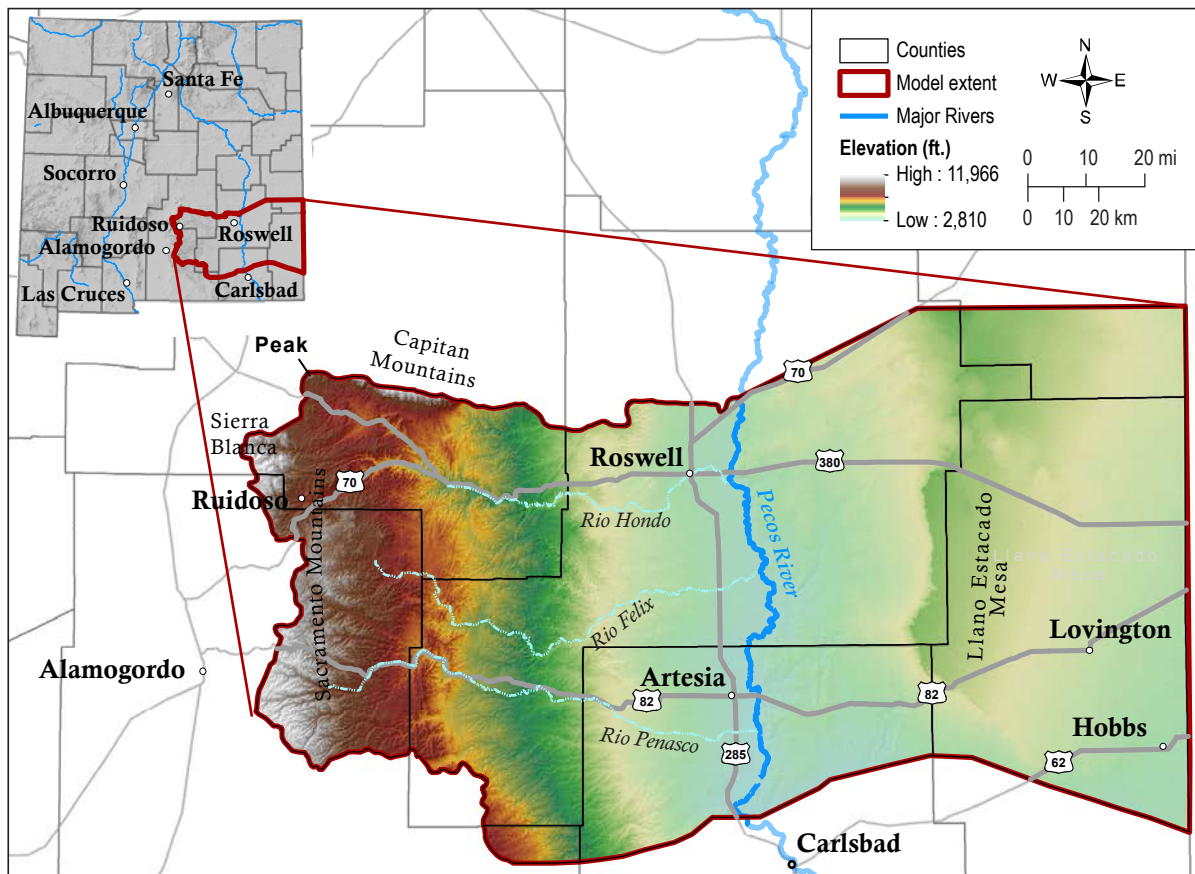


**Figure 1.** Area of hydrogeologic study and 3D model within New Mexico. The study covers variable terrain, including the Sacramento and Capitan mountains at elevations just over 11,000 ft., the Pecos River Valley, and the arid Southern High Plains.



The Pecos River flows from north to south and is the major surface water feature in the region (Fig. 1). Its three principal tributaries (the Rio Hondo, Rio Felix, and Rio Peñasco) originate in the Sacramento Mountains. These streams and their lesser tributaries are fed by hundreds of springs and flow eastward across the Pecos Slope toward the Roswell Artesian Basin and the Pecos River. The streams are perennial in the Sacramento Mountains but become intermittent losing streams as they flow across the Pecos Slope where most of their flow enters the subsurface through solution-enlarged fissures in bedrock streambeds. This subsurface flow ultimately contributes to groundwater recharge in the Roswell Basin (Land and Newton, 2008).

Elevation ranges from 11,981 ft at Sierra Blanca (the highest mountain in southern New Mexico) to 3,300 ft in the Lower Pecos Valley. Average annual rainfall corresponds to elevation, ranging from 26 inches in the high mountains to less than 12 inches in

the Artesian Basin. Most precipitation falls as summer monsoon rains. Winter snowfall, although highly variable, accounts for about 20% of precipitation in the Sacramento Mountains. Vegetation reflects variations in elevation and rainfall, with a mixed conifer forest at higher elevations and piñon-juniper and grassland at lower elevations (Newton et al., 2012; Land and Timmons, 2016).

## Geologic Setting

The southeast region of New Mexico is composed generally of sedimentary and volcanic rock types overlying Precambrian basement and intruded by plutonic rocks. Exposed sedimentary and volcanic units are Permian to Quaternary in age, while exposed intrusions are of Tertiary age. Strata span multiple depositional settings including platform

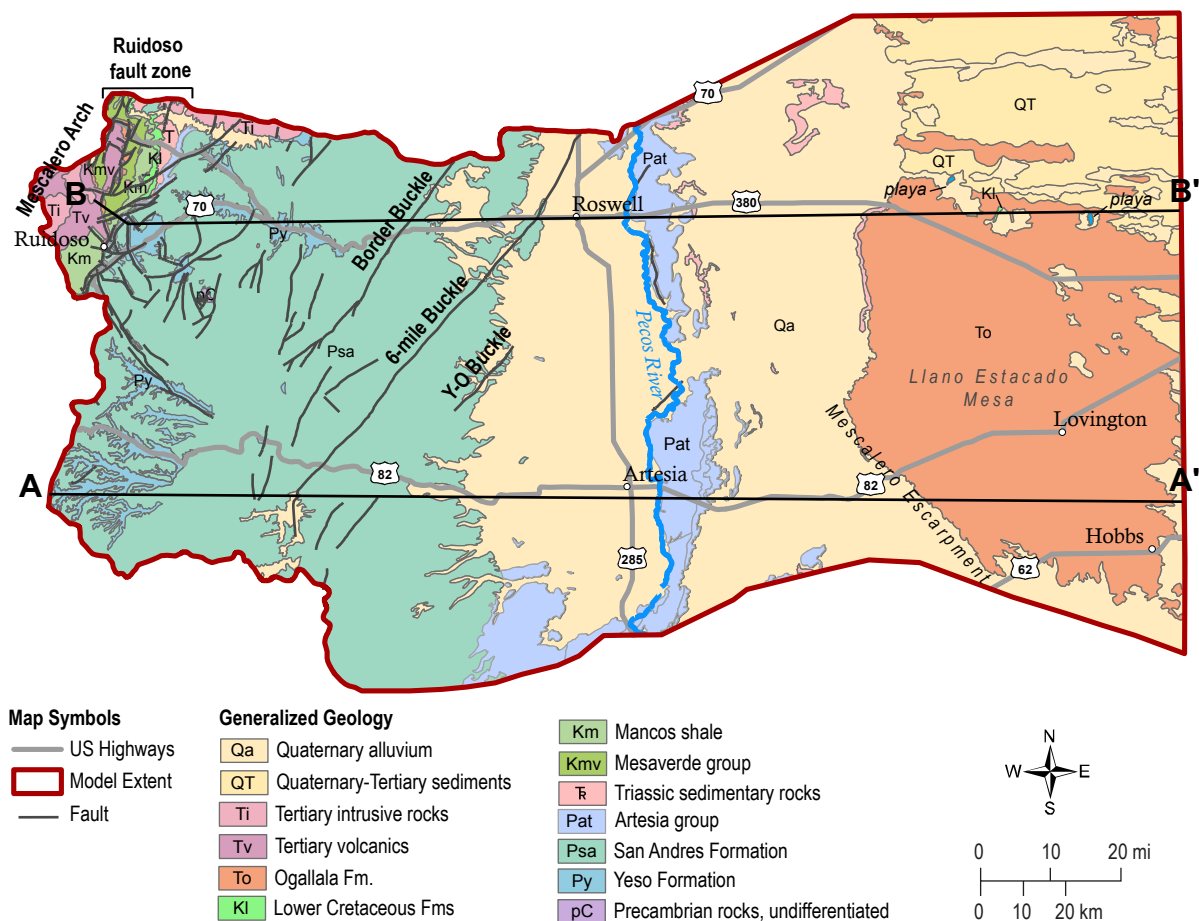


**Figure 2.** Generalized surficial geologic map of study area. Permian sedimentary units dominate the surficial geology west of the Pecos River and dip gently to the east. Large swaths of alluvium cover the central study area surrounding the Pecos River, while the near flat lying lower Cretaceous Edwards–Trinity Formations and Tertiary Ogallala Formation form the Llano Estacado Mesa from the Mescalero Escarpment to the New Mexico–Texas border. The series of NE–SW trending buckles west of the Pecos River, known as the Pecos Buckles, are conduits to groundwater flow in the Permian Aquifer System, resulting in a number of mountain springs.



marine to marginal marine, mudflat to sabkha, and fluvial settings in the Permian; continental fluvial settings in the Triassic; fluvial to shallow marine settings during the Cretaceous; and finally fluvial and eolian environments in the late Cenozoic. Middle Permian rocks of the San Andres and Yeso Formations crop out throughout most of the Sacramento Mountains and the Pecos Slope (Fig. 2). North of Ruidoso Creek the bedrock consists of Mesozoic and Cenozoic clastic rocks within the Laramide-age Sierra Blanca Basin, overlain and crosscut by intrusive and extrusive igneous rocks of the Sierra Blanca volcanic complex (Rawling and Newton, 2016). The Tertiary-aged Ogallala formation crops out throughout the eastern portion of the region and overlies Lower Cretaceous and Dockum Group sedimentary rocks, which overlie the Permian sedimentary units that crop out throughout the Sacramento Mountains. Sedimentary units east of the Sacramento Mountains dip gradually to the east (Fig. 3). Alluvium lines the floor of the Pecos River Valley (Fig. 2).

Three episodes of regional deformation shaped the greater Sacramento Mountains and adjacent areas: 1) the late Paleozoic Ancestral Rocky Mountains orogeny, 2) the late Cretaceous-early Tertiary Laramide orogeny, and 3) mid-to-late

Tertiary extensional tectonics associated with opening of the Rio Grande Rift. There is abundant evidence for reactivation of older basement structures (Cather, 1991). The east flank of the Sacramentos grades into the Pecos Slope, a gentle homocline with regional eastward dip of less than  $1^\circ$  toward the Pecos Valley. The general structural slope is modified by numerous faults and fold belts including the Dunken–Tinnie Anticlinorium, which defines the eastern foothills of the Sacramentos, and the Pecos Buckles (Fig. 2, 4). These latter structures, which include from west to east the Border, Six-Mile, and Y-O Buckles, are interpreted as wrench faults of probable Laramide age with right-lateral displacement. The buckles are remarkably straight and uniformly spaced, extending southwest-northeast for up to 80 miles across the Pecos Slope and projecting beneath the northern Roswell Artesian Basin (Motts and Cushman, 1964; Havenor, 1968; Kelley, 1971).

In the northern Sacramento Mountains, the Mescalero Arch forms a broad structural divide separating the Pecos Slope to the east from structurally lower areas of the Tularosa and Sierra Blanca Basins to the west (Fig. 2, 5) (Pray, 1961; Kelley, 1971). The Mescalero Arch coincides with the crest of the Sacramento Uplift and plunges gently north-northeast, passing about six miles east of Ruidoso and intersecting the mid-point of the Capitan Mountains batholith. The position of the Arch also roughly corresponds to the axis of the late Paleozoic Pedernal Uplift (Kelley & Thompson, 1964; Kelley, 1971; Cather, 1991). The west limb of the Arch is much steeper and more irregular than the gently dipping

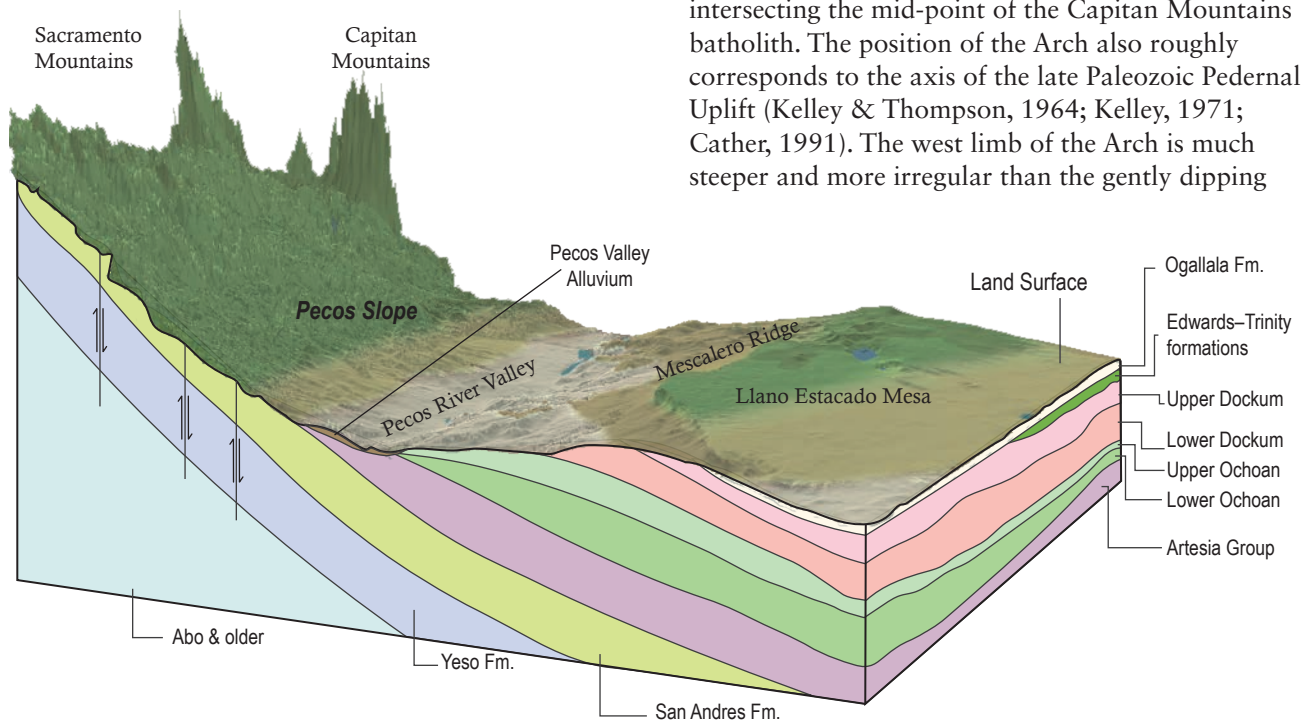


**Figure 3.** Block diagram showing simplified regional subsurface geology and surficial landscape. View is W-NW. Units dip approximately 3 degrees E from the Sacramento Mountains. Primary aquifer units include the Yeso Fm., San Andres Fm., Pecos Valley Alluvium, the Ogallala Fm., and the Edwards–Trinity Fms. Confining units or low-permeability barriers to flow include the Abo Fm., Artesia Group, upper and lower Ochoan Fms, and units within the upper and lower Dockum Group.



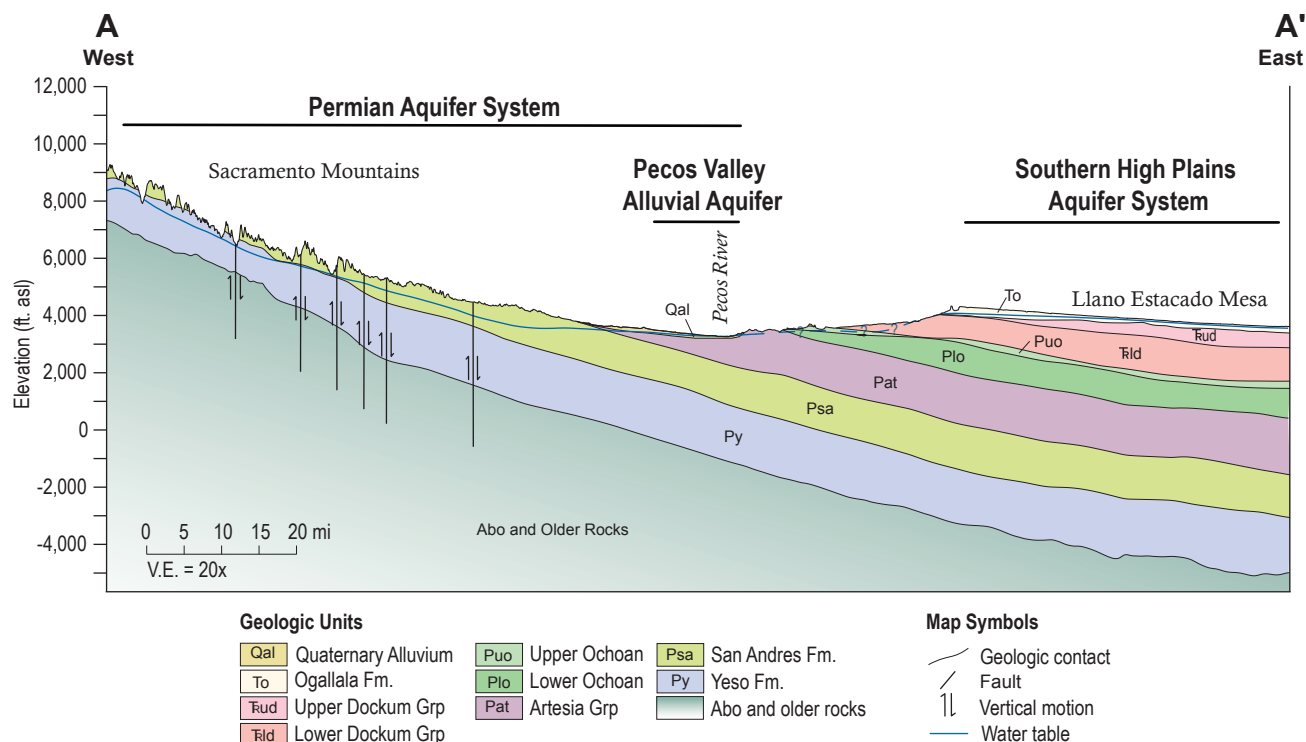


**Figure 4.** A-A' west-east cross-section of southern half of study area displaying subsurface geology and water-table elevation. Surficial extent of aquifer systems is noted. Vertical exaggeration = 20x.

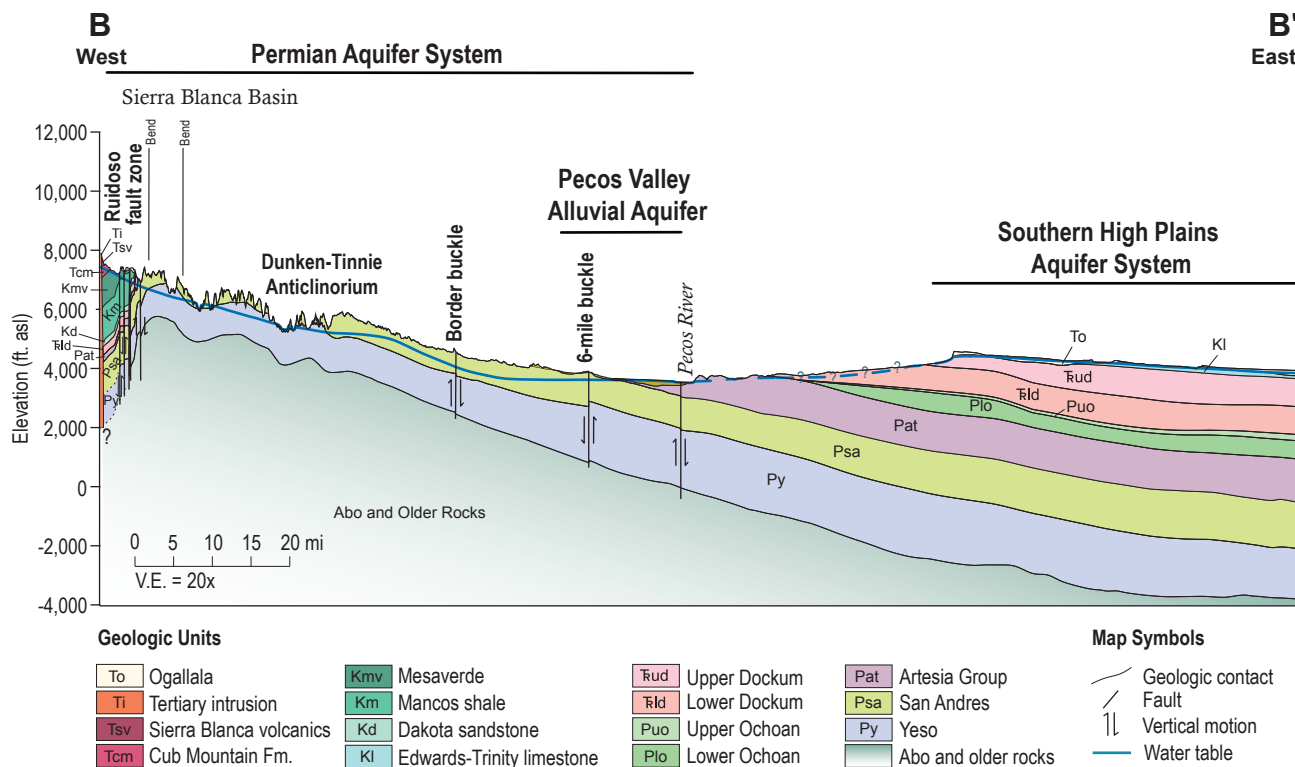


**Figure 5.** B-B' west-east cross-section of northern half of study area displaying complex geologic structure and stratigraphy of the northern Sacramento Mountains (Ruidoso Fault Zone), and the Pecos Buckles. Water-table elevation is displayed. Surficial extent of aquifer systems is noted. Insufficient data was available to confidently contour the water-table surface in the valley east of the Pecos River.



east limb, descending across several northeast-trending faults into the Sierra Blanca Basin. This basin is an asymmetric structural depression of late Laramide age which subsequently became a center for late Eocene–Miocene plutonism and volcanism (Cather, 1991).

Many studies go into further detail on the geologic history of the area and are included in the references section of this report. Additional geologic studies not already mentioned include Adams and Keller (1996), Bachman (1980), Cather (2004), Erdlac (1993), Goff et al. (2014), Gustavson and Holliday (1999), Hawley (1993), Hayes (1964), Johnson (1993), Kelley et al. (2014), Koning et al. (2014, 2014a, 2014b), Kues and Giles (2004), Lehman and Chatterjee (2005), Loucks (2009), Lucas and Anderson (1993), Lucas et al., (2001), Lucas (2004), Lyford (1973), Mack and Bauer (2014), McGown et al. (1977), Meyer (1966), Motts (1972), Nance (2009), Nummedal (2004), Pazzaglia and Hawley (2004), Powers (2003), Rawling (2014), Riggs et al. (1996), Schiel (1988), and Seager (2004).

## Hydrogeologic Overview

Groundwater in the region is divided into three generalized aquifer systems based on the 3D geologic framework, current water levels, and previous

research. The three aquifer systems include: 1) the Permian Aquifer System comprised of east-dipping limestones exposed in the Sacramento Mountains which continue in the subsurface through the Roswell Artesian Basin, 2) the Pecos Valley Alluvial Aquifer composed of alluvial sediments surrounding the Pecos River, and 3) the Southern High Plains Aquifer System encompassing the area east of the Mescalero Escarpment and west of the New Mexico–Texas border (Fig. 6). Analysis of water levels measured after 2010 show groundwater flow within systems is interconnected between geologic formations, flowing cross-formationally between hydrostratigraphic units and possibly, though less frequently, between aquifer systems. The Pecos River bisects the study area and acts as the major point of discharge for the Permian Aquifer System and the Pecos Valley Alluvial Aquifer. Groundwater in the Southern High Plains Aquifer System flows principally southeast down stratigraphic dip into Texas. Subsurface geology and structure play a major role in groundwater storage and flowpaths. Confined, unconfined, perched, and artesian aquifers all exist in the study area.

Water quality varies considerably as a result of groundwater flow paths, geochemistry, and irrigation practices. Water quality was contoured in three

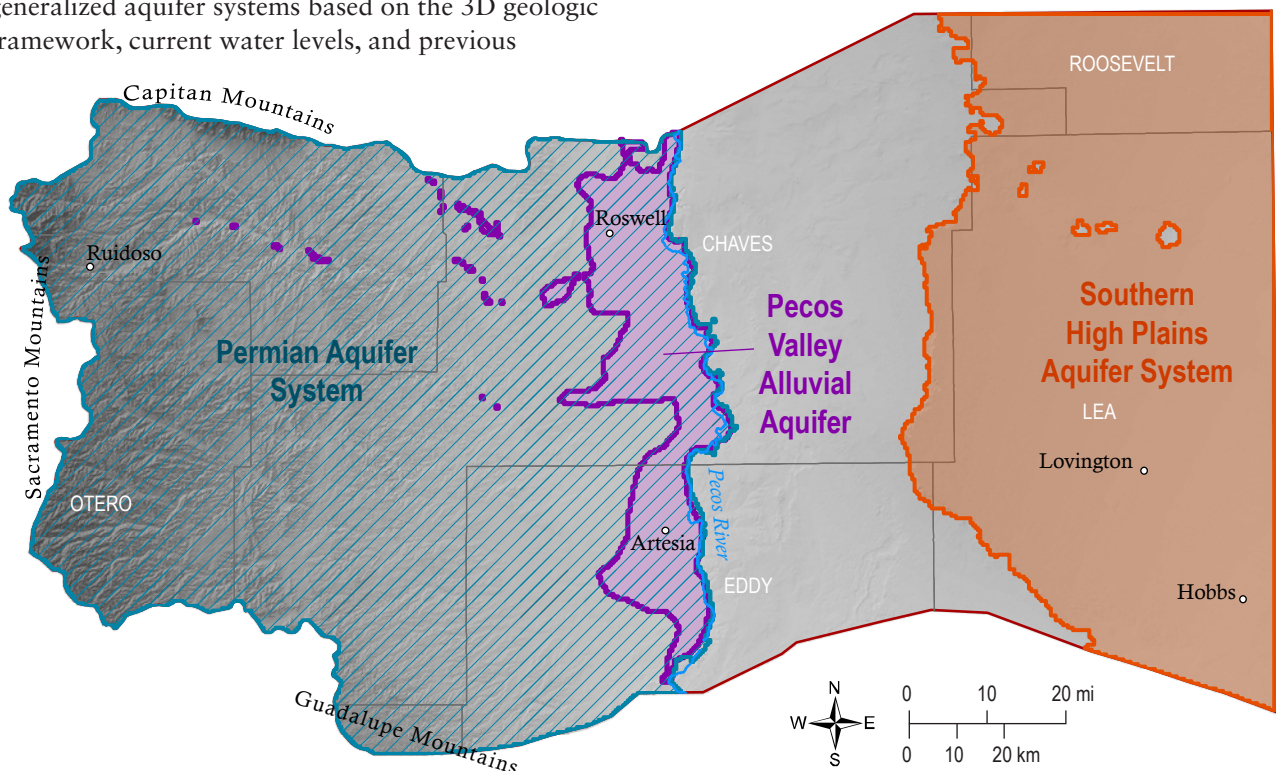


**Figure 6.** Areal extent of relevant aquifer systems/aquifer units. Extent is delineated based on lateral extent of subsurface aquifer units and water quality with TDS <3,000 mg/L.



dimensions and divided into two zones: 1) fresh to low-salinity brackish, and 2) brackish to saline, based on total dissolved solids (TDS) content (Fig. 7). The 3-dimensional display of water quality highlights the regional spatial variability in salinity (Fig. 7), and furthermore, could potentially provide estimations of brackish water resources in future studies. Water quality was grouped into two categories, with shallow groundwater (<2,000 ft) typically being fresh to

low-salinity brackish (TDS <3,000 mg/L), and increasing to higher salinities (TDS >35,000 mg/L) with depth (Fig. 7a, 7b). Contouring water quality in three dimensions provided additional considerations for aquifer boundaries with depth, and facilitated in estimating the volume of known groundwater resources in the region (Fig. 7). Aquifer system characteristics are described in further detail in subsequent sections.

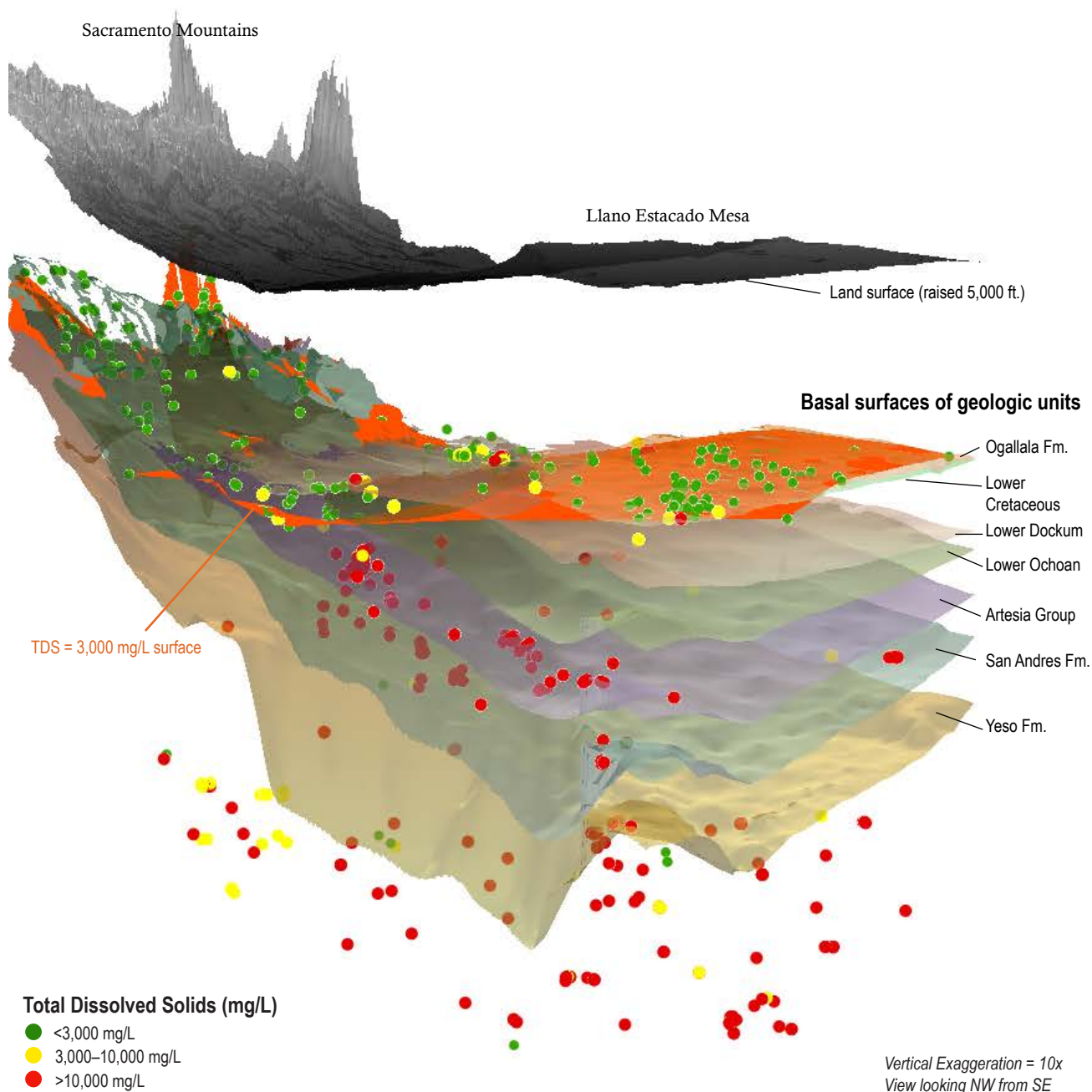
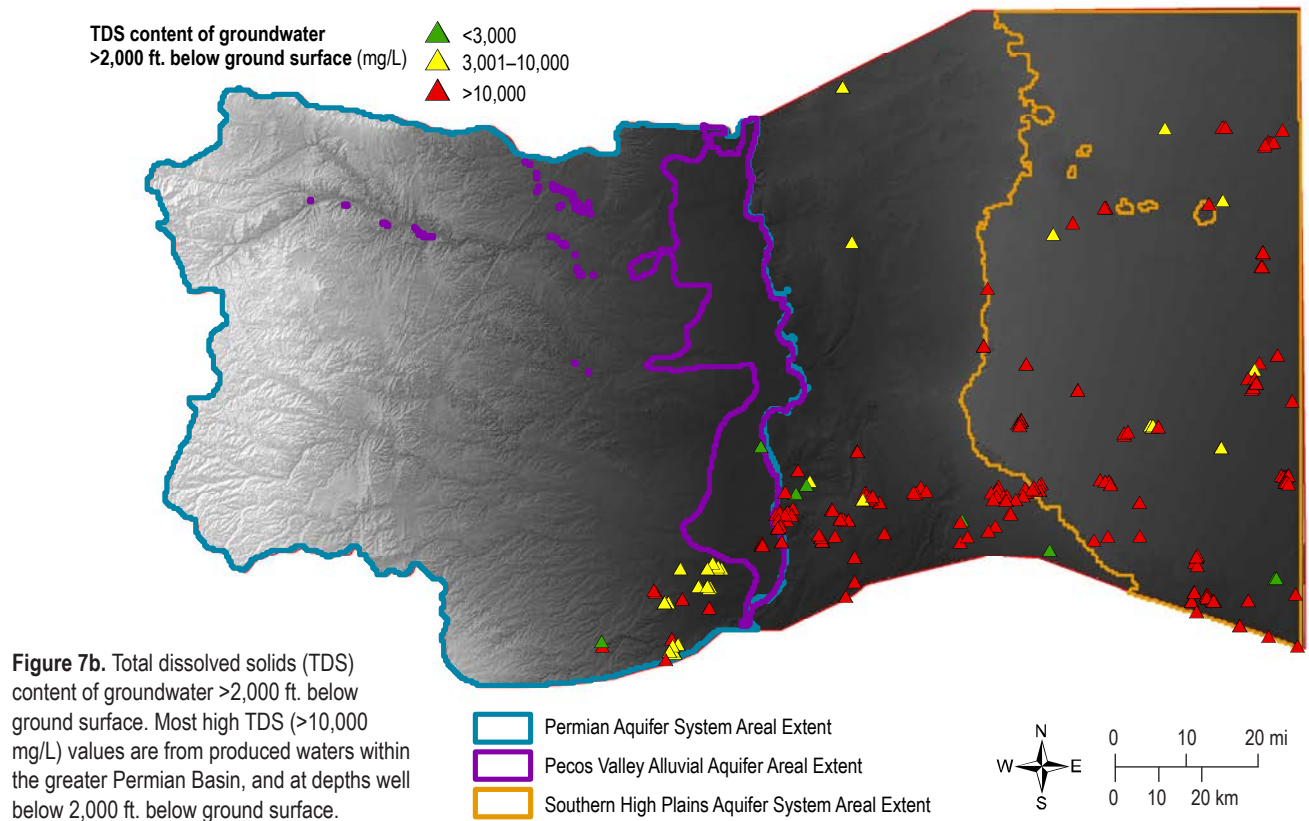
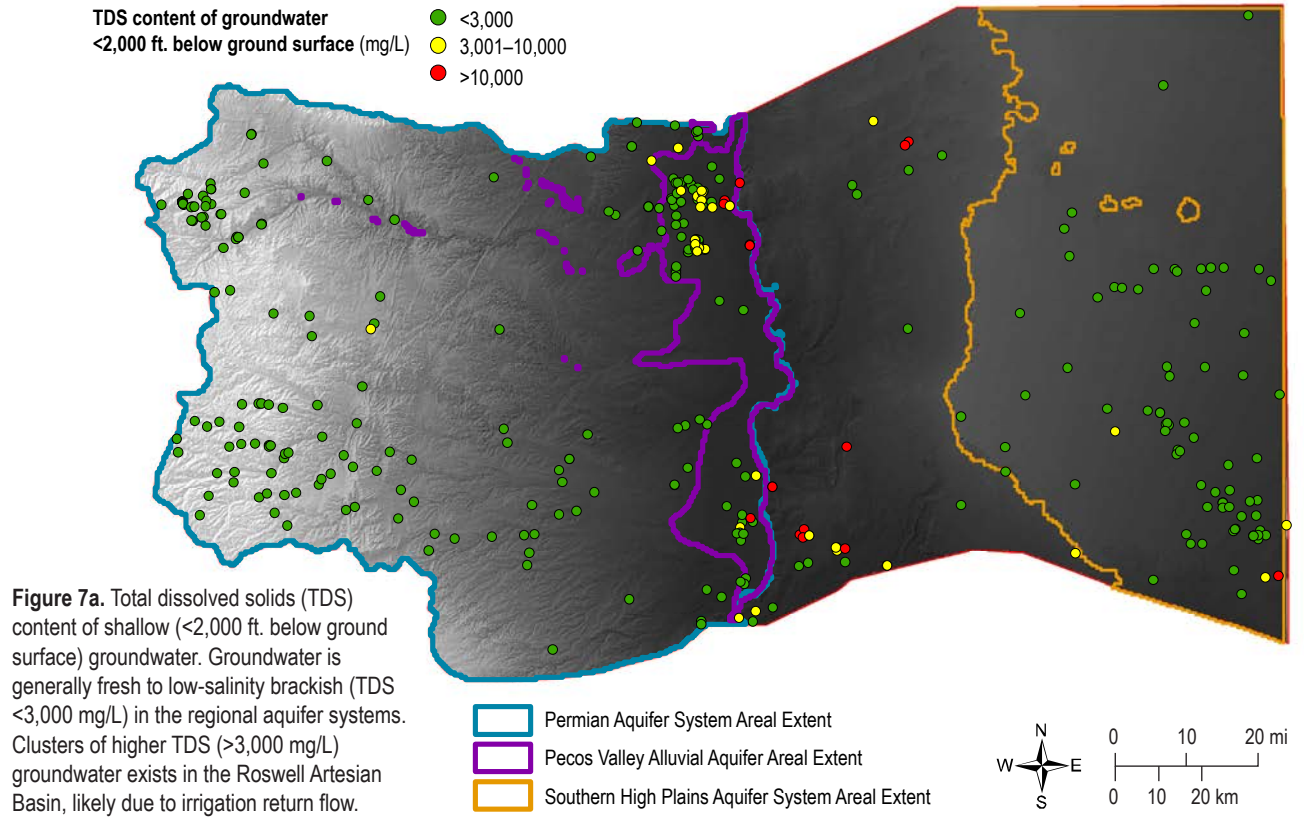


**Figure 7.** Three-dimensional representation of total dissolved solids concentration within study area. View is looking NW from SE. Land surface has been raised 5,000 ft. and geologic layers were made transparent to expose subsurface TDS distribution. A surface representing a TDS value of 3,000 mg/L is displayed and was used to estimate the approximate base of treatable groundwater for respective aquifers in the region. TDS points are plotted at their recorded well depths. The zone of high TDS water (>10,000 mg/L) is associated with produced waters from oil and gas operations in southeast NM.









Willis Canyon in the crest area, the recharge zone for the Pecos Slope, of the Sacramento Mountains.  
*Photograph by Lewis Gillard.*



### III. METHODS

#### Overview

Using existing geologic and hydrologic data and robust geostatistical tools available in ESRI's ArcGIS, a suite of geologic surfaces and hydrologic surfaces were created and compiled into an ArcGIS map package available for download. A detailed report on the methodology involved in creating these geologic surfaces is available in the previous chapter. Detailed methods for the development of aquifer surfaces and volume calculations are described in Appendix 1. A general summary of the methodology is described here.

Overall, the 3D hydrogeologic model was developed in two parts: 1) the development of geologic surfaces, and 2) the development of aquifer surfaces. Both parts of the process utilized solely existing data in various forms, i.e., no additional data was collected for this project. Three-dimensional geologic and hydrologic surfaces were created by first compiling and organizing existing data into ArcGIS relational databases. Input data for geologic surfaces included: land surface digital elevation models (DEMs) derived from Intermap Technologies (2008) 4.5-meter resolution digital terrain models (DTMs); surface geology and faults acquired from the 1:500,000-scale statewide surface geologic map of New Mexico (NMBGMR, 2003) and Precambrian subsurface mapping by Broadhead et al. (2009); subsurface formation picks from well control sources including databases provided by Ron Broadhead at NMBGMR, the Texas Water Development Board (TWDB), and the New Mexico Oil Conservation Division (NM OCD); digitized cross-sections available from NMBGMR; structure contours produced from several studies; and existing raster surfaces from TWDB-sponsored aquifer studies. Input data for aquifer surfaces included: resulting 3D geologic surfaces; water-level data from sources including the USGS, several studies published by NMBGMR, and static water-level data available from the New Mexico Water Rights Reporting System (NM WRRS) provided by the New Mexico Office of the State Engineer (NM OSE); and water-quality data sourced from several studies done in the region by NMBGMR, Sandia National Labs (SNL), and TWDB.

Raster surfaces were created by interpolating between control points using geostatistical tools available in ArcGIS. Rigorous quality control procedures for geologic surfaces were implemented and are outlined in chapter by Cikoski. Aquifer top surfaces were interpolated from water level control data, from sources with recorded water levels taken in the last decade (year 2010–present). Aquifer basal surfaces were estimated using a combination of visual and computational interpretation of water quality (total dissolved solids) and geologic boundaries at depth. This process involved mosaicking geologic bounding surfaces with water quality bounding surfaces to create an approximate freshwater aquifer “bottom” boundary in the subsurface. For the purposes of this study, freshwater is considered to be groundwater with total dissolved solids (TDS) concentrations <3,000 mg/L. Identifying and creating aquifer bottom surfaces allowed freshwater volumes to be estimated using methods outlined in Appendix 2.

Cikoski provides a thorough statistical analysis of the feasibility of using ArcGIS to build a 3D geologic model, using the Pecos Slope region as a pilot study area. This process provides a new technique in which aquifer boundaries can be interpreted, estimated, and visualized in the subsurface. The cross-sections shown in this report were generated from the 3D framework, and are an example of the types of informative products that can be developed from 3D maps. Additionally, the development of the 3D model allowed for identification and correction of errors in subsurface data, and highlighted regions where subsurface data is lacking.

#### Water Data Summary

The water data network in the study area is dense—a total of 31,151 water-well and spring locations were pulled from agencies including NMBGMR, NM OSE, and USGS. Well-depth data was used in conjunction with geologic surface data to assign aquifer units to wells. Water levels were then assigned to aquifer systems based on aquifer



units. Table 1 outlines the number of wells used to create hydrologic surfaces for each aquifer system in the study area. Only water levels collected and/or reported after year 2009 were used to create water-table maps for each aquifer system:

From the 31,151 water-well and spring locations in the study area, 2,563 locations had water-level

**Table 1.** Aquifer assignment based on well depth. The 3D geologic framework was used to assign a geologic unit to each well in the study area. Wells with water levels reported after year 2009 were used to create water-table maps for each aquifer system.

Geologic unit of well depth	No. of wells used in model	Aquifer system assigned
Yeso Fm., San Andres Fm., Upper Cretaceous Fm., Sierra Blanca Volcanics	494	Permian Aquifer System
Pecos Valley Alluvium	307	Pecos Valley Alluvial Aquifer
Ogallala Fm., Edwards–Trinity Fm., Upper Dockum Group.	950	Southern High Plains Aquifer System

measurements reported after 2009. Of these, a total of 1,639 water-level measurements were within aquifer system boundaries. The final water-level data coverage used in the hydrologic model is shown in Figure 8.

The data compilation phase of model development provided an opportunity to analyze the water data density of the region. Recent water-level data (post year 2009) density is sparse in many areas, especially when compared to the nearly 32,000 well and spring locations documented in the initial data compilation. Figure 8 displays the post-2009 water-level network used in the model. Data gaps can be seen in all aquifer systems, namely in the central to south-central portion of the Permian Aquifer System, the western portion of the Pecos Valley Alluvial Aquifer, and the northern half of the Southern High Plains Aquifer System. Wells that tapped some formations were left out of water-table analyses all together due to lack of data. Wells that tap these formations are displayed in Figure 9. The large swath of land between the Southern

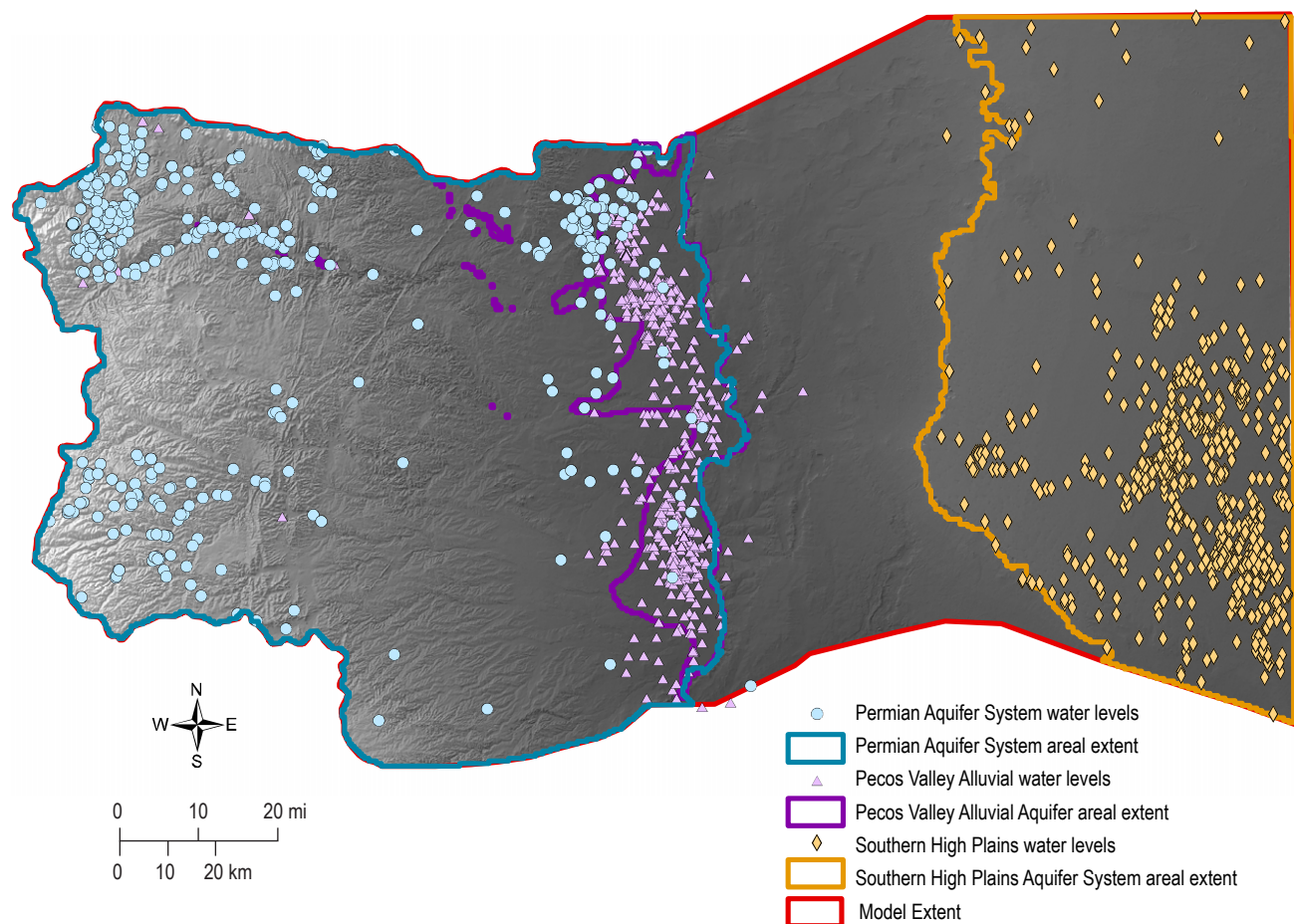


**Figure 8.** Locations of water-level measurements used in model development for each aquifer system. Table 1 summarizes the number of wells with relevant water-level data. Over 30,000 data points existed from the initial data compilation effort, from sources including the New Mexico Bureau of Geology, the United States Geologic Survey, and the New Mexico Office of the State Engineer, with water-level measurements dating back to the early 1900s. Of these 30,000 data points, 1,639 had measurements post-dating 2009 and were subsequently used in development of the 3D model.



High Plains Aquifer System and the Pecos River contains Ochoan and Dockum strata. Well networks in this region are sparse, and associated water-level and water-quality data are also lacking. TDS data in shallow groundwater (Fig. 7a) is most dense in the Sacramento Mountains region, the northern

Roswell Artesian Basin, and the Southern half of the High Plains region. Areas where brackish water (yellow) and saline water (red) are more abundant are options to sample in future studies for brackish water resources. The northern half of the Southern High Plains system is also lacking sufficient TDS data.

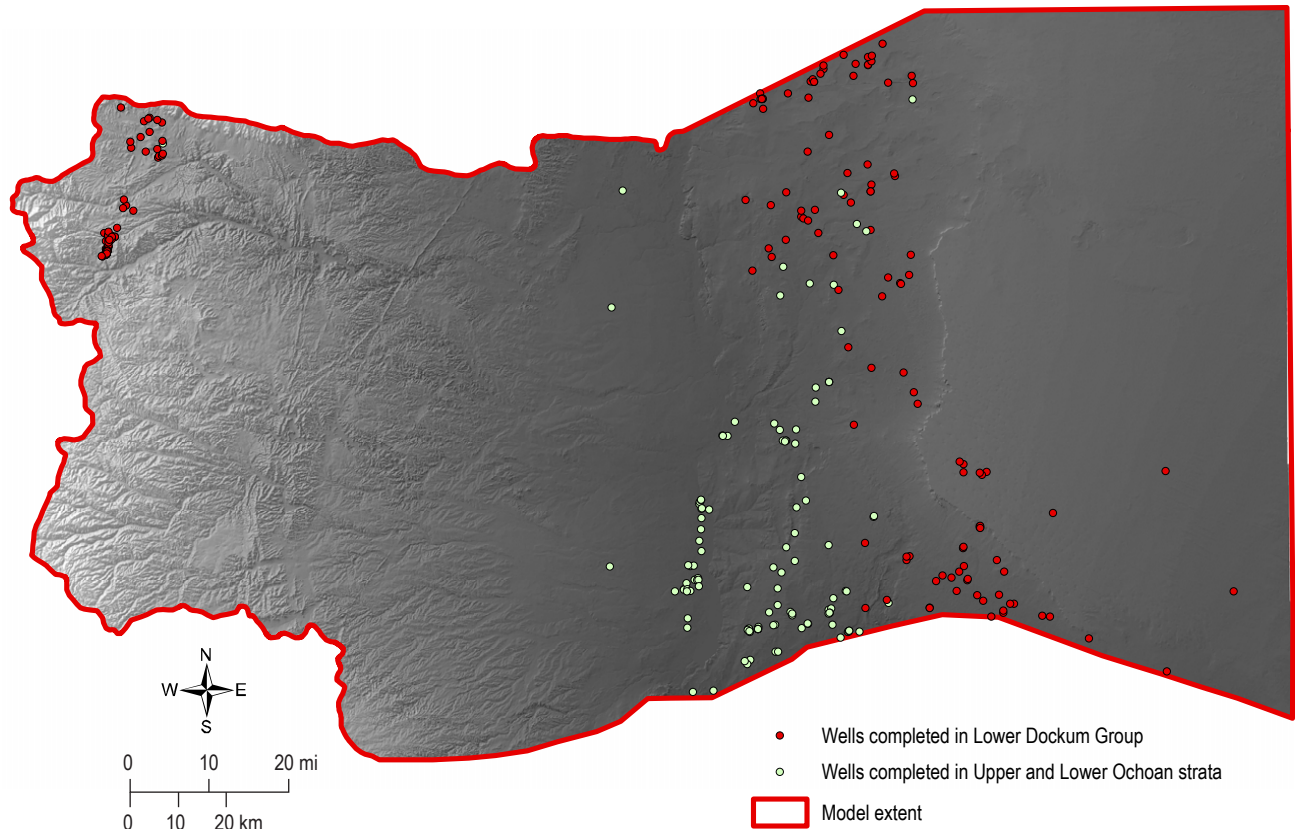


**Figure 9.** Network of wells not used in aquifer characterization of this region. These wells include those drilled into the Lower Dockum Group and the Upper and Lower Ochoan formations. Water-level and water-quality data for these formations is lacking, therefore groundwater flow was unable to be adequately analyzed in the large swath of land between the Southern High Plains and the Pecos Valley Alluvium.





Bitter Lake is sourced from the Lost River (also known as Bitter Creek). The lake is seasonally dessicated, as in this July 2016 photo.  
*Photograph by David J. McCraw*



## IV. REGIONAL AQUIFER SYSTEMS

### Permian Aquifer System

#### Overview

The Pecos Slope is a geologically defined structural ramp to the west of the Pecos River (Kelley, 1971). Its western extent is defined by the Mescalero Arch in the north, the crest of the Sacramento Mountains, and the crest of Guadalupe Mountains in the south (Fig. 6). The northern boundary of the study area runs from Carrizo Peak in the northwest, east along the crest of the Capitan Mountains, down slope to the Pecos River. The eastern boundary is defined by the Pecos River, which runs roughly north-south. The southern boundary runs east-west, roughly 10 miles south of Artesia, extending west to where it reaches the ridge of the Sacramento Mountains. Elevation ranges from the high at Sierra Blanca of 11,981 ft descending to the west, down to 3,300 ft on the valley floor along the Pecos River (Fig. 1).

The south-flowing Pecos River is the primary surface water feature in the area. Several other smaller rivers flow eastward from their headwaters in the upper Sacramento Mountains; the Rio Hondo in the north, the Rio Felix, and the Rio Penasco (Fig. 1). The upper reaches of these rivers flow year-round, however, natural recharge to the aquifers, and irrigation along eastern reaches of the rivers siphons off much of the natural flow. These rivers are typically dry by the time they reach the lower basin except after storms and during spring runoff.

The primary population centers within the study area include Ruidoso, Roswell, and Artesia (Fig. 1). The Roswell Artesian Basin in the Pecos Valley is one of the most intensively farmed areas in the state. The principal crops are alfalfa, cotton, sorghum, chiles and pecans (Land and Newton, 2008). The basin derives the majority of its irrigation water from groundwater stored in a shallow alluvial aquifer and from the underlying confined Permian aquifer. Because of the long history of agriculture and settlement in the region, this region has one of the best water-level measurement networks in the state.

The Permian Aquifer System can be subdivided into three distinct groundwater flow systems, and

has commonly been delineated by the following in previous studies: 1) The High Mountain Aquifer System, consisting of principally the Yeso Formation in the higher elevations of the Sacramento Mountains; 2) The Pecos Slope Aquifer, consisting principally of the San Andres Formation, located on the lower slope of the Sacramento Mountains foothills; and 3) The Roswell Artesian Basin, consisting of the San Andres Formation where it underlies the Artesia confining unit, located mostly beneath the Pecos River and surrounding Pecos Valley Alluvium (Rinehart and Mamer, 2017). While these three systems have distinct defining characteristics, groundwater is largely interconnected between them and hence for the purposes of this study they are mapped as one aquifer system.

#### Geologic units

The primary geologic units found in the study area that play a role in the hydrologic model, from oldest to youngest, are the Permian Yeso Formation, the San Andres Formation, and the Artesia Group (Land and Newton, 2008). The Permian units are tilted, dipping roughly 1 degree to the east (Fig. 3). There is very poor exposure of the Yeso Formation, as it is usually covered by the more resistant San Andres Formation, however, it crops out in the eroded upper reaches of drainages in the Sacramento Mountains (Fig. 2). This is displayed in the 3D geologic model, as patches of the San Andres basal surface are absent in the distinctive form of drainage patterns in the western-most portion of the model. Where the Yeso Formation is exposed, it is prone to dissolution and weathering. The San Andres is exposed throughout much of the Sacramento Mountains and across the Pecos Slope, where it is overlain by the Artesia Group along the lower flanks (Fig. 3). The valley floor is covered by the alluvium and older basin fill (Land and Newton, 2008) (Fig. 2).

The Yeso Formation (~2,000 ft thick) is a heterogeneous formation composed of discontinuous limestone, siltstone, and sandstone, dipping gently to the east. Abundant fractures and karst features make it a productive aquifer (Fig. 10). Above the



Yeso Formation, the San Andres Formation (~1,000 ft thick) is made up of light-to-dark-gray and bluish-gray carbonate rocks (Land and Newton, 2008). This group of carbonate and siliciclastic units make up the variably confined Permian aquifer system. Above the San Andres is the low permeability Artesia Group, largely composed of siliciclastic and evaporite deposits. The Artesia group was part of a back reef environment where thick evaporite deposits were deposited. Moving south this formation grades into the Capitan Reef.

There are four prominent pre-Permian to late Permian structural zones of folding and faulting that transect the Pecos Slope and extend into the Roswell Artesian Basin (Kelley, 1971; Fiedler and Nye, 1933). All four of these structural zones run parallel to each other, trending southwest to northeast (Fig. 2). In addition to these structure zones is the Pecos River Fault that trends north to south along the path of the Pecos River. The impact of these structural zones

on the hydrogeology of the basin is not well understood, though DBS&A (1995) found structural zones coincided with changes in spacing of the potentiometric contours.

### Water data

Water data in the Permian Aquifer System is generally abundant. Data compiled for this study included water-well locations, water levels, and TDS content. The total water-well network with associated geologic model units is shown in Figure 11. Wells used in water-table development are displayed in Figure 12. Data coverage is summarized in Table 2.

Wells with reported TDS content totaled 289 data points within the Permian Aquifer System extent. Sample dates range from years 1926 to 2018. TDS content ranges from 1 mg/L to 219,490 mg/L, with a mean TDS value of 13,054 mg/L. All available TDS data was used in model development (Fig. 7a, 7b).

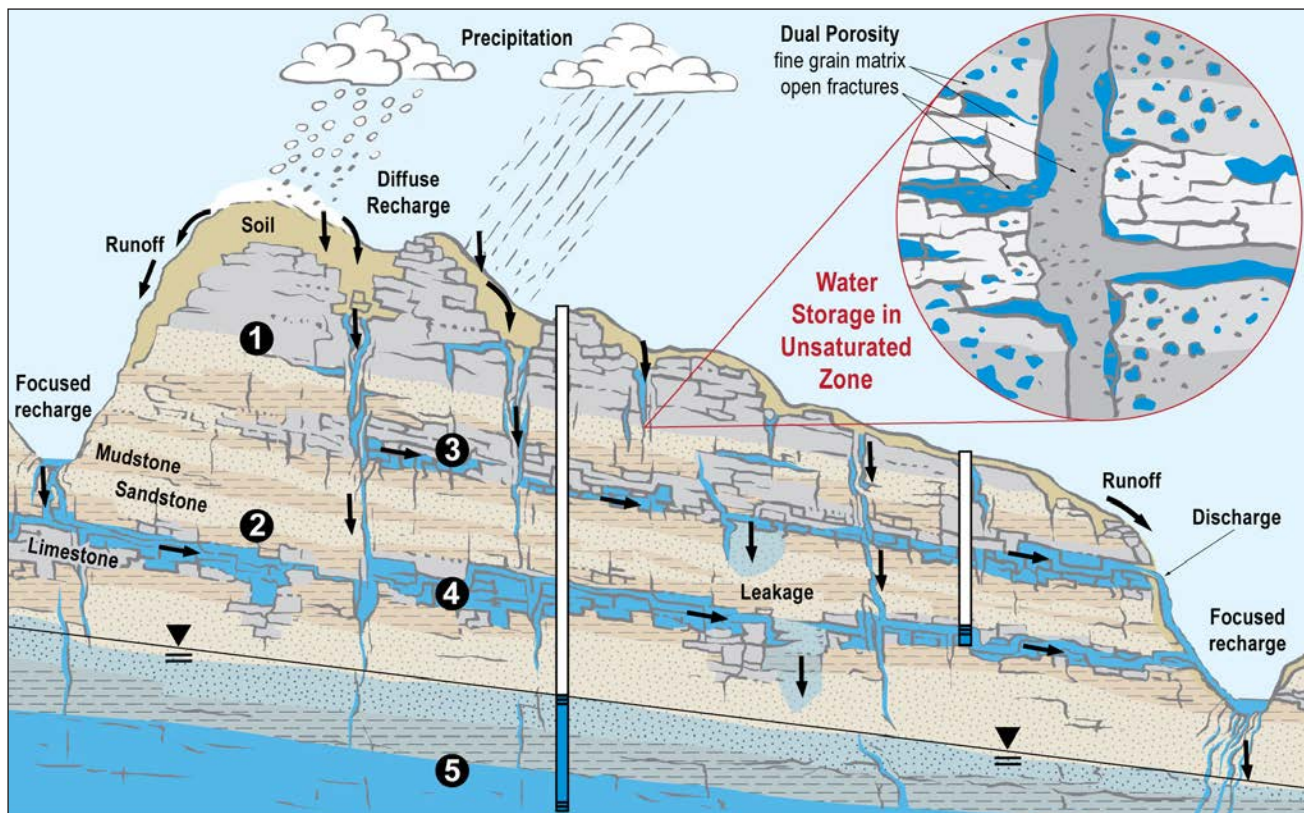


**Figure 10.** Conceptual model of Yeso aquifer in the Sacramento Mountains. 1) An upper vadose zone is the unsaturated bedrock that exists above local perched aquifers. Water can be stored in fractures, epikarst, and pores in this zone. 2) An intermediate vadose zone is unsaturated bedrock located between two saturated carbonate aquifers. 3) A local perched aquifer is the upper-most perched aquifer that is recharged by infiltration from directly above and discharges at a spring in the local watershed. 4) An intermediate perched aquifer is located beneath at least one other perched aquifer and is recharged by focused recharge from one or more watersheds and leakage from overlying aquifers. This aquifer discharges to springs. 5) A regional aquifer is primarily recharged by focused recharge from several streams and leakage from perched aquifers. These aquifers are deep enough to avoid groundwater/surface water interactions and likely merge with the Pecos Slope aquifer.



**Location of wells completed  
in the following  
geologic formations:**

- Sierra Blanca Volcanics
- Upper Cretaceous Fm.
- San Andres Fm.
- Yeso Fm.
- Model extent
- Permian Aquifer System

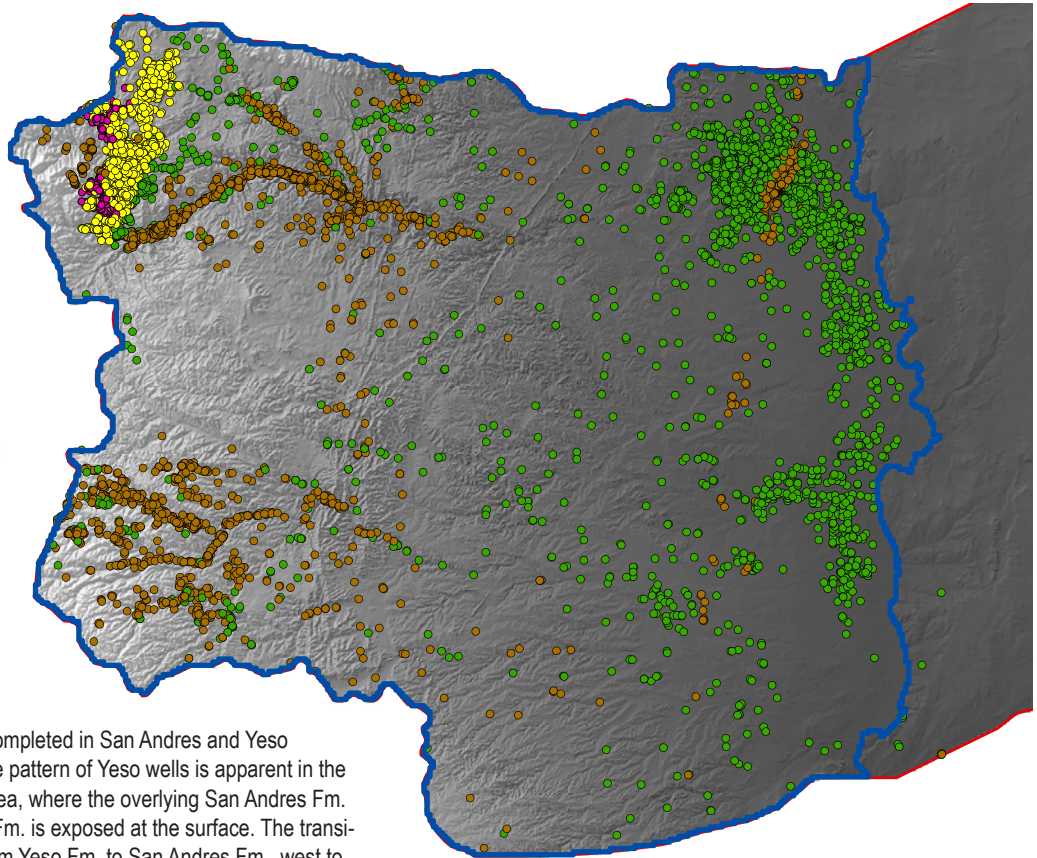
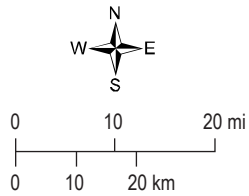


**Figure 11.** Location of wells completed in San Andres and Yeso Formations. A distinct drainage pattern of Yeso wells is apparent in the western-most portion of the area, where the overlying San Andres Fm. is eroded away and the Yeso Fm. is exposed at the surface. The transition in principal aquifer unit from Yeso Fm. to San Andres Fm., west to east, is apparent.

- Permian Aquifer System  
water-level locations  
2009-present
- Model extent
- Permian Aquifer System

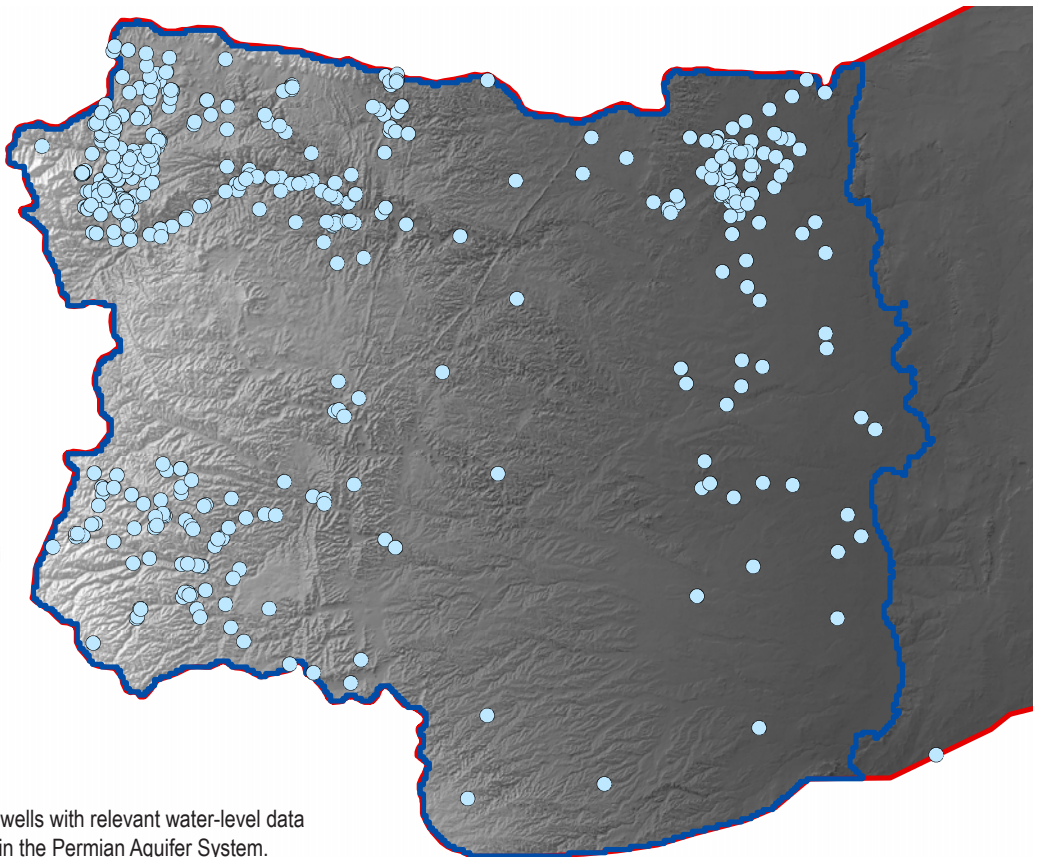
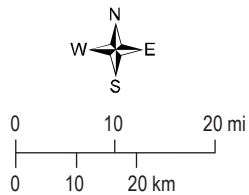


**Figure 12.** Locations of water wells with relevant water-level data (sample date post year 2009) in the Permian Aquifer System.



**Table 2.** A summary of water-well coverage in the Permian Aquifer System extent. Table displays the total number of wells completed in corresponding geologic formations, the number of wells used in development of water-table maps/surfaces for this study, and the average well depth of wells used in the study, measured in feet below ground surface. Relevant water-level data corresponds to water levels reported after year 2009.

Geologic Formation	Total no. of wells	No. of wells with relevant water-level data	Average well depth (ft. bgs)
Sierra Blanca Volcanics	328	21	269.8
Upper Cretaceous	1688	138	375.2
San Andres Fm.	3373	147	395.0
Yeso Fm.	2825	188	315.2
<b>TOTAL</b>	<b>8214</b>	<b>494</b>	<b>-</b>

### Water quality

Detailed chemical analyses of groundwater published in the comprehensive Sacramento Mountains Hydrogeology Study by Newton et al. (2012) is summarized here. Total dissolved solids (TDS) content of the Permian Aquifer System in the Sacramento Mountains and on the Pecos Slope is generally <1,000 mg/L and is considered fresh water (Fig. 13). Specific conductance (SC) of spring water is lower than for well water, suggesting that water discharging at springs has undergone slightly less mineral/water interaction than water collected from wells. SC for wells and springs in the Sacramento Mountains is

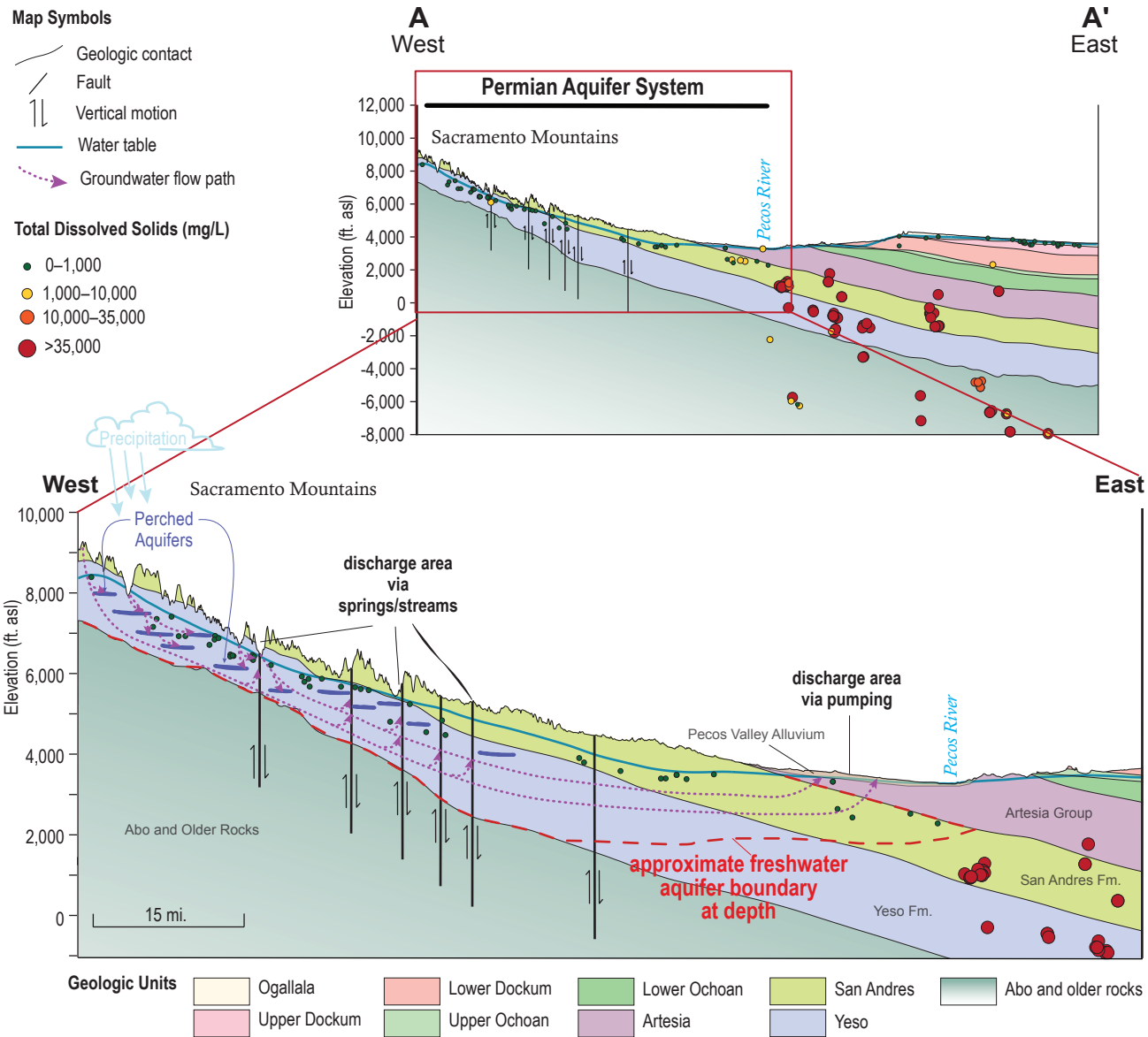


**Figure 13.** Hydrostratigraphic cross-section of the Permian Aquifer System and Pecos Valley Alluvial Aquifer, inset from Figure 4. Dashed line shows approximate bottom of freshwater aquifer at depth, defined by drastic increase in TDS content down stratigraphic dip. TDS data projected from data points within a radius of 15 km. of cross-section line A-A'. Cross-section created from 3D hydrogeologic framework.



generally lower than in the Pecos Slope portion of the aquifer. Total dissolved solids content has an inverse correlation with elevation, and increases significantly down dip east of the Pecos River (Fig. 13). This sharp degradation in water quality constitutes a lower and eastern boundary for the Permian Aquifer System. According to Newton et al. (2012), similar trends are also apparent for sulfate and magnesium content, which increase west to east as well as south to north. Bicarbonate decreases downgradient, and calcium and chloride were shown to have no significant trend with elevation. Oxidation reduction potential (ORP) and dissolved oxygen (DO) were found to be variable. In general, ORP was positive, indicating oxidizing conditions, which is supported by recorded DO values being greater than 5 mg/L.

### Depth to water

Depth to water in the Permian Aquifer System ranges from <100 ft. below ground surface (bgs) to nearly 400 ft bgs. Depth to water measurements reported by the NMBGMR and the USGS were converted to groundwater elevations. These were combined with water levels downloaded from the NM OSE Water Rights Reporting System (WRRS) to create and interpret the regional groundwater flow map displayed in Figure 14. Additionally, this surface was used as the “aquifer top” surface in creation of the 3D aquifer map. Groundwater elevation ranges from >8,000 ft. asl in the Sacramento Mountains to <3,000 ft. asl near the Pecos River (Fig. 14). Depth to water and groundwater elevations are estimated based on water levels taken from year 2010-present. The geology of the Pecos Slope and Roswell Artesian Basin plays a crucial role in the groundwater system’s recharge, groundwater flow and hydraulic properties. The Permian Aquifer System, comprised of the Yeso Formation and San Andres Limestone, forms an unconfined aquifer high on the slope of the Sacramento Mountains. Within the high mountains the high degree of heterogeneity within the exposed outcrop of the Yeso Formation, combined with regional fracture systems, results in a complex hydrologic system that allows a significant portion of high-altitude precipitation to move relatively quickly into the aquifers (Fig. 10). Water-level, geochemical, age dating, and isotope data indicates that the primary recharge source is precipitation in the high mountains above 8,200 feet Newton et al. (2012). Under certain conditions, summer precipitation can also contribute significant recharge to the regional groundwater systems from monsoon storm runoff. Recharge

estimates indicate that up to 22% of high elevation precipitation recharges adjacent regional aquifers to the east and south. Age dating data indicates that it may take up to 1,300 years for groundwater to flow from the Sacramento Mountains to the eastern extent of the Pecos Slope. Groundwater flows from the top of the mountains in the west to lower elevations to the east and south (Fig. 14), eventually moving into the San Andres Formation. Beneath the Pecos River, groundwater is discharged by way of pumping in the Roswell Artesia Basin. Groundwater that is not discharged continues its flow path to the east. At this point, many miles of mineral-water interaction with limestones of the Yeso and San Andres has caused the groundwater quality to degrade significantly.

The primary aquifer unit transitions from the Yeso Formation to the San Andres Formation roughly midway between the crest of the Sacramento Mountains and the Pecos River (Fig. 11, 13). This transition is characterized by a flatter hydraulic gradient (Fig. 14) reflecting the high transmissivity of large cavernous fractures and sinkholes typical of the San Andres Fm. (Newton et al., 2012).

Moving east, lower down the slope, the Permian Aquifer System is superimposed by the low-permeability Artesia Group, leading to confined aquifer conditions (Fig. 13). In the early 1900s, when this confined aquifer system was first drilled into, there were reports of water gushing hundreds of feet into the air. Today, however, the artesian pressure has been reduced and, for the most part, the potentiometric surface is below ground surface (Fig. 13).

Aquifer test data published by DBS&A (1995) indicate that transmissivity in the San Andres Fm. is highly variable in the Roswell Artesian Basin, ranging from 1,600 ft<sup>2</sup>/d to over 400,000 ft<sup>2</sup>/d. The storage coefficients used to quantify storage change for the aquifers were found in DBS&A (1995) which compiled published storage coefficients from numerous studies conducted on the Permian aquifer system, and further refined the values with a calibrated groundwater flow model. Results of the study found a specific yield value of 0.05 and a storativity value of 0.0005 to be representative of unconfined and confined portions of the aquifer system, respectively.

### 3D geometry

Information outlined above regarding geologic features, groundwater elevations, water quality, and well networks, were all combined to delineate the three dimensional extent of the Permian Aquifer System. Areal extent of the Permian Aquifer System was



largely determined by the bounding mountain ranges of the eastern Sacramento Mountains watershed. The west and north boundaries follow the ridgeline of the Sacramento and Capitan mountains (Fig. 6), which constitute locations of known groundwater divides. The southern boundary follows the northeast extent of Otero Mesa and the Guadalupe Mountains. The eastern boundary was defined as the eastern extent of the Pecos Valley Alluvium; at this point, wells are no longer located in the San Andres Fm (Fig. 11).

As groundwater flows through the Yeso and San Andres formations of the Permian Aquifer System, minerals in the rocks of the limestones interact with the groundwater. West to east, TDS content increases

with distance from the recharge area in higher elevations (Newton et al., 2012). A cross-sectional view of groundwater flow paths and TDS content, generated from the 3D hydrogeologic framework, is shown in Figure 13. The cross section displayed in Figure 10 is an example of the informative products that can be created from 3D maps in ArcGIS—similar cross sections can be generated anywhere within the study area boundary. Just east of the Pecos River, TDS content increases sharply to greater than 10,000 mg/L in the subsurface. The intersection of the TDS = 3,000 mg/L surface and the base of the Artesia Group creates an approximate eastern boundary of the aquifer system in the subsurface. After areal aquifer

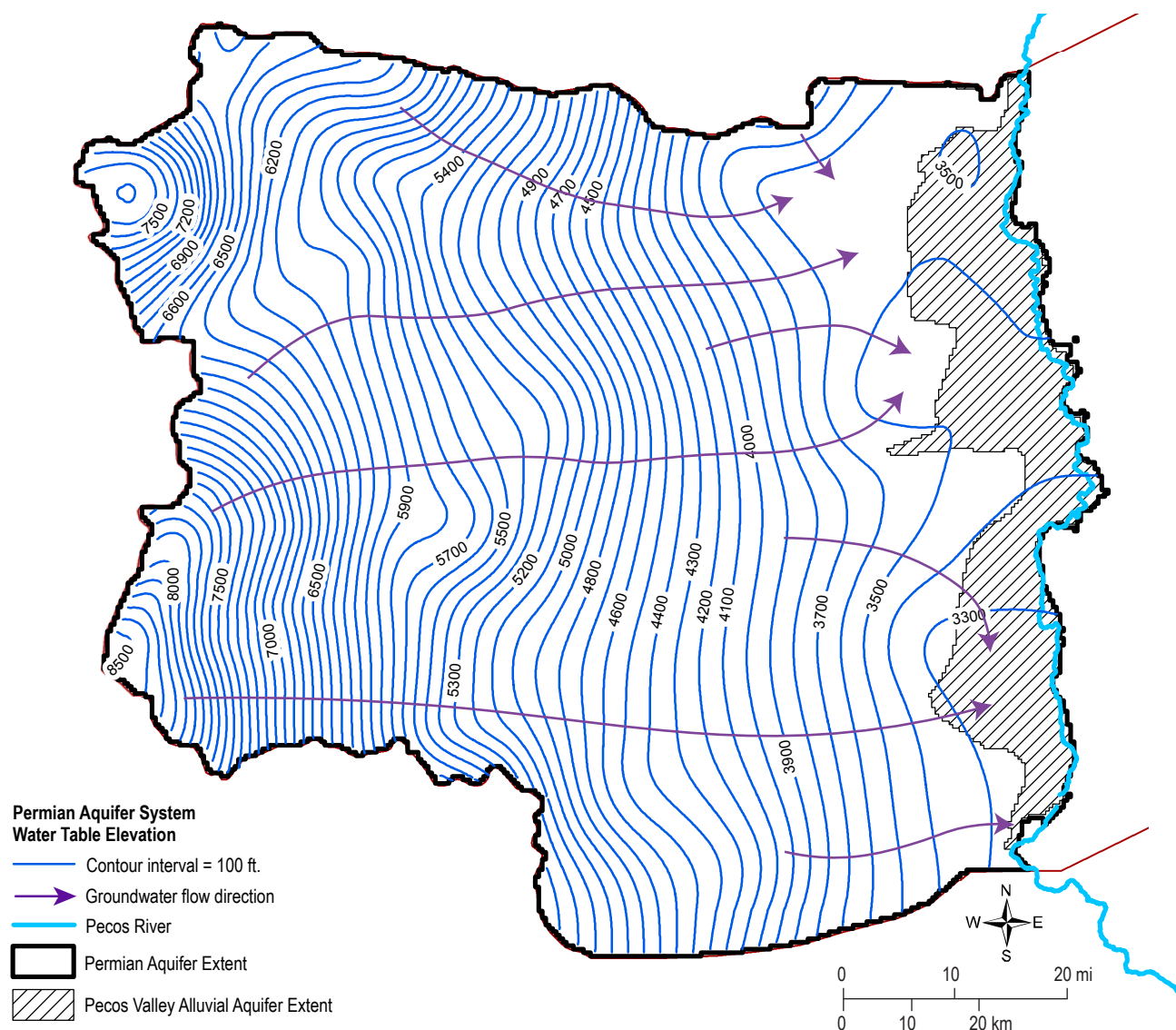


**Figure 14.** Potentiometric surface map of the Permian Aquifer System. Groundwater flows generally from its recharge location in the Sacramento Mountains eastward into the Roswell Artesian Basin, eventually discharging into the Pecos River, by way of pumping by Roswell and Artesia for irrigation, or continues flowing east down stratigraphic dip.



extents were delineated, top and bottom surfaces were created, displayed in Figure 15a and 15b. Figure 15c shows the resulting thickness of fresh groundwater within the aquifer system. This thickness was used to conservatively estimate groundwater volume.

### Water quantity

From the 1900s through the 1950s storage change in the Permian Aquifer was relatively minor, on the order of 0.05 million acre-feet (Maf) (Rinehart and Mamer, 2017). From the 1950s to 1960s, the Permian aquifer saw the largest withdrawals, almost 0.5 Maf in 10 years. In 1956 the adjudication of water rights began and led to the retirement of 12,000 acres (Shomaker, 2003). In 1967, the Pecos Valley Artesian Conservancy District (PVACD) required irrigation wells in the basin to be metered; this ensured that landowners were only accessing their allotted water rights (Shomaker, 2003). From the 1970s through the 1990s, groundwater storage appeared to recover before declining slightly in the 2010s. The groundwater policy implementations of the 1960s seems to have had a significant impact on the storage change.

Potential leakage between confined and unconfined aquifers in the system is an additional concern. Since the artesian system was first discovered, thousands of wells have punctured the confining unit to tap the pressurized system beneath. In an effort to reduce leakage between the aquifers, the PVACD has plugged more than 1500 leaky or abandoned artesian wells (Shomaker, 2003). Originally, the effort focused on preventing the upward flow from the confined aquifer into the alluvial aquifer. Recently, however, the potentiometric surface of the confined system has dropped below the water table in the alluvial system. As there is currently a downward gradient in places between the two aquifers, water is potentially leaking from the alluvial system into the confined aquifer.

While the total change in groundwater storage in the Permian Aquifer System has been relatively small, in the confined area between Roswell and Artesia, there have been significant declines in the potentiometric surface. In the Roswell area, the potentiometric surface has dropped by 50 to 60 ft over the 120 year measurement record. This demonstrates how rapidly the potentiometric surface can decline in confined areas due to extraction of small volumes of water.

Estimating the volume of groundwater present in the Permian Aquifer System is complex due to the heterogenous stratigraphy of the Yeso Formation, the karstic nature of the San Andres Formation, the transition from confined to unconfined conditions

with the presence of the Artesia Group, and the degradation of water quality in the San Andres and Yeso formations down stratigraphic dip. Freshwater volumes were estimated for the confined and unconfined portions of the aquifer system and combined for a total estimate. A storage coefficient of  $4e-5$  (DBS&A, 1995) was used for the confined portion, and a specific yield range of 0.05–0.15 was used for the unconfined. It should be noted that karst features and perched aquifers in the unconfined portion of the aquifer system cause hydrogeologic properties, including specific yield values, to vary by orders of magnitude within individual units. A total volume estimate of treatable groundwater (TDS content  $<3,000$  mg/L) within the Permian Aquifer System ranges from 86.7 to 259.8 Maf for the extent outlined in Figure 6. This estimate was calculated using boundaries delineated by the 3D hydrogeologic framework shown in Figure 12. The appendix included in this report outlines the methodology in calculating freshwater volumes. Table 5 summarizes the volumes calculated for each aquifer system.

## Pecos Valley Alluvial Aquifer

### Overview

The Pecos Valley Alluvial aquifer bisects the study area north to south. The Pecos River Valley extends north to Mora County and south into Texas – this portion of the alluvial aquifer, located in Chaves County, is typically grouped with the Roswell Artesian Basin due to its identical physiographic location as the underlying artesian aquifer. The alluvial aquifer consists of alluvium deposited by and surrounding the Pecos River. This depositional environment results in an aquifer geometry that is thickest near the river and thins with distance from the river.

Roswell and Artesia are the two main population centers within the extent of the alluvial aquifer. Surface water withdrawal from the Pecos River is minimal, and totaled just 7,388 acre-ft in 2015 (Magnuson et al., 2015). This is likely due to the Pecos River Compact—a requirement that New Mexico delivers a certain amount of water to Texas via the Pecos River every year. Groundwater withdrawal in Chaves County totaled just under 232,000 acre-ft in 2015 (Magnuson et al., 2015), suggesting that the overwhelming majority of water is sourced from the alluvial aquifer and the underlying artesian



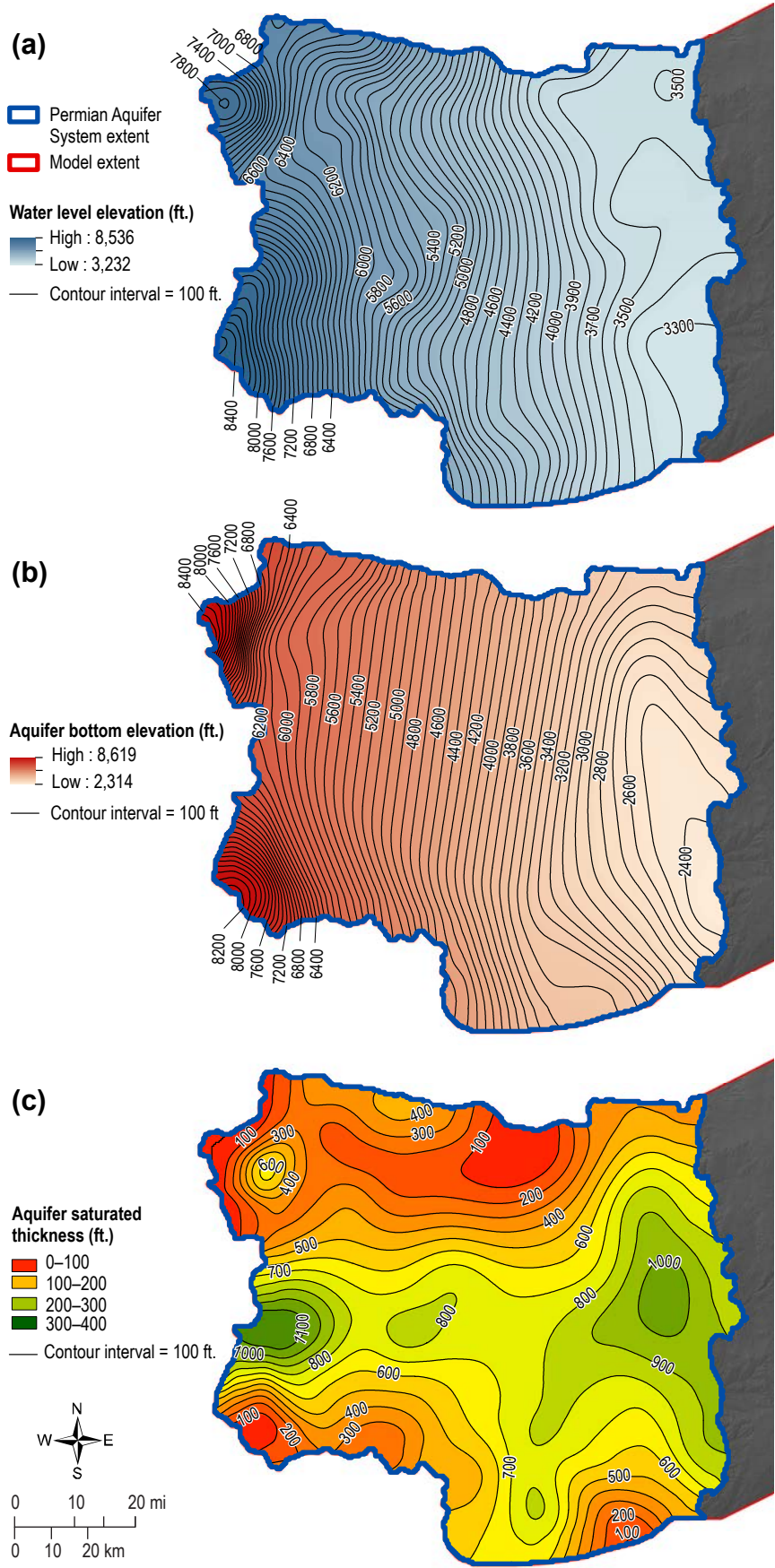
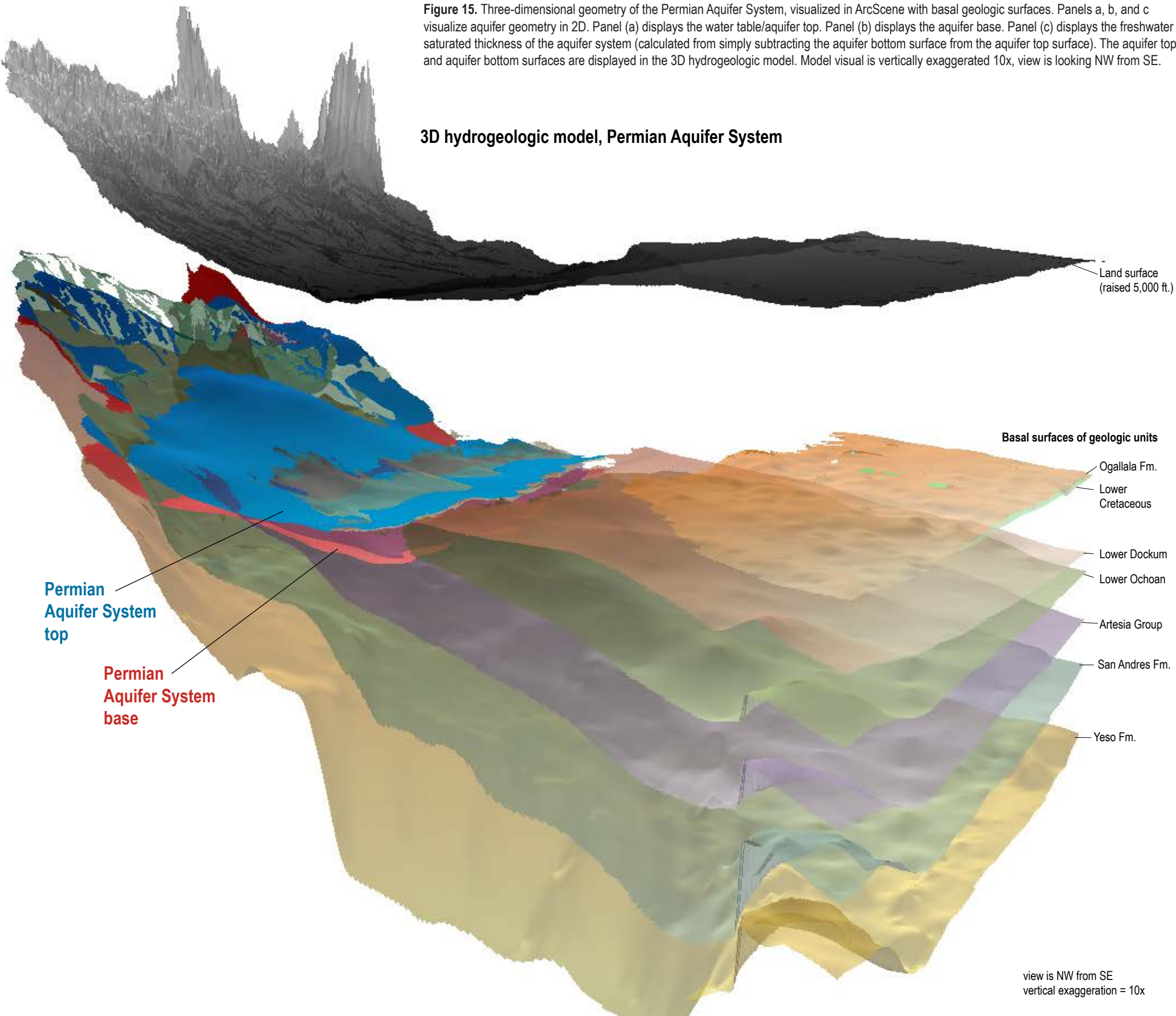


**Figure 15.** Three-dimensional geometry of the Permian Aquifer System, visualized in ArcScene with basal geologic surfaces. Panels a, b, and c visualize aquifer geometry in 2D. Panel (a) displays the water table/aquifer top. Panel (b) displays the aquifer base. Panel (c) displays the freshwater saturated thickness of the aquifer system (calculated from simply subtracting the aquifer bottom surface from the aquifer top surface). The aquifer top and aquifer bottom surfaces are displayed in the 3D hydrogeologic model. Model visual is vertically exaggerated 10x, view is looking NW from SE.





portion of the Permian Aquifer System. Water is used mainly for irrigated agriculture (Magnesun et al., 2019).

### Geologic units

Above the Artesia group, the Pecos Valley Alluvium (~350 ft thick) hosts the unconfined alluvial aquifer (Daniel B. Stephens & Associates (DBS&A), 1995) (Fig. 6). It is primarily made up of sand and gravel that originates from streams in the Pliocene, Pleistocene and Holocene times that drained off the Sacramento Mountains and deposits from the Pecos River (Fig. 2). The Pecos River flows through the center of the alluvial fill and is shown to be well connected with the alluvial aquifer (Fig. 16). The alluvial aquifer ranges in thickness from 0 to 380 ft. Reported hydraulic conductivity values in the alluvium vary drastically from 15 to 55 ft/day. Specific yield estimates range from 0.1 to 0.2.

### Water data

There is a dense network of water data in Pecos Valley. Over 7,000 water data locations were pulled from sources listed previously in this report (Fig. 17). Figure 18 displays the location of wells used in model development. Well networks shown in Figures 17 and 18 include wells completed in both the alluvium and the underlying Artesia Group, with the assumption that wells completed in the Artesia Group are screened in the alluvial unit.

### Water quality

Water quality is generally good in the Pecos Valley Alluvial Aquifer, with TDS values mostly <1,000 mg/L (Fig. 7a). Minimal water samples have TDS values in the brackish category, however, a handful of wells exhibit TDS content up to 10,000 mg/L in regions

close to major population centers, Roswell and Artesia (Fig. 7a). Higher salinity zones are likely the result of recharge to the aquifer from irrigation return flow, as the majority of groundwater use in Chaves County is for irrigated agriculture (Magnesun et al., 2019).

### Depth to water

Depth to water in the alluvial aquifer ranges from <20 ft below ground surface to nearly 300 ft. below ground surface according to water-level data taken

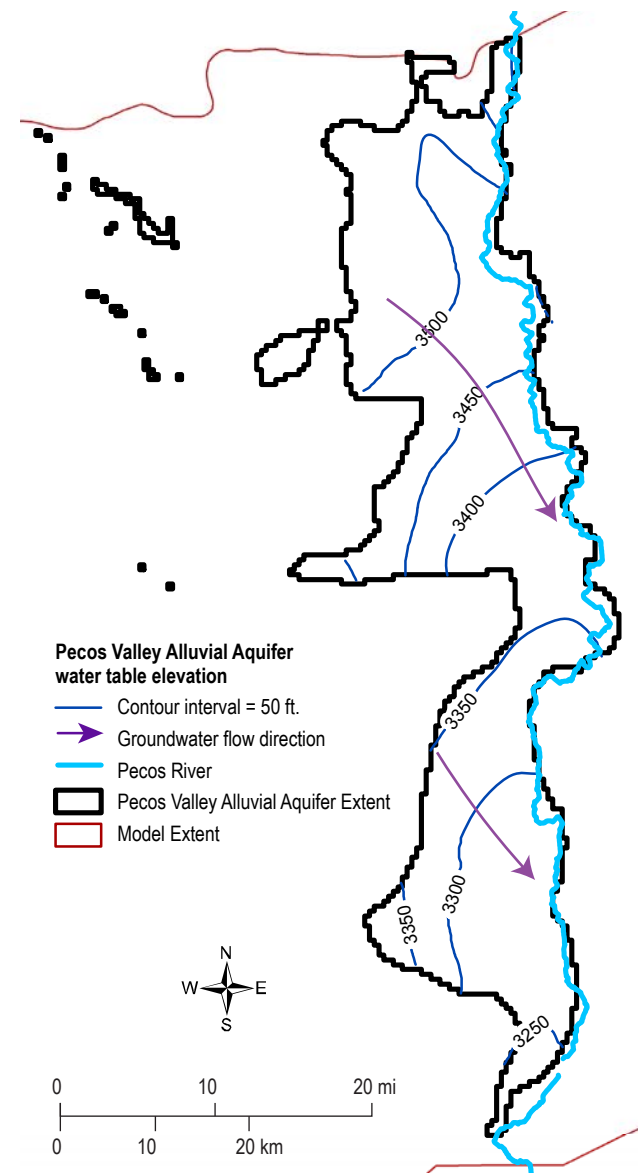


**Figure 16.** Potentiometric surface map of the Pecos Valley Alluvial Aquifer. Groundwater is recharged principally by irrigation return flow, and by runoff from major tributaries Rio Hondo and Rio Felix. Groundwater is discharged to the Pecos River and by way of pumping.

**Table 3.** A summary of water-well coverage in the Pecos Valley Alluvial Aquifer extent. Table displays the total number of wells completed in corresponding geologic formations, the number of wells used in development of water-table maps/surfaces for this study, and the average well depth of wells used in the study in feet below ground surface (ft. bgs). Relevant water-level data corresponds to water levels reported after year 2009.

Geologic Formation	Total no. of wells	No. of wells with relevant water-level data	Average well depth (ft. bgs)
Pecos Valley Alluvium	4179	307	123.5
Artesia Group	3255	282	244.7
TOTAL	7434	589	-



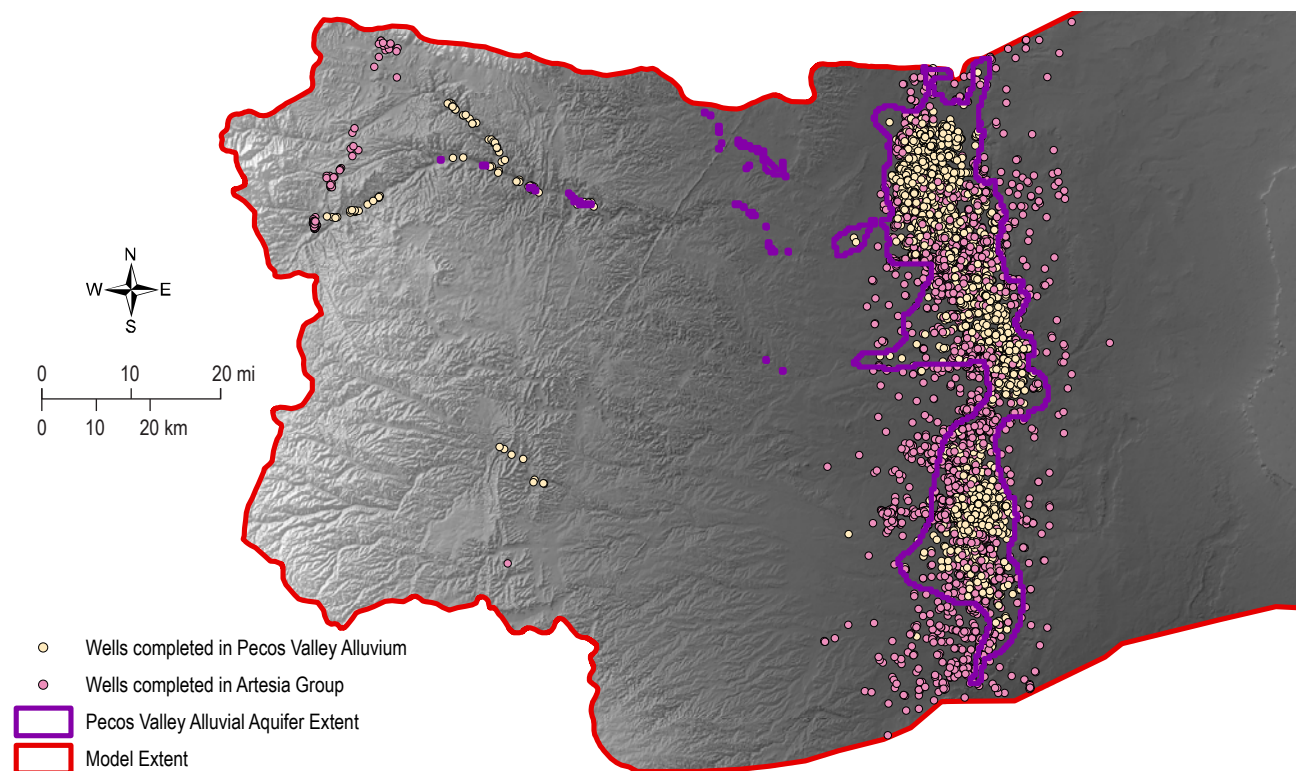


**Figure 17.** Location of wells completed in the Pecos Valley Alluvium or the Artesia Group. Due to the confining nature of the Artesia group, an assumption can be made that most wells are screened in the alluvium, therefore these two formations are grouped. Water levels from this well network used in the hydrologic model are shown in Figure 18.

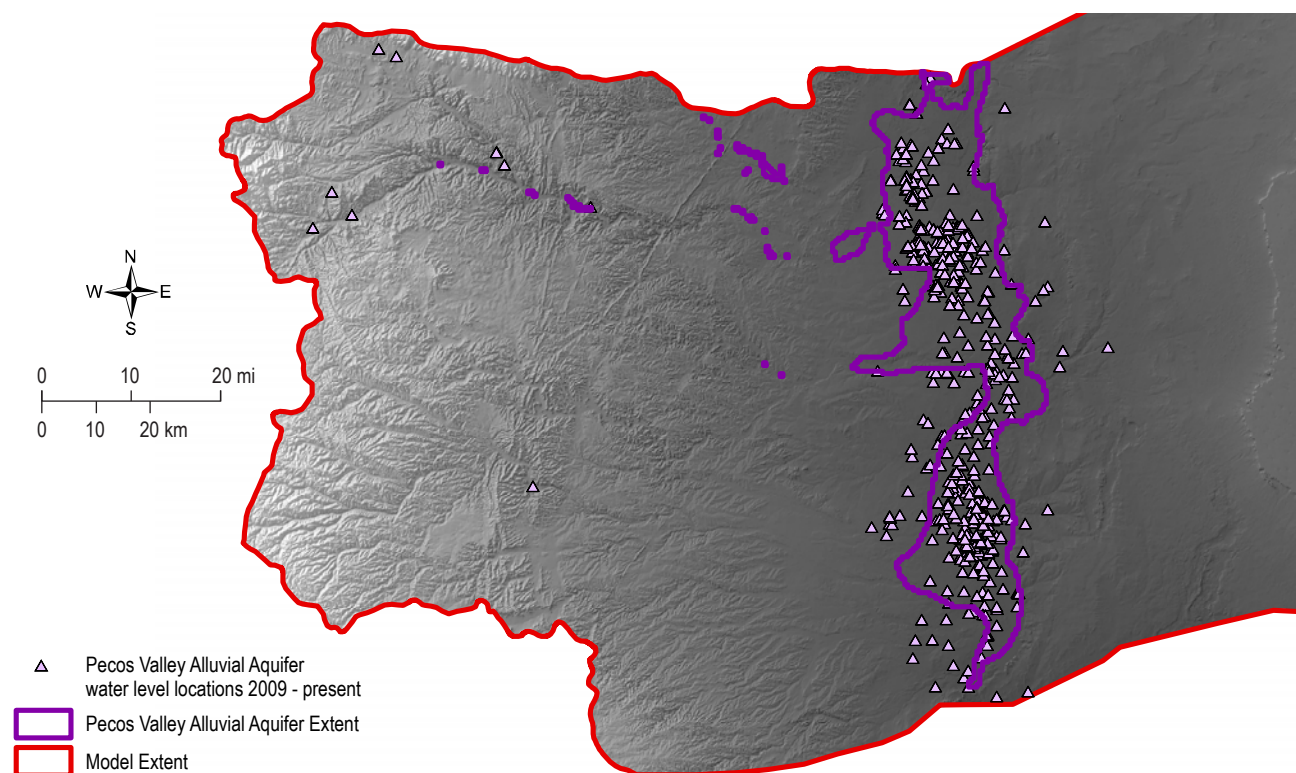


**Figure 18.** Locations of wells with water levels reported after 2009 for the Pecos Valley Alluvial Aquifer. The final extent of the Pecos Valley Alluvium is shown in purple.



from year 2010 to present. Groundwater elevations range from approximately 3,600 ft asl in the higher elevations to the north and east down to roughly 3,200 ft asl to the south (Fig. 16). Groundwater generally flows from west to east, eventually discharging into the Pecos River (Fig. 16). Groundwater is also present in alluvial material in drainages to the west with saturated thicknesses reaching up to 200 feet (Fig. 19a),

### 3D geometry

The Pecos Valley Alluvial Aquifer extent was simply defined by the extent and thickness of its host unit, the Pecos Valley Alluvium. The final areal extent of the aquifer was defined based on where the water-table elevation was higher than the elevation of the base of the alluvium. This final extent is shown in Figures 17 and 18. The upper aquifer surface was created from water-level measurements (locations in Figure 18) to form the potentiometric surface (Fig. 19a). The basal surface was simply the base of the Pecos Valley Alluvium (Cikoski chapter) (Fig. 19b). Subtracting lower surface elevation from the upper surface elevation revealed a saturated thickness ranging from 0 ft. to 400 ft, consistent with previous thickness estimates (Fig. 19c). The aquifer unit thins out to the west. Figure 19 shows the resulting aquifer surfaces within the geologic framework.

### Water quantity

Decreases in groundwater storage in the alluvial aquifer have been significant, with steady decline since the 1940s. In the 1980s, the rate of decline began to slow, though withdrawals remained significant. The 1990s saw a brief period of recovery before declining again. An estimated 3.75 Maf of water has been extracted from the alluvial aquifer since the 1940s (Rinehart and Mamer, 2017). The current volume estimate for the Pecos Valley Alluvial Aquifer (Fig. 19) ranges from 3.64 to 6.18 Maf. This estimate was calculated using water levels taken between year 2010–present and a specific yield range of 0.1–0.17. The appendix included in this report outlines the methodology in calculating freshwater volumes. Table 5 describes the volumes calculated for each aquifer system.

## Southern High Plains Aquifer System

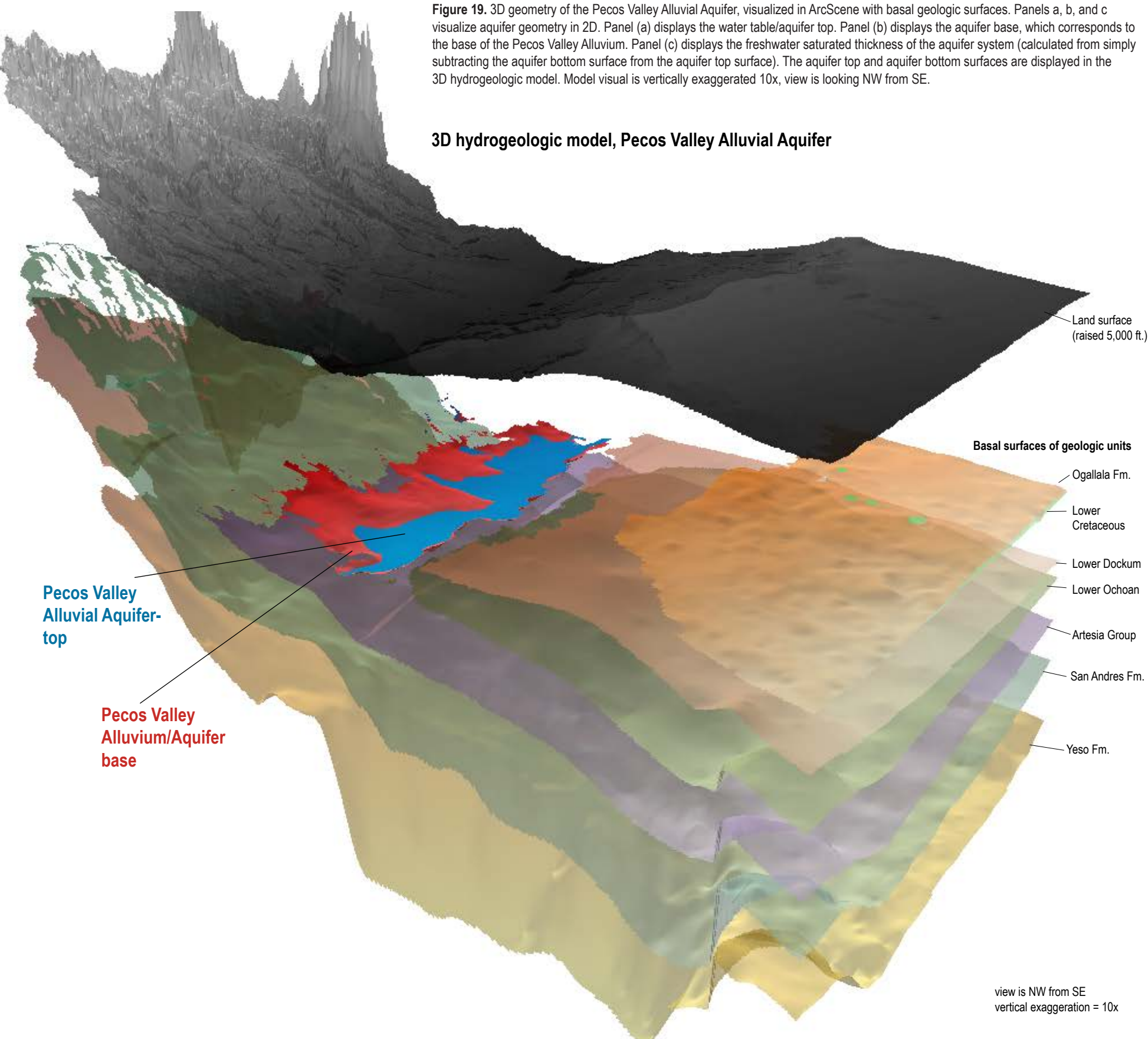
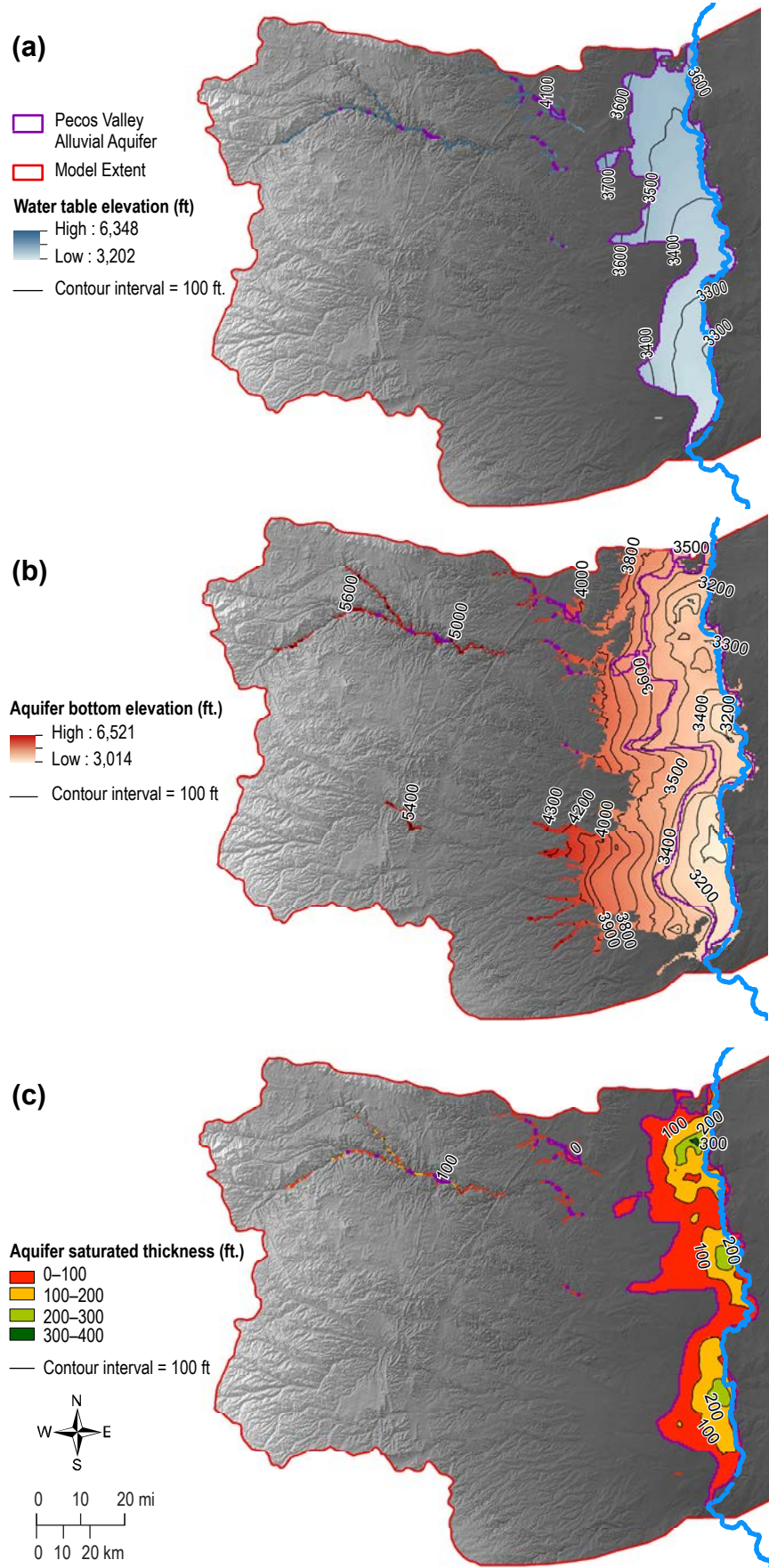
### Overview

In east-central and southeast New Mexico, the Southern High Plains and their namesake aquifer are bounded on the north and west by the cliffs of the Mescalero Ridge escarpment, and encompass northern Lea and southern Roosevelt counties (Fig. 1, 6). Elevations range from 5,500 ft. in the northwest part of the region to 3,600 ft. near Hobbs. The land surface forms a gently east to southeast-dipping upland, most of which is a very low relief and nearly featureless grassland. There are no perennial streams, and most of the land surface is undissected by drainages; Frio and Running Water Draw north of Clovis are notable exceptions. However, broad, shallow depressions, known as *playa* basins, are common. These range in size from less than a square mile to many square miles, and they are usually dry and only contain water after heavy rains. The majority of the High Plains area is rural farm and ranch country. A variety of crops are grown in the region: corn, cotton, sorghum, alfalfa hay, and peanuts. Nearly all of this agriculture is irrigation-dependent. Cattle ranching is prevalent on much of the open grassland that is not intensively farmed. This region additionally comprises part of the greater Permian Basin oil patch, and oil and gas are produced from thousands of wells in Lea and southern Roosevelt Counties. The economy in the southern high plains region is driven largely by oil and gas development and by groundwater irrigated agriculture (Lea County Regional Water Plan, 2016). The vast majority (82%) of water use is for irrigated agriculture (Magnesun et al., 2019). Use of hydraulic fracturing in horizontal wells has created concerns that fresh water used for oil well development is depleting water resources from an already stressed aquifer (Lea County Regional Water Plan, 2016).

### Geologic units

The Southern High Plains Aquifer system is comprised principally of the Ogallala Formation, and includes the underlying Lower Cretaceous Edwards–Trinity Formations where present in the northern portion of Lea County and southern portion of Roosevelt County (Fig. 3). The Ogallala Formation is a complex sedimentary unit consisting of gravel and sand along paleovalleys capped by fine sand, silt, and clay of dominantly eolian origin (Gustavson and Holliday, 1999). It may be loosely lithified like modern gravels or well-cemented into a hard rock that will hold up







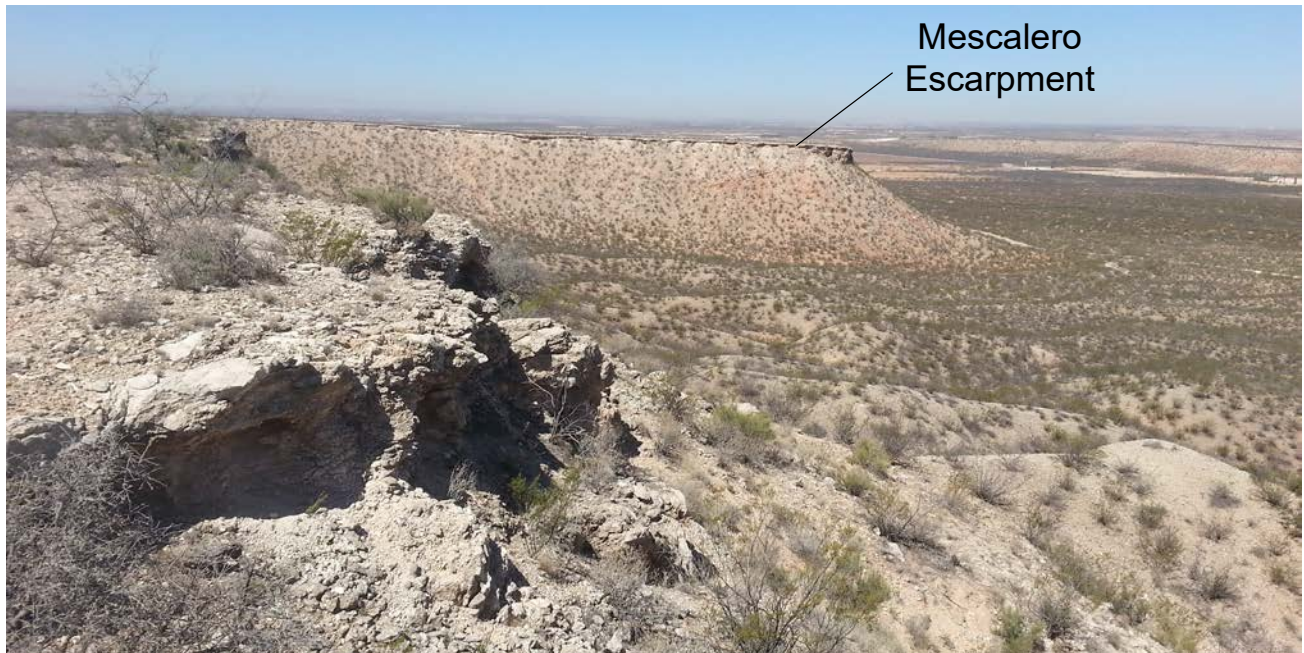


**Figure 20.** Upper caliche caprock of Ogallala Formation forming the Mescalero Escarpment in southeast New Mexico.

cliffs, such as those along the Mescalero Escarpment (Fig. 20). A defining characteristic of the Ogallala is the sandy calcium carbonate soil deposit, known as caliche, that is ubiquitous at the top of the formation and may be up to several meters thick. The Ogallala Formation is exposed at the surface in central and northern Lea County. Very young to modern sand-sheets and sand dunes stabilized by vegetation are common in southern Lea County beyond the extent of the Ogallala Formation and the High Plains Aquifer.

The Ogallala Formation overlies nearly flat-lying Lower Cretaceous sandstone, shale, and minor limestone in southeast Roosevelt and northeast Lea Counties, and Upper Triassic sandstone, shale, and mudstone elsewhere (Fig. 3). The base of the Ogallala is a profound unconformity that is highly channelized, with backfilled and buried paleovalleys trending eastward in the subsurface containing greater thicknesses of deposits that are prime targets for groundwater resource development. The Lower Cretaceous section is a locally-preserved remnant of a regional sequence of strata that is better preserved and more extensive outside the study area in west-central Texas, and includes variable thicknesses of the Antlers, Walnut, Comanche Peak, Kiamichi, and Duck Creek Formations (Fallin, 1988). The Ogallala and Lower Cretaceous intervals are commonly well-connected hydraulically, and groundwater in the Cretaceous is commonly fresh (Fallin, 1988). There are no significant faults or geologic structures mapped in this

region that clearly influence groundwater flow—the main physical influence of the regional geology on the High Plains Aquifer is the depth to bedrock beneath the Ogallala Formation.

#### Water data

An extensive water data network exists in the Southern High Plains. Nearly 14,500 well locations were pulled from sources listed previously (Fig. 21). The number of data points pulled from various sources vs. the number of data points used in creating the hydrologic model is summarized in Table 4. Water-level measurements for wells completed in the Ogallala Fm., Edwards–Trinity

**Table 4.** A summary of water-well coverage in the Southern High Plains Aquifer System extent, including total number of wells completed in corresponding geologic formations, the number of wells used in development of water-table maps/surfaces for this study, and the average depth of the wells used in the study, measured in feet below ground surface (ft. bgs). Relevant water-level data corresponds to water levels reported after year 2009.

Geologic Formation	Total no. of wells	No. of wells with relevant water-level data	Average well depth (ft. bgs)
Ogallala Fm.	10,311	404	147.9
Edwards–Trinity Fms.	652	26	149.1
Upper Dockum Group	3,462	520	216.1
<b>TOTAL</b>	<b>14,425</b>	<b>950</b>	<b>-</b>



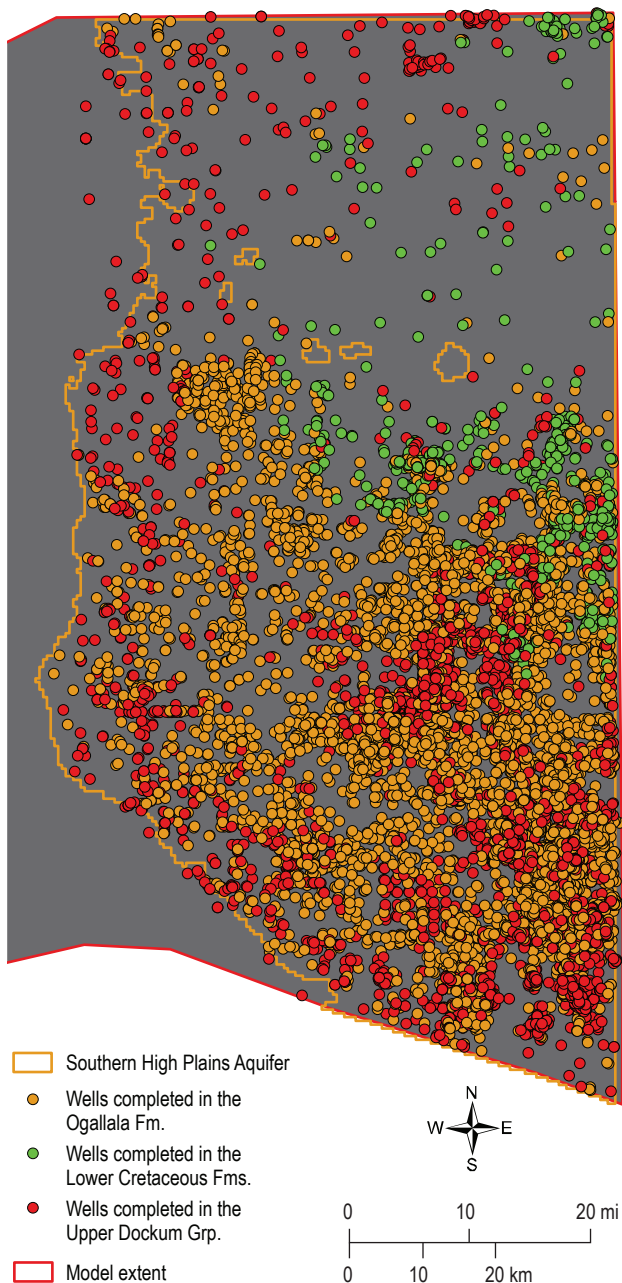


**Figure 21.** Location of wells completed in Southern High Plains Aquifer System units, from oldest to youngest: the Upper Dockum Group; Lower Cretaceous formations; and the Ogallala Formation. The Ogallala Fm. thins to the north, as can be seen by the lack of Ogallala Fm. wells and the appearance of Lower Cretaceous wells. The well network is less dense in the northern half of the area. Future work is needed to parse out Upper Dockum wells from its overlying units, due to unknown screen intervals and documented upward flow from the Upper Dockum Group to the Ogallala/Lower Cretaceous Fms. For the purposes of this study, water-level measurements from wells which reached depths into the Upper Dockum Group were included in analyzing the water table for the Southern High Plains Aquifer System.

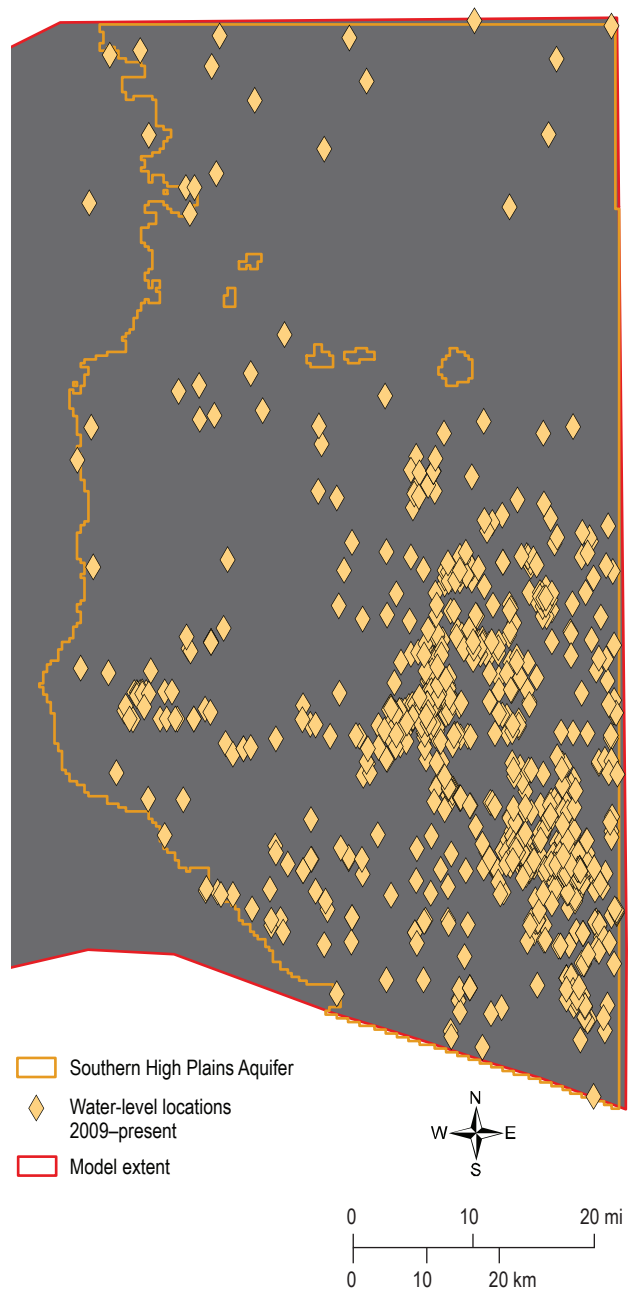


**Figure 22.** Locations of wells with water levels reported after 2009 for the Southern High Plains Aquifer System. Water-level measurements from these wells were used in final model development.



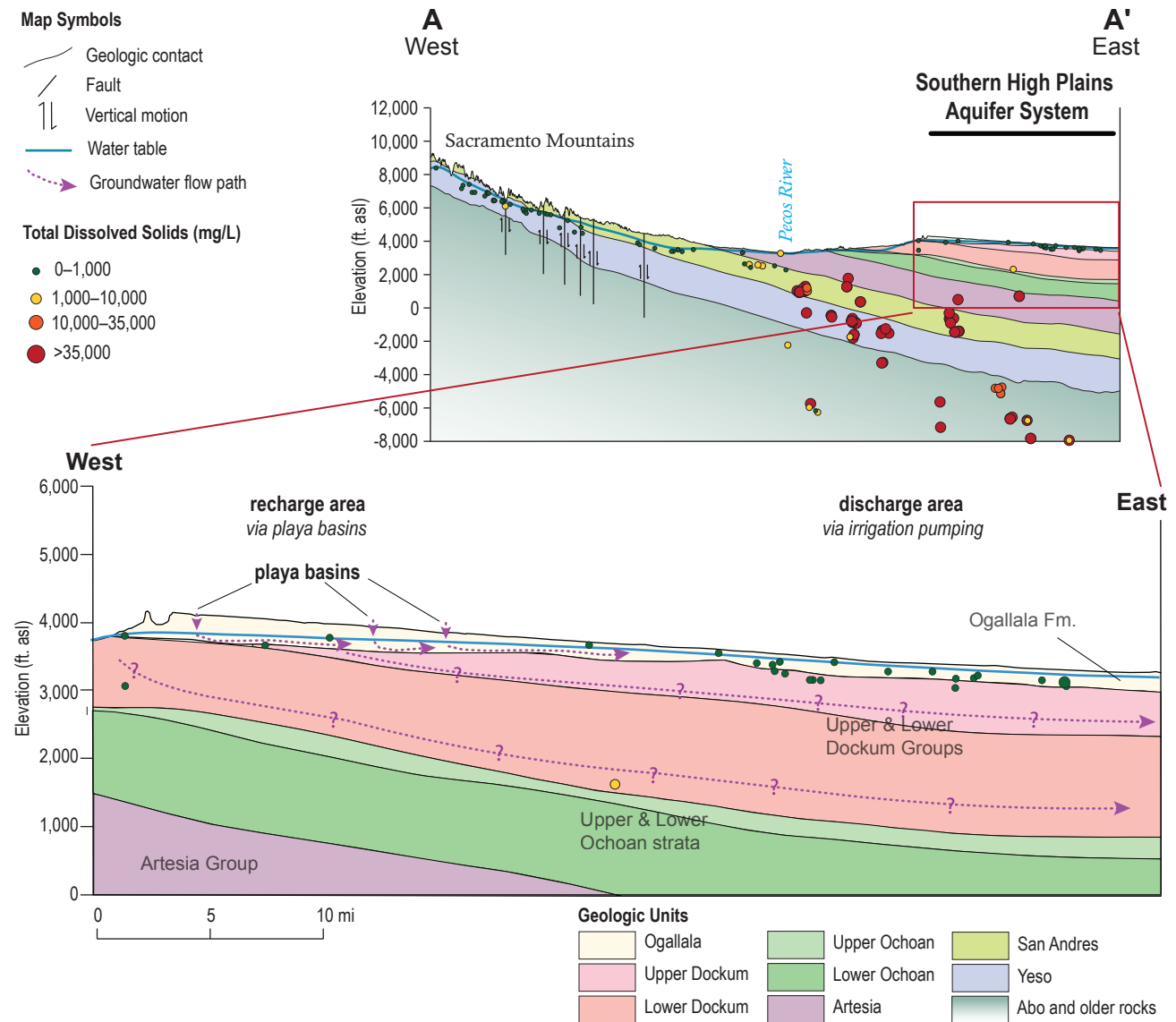
Formations, and Upper Dockum Group were included in the final model.

Figure 21 displays the entire water-well network and corresponding geologic formations of well depths in the Southern High Plains region. The transition from wells being principally completed in the Ogallala Fm. to wells completed in the underlying Edwards–Trinity Formations is apparent. Additionally, well density decreases significantly at this transition, displaying the prolific water-bearing qualities of the Ogallala Fm. Figure 22 displays the number of wells with relevant water data used in model development.

Lack of recent data is evident in much of the Southern High Plains Aquifer System.

### Water quality

Water quality is good in most of the High Plains Aquifer in New Mexico (Fig. 23). In Lea County TDS content is usually below 1,000 mg/L (Fig. 7a). Notable differences exist in southeast Roosevelt County where the aquifer is relatively thin and underlain by Cretaceous rocks. Here many sampled waters are slightly saline (between 1,000 and 3,000 mg/L).



**Figure 23.** Hydrostratigraphic cross-section of Southern High Plains Aquifer System, displaying water quality projected from data points within a radius of 15 km of cross-section line A-A' (Fig. 2). Recharge is typically low through playa basins. Discharge is by way of pumping for irrigation purposes. Shallow groundwater is mostly fresh (TDS <1,000 mg/L). Groundwater flows generally south-southeast down stratigraphic dip. There was insufficient data to characterize groundwater flow within the Dockum Group, although it presumably follows a similar flow direction where groundwater is present (Deeds et al., 2015).



TDS). These waters are variable in mineral content but tend towards high sodium, magnesium, chloride, and sulfate. Locally some constituents such as arsenic, chloride, uranium and fluoride exceed drinking water standards. These constituents and the high TDS values may result from dissolution of volcanic ash beds in the Ogallala Formation and/or upward leakage of a small amount of highly mineralized water from the Cretaceous bedrock. Below Ochoan strata, water quality degrades significantly within the underlying Permian layers. Most of these wells contain produced water from oil and gas drilling into the Delaware basin, and TDS content ranges from 35,000 mg/L to greater than 200,000 mg/L (Fig. 7b). The spatial patterns of water chemistry within the High Plains aquifer have not changed significantly since the 1950s even with large water withdrawals for irrigation.

### Depth to water

Depth to water reaches a maximum depth of approximately 200 ft. below land surface in Ogallala and Edwards–Trinity formations, with water-table elevations ranging from 3,450 ft. to 4,300 ft. above sea level (Fig. 24). The aquifer top is defined by the water table as measured in wells, and the bottom by the base of the Ogallala Formation or the Edwards–Trinity Group where present. Hydraulic conductivity and specific yield are highly variable across the Ogallala Formation and are largely determined by the lithology of the aquifer materials. Hydraulic conductivity values range from less than 5 ft/day to 500 ft/day (Deeds et al., 2015). The hydraulic conductivity and specific yield both tend to be high in gravels and coarse sands that predominate in the paleochannels at the base of the aquifer. In areas of the aquifer dominated by finer materials such as sand and silt the hydraulic conductivity and specific yield tend to be much lower. In the northeast corner of the study area, the underlying Edwards–Trinity Formation has significantly lower variability in hydraulic conductivity, ranging from 0 ft/day to 12 ft/day (Deeds et al., 2015). The Ogallala and Edwards–Trinity aquifers are hydraulically connected, and recharge to the Ogallala is partially sourced from upward flow from the Edwards–Trinity unit.

Many studies identify sandsheets, dunes, and especially playa basins as potentially important recharge locations. Natural recharge outside of these locations is essentially zero. Most recharge appears to occur under playa lakes after they fill with water from heavy rains. A small amount of pumped irrigation water infiltrates back into the aquifer beneath

irrigated fields; however, this is not “new” water but rather a return of some water removed by pumping. Natural discharge is extremely small as it may only exist as leakage into some of the large playas after they are saturated. Groundwater flows from west to east-southeast into Texas.

### 3D geometry

Information outlined above regarding groundwater elevations, water quality, and well networks, were all

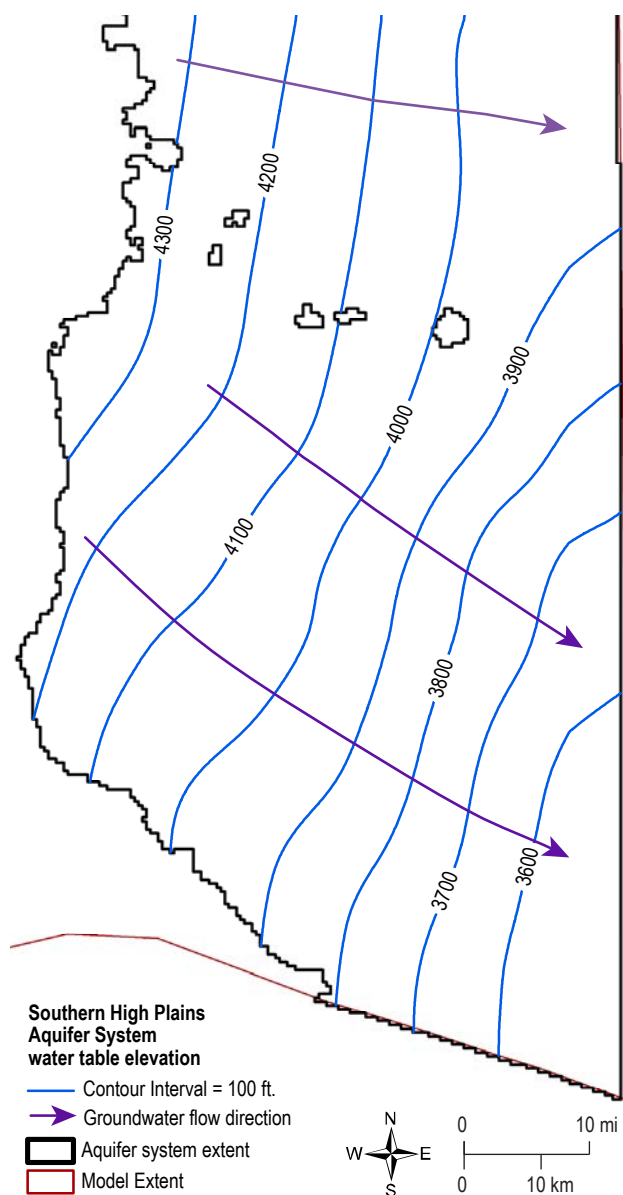
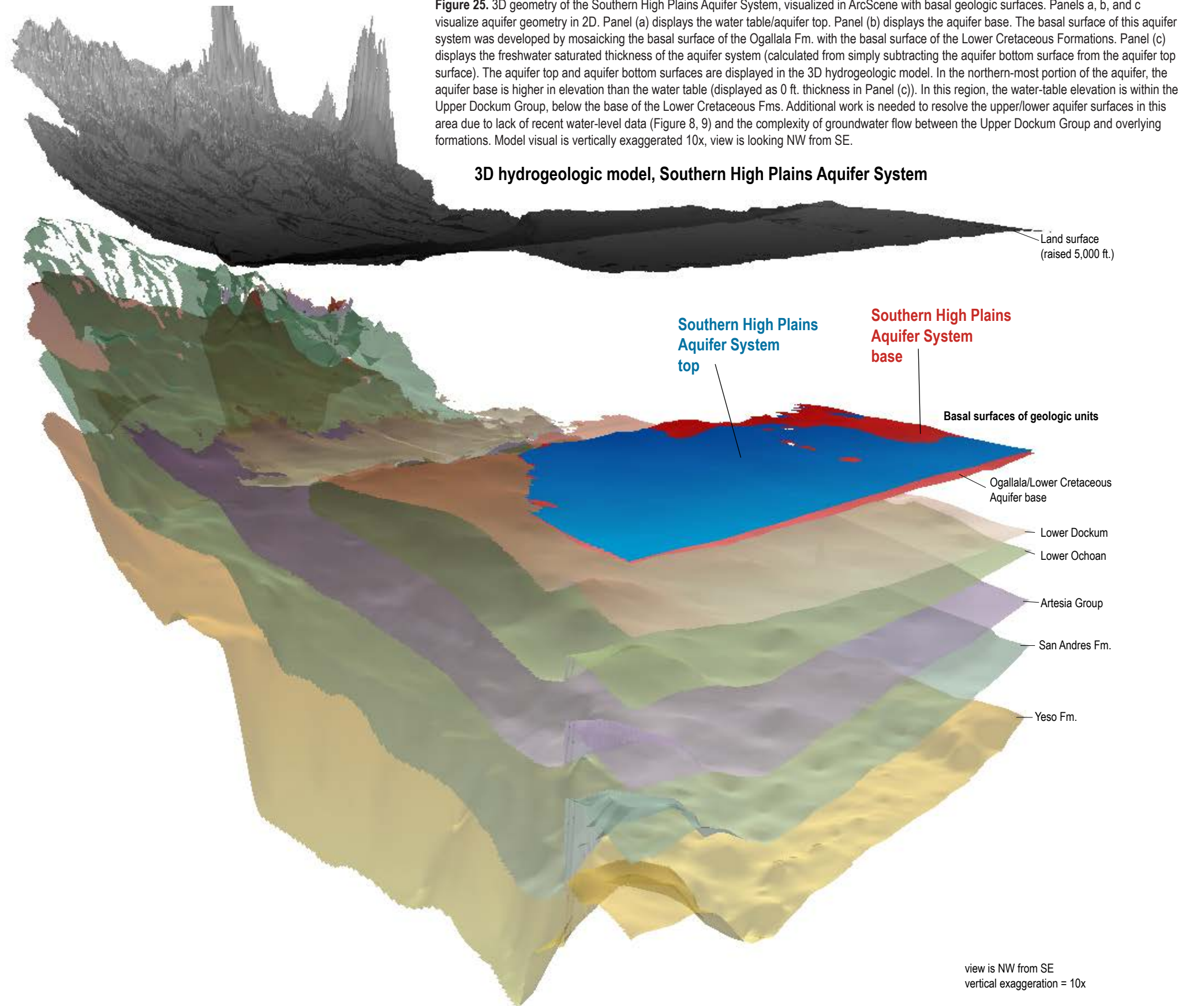
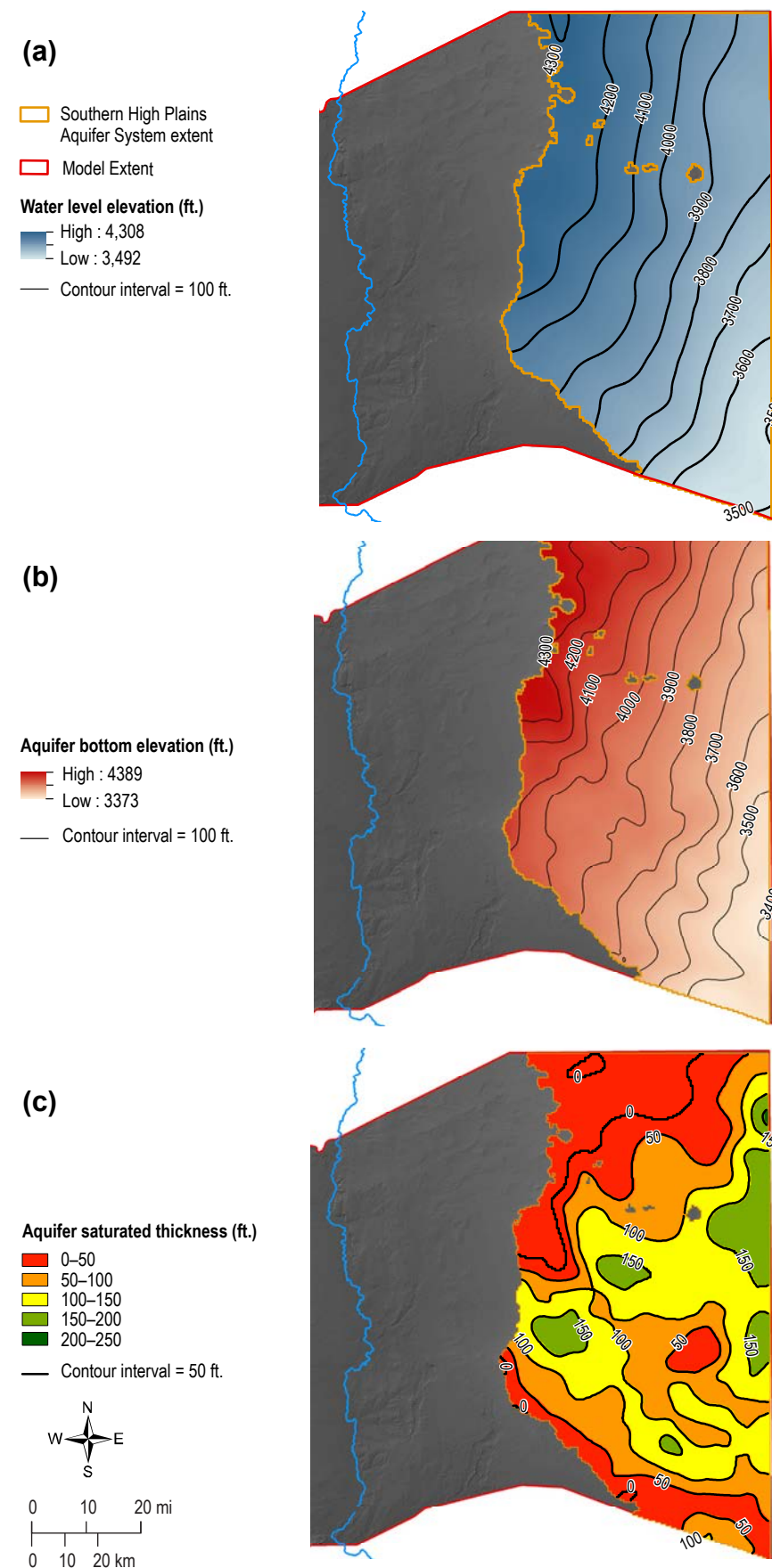


**Figure 24.** Potentiometric surface map of the Southern High Plains Aquifer System. Groundwater flows generally from NW to SE down stratigraphic dip into Texas. The Ogallala Fm. thins to the north, and a portion of the groundwater is presumed to be upward leakage from the underlying Dockum Group.







combined to delineate the three dimensional extent of the Southern High Plains Aquifer System. The areal extent of the aquifer system is simply the areal extent of the Ogallala and Edwards–Trinity Formations. The water-table elevation constituted the upper surface (Fig 25a) and a mosaic of the base of the Ogallala with the base of the Edwards–Trinity Formation constituted the lower surface (Fig. 25b). The thickness of this unit ranged from 0 ft to 250 ft (Fig. 25c). The final 3D model in Figure 25, at a vertical exaggeration of 10x, displays just how thin the Southern High Plains Aquifer System is in southeast NM. In the northern-most portion of the aquifer, the aquifer base is higher in elevation than the water table (Fig. 25) (displayed as 0 ft thickness in Fig. 25c). In this region, the water-table elevation is within the Upper Dockum Group, below the base of the Lower Cretaceous Fms. Complexities arose when developing the 3D framework for this portion of the aquifer system, as there is evidence of vertical flow upwards from the Upper Dockum Group. The overwhelming majority of wells did not have a screen interval specified, therefore water levels from wells completed in the Upper Dockum Group were included in upper surface development. Current geometry, water quality, and water-level data regarding the Upper Dockum Group is lacking, therefore it was decided that the lower surface of the aquifer would be at the base of the Ogallala and Edwards–Trinity Formations. However, the Dockum Group is known to be a water-bearing

unit (Deeds et al., 2015). Parsing out which portions of the Upper Dockum are water-bearing is in the scope of future work for this area.

### Water quantity

Groundwater is contained principally within Ogallala and Edwards–Trinity Formations. The two aquifers are connected by a semi-permeable contact and upward flow is likely present from the Edwards–Trinity Formation to the Ogallala Formation (Deeds et al., 2015). Nativ and Gutierrez (1998) additionally suggest likely upward flow from the Dockum Group to the Edwards–Trinity Formations in Lea and Roosevelt County, based on lithology, water-level, and water-chemistry data.

The estimated volume of known and potential groundwater resources in the Southern High Plains Aquifer System ranges from 20.5–51.3 Maf for a specific yield range between 0.1 and 0.25 (Table 5). This volume estimate was made using water levels taken from the year 2010 to present and takes into account variable saturated thickness within the aquifer system, however does not take into account heterogeneities within the aquifer units. This is a conservative estimate of current available groundwater resources in the aquifer system. Groundwater storage has declined significantly since the 1960s according to research done by Rawling and Rinehart (2018), with a cumulative decline of 3 Maf from 1960 to 2010.



## V. SUMMARY

Development of a 3D hydrogeologic framework has provided a modern look at current water levels, water quality, and geometry, of aquifer systems in the Pecos Slope and Southern High Plains region of southeast New Mexico. This report summarizes the aquifer systems using products created from 3D map development, including 2D map visuals, cross-sections, and 3D map visuals using ArcScene. A comprehensive 3D visual is shown in Figure 26.

In summary, three major aquifer systems were mapped in the study area, based on literature review, the 3D geologic framework, and current water data: 1) the Permian Aquifer System, 2) the Pecos Valley Alluvial Aquifer, and 3) the Southern High Plains Aquifer System. The 3D hydrogeologic framework provided the means to create high quality, accurate, hydrostratigraphic cross-sections through any point in the model area, shown in Figures 4, 5, 13, and 23. It allowed for estimates of groundwater volumes to be calculated, which are summarized in Table 5. Combined with well depth data, the geologic framework facilitated estimation of water well formation depth (Fig. 9, 11, 17, 21) and water quality depth (Fig. 7, 7a, 7b), allowing for a more accurate representation of relevant water data for each aquifer system. Inherent uncertainties exist when developing products based on subsurface data. Uncertainties in geologic digital data are documented in chapter by Cikoski. Uncertainties associated with groundwater volume calculations and digital aquifer data are documented in Appendix 2. Robust quality control and geostatistical procedures combined with human interpretation were implemented during the 3D mapping process to

develop an accurate representation of the subsurface in this region. However, digital data accompanying this report is intended for use at the county-to-state scale (approximately 1:500,000 to 1:1,000,000), and is not appropriate for use in site-specific studies.

This study has accomplished creating and analyzing 3D digital subsurface data, in the form of raster surfaces and contour maps, from existing geologic and hydrologic data using tools available in ArcGIS. Aquifer mapping was accomplished in 3D with the use of 3D geologic surfaces and a TDS bounding surface to delineate aquifers based on geology and water quality. Future work will make efforts to include additional water quality parameters for aquifer boundary evaluation. The ability to interact with subsurface geology and hydrogeology in 3D, using programs such as ArcScene, has proved invaluable when it comes to analyzing water data and mapping groundwater resources. The 3D data accompanying this report allows various agencies and communities to have an enhanced understanding of the aquifer systems in this region.

**Table 5.** Summary of estimated aquifer volumes. Sy refers to specific yield (property of unconfined aquifers), S refers to storativity (property of confined aquifers), Maf = million acre-ft.

Aquifer system	Sy or S range (unitless)	Freshwater volume (Maf)
Permian Aquifer System	Sy = 0.05–0.15 S = 0.00004	86.7–259.8
Pecos Valley Alluvial Aquifer	Sy = 0.1–0.17	3.64–6.18
Southern High Plains Aquifer System	Sy = 0.1–0.25	20.5–51.3



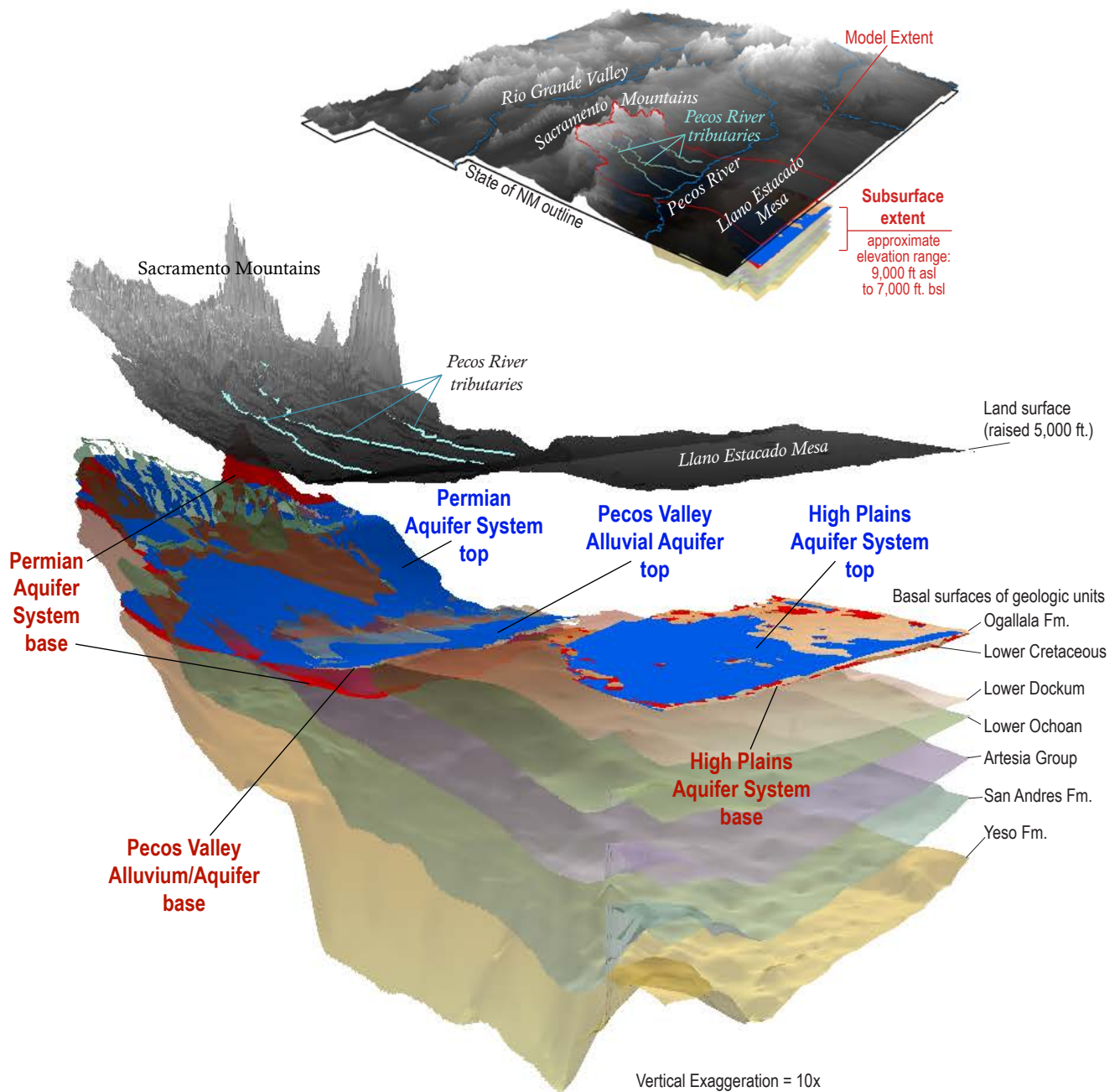


**Figure 26.** 3D hydrogeologic model of Lower Pecos Slope and Southern High Plains region of southeast New Mexico. Aquifer systems are displayed within the geologic framework. Aquifer tops are displayed in blue, aquifer bottoms are displayed in red. The hydrogeologic model encompasses approximately 11,500 sq. miles in areal extent and nearly 16,000 ft. of subsurface geology.



## ACKNOWLEDGMENTS

This project could not have been completed without the advice and guidance from many members of the NMBGMR Aquifer Mapping Program. Specifically, I'd like to thank Kitty Pokorny (NMBGMR) for her assistance with data compilation, Phil Miller (NMBGMR) for his invaluable ArcGIS instruction, and Colin Cikoski (formerly NMBGMR) for his guidance and company while working through the iterative processes this project required. Lastly, I thank Stacy Timmons and Laila Sturgis (NMBGMR) for their valuable report edits and assistance in completing the many products of this project.

## REFERENCES

- Adams, D.C., and Keller, R.G., 1996, Precambrian basement geology of the Permian basin region of west Texas and eastern New Mexico: A geophysical perspective: *American Association of Petroleum Geologists, Bulletin*, v. 80, no. 3, p. 410–431.
- Bachman, G. O., 1980, Regional geology and Cenozoic history of Pecos region, southeastern New Mexico: U.S. Geological Survey, Open-File Report 80-1099, 116 p.
- Broadhead, R.F., Mansell, M.M., and Jones, G., 2009, Carbon dioxide in New Mexico: Geologic distribution of natural occurrences: New Mexico Bureau of Geology and Mineral Resources, Open-File Report 514, 131 p.
- Cather, S.M., 1991, Tectonic overview of the Ruidoso region: New Mexico Geological Society, 42nd Field Conference Guidebook, p. 37–39.
- Cather, S. M., 2004, Laramide orogeny in central and northern New Mexico and southern Colorado, *in* Mack, G. H., and Giles, K. A., eds., “The Geology of New Mexico: A Geologic History”: New Mexico Geological Society, Special Publication 11, p. 203–248.
- Daniel B. Stephens and Associates, Inc. (DBS&A), 1995, Comprehensive Review and Model of the Hydrogeology of the Roswell Basin, Volumes I and II, prepared for The New Mexico State Engineer Office, Santa Fe, New Mexico, 284 p.
- Deeds, N.E., Harding, J.J., Jones, T.L., Singh, A., Hamlin, S., Reedy, R.C., Yan, T., Jigmond, M., Lupton, D., Scanlon, B.R., Seni, S., and Dutton, A., 2015, Final conceptual model report for the High Plains aquifer system groundwater availability model: report to the Texas Water Development Board, 546 p.
- Erdlac, R.J., 1993, Small-scale structures in the Guadalupe Mountains region: Implication for Laramide stress trends in the Permian basin, *in* Love, D. W., Hawley, J. W., Kues, B. S., Austin, G. S., and Lucas, S. G., eds., “Carlsbad Region (New Mexico and West Texas)”: New Mexico Geological Society, Fall Field Conference Guidebook 44, p. 167–174.
- Fallin, J.A.T., 1988, Hydrogeology of Lower Cretaceous strata under the southern High Plains of Texas and New Mexico: *New Mexico Geology*, v. 10, no. 1, p. 6–9.
- Fallin, J.A.T., 1989b, Hydrogeology of Lower Cretaceous strata under the southern High Plains of Texas and New Mexico: Texas Water Development Board, Report 314, 39 p.
- Fiedler AG, Nye SS. 1933. Geology and ground-water resources of the Roswell Basin, New Mexico. U.S. Geological Survey Water-Supply Paper 639.
- Goff, F., Roback, R.C., McIntosh, W., Goff, C.J., and Kluck, E.C., 2014, Geochemistry and geochronology of intrusive and volcanic rocks of the Three Rivers stock, Sierra Blanca, New Mexico, *in* Rawling, G., McLemore, V. T., Timmons, S., and Dunbar, N., eds., “Geology of the Sacramento Mountains Region”: New Mexico Geological Society, Fall Field Conference Guidebook 65, p. 183–196.
- Gustavson, T.C., and Holliday, V.T., 1999, Eolian sedimentation and soil development on a semiarid to subhumid grassland, Tertiary Ogallala and Quaternary Blackwater Draw Formations, Texas and New Mexico High Plains: *Journal of Sedimentary Research*, v. 69, no. 3, p. 622–634.
- Havenor, K. C., 1968, Structure, stratigraphy, and hydrogeology of the northern Roswell Artesian Basin, Chaves County, New Mexico: New Mexico Bureau of Mines and Mineral Resources, Circular 93, 30 p.
- Hawley, J. W., 1993, The Ogallala and Gatuna Formations in the southeastern New Mexico region: A progress report, *in* Love, D. W., Hawley, J. W., Kues, B. S., Austin, G. S., and Lucas, S. G., eds., “Carlsbad Region (New Mexico and west Texas)”: New Mexico Geological Society, Fall Field Conference Guidebook 44, p. 261–269.



- Hayes, P.T., 1964, *Geology of the Guadalupe Mountains, New Mexico*: U.S. Geological Survey, Professional Paper 446, 69 p.
- Intermap Technologies, Inc., 2008, *Digital Terrain Models, Core Product Version 4.2, Edit Rule Version 2.2*: Englewood, CO.
- Johnson, K.S., 1993, Dissolution of Permian Salado salt during Salado time in the Wink area, Winkler County, Texas, *in* Love, D. W., Hawley, J. W., Kues, B. S., Austin, G. S., and Lucas, S. G., eds., "Carlsbad Region (New Mexico and west Texas)": New Mexico Geological Society, Fall Field Conference Guidebook 44, p. 211–218.
- Kelley, S., Koning, D.J., Goff, F., Cikowski, C.T., Peters, L., and McIntosh, W., 2014, Stratigraphy of the northwestern Sierra Blanca volcanic field, *in* Rawling, G., McLemore, V. T., Timmons, S., and Dunbar, N., eds., "Geology of the Sacramento Mountains Region": New Mexico Geological Society, Fall Field Conference Guidebook 65, p. 197–208.
- Kelley, V.C., 1971, *Geology of the Pecos country, southeastern New Mexico*: New Mexico Bureau of Mines and Mineral Resources, Memoir 24, 78 p.
- Kelley, V.C. and Thompson, T.B., 1964, Tectonics and general geology of the Ruidoso-Carrizozo region, central New Mexico: New Mexico Geological Society, 15th Field Conference Guidebook, p. 110–121.
- Koning, D.J., and Roberts, L., 2014, Redefinition of the base of the Cub Mountain Formation and preliminary depositional and tectonic interpretations of the Early-Middle Eocene strata in the Sierra Blanca basin, New Mexico, *in* Rawling, G., McLemore, V. T., Timmons, S., and Dunbar, N., eds., "Geology of the Sacramento Mountains Region": New Mexico Geological Society, Fall Field Conference Guidebook 65, p. 273–286.
- Koning, D.J., Kelley, S., and Goff, F., 2014a, Preliminary geologic map of the northeastern Tularosa basin and western Sierra Blanca basin, Lincoln and Otero Counties, New Mexico: New Mexico Bureau of Geology and Mineral Resources, Open-File Report 563, scale 1:50,000.
- Koning, D.J., Rawling, G.C., Kelley, S., Goff, F., McIntosh, W., and Peters, L., 2014b, Structure and tectonic evolution of the Sierra Blanca basin, *in* Rawling, G., McLemore, V. T., Timmons, S., and Dunbar, N., eds., "Geology of the Sacramento Mountains Region": New Mexico Geological Society, Fall Field Conference Guidebook 65, p. 209–226.
- Kues, B.S., and Giles, K. A., 2004, The Late Paleozoic ancestral Rocky Mountains system in New Mexico, *in* Mack, G. H., and Giles, K. A., eds., "The Geology of New Mexico: A geologic history": New Mexico Geological Society, Special Publication 11, p. 95–136.
- Land, L., 2003a, Regional geology of the Pecos Country, *in* Johnson, P.S., Land, L., Price, L.G., & Titus, F., eds., *Water Resources of the Lower Pecos Region, New Mexico: Science, Policy, and a Look to the Future*: New Mexico Bureau of Geology and Mineral Resources, 2003 New Mexico Decision Makers Guidebook, p. 9–13.
- Land, L. and Newton, B. T., 2008, Seasonal and long-term variations in hydraulic head in a karstic aquifer: Roswell Artesian Basin, New Mexico: *Journal of the American Water Resources Association*, v. 44, p. 175–191.
- Land L, Timmons S. 2016. Evaluation of groundwater residence time in a high mountain aquifer system (Sacramento Mountains, USA): Insights gained from use of multiple environmental tracers. *Hydrogeology Journal* 24 (4): 787–804.
- 2016, Lea County Regional Water Plan, in State of New Mexico, I. S. C., Office of the State Engineer, ed., p. 155.
- Lehman, T.M., and Chatterjee, S., 2005, Depositional setting and vertebrate biostratigraphy of the Triassic Dockum Group of Texas: *Journal of Earth System Science*, v. 114, no. 3, p. 325–351.
- Loucks, R., 2009, Review of the Lower Ordovician Ellenburger Group of the Permian basin, west Texas, *in* Ruppel, S. C., ed., "Integrated synthesis of the Permian Basin: Data and models for recovering existing and undiscovered oil resources from the largest oil-bearing basin in the U.S.", prepared for the U.S. Department of Energy contract DE-FC26-04NT15509, p. 15–106.
- 2016, Lower Pecos Valley Regional Water Plan, in State of New Mexico, I. S. C., Office of the State Engineer, ed., p. 264.
- Lucas, S. G., 2004, The Triassic and Jurassic Systems in New Mexico, *in* Mack, G. H., and Giles, K. A., eds., "The Geology of New Mexico: A geologic history": New Mexico Geological Society, Special Publication 11, p. 137–152.
- Lucas, S. G., and Anderson, O.J., 1993, Stratigraphy of the Permian-Triassic boundary in southeastern New Mexico and west Texas, *in* Love, D. W., Hawley, J. W., Kues, B. S., Austin, G. S., and Lucas, S. G., eds., "Carlsbad Region (New Mexico and west Texas)": New Mexico Geological Society, Fall Field Conference Guidebook 44, p. 219–230.
- Lucas, S. G., Heckert, A.B., and Hunt, A.P., 2001, Triassic stratigraphy, biostratigraphy and correlation in east-central New Mexico, *in* Lucas, S. G., and Ulmer-Scholle, D., eds., "Geology of Llano Estacado": New Mexico Geological Society, Fall Field Conference Guidebook 52, p. 85–102.
- Lyford, F.P., 1973, Valley fill in the Roswell-Artesia area, New Mexico: United States Geological Survey, Open-File Report 73-163, 26 p.
- Mack, G.H., and Bauer, E.M., 2014, Depositional environments, sediment dispersal, and provenance of the early Permian (Leonardian) Glorieta Sandstone, central New Mexico, *in* Rawling, G., McLemore, V. T., Timmons, S., and Dunbar, N., eds., "Geology of the Sacramento Mountains Region": New Mexico Geological Society, Fall Field Conference Guidebook 65, p. 261–271.
- Magnuson, M. L., Valdez, J. M., Lawler, C. R., Nelson, M., and Petronis, L., 2019, *New Mexico Water Use by Categories 2015*. Technical Report 55. 142 p.
- McGowen, J.H., Granata, G.E., and Seni, S.J., 1977, Depositional systems, uranium occurrence and postulated groundwater history of the Triassic Dockum Group, Texas Panhandle-eastern New Mexico: The University of Texas at Austin, Bureau of Economic Geology, contract report prepared for the United States Geological Survey, 104 p.
- Meyer, R.F., 1966, *Geology of Pennsylvanian and Wolfcampian rocks in southeast New Mexico*: New Mexico Bureau of Mines and Mineral Resources, Memoir 17, 123 p.
- Motts, W. S. and Cushman, R. L., 1964, An appraisal of the possibilities of artificial recharge to ground-water supplies in part of the Roswell Basin, New Mexico: U.S. Geological Survey Water-Supply Paper 1785, 86 p.
- Motts, W.S., 1972, Geology and paleoenvironments of the northern segment, Capitan shelf, New Mexico and west Texas: *Geological Society of America Bulletin*, v. 83, p. 701–722.
- Nance, H.S., 2009, Guadalupian (Artesia Group) and Ochoan shelf succession of the Permian basin: Effects of deposition, diagenesis, and structure on reservoir development, *in* Ruppel, S. C., ed., "Integrated synthesis of the Permian Basin: Data and models for recovering existing and undiscovered oil resources from the largest oil-bearing basin in the U.S.", prepared for the U.S. Department of Energy contract DE-FC26-04NT15509, p. 847–946.



- Nativ, R., and Gutierrez, G.N., 1988, Hydrogeology and hydrochemistry of Cretaceous aquifers, exas pan-handle and eastern New Mexico: The University of Texas at Austin, Bureau of Economic Geology, Geological Circular 88-3.
- Newman, B. D., Havenor, K. C., and Longmire, P., 2016, Identification of hydrochemical facies in the Roswell Artesian Basin, New Mexico (USA), using graphical and statistical methods: Hydrogeology Journal, v. 24, no. 4, p. 819–839.
- Newton BT, Rawling GC, Timmons S, Land L, Johnson PS, Kludt TJ, Timmons JM. 2012. Sacramento Mountains hydrogeology study. New Mexico Bureau of Geology and Mineral Resources Open-File Report 543: <http://geoinfo.nmt.edu/publications/openfile/details.cfm?Volume=543>
- NMBGMR, 2003, Geologic map of New Mexico: New Mexico Bureau of Geology and Mineral Resources, scale 1:500,000.
- NMBGMR., 2018, New Mexico geologic map search [on-line], from: <https://geoinfo.nmt.edu/publications/maps/geologic/home.cfm>, New Mexico Bureau of Geology and Mineral Resources.
- Nummedal, D., 2004, Tectonic and eustatic controls on Upper Cretaceous stratigraphy of northern New Mexico, *in* Mack, G. H., and Giles, K. A., eds., “The Geology of New Mexico: A Geologic History”: New Mexico Geological Society, Special Publication 11, p. 169–182.
- Pazzaglia, F.J., and Hawley, J. W., 2004, Neogene (rift flank) and Quaternary geology and geomorphology, *in* Mack, G. H., and Giles, K. A., eds., “The geology of New Mexico: A geologic history”: New Mexico Geological Society, Special Publication 11, p. 407–437.
- Powers, D. W., 2003, Geohydrological conceptual model for the Dewey Lake Formation in the vicinity of the Waste Isolation Pilot Plant (WIPP): Sandia National Laboratories, Test Plan TP 02-05, Rev. 0, 32 p.
- Pray LC. 1961. Geology of the Sacramento Mountains escarpment, Otero County, New Mexico. New Mexico Bureau of Mines and Mineral Resources Bulletin 35.
- Rawling, G.C., 2014, Geology of the Capitan and Nogal quadrangles, Lincoln County, New Mexico: New Mexico Bureau of Geology and Mineral Resources, Open-File Report 538, scale 1:24,000.
- Rawling, G.C. and Rinehart A.J., 2018, Lifetime Projections for the High Plains Aquifer in East-central New Mexico: New Mexico Bureau of Geology and Mineral Resources, Bulletin-162.
- Rawling GC, Newton BT. 2016. Quantity and location of groundwater recharge in the Sacramento Mountains, south-central New Mexico (USA), and their relation to the adjacent Roswell Artesian Basin. Hydrogeology Journal 24 (4): DOI 10.1007/s10040-016-1399-6.
- Rinehart, A.J. and Mamer, E., 2017, Groundwater Storage Change in New Mexico Aquifers: New Mexico Bureau of Geology and Mineral Resources, Technical Completion Report.
- Riggs, N.R., Lehman, T.M., Gehrels, G.E., and Dickinson, W.R., 1996, Detrital zircon link between headwaters and terminus of the Upper Triassic Chinle-Dockum paleoriver system: Science, v. 273, p. 97–100.
- Schiel, K.A., 1988, The Dewey Lake Formation: End stage deposit of a peripheral foreland basin [M.S. Thesis]: The University of Texas at El Paso, El Paso, Texas, 180 p.
- Seager, W.R., 2004, Laramide (Late Cretaceous-Eocene) tectonics of southwestern New Mexico, *in* Mack, G. H., and Giles, K. A., eds., “The Geology of New Mexico: A Geologic History”: New Mexico Geological Society, Special Publication 11, p. 183–202.
- Shomaker JW. 2003. How we got here: A brief history of water development in the Pecos Basin. In: Johnson PS, Land L, Price LG, Titus F, editors. Water Resources of the Lower Pecos Region, New Mexico: Science, Policy, and a Look to the Future. New Mexico Bureau of Geology and Mineral Resources, 2003 New Mexico Decision Makers Guidebook, p. 61–64.





About 45 miles east of Roswell in the Southern High Plains is the Mescalero Sands North Dune area adjacent to Mescalero Ridge or Caprock Escarpment. *Photograph by Peter A. Scholle.*



# APPENDIX I

## MODEL ASSESSMENT

A final assessment of the geologic model was the comparison of the modeled contact surfaces to contours drawn by separate authors. This analysis was conducted in a geographic information system (GIS) using Esri ArcMap, and several of the comparisons are shown in Figures 1–5 (not sure what the numbering scheme is for these—originally Plates A1.1–A1.5). This analysis was limited to contact surfaces where independent studies were available for comparison. For further discussions of the results of some individual states (quality assessment, offset control estimate generation, regional trend and local deviance model interpolations) please see the main report.

Discussions of the results of some individual stages (quality assessment, offset control estimate generation, regional trend and local deviance model interpolations) are above. The final contact surfaces are assessed by comparing contours drawn along the contact surfaces of the model to contours drawn or generated by separate authors in a GIS using Esri ArcMap, and several of these comparisons are shown in Plates A1.1 through A1.5. For only some contact surfaces were independent studies available for this comparison.

### Dockum model units

The bases of the Upper and Lower Dockum model units can be compared to similar contacts contoured by McGowen et al. (1977), Schiel (1988), Ewing et al. (2008), and Deeds et al. (2015). The base of the Lower Dockum can be directly compared to the hand-drawn structure contours for the base of the Dockum from McGowen et al. (as digitized by Ewing et al.; Plate A1.1). These contours in a large part mirror one another, with similar spacing and trends, and contour lines are typically within 1–2 km of each other across the study area. Some structural troughs in the work of McGowen et al. (1977) are not apparent in the model contours, however. Lower Dockum base contours can also be compared to the contours for the Dewey Lake–Santa Rosa contact from Schiel, at least for the small area in the far southeast corner of the study area. Here, the contours are typically in agreement; both locate a high of about 2,600 ft amsl at the mutual corner of T19S R36E, T19S 37E, T20S R36E, and T20S R37E from which the contact descends in all directions, with continued descent to the east and northeast, and eventual rise to the west and northwest. Contours diverge somewhat, but differences appear less than about 200 ft.

Less agreement is observed between the contours for the base of the Upper Dockum model unit and the base of the Upper Dockum from Ewing et al. (2008) (Plate A1.2). It is worth noting that these Ewing et al. contours are themselves interpolations generated by combining the base of the Lower Dockum structure contours, top of the Upper Dockum structure contours, and isopach contours for the thickness of the Lower Dockum (all from McGowen et al., 1977) to estimate the contours for the base of the Upper Dockum. It is also worth noting that the original data used to generate these contours were not available for this study. In fact, overlaying data points for the base of the Upper Dockum from either the BRACS database or from Deeds et al. (2015) suggests that the contours from Ewing et al. may be in error, as these well control data points contrast with the Ewing et al. (2008) contours but generally agree with the contours for the base of the Upper Dockum model unit from this study. Acquisition of the original data used by McGowen et al. (1977) would be necessary to fairly compare the Ewing et al. (2008) contours to the contours from this study. That said, at a large scale the two contour sets do show similar trends and contour spacing, if not the exact same elevations.

Deeds et al. (2015) released surfaces for the bases of the Lower and Upper Dockum using very similar datasets as used here. These were contoured in a GIS, and these contours were compared to the contours for the model unit contact surfaces from this study (e.g., Plate A1.3). Not surprisingly, the contours from the Deeds et al. (2015) study and this project are nearly identical, as each used very similar datasets. The comparison is useful, however, as it suggests no errors or biases were introduced in this study by the interpolation method used.

### San Andres model unit

The contours for the base of the San Andres model unit can be compared to the contours of the top of the Rio Bonito Member of the San Andres Formation released by Kelley (1971) (Plate A1.4). Although these are not the same surface, as the Rio Bonito lies entirely within the San Andres, the two surfaces should be commonly parallel to one



another. Therefore, the exact values of contours cannot be compared, but the trends and contour spacings should be comparable. However, Kelley illustrated numerous small-scale (wavelengths <1 km) folds and faults particularly in the northwest corner of the study area that would be impossible to capture with a model of this resolution. Therefore, the comparison is inexact by nature, as some details cannot be expected to appear in this model that are depicted in detail by Kelley.

Along the east side of the study area, the eastward decent along the Pecos Slope appears identical in the two sets of contours, with very similar trends and contour spacings. Southward, into the Delaware Basin, the model shows a steeper descent than is shown by Kelley (1971). This may be geologically reasonable, as syndepositional subsidence of the basin could result in a steeper base of the San Andres as compared to the top of a member within the San Andres. Westward from the Delaware Basin, the two contour sets are decently subparallel and equally spaced up the Huapache monocline and onto the Dunken Uplift, with some deviations along the Huapache monocline, particularly along the Artesia–Vacuum arch trend. Westward from the Dunken Uplift, both sets of contours depict a sharp descent into the Elk Basin; however, the location of the lowest part of the basin is in disagreement, as the model shows the basin further south than is shown by Kelley. Further west, the two contour sets are again in agreement along the gentle structural climb to the Sacramento Mountains crest. Thus, the contours from Kelley and the contours for the base of the San Andres model unit are, at least through the northeast, southeast, and southwest corners of the study area, typically subparallel, with local divergences associated with small-scale folds that would be difficult to capture with this model given its resolution.

Substantially more structural deformation is apparent in the northwest corner of the study area, where Kelley (1971) maps numerous small folds and faults. Here, large scale trends in contour sets were examined, rather than exact contour details. From around Pajarito Mountain Dome northward and northwestward into the Sierra Blanca Basin, the two contour sets are generally in agreement. Some exceptions occur directly around faults and around the Sierra Blanca volcanic field intrusions. South and southeast of the Capitan intrusion, particularly through the Hondo Basin and Tinnie fold belt southward onto the northern tip of the Dunken Uplift, the contour sets diverge considerably. Tight folds along the fold belt are not captured by the model surface, and the model surface is significantly smoother than the hand-drawn contours. The Hondo Basin and nearby Talley Basin are merged as one structural low in the model surface, but separated by a structural high along the Tinnie fold belt in Kelley's contours. Additionally, along the Pecos Buckles, Kelley maps several tight folds that are not captured by the model surface. In between the individual buckles, the two contour sets are typically in agreement, but directly along the buckles there is divergence associated with folding along these faults.

This comparison generally confirms the expectation that areas with higher structural complexity will also be areas of greater uncertainty in the model results. Large-scale trends appear well-captured by the model, while small-scale deformations are more difficult to capture.

### Yeso model unit

The contours of the base of the Yeso model unit can be compared to contours for the top of the Abo Formation produced by Broadhead et al. (2005) (Plate A1.5). From the south flank of the Roosevelt Dome southward across the Northwest Shelf and beneath the Southern High Plains to the edge of the Delaware Basin, the two contour sets are nearly identical. This is not surprising, as the data used for the model surface was largely derived from Broadhead et al. (2005) compilation of well data. Significant deviations occur along the margin of the Delaware Basin, however, where the contours from Broadhead et al. (2005) remain relatively low gradient, while the model surface contours bend to follow the margin of the Basin and descend rapidly into the Basin. This is perhaps due to the different methods of handling the transition from shelf to basin facies. Broadhead et al. (2005) collected data for solely the shelf area, whereas this project combined equivalent shelf and basin facies data into single model units, such that the base of the Yeso model unit is continued into the base of the Bone Spring Limestone within the Delaware Basin. This choice causes a deflection and sharp descent in the contours around the margin of the basin. The two contour sets also diverge west of the Delaware Basin along the trend of the Huapache monocline, where model contours strike dominantly northwest-southeast, while contours from Broadhead et al. (2005) trend more north-northwest-south-southeast. Regionally, the Huapache monocline is a northwest-southeast striking monocline, and hence one would expect that contacts through here should strike northwest-southeast as well, although Kelley (1971) does show some north-south striking contours where his Artesia–Vacuum arch intersects the monocline (cf., Plate A1.4). The two contour sets also diverge in the vicinity of the Pecos Buckles. Typically, in this area, in between the individual buckles the two contour sets colocate, but close to each buckle the contour sets diverge. This likely simply reflects the different interpolation methods used; this model directly incorporates each of the buckles as a barrier in the interpolation, while Broadhead et al. (2005) uses a smooth interpolation strategy that does not include discrete breaks.



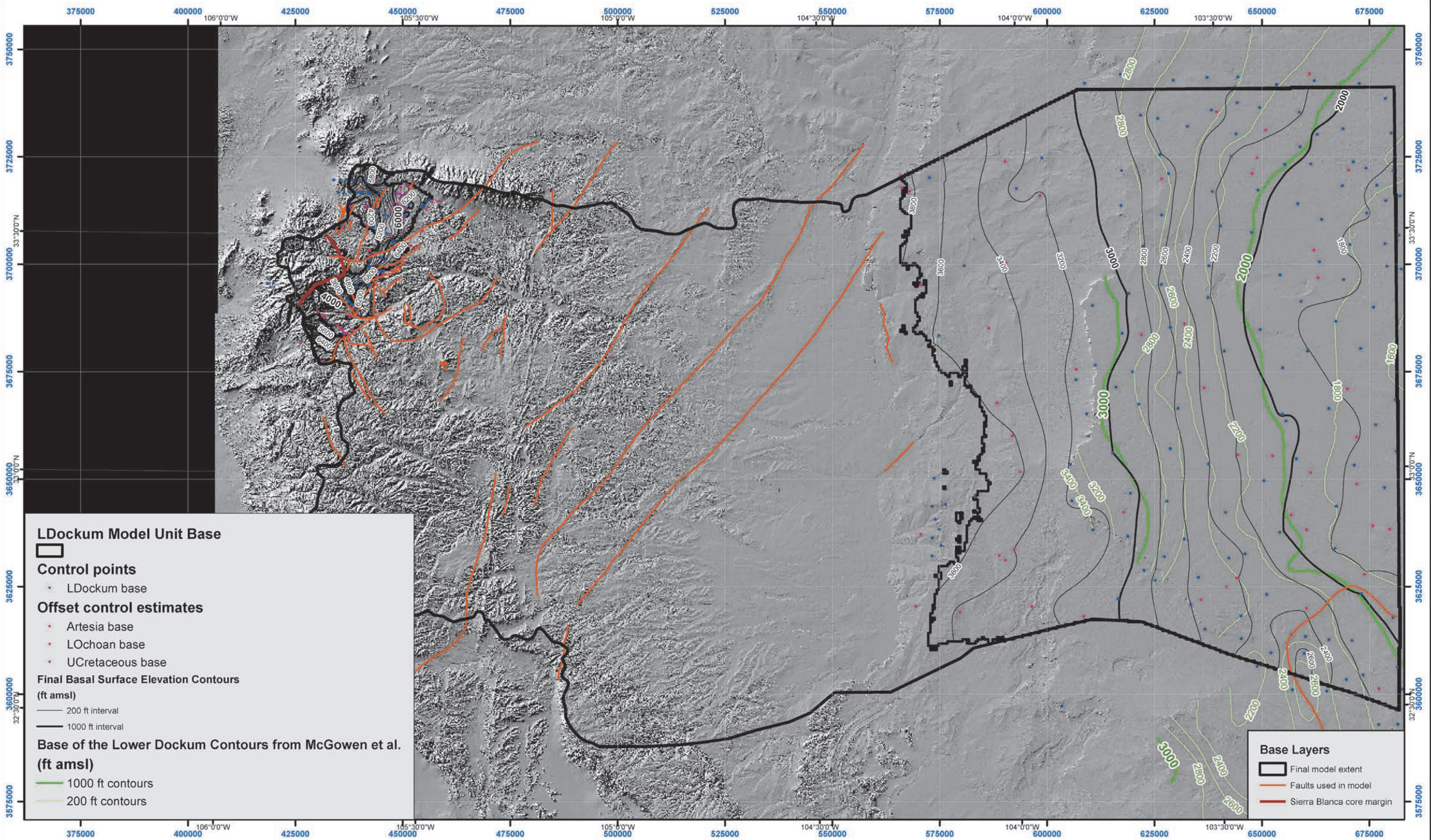


Plate A1.1. Comparisons to prior work Lower Dockum Formation.

Coordinate System: NAD 1983 UTM Zone 13N  
Projection: Transverse Mercator  
1:800,000





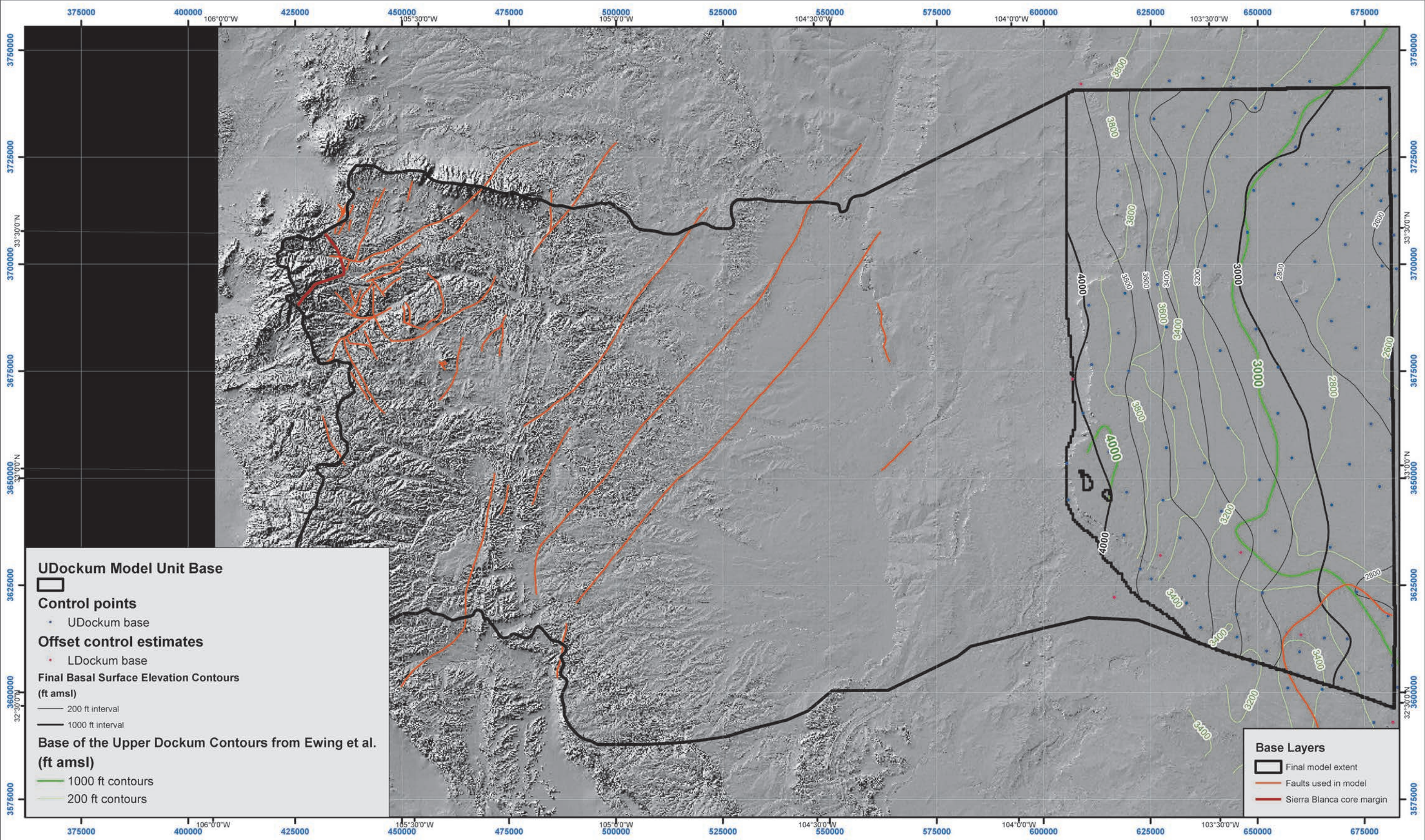
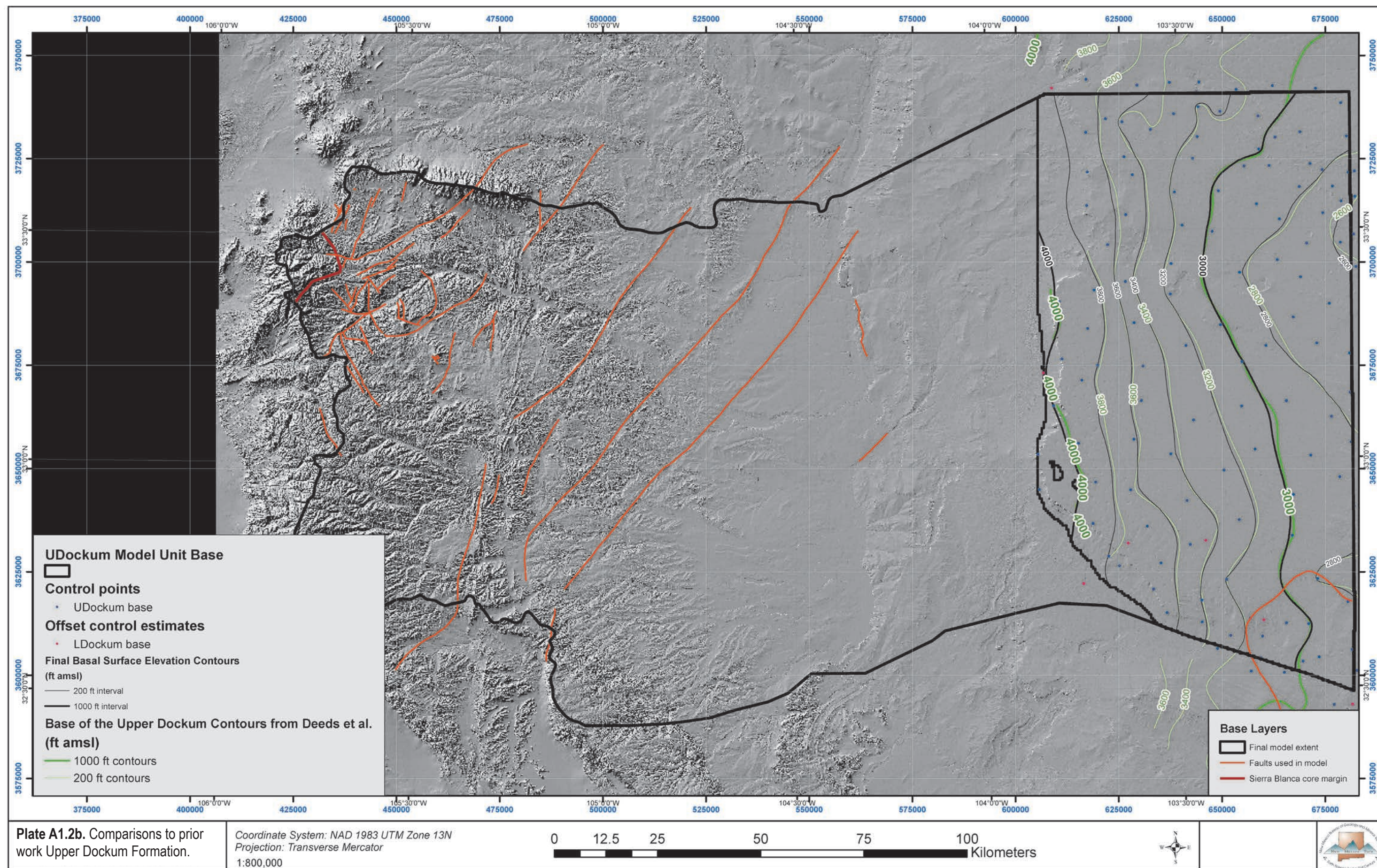


Plate A1.2a. Comparisons to prior work Upper Dockum Formation.

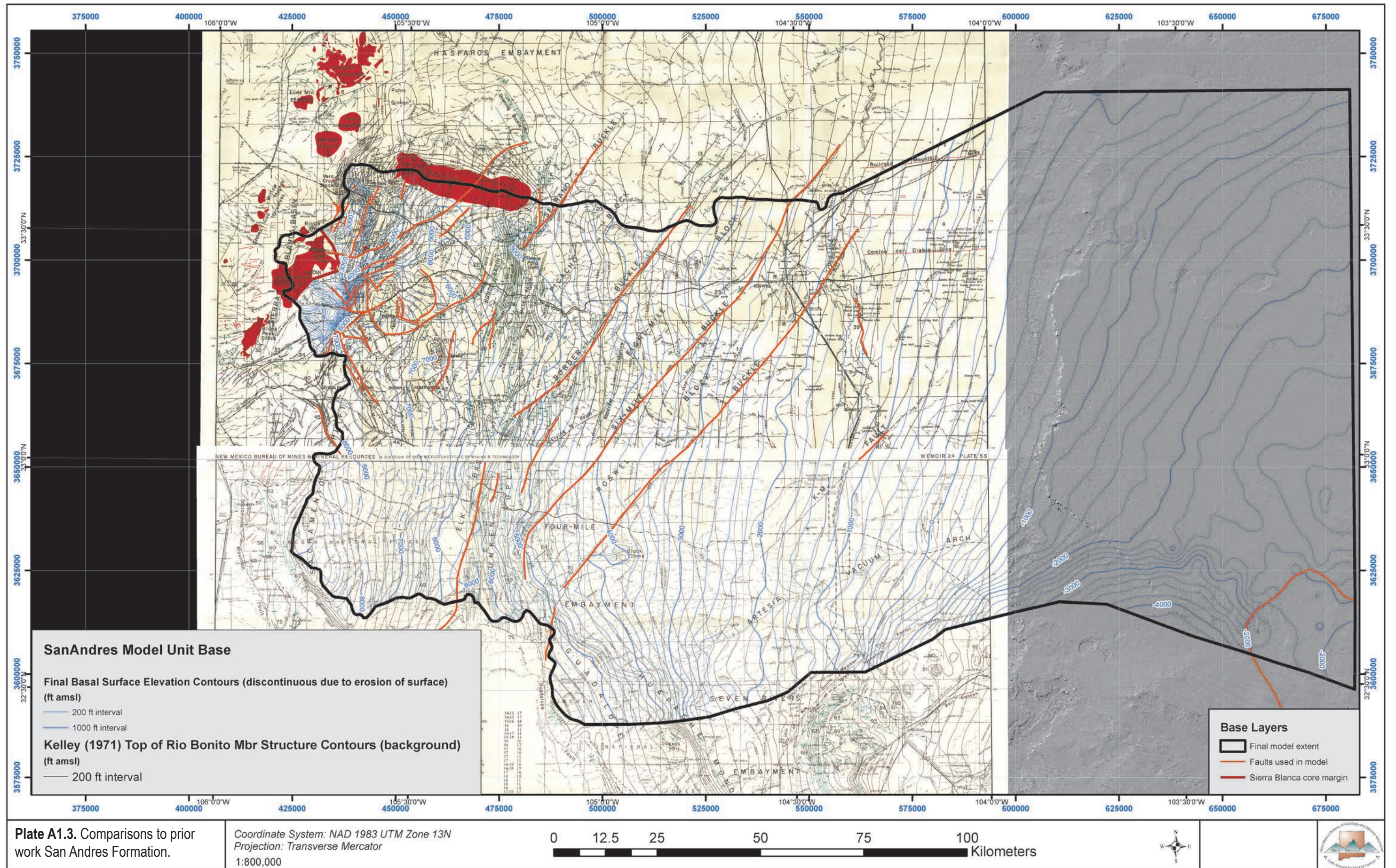
Coordinate System: NAD 1983 UTM Zone 13N  
Projection: Transverse Mercator  
1:800,000



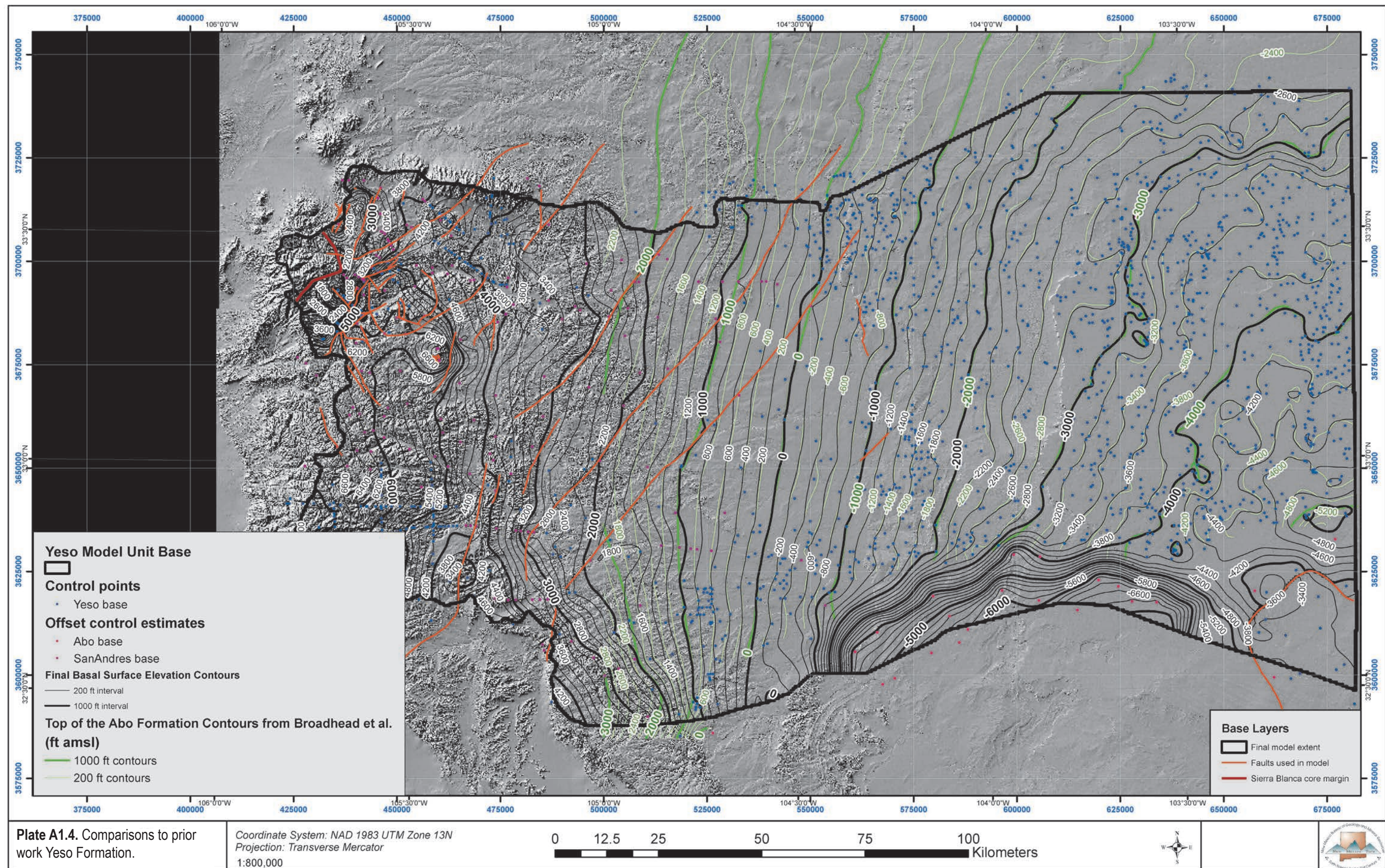
















Pecos floodplain near Bitter Lake National Wildlife Refuge.  
*Photograph by Peter A. Scholle.*



## APPENDIX 2

# AQUIFER VOLUME CALCULATION METHODS

The development of a 3D hydrogeologic framework enabled the estimation of total groundwater volume within each aquifer system. This appendix outlines the methods, assumptions, and results of the analysis to estimate the total volume of treatable groundwater for the Permian Aquifer System, the Pecos Valley Alluvial Aquifer, and the Southern High Plains Aquifer System within the Lower Pecos Slope/Southern High Plains region of southeast New Mexico. Total volume estimation considered areal aquifer boundaries, variable hydrogeologic properties within aquifer units, saturated thickness, and estimated depth of treatable groundwater. Analysis was done using the suite of tools available in ArcGIS and Python scripts, and the methodology is based largely on Kohlrenken (2013). Volumes were calculated using a combination of raster surfaces taken directly from the 3D hydrogeologic framework outlined in the main body of this report.

### Input Data

#### Sources of data

Geologic raster surfaces utilized in volume calculations were created from various sources of data outlined in Chapter 1, Pecos Slope Digital Framework Geologic Model—Overview of Methods, by Cikoski. Input data used to create geologic surfaces includes surface geologic mapping; well data compilations and individual well logs and records; cross-section and structure contour interpretations; and existing published georeferenced rasters of geologic contact elevations, Chapter 1, Pecos Slope Digital Framework Geologic Model—Overview of Methods. Hydrologic raster surfaces were created from data sourced from the Office of the State Engineer (OSE), the NMBGMR, the USGS, and Sandia National Laboratories (SNL). All raster surfaces were resampled to 500m x 500m resolution for volume calculations. Raster surfaces used in volume calculations are described in subsequent sections and summarized in Table A1. Aquifer properties, such as storage coefficients and specific yields, were compiled from aquifer tests conducted by Daniel B. Stephens & Associates (DBS&A) (1995) in the Roswell Artesian Basin, and estimated from previous research reported by Rinehart and Mamer (2017) for the Southern High Plains Aquifer System. These values are also summarized in Table A1.

### Methods

#### General

To calculate the volume of groundwater within each aquifer system, aquifer system boundaries were delineated laterally and at depth based on a variety of factors, including geologic boundaries (confining units, low-permeability barriers to groundwater flow) and water quality boundaries (TDS = 3,000 mg/L surface). 500m x 500m raster surfaces were created in ArcGIS to represent aquifer tops (water-level surface, confining units) and aquifer bottoms (water quality boundary, geologic contact with low-permeability unit). The volume of groundwater within each 500m x 500m cell was calculated using storage equations outlined in Kohlrenken (2013). Cell volumes were then summed to estimate the total groundwater volume within each respective system. Total groundwater volume was estimated for the following aquifer systems:

- Pecos Valley Alluvial Aquifer
- Southern High Plains Aquifer System
- Permian Aquifer System



### Aquifer Boundary Assessment

Bounding surfaces for aquifers were delineated based on previous research done on groundwater flow within the region (Newton et al., 2012; Deeds et al., 2015), including lateral and vertical extent of freshwater (total dissolved solids (TDS) concentration <3,000 mg/L), cross-formational flow, changes in confined/unconfined conditions, and hydrogeologic properties. The aquifer systems contain single or multiple water-bearing units (Table A2.1). Aquifer properties were assigned based on appropriate ranges of specific yield/storage coefficient values estimated from published values in literature. Ranges in specific yield/storativity for the Permian Aquifer System and Pecos Valley Alluvial Aquifer were published in DBS&A (1995) and Rinehart and Mamer (2017). Ranges of specific yield in the Southern High Plains Aquifer System were published in Rinehart and Mamer (2017). These values are summarized in Table A1.

**Table A2.1.** Summary of significant aquifer system properties used to create aquifer surfaces and consequently used in volume calculations. The Pecos Valley Alluvial Aquifer and Southern High Plains Aquifer System are both unconfined aquifer systems, while the Permian Aquifer System is considered a variably-confined aquifer system. The hydrogeologic properties and surfaces differed for the confined vs. unconfined portion of the Permian aquifer and are outlined separately below. "Surfaces" refer to 500m x 500m raster surfaces created in ArcGIS. Water-level surfaces were created by interpolating water-level data taken between year 2010-present in order to display the most up-to-date picture of water levels in the region. Mosaicking of surfaces was done by the ArcGIS Mosaic to New Raster tool and allowed for multiple surfaces to be combined when appropriate. Specific yield is a property of unconfined aquifers and is unitless. Storativity is a property of confined aquifers and is unitless.

Aquifer system	Type	Principal water-bearing unit(s)	Upper surface(s) used in calculation	Lower surface(s) used in calculation	Specific yield range (unitless)	Storativity range (unitless)
<b>Pecos Valley Alluvial Aquifer</b>	Unconfined	Pecos Valley Alluvium	Water-level surface	Pecos Valley Alluvium base	0.1–0.17	n/a
<b>Southern High Plains Aquifer System</b>	Unconfined	Ogallala Fm., Edwards–Trinity Fms.	Water-level surface	Mosaic of Ogallala base and Edwards–Trinity base	0.1–0.25	n/a
<b>Permian Aquifer System</b>	Unconfined	Yeso Fm., San Andres Fm.	Mosaic of water-level surface and Artesia Group base	Mosaic of TDS = 3,000 mg/L surface and Yeso Fm. base	0.05–0.15	n/a
<b>Permian Aquifer System</b>	Confined	San Andres Fm.	Water-level surface	Artesia Group base	n/a	0.0004

Aquifer boundaries varied between aquifer systems, and were chosen based on spatial variability of TDS data and known geologic boundaries:

Bounding surfaces for the Pecos Valley Alluvial Aquifer are relatively straight-forward. The water-level surface served as the aquifer top, and the base of the Pecos Valley Alluvium served as the aquifer bottom.

The Southern High Plains Aquifer System aquifer top was defined by the water-level surface. The base of the Ogallala or the base of the Edwards–Trinity Formations served as the aquifer bottom, whichever surface was deeper. The Dockum Group was not included in volume calculations for the Southern High Plains Aquifer System, although there is evidence that upward flow from the Dockum into the Edwards–Trinity and Ogallala formations does exist (Deeds et al., 2015).

The Permian Aquifer System was first split into confined and unconfined sections due to differences in aquifer properties. For the unconfined portion, the water-level surface was used as the aquifer top until it intersected the base of the confining unit (Artesia Group), where the base of the Artesia Group then became the aquifer top. The aquifer bottom was defined as the base of the Yeso Fm., or the TDS = 3,000 mg/L water quality boundary, whichever was shallower. For the confined portion, the aquifer top was defined as the water-level surface, and the aquifer bottom was defined as the top of the Artesia Group.

### Surface generation

Generally, water-level surfaces were used as upper aquifer surfaces for all calculations. Water-level surfaces were created using interpolation of water levels taken from year 2010 to present. This was done using the ArcGIS Topo to Raster tool. The Permian Aquifer System required two calculations to be made: 1) the unconfined portion of the aquifer, and 2) the confined portion of the aquifer where the confining Artesia Group is present. Upper and basal surfaces were mosaicked together using the ArcGIS Mosaic to New Raster tool when more than one surface qualified as a boundary. This allowed for the combination of multiple surfaces as one aquifer upper or basal surface and consequently a more accurate groundwater volume calculation.



### Volume calculation

The total volume of groundwater in each aquifer system was calculated using the following equations for confined and unconfined portions of aquifer systems. A detailed explanation of total recoverable storage and how the definition varies between confined and unconfined systems can be found in Kohlrenken, (2013):

- For unconfined aquifer systems:

$$\text{Total Storage} = V_{\text{drained}} = A * S_y * \Delta h$$

where:

- $V_{\text{drained}}$  = storage volume due to water draining from the formation (acre-ft),
- $A$  = aquifer area (acre),
- $\Delta h$  = saturated thickness of water column, and
- $S_y$  = specific yield

- For confined aquifers, or confined portions of variably-confined aquifer systems:

$$\text{Total Storage} = V_{\text{confined}} = A * S \text{ (water level - top)}$$

where:

- $V_{\text{confined}}$  = storage volume due to elastic properties of the aquifer and water (acre-ft),
- $A$  = aquifer area (acre),
- water level = groundwater elevation (ft. above mean sea level)
- top = elevation of the aquifer top (ft. above mean sea level)
- $S$  = storativity or storage coefficient (unitless)

The volume of groundwater was calculated on a 500mx500m cell by cell basis, then cell volumes were summed within each aquifer system to estimate total groundwater storage. Two volumes were calculated for the Permian Aquifer System—one for the confined portion in the Roswell Artesian Basin and one for the unconfined portion in the Sacramento Mountains down through the Pecos Slope. The two volumes were then summed to estimate a total groundwater storage for the entire aquifer system. Volumes varied based on  $S_y$  and  $S$  values used in calculations based on oftentimes highly variable geologic properties. Results of volume calculations are summarized in Table A2:

**Table A2.2.** Total groundwater volume ranges in Lower Pecos Slope and Southern High Plains Region, Southeast New Mexico.

Aquifer system	Sy or S range (unitless)	Groundwater volume range (Maf)
Permian Aquifer System	Sy = 0.05–0.15 S = 0.00004	86.7–259.8
Pecos Valley Alluvial Aquifer	Sy = 0.1–0.17	3.64–6.18
Southern High Plains Aquifer System	Sy = 0.1–0.25	20.5–51.3

### Assumptions and limitations

There exists inherent uncertainty when calculating volume of groundwater. Assumptions used in volume calculations are as follows:

- Aquifer properties were assumed to be homogenous within respective aquifer systems, with the exception of distinguishing between confined and unconfined conditions.
- Water tables were created based on available water-level data from the year 2010 to present. Data gaps exist and therefore the uncertainty in groundwater elevation is greater where data density is poor. Data gaps are discussed in the main body of this report.
- Uncertainty in geologic subsurface elevations are documented in detail in chapter by Cikoski.
- TDS values were plotted at the corresponding well depth elevation, then contoured in three dimensions to create a water quality bounding surface. This surface is an estimate of the TDS = 3,000 mg/L water quality boundary at depth across the entire region, and uncertainty is greater where water quality data density is poor.

The calculated volume ranges are estimates and can be used to inform decision making but should not be used to make decisions.



## References

- Daniel B. Stephens and Associates, Inc., 1995, Comprehensive Review and Model of the Hydrogeology of the Roswell Basin, Volumes I and II, prepared for The New Mexico State Engineer Office, Santa Fe, New Mexico, 284 p.
- Deeds, N.E., Harding, J.J., Jones, T.L., Singh, A., Hamlin, S., Reedy, R.C., Yan, T., Jigmond, M., Lupton, D., Scanlon, B.R., Seni, S., and Dutton, A., 2015, Final conceptual model report for the High Plains aquifer system groundwater availability model: report to the Texas Water Development Board, 546 p.
- Kohlrenken, W., 2013 GAM Task 13-042: Total Estimated Recoverable Storage by County for Aquifers in High Plain Underground Water Conservation District No. 1, Texas Water Development Board Groundwater Resources Division, Groundwater Availability Modeling Section, 16 p.
- Newton, B.T., Rawling, G.C., Timmons, S.S., Land, L., Johnson, P.S., Kludt, T.J., and Timmons, J.M., 2012, Sacramento Mountains hydrogeology study: Final technical report, prepared for Otero Soil and Water Conservation District: New Mexico Bureau of Geology and Mineral Resources, Open-File Report 543, 77 p.
- NMBGMR, 2003, Geologic map of New Mexico: New Mexico Bureau of Geology and Mineral Resources, scale 1:500,000.
- NMBGMR, 2018, New Mexico geologic map search [on-line], from: <https://geoinfo.nmt.edu/publications/maps/geologic/home.cfml>, New Mexico Bureau of Geology and Mineral Resources.
- Rinehart, A.J., and Mamer, E., 2017, Groundwater Storage Change in New Mexico Aquifers, Part 1. Method for Estimating Groundwater Storage Change in Variably Confined Aquifers in New Mexico, Part 2. Estimates for Groundwater Storage Change in the New Mexico Southern High Plains Aquifer, Technical Completion Report, 58 p.





New Mexico Bureau of Geology and Mineral Resources

A Research Division of New Mexico Institute of Mining and Technology

Socorro, NM 87801  
(575) 835-5490  
[geoinfo.nmt.edu](http://geoinfo.nmt.edu)